

Mechanism suppressing proteostasis collapse in pluripotent stem cells and its demise in Huntington's disease

Inaugural-Dissertation

zur

Erlangung des Doktorgrades

der Mathematisch-Naturwissenschaftlichen Fakultät

der Universität zu Köln



vorgelegt von

Seda Koyuncu

aus Ankara, Türkei

Köln 2019

Berichterstatter: Dr. David Vilchez
Prof. Dr. Thorsten Hoppe
Prof. Dr. Harm Kampinga

Tag der mündlichen Prüfung: 15.02.2019

Table of Contents

ABSTRACT	8
Zusammenfassung.....	10
1.INTRODUCTION	12
CHAPTER 1) The role of the ubiquitin-proteasome system in embryonic stem cell identity	12
1.1) The hallmarks of aging.....	12
1.2) The Ubiquitin-Proteasome system (UPS) and loss of UPS in aging process	14
1.2.1) The Ubiquitin-Proteasome System.....	14
1.2.2) The Alterations of Ubiquitin-Proteasome system activity during aging	19
1.2.3) The role of Ubiquitin-Proteasome system in stem cell identity	20
CHAPTER 2) Proteostasis of Huntingtin	22
2.1) Huntington's Disease (HD).....	22
2.2) The chaperone node in Huntington's Disease	23
2.3) The UPS in Huntington's Disease	25
2.4) The Autophagy-Lysosome system in Huntington's Disease	26
2.5) Modeling Huntington's Disease in Pluripotent Stem Cells	27
2) OBJECTIVES AND RATIONALITIES	30
3) PUBLICATIONS.....	32
4) DISCUSSION.....	158
1) Analysis of the role of E3 ligases in pluripotency.....	158
2) The investigation of the role of UBR5 in the proteostasis of HTT.....	161
5) CONCLUSIONS	166
6) DECLARATION OF CONTRIBUTION AS CO-AUTHOR	167
7) REFERENCES	168
8)Erklärung.....	180

Table of Figures

FIGURE I) The nine hallmarks of aging in molecular and cellular level	14
FIGURE II) The ubiquitin proteasome system (ups).....	18
FIGURE III) The collapse in different proteostasis network upon accumulation of mhtt aggregation.....	23

Abbreviations

AD	Alzheimer's disease
ALS	amyotrophic lateral sclerosis
ATP	Adenosine Triphosphate
ATXN3	ataxin-3
BDNF	brain-derived neurotrophic factor
<i>C. elegans</i>	<i>Caenorhabditis elegans</i>
CMA	chaperone mediated autophagy
CRLs	cullin-RING ligases
DNA	Deoxyribonucleic acid
DUBs	deubiquitinating enzymes
E1	ubiquitin-activating enzyme
E2	ubiquitin conjugating enzymes
E3	ubiquitin ligases
ER	endoplasmic reticulum
ERAD	endoplasmic reticulum-associated degradation
ESCs	embryonic stem cells
EXOC5	Exocyst complex component 5
FoxO	forkhead transcription factor
GWA	genome-wide association
HD	Huntington's disease
hESCs	human embryonic stem cells
HECT	Homologous to the E6-AP Carboxyl Terminus
HK2	hexokinase II
HSCs	hematopoietic stem cells
HSP	heat shock protein
HTT	Huntingtin
IGF-1	Insulin-like growth factor 1
IIS	Insulin/Insulin-like growth factor signaling
iPSCs	induced pluripotent stem cells
IB	Inclusion bodies
K	lysine
LIF	leukemia inhibitory factor

Met	methionine
MHC	major histocompatibility complex
MJD	Machado-Joseph disease
mRNA	messenger RNA
MSCs	mesenchymal stem cells
mHTT	mutant Huntingtin
mTOR	The mechanistic target of rapamycin
NF- κ B	nuclear factor-kappa B
NPC	neural progenitor cells
NSCs	neural stem cells
PD	Parkinson's disease
polyQ	polyglutamine repeats
Proteostasis	protein homeostasis
RBR	RING-between-RING
RCC1	regulators of chromosome condensation 1
RING	Really Interesting New Gene
RLDs	(RCC1)-like domains
RNA	Ribonucleic acid
RNAi	RNA interference
SCs	stem cells
SG	stress granules
TRiC	TCP-1 Ring Complex
Ub	ubiquitin
UPS	ubiquitin-proteasome system
WW	tryptophan-tryptophan

ABSTRACT

With the significant extension in human life expectancy during the last decades, the number of older people is increasing dramatically. As a consequence, the incidence of age-related diseases such as cancer, neurodegenerative and cardiovascular diseases is also increasing. Our ever-aging population also has considerable social and economic impact. Therefore, understanding the underlying molecular mechanisms of the aging process is of central importance to improve the quality of life and develop novel therapeutic approaches for aging-related diseases.

A decline in protein homeostasis (proteostasis) in somatic cells is a hallmark of aging. On the other hand, pluripotent stem cells such as human embryonic stem cells (hESCs) have shown to be immortal in culture and do not age, correlating with higher proteostasis mechanism. Thus, we hypothesized that understanding the regulation of the proteostasis network in pluripotent stem cells may provide valuable information for the better understanding of pluripotent stem cell identity and the aging process.

In the first part of this study, we aimed to investigate how proteostasis pathways regulate hESC identity and function. hESCs have higher proteasome activity which is essential to maintain their self-renewal and pluripotency as well as their ability to differentiate. However, the underlying mechanisms by which enhanced proteasome activity regulates hESCs identity and function remain unknown. We hypothesized that increased proteasome activity could be essential to maintain proper concentration of many regulatory proteins. Since E3 ubiquitin ligases are responsible for the ubiquitin transfer to the specific substrate, we first identify which E3 ligases are up-regulated in hESCs compared with their differentiated counterparts. We found that some HECT-domain E3 enzymes such as HERC2 and UBE3A and some RING-domain E3 enzymes such as UBR7 and RNF181 are highly expressed in hESCs. Our interactome data indicates a possible link of these enzymes with hESC identity function. Interestingly, loss of different up-regulated E3 ligases leads to significant changes at both the transcriptome and proteome of hESCs. Nevertheless, these changes do not have strong effect on either pluripotency markers or differentiation capacity. On the contrary, by using a shot label-free proteomics approach, we show that global proteasome inhibition induces an alteration in key biological processes of hESCs identity such as protein synthesis, RNA biogenesis, telomere function. Therefore, our data suggests that enhanced proteasome activity is connected with other biological pathways of hESCs identity.

In the second part of this study, we aimed to investigate how enhanced proteasome activity determines proteostasis of mutant HTT (mHTT) in pluripotent stem cells by specifically focusing on the intrinsic E3 ubiquitin ligase network. Proteostasis is essential for organismal development and cell function. Impairment of proteostasis leads to accumulation of damaged, misfolded and aggregated proteins, a process linked with the onset of age-related diseases such as Huntington's disease (HD). HD is caused by abnormal expansions of polyglutamine repeats (polyQ) in the Huntingtin protein, leading to its aggregation and concomitant toxicity. Remarkably, the length of pathological polyQ does not influence survival, self-renewal and pluripotency of induced pluripotent stem cells (iPSCs) derived from HD patients (HD-iPSCs). These results suggest that iPSCs might have enhanced mechanisms to maintain proteostasis of mutant HTT. Here, we examined the mechanisms by which iPSCs maintain proteostasis of HTT. We find that proteasome activity determines HTT levels and prevents the accumulation of polyQ aggregates in HD-iPSCs. Notably, iPSCs have increased levels of the E3 ubiquitin ligase UBR5, which interacts with HTT and regulates the degradation of both mutant and wild-type HTT protein levels. Moreover, loss of UBR5 results in accumulation of HTT protein as well as polyQ-expanded aggregates in HD-iPSCs. Furthermore, we find that knockdown of the orthologue of UBR5 hastens polyQ-expanded aggregation and neurotoxicity in a *C. elegans* model of HD. Strikingly, ectopic expression of UBR5 is sufficient to induce polyubiquitination and degradation of mutant HTT, decreasing polyQ aggregates in HD cell models. Moreover, higher UBR5 expression determines global proteostasis of iPSCs preventing the aggregation of misfolded proteins ensued from normal metabolism. Thus, our data put UBR5 as a novel modulator of super-vigilant proteostasis of iPSCs.

Zusammenfassung

In den letzten Jahren hat die Lebenserwartung der Menschen stark zugenommen, wodurch auch die Anzahl älterer Menschen dramatisch gestiegen ist. Dementsprechend hat die Anzahl der altersbedingten Krankheiten wie Krebs, neurodegenerative Erkrankungen und Erkrankungen des Herz-Kreislauf-Systems ebenfalls stark zugenommen. Die immer weiter alternde Gesellschaft hat einen starken sozialen und wirtschaftlichen Effekt. Ein besseres Verständnis der molekularen Abläufe, die den Alterungsprozess steuern, ist von zentraler Bedeutung, um die allgemeine Lebensqualität zu verbessern und für die Entwicklung von neuen therapeutischen Behandlungen für altersassoziierte Krankheiten.

Ein Zeichen der Alterung ist die Abnahme der Proteinhomöostase (Proteostasis) in somatischen Zellen. Allerdings sind pluripotente Zellen, so wie embryonale Stammzellen (hESCs), unsterblich in Zellkultur und altern nicht, was man auf ihre erhöhte Proteinhomöostase zurückführen kann. Wir vermuten, dass ein besseres Verständnis der Regulierung der Proteinhomöostase in pluripotenten Stammzellen wichtige Informationen über die Identität pluripotenter Stammzellen und ihres Alterungsprozesses liefern wird.

Im ersten Teil unserer Studie untersuchten wir, wie Homöostasesignalwege die Identität und Funktion von hESCs regulieren. hESCs haben eine erhöhte proteasomale Aktivität, was ihnen die Fähigkeiten zur Selbsterneuerung, Pluripotenz und Differenzierung erlaubt. Allerdings ist der genaue Mechanismus, wie die erhöhte proteasomale Aktivität, Identität und Funktion der hESCs reguliert wird, nicht bekannt. Unserer Hypothese besagt, dass erhöhte proteasomale Aktivität essenziell zur Erhaltung der idealen Konzentration von Regulationsproteinen ist. E3 Ubiquitinligasen sind Enzyme, die Ubiquitin auf ihre spezifischen Substrate übertragen. Hier haben wir zuerst alle E3 Ubiquitinligasen identifiziert, die nur in hESCs hochreguliert sind und nicht in differenzierten Formen. Unsere Ergebnisse haben gezeigt, dass bestimmte HECT E3 Ligasen wie HERC2 und UBE3A, so wie Enzyme mit RING-Domäne, wie UBR7 und RNF181 in hESCs stark exprimiert sind. Unserer via massenspektrometrischer Analyse erstelltes Interaktom deutete eine Verbindung zwischen den genannten Proteinen und hESC Identität an. Bei einem Verlust von hochregulierten E3 Ligasen kann man signifikante Veränderungen im Transkriptom und im Proteom von hESCs feststellen. Allerdings haben keine dieser Veränderungen einen starken Einfluss auf Marker der Pluripotenz oder auf die Differenzierungsfähigkeit von Zellen. Nichtsdestotrotz hat die massenspektrometrische Analyse gezeigt, dass die globale, proteasomale Inhibierung wichtige biologische Prozesse ändert und die hESC Identität mit beeinflusst. Ebenfalls beeinflusst werden Proteinsynthese, RNA Biogenese und die Telomerfunktion. Insgesamt zeigt unsere

Analyse, dass proteasomale Aktivität mit biologischen Prozessen verbunden ist, welche die hESC Identität beeinflussen.

In dem zweiten Teil dieser Arbeit wurde untersucht, wie erhöhte proteasomale Aktivität die Proteostase von mutiertem HTT (mHTT) in pluripotenten Stammzellen beeinflusst. Der besondere Fokus lag auf dem inhärenten E3 Ubiquitin-Ligasenetzwerk. Proteostase ist für Zellen lebensnotwendig für die Entwicklung des Organismus und für die Zellfunktion. Eine Störung der Proteostase führt zu einer Anreicherung von beschädigten, falsch gefalteten und aggregierten Proteinen. Dieser Prozess ist eng verlinkt mit altersbedingten Krankheiten wie Huntington-Krankheit (HD). HD entsteht durch abnormale Zunahme der Polyglutamine-Wiederholungen (polyQ) des Huntington Proteins, was zu seiner Aggregation mit anschließender Toxizität führt. Besonders bemerkenswert ist, dass die Länge von pathologischem PolyQ kein Einfluss auf die Überlebensfähigkeit, Selbsterneuerung oder auf die Pluripotenz induzierte Stammzellen hat, die von huntington-kranken Patienten (HD-iPSCs) isoliert wurden, hat. Diese Beobachtung legt die Vermutung nahe, dass diese Zellen einen Mechanismus haben, der ihnen erlaubt, die Proteostase von mutiertem HTT zu wahren. In dieser Arbeit haben wir den Mechanismus untersucht, durch den iPSCs ihre Proteostase erhalten können. Unsere Ergebnisse zeigen, dass proteasomale Aktivität die Menge von HTT reguliert und die Anreicherung von PolyQ-Aggregaten verhindert. Es ist beachtenswert, dass iPSCs eine hohe Menge der E3 Ligase UBR5 generieren, welche direkt mit HTT interagiert und die Proteinmengen von sowohl Wildtyp, als auch von Mutanten reguliert. Ein Verlust des Proteins UBR5 führt zu einer starken Akkumulation von HTT und PolyQ-Aggregaten in HD-iPSCs. Weiterhin haben wir herausgefunden, dass der Verlust von UBR5 Orthologen in *C. elegans* zur schnelleren Bildung von PolyQ-Aggregaten und zu Neurotoxizität führt. Auffällig ist, dass die ektopische Expression von UBR5 ausreichend ist, um Polyubiquitylierung zu induzieren und mutiertes HTT zu degradieren, was in den HD Modelzellsystemen zur Abnahme von PolyQ-Aggregaten führt. Ferner bestimmt eine erhöhte Expression von UBR5 die globale Proteostase in iPSCs. Außerdem verhindert sie Aggregatbildung von falsch gefalteten Proteinen, die aus dem normalen Metabolismus resultieren. Zusammenfassend zeigt unsere Arbeit, dass UBR5 als ein besonderer Modulator der supervorsichtigen Proteostase in iPSCs dient.

1.INTRODUCTION

CHAPTER 1) The role of the ubiquitin-proteasome system in embryonic stem cell identity

1.1) The hallmarks of aging

During the last decades, the average age of human population has increased significantly due to the advances in medical care, improvements in healthier food and drug development. This increase in older age population results in a higher incidence of age-related diseases such as cancer, neurodegenerative disorders, diabetes, cardiovascular disorders, which have social and economic impacts (Carmona and Michan 2016). Therefore, understanding the underlying molecular and cellular mechanisms of aging and the susceptibility to age-related disease is necessary to identify novel interventions that can improve the quality of life at older ages.

Aging is a gradual, physiological deterioration process which is associated with decline in molecular and cellular function, causing causes vulnerability to disease and death (Carmona and Michan 2016). There are many theories have been proposed to explain organismal aging and they are categorized into two main groups: programmed and error theories (Jin 2010). In the programmed theories, aging follows a biological timetable and it is regulated by changes in gene expression that influence biological systems responsible for repair, maintenance, and defense mechanisms. The error theories are based on the concept that damage accumulates at various levels throughout the entire lifespan due to environmental assaults and causes aging (Jin 2010). Among a number of theories, antagonistic pleiotropy and disposable soma theory stand out. In the first theory, it has been suggested that a decrease in force of natural selection with age results in aging (Rose, Flatt et al. 2012). The extrinsic risks such as starvation, infection or predators lead to limitation of organismal lifespan and decrease in the natural aging population. Therefore, natural selection can cause elimination of genes which are drivers for deleterious effects (Rose, Flatt et al. 2012). However, the genes which are important in early-life survival cannot be eliminated and they may also drive aging in late-life, which is a concept known as antagonistic pleiotropy (Baig, Bhadbhade et al. 2014). According to the disposable soma theory, the higher energy expense used for growth and reproduction has a considerable cost on the somatic maintenance. The accumulation of cell damage over time limits the functioning of important organ systems and lifespan (Hughes, Alipaz et al. 2002). The main characteristic of aging is the loss of function (degeneration) at molecular, cellular and organismal levels. In mammals, age-related degeneration is a hallmark of distinct

pathologies such as neurodegenerative diseases (Alzheimer's (AD), Huntington's (HD) and Parkinson's diseases (PD)), atherosclerosis and diabetes (Carmona and Michan 2016). Moreover, in multicellular organisms, aging can also lead to a gain of function which causes inappropriate cell proliferation called hyperplasia (Rose, Flatt et al. 2012).

The aging process is characterized by nine hallmarks at the molecular and cellular level: instability in genome (accumulation of damage in genome throughout life), telomere attrition (deterioration of telomere region), epigenetic alterations (i.e., change in DNA methylation level, chromatin remodeling and posttranslational modification of histone) , impairment in proteostasis (i.e., deficiency in degradation pathways such as proteasome and autophagy and impairment in folding capacity of proteins) , deregulated nutrient sensing (i.e., variation in insulin and IGF-1 (insulin-like growth factor type 1) signaling (IIS) pathway, mTOR pathway), impairment in mitochondrial fitness (i.e., decline in the efficiency of the respiratory chain) , cellular senescence (irreversible arrestment in cell proliferation), changed intercellular communication and stem cell exhaustion (Lopez-Otin, Blasco et al. 2013) (Figure I).

Over recent years, studies based on several organisms ranging from yeast to humans have suggested that dietary restriction, genetic and pharmacological interventions may promote protection against aging-related cellular and molecular declines by improving cellular homeostasis and stress resistant, resulting in longer lifespan and healthspan (Lin, Seroude et al. 1998, Smith, Kaeberlein et al. 2008, Saraswat and Rizvi 2017). A range of signaling pathways such as mTOR, sirtuins, insulin/IGF-1 have been identified as having a role in the regulation of aging process (Tatar, Bartke et al. 2003, Longo and Kennedy 2006, Johnson, Rabinovitch et al. 2013).



Figure I) The nine hallmarks of aging in molecular and cellular level. Aging is a gradual, physiological decline in function of multiple cells and tissues. Aging is characterized by the nine hallmarks including; stem cell exhaustion, altered intercellular communication, genomic instability, telomere attrition, epigenetic alterations, loss of proteostasis, deregulated nutrient sensing, mitochondrial dysfunction, cellular senescence. Figure reprinted from Ref. (Lopez-Otin, Blasco et al. 2013), with permission from Elsevier.

1.2) The Ubiquitin-Proteasome system (UPS) and loss of UPS in aging process

1.2.1) The Ubiquitin-Proteasome System

Maintenance of protein homeostasis by the Ubiquitin-Proteasome System (UPS) is important for cellular function and their viability. UPS regulates intracellular protein degradation which is a vital process for determining the protein half-life and preventing damaged proteins or aggregates to accumulate (Powers, Morimoto et al. 2009). UPS is involved in a variety of biological functions such as regulation of gene transcription, cell cycle, immunological response, aging and stem cell identity (Eldridge and O'Brien 2010).

For targeting a protein to the UPS, first it is required the attachment of ubiquitin, a protein which is 76 amino acids long. Ubiquitin has seven lysine residues (K6, K11, K27, K29, K33,

K48, K63) and a N-terminal methionine (Met1) residue which can be linked to other ubiquitin to form multi or polyubiquitin chain. The pattern and type of ubiquitinylation determine the fate of a protein. Monoubiquitylation or multiubiquitylation (multiple monoubiquitylation of a target protein) are involved in different biological functions such as endocytosis, DNA repair, protein sorting. On the contrary, polyubiquitination signals are involved in protein degradation, kinase regulation and activation/inhibition of transcription factors (Jana, Zemskov et al. 2001, Sun and Chen 2004). For example, K63 linked polyubiquitination has a key role in the regulation of DNA damage response and endocytosis. On the contrary, K48 linked polyubiquitination targets proteins to the proteolytic complex, 26S proteasome, for degradation (Adams 2003). Moreover, linear types of ubiquitination chain can be formed by conjugation of the one of the carboxy-terminal glycine of ubiquitin to lysine residue of another ubiquitin. This ubiquitination plays role in nuclear factor-kappa B (NF- κ B) activation (Iwai and Tokunaga 2009). Ubiquitination of target protein is accomplished through a three-step cascade mechanism (Pickart and Eddins 2004). Initially, ubiquitin is activated in an ATP-dependent manner by a ubiquitin-activating enzyme (E1) that forms a thioester bond between a cysteine residue and carboxy-terminal of ubiquitin (Hochstrasser 1996). The activated ubiquitin is transferred to ubiquitin conjugating enzymes (E2s) via formation of E2-Ub thioester structure (Pickart 2001). In the final step, E3 ligase catalyze the attachment of ubiquitin to the target protein by binding to both the E2-Ub thioester structure and target protein (Hochstrasser 1996).

E3 ubiquitin ligases are essential components of the ubiquitination cascade reaction due to their role in both controlling the efficiency and substrate specificity. Due to the requirements of a specific substrate targeting, there are more than 600 human E3s encoded by the human genome. The E3s are classified into three different families based on their structural domains and mechanism for ubiquitin transfer from the E2 enzyme to the target substrate protein: the (RING) E3s family, the homologous to the E6AP carboxyl terminus (HECT) E3s family and the RING-between-RING (RBR) E3s family (Deshaies and Joazeiro 2009, Metzger, Hristova et al. 2012, Spratt, Walden et al. 2014). RING E3 enzymes represents the biggest E3 ligase family. It contains a RING or U-box domain which is required for binding both to the E2 enzyme and the target protein. The RING domain is characterized by two zinc ions while the U-box domain does not contain zinc ions but adopts the same folding of the RING domain. By binding both to the E2-Ub thioester and the target protein, these E3s ligases transfer ubiquitin directly from the E2 enzymes to the target proteins (Metzger, Hristova et al. 2012). RING E3 ligases can function in diverse ways including monomers, homodimers and heterodimers. Moreover, some RING E3s such as the cullin-RING ligases (CRLs) are composed by multi-

subunits (Deshaies and Joazeiro 2009). U-box proteins are also a part of the RING E3 ligase family as they transfer ubiquitin through the same mechanism and resemble the structure of the RING domain. U box proteins can also function as monomers or homodimers such as UBE4B and CHIP respectively (Buetow and Huang 2016). On the other hand, HECT E3 and RBR E3s family catalyze ubiquitin transfer in a two-step reaction which first transfers ubiquitin from E2 to an active site cysteine of the E3 ligase and in the second step, from the E3 ligase to the target protein (Metzger, Hristova et al. 2012, Spratt, Walden et al. 2014). In humans, 28 HECT E3s are found. HECT E3s have a HECT domain and a N-terminal substrate-binding domain (Rotin and Kumar 2009). The HECT domain is located at the C-terminal and is involved in catalysis of ubiquitin conjugation and transfer while the N-terminal substrate-binding domain interacts with E2-Ub. HECT E3s are divided into 3 subfamilies: the NEDD4 family, which comprises tryptophan-tryptophan (WW) motifs, the HERC family, which has regulators of chromosome condensation 1 (RCC1)-like domains (RLDs) and “other” HECTs with various protein-protein interactions domain (Metzger, Hristova et al. 2012). Like HECT E3s, RBR E3s catalyze the ubiquitin transfer in two-step reaction. In humans, 14 RBR E3s are described and they comprise two RING fingers, RING1 and RING2 and are separated with an in-between-RINGs zinc-binding domain (Spratt, Walden et al. 2014). RBR E3s are defined as a hybrid of HECT and RING E3s. RING1 domain recruits E2-Ub and RING2 domain has a catalytic cysteine (Buetow and Huang 2016). In addition to E3 ligases, the UPS is also regulated by a number of deubiquitinating enzymes (DUBs) (Wilkinson 2000). DUBs are responsible for removal of ubiquitin chain from substrate before substrates enter the proteolytic core of proteasomes. DUBs act by direct or indirect association with the proteasome (Wilkinson 2000). The classical DUBs are classified into two main families according to their enzymatic cleavage mechanism: zinc metalloproteases and cysteine proteases (Pfoh, Lacdao et al. 2015).

The polyubiquitin chain is made by the addition of a C-terminal Gly residue of one ubiquitin to another ubiquitin's lysine residue. This polyubiquitin chain acts like a degradation signal which is recognized by the 26S proteasome complex (Glickman and Ciechanover 2002). The proteasome is a well conserved complex composed of a central unit (20S) and a regulatory subunit (19S). 19S is composed of the two subcomplexes; the base and the lid which consist of 20 subunits. The lid consists of nine non-ATPase subunits (Rpn3, Rpn5-9, Rpn11, Rpn12, and Rpn15) whereas the base consists of three non-ATPases (Rpn1, Rpn2, and Rpn13) and six AAA-type ATPases (Rpt1-6) (Gumeni and Trougakos 2016). The 19S is responsible for the recognition of polyubiquitylated proteins (da Fonseca, He et al. 2012). The central unit 20S is composed of four rings; two central and identical heptameric rings called β -rings and two outer

rings called α -rings. β subunits include three catalytic subunits - $\beta 1$, $\beta 2$, $\beta 5$ - which have caspase-like, trypsin-like activity and chymotrypsin-like activity, respectively (Groll, Ditzel et al. 1997). After the proteins enter into the 20S complex, they are targeted by a N-terminal threonine residue of the catalytic subunits of the 20S (Adams 2003). (Figure II). There is also a specialized form of proteasome which is called immunoproteasome. In the immunoproteasome, the catalytic subunits $\beta 1$, $\beta 2$, $\beta 5$ of proteasome are replaced by the cytokine inducible $\beta 1i$, $\beta 2i$, $\beta 5i$ subunits. The immunoproteasome is stimulated by proinflammatory cytokines such as interferons as well as oxidative stress (Ferrington and Gregerson 2012). Moreover, in the immunoproteasomes, the regulatory subunits 19S is replaced by the PA28 activator (11S) (Borissenko and Groll 2007). Immunoproteasomes promote increased cleavage after hydrophobic residues and decreased cleavage after acidic residues. This leads to the generation of peptides with higher affinity to bind to the MHC class I complex, which is one of the primary classes of major histocompatibility complex (Ferrington and Gregerson 2012).

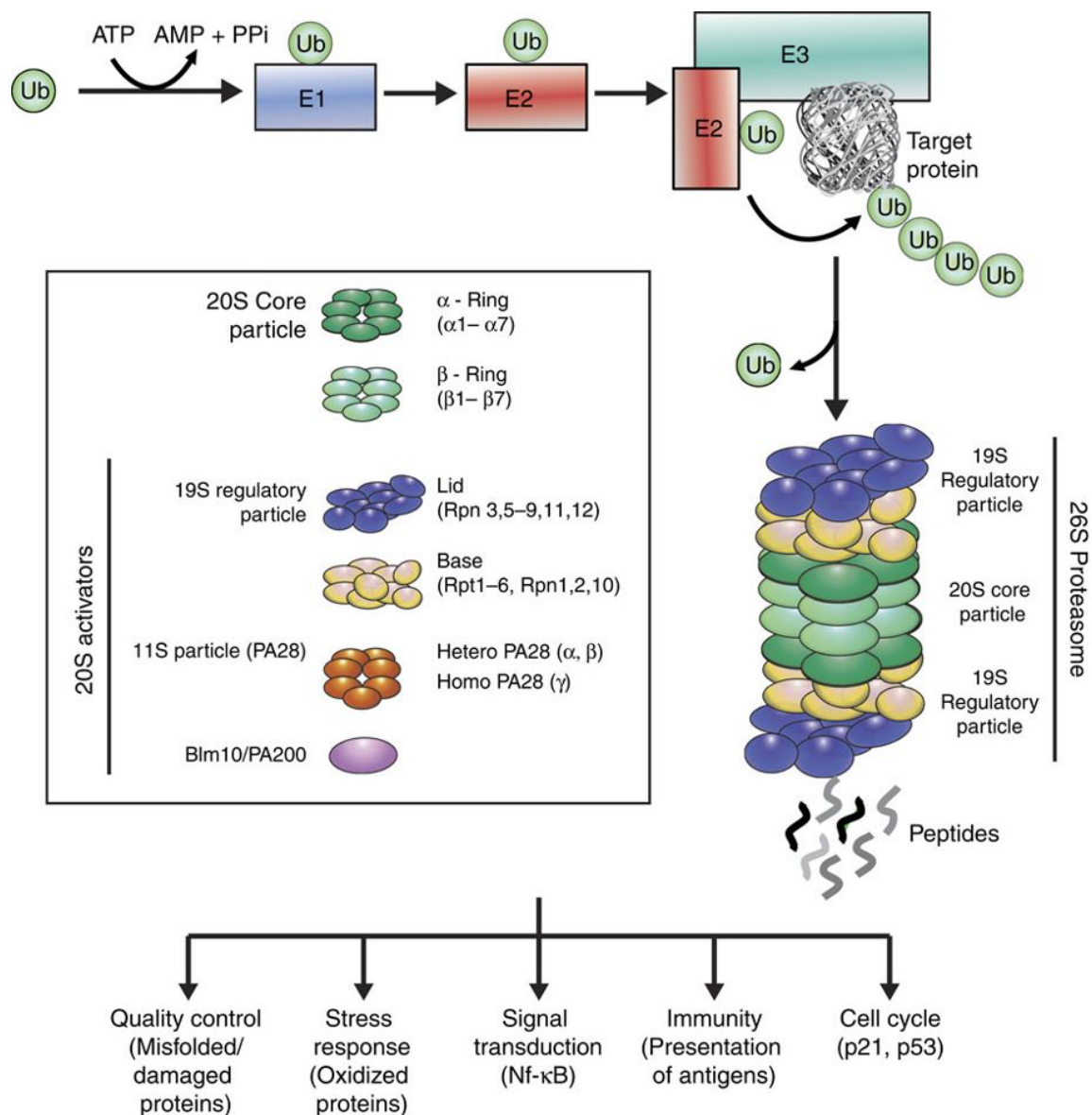


Figure II) The ubiquitin proteasome system (UPS). UPS regulates intracellular protein degradation and targeting a protein to UPS, first it is needed the attachment of ubiquitin to substrate protein. Ubiquitination of substrate protein is achieved through a three-step cascade mechanism. Firstly, ubiquitin is activated in a ATP-dependent manner by E1. The activated ubiquitin is transferred to E2s via formation of E2-Ub thioester structure. Finally, E3 ligase catalyze the ubiquitin attachment to the substrate protein by binding to both the E2-Ub thioester structure and substrate protein. The same cascade reaction is repeated to form a ubiquitin chain. After ubiquitination, this polyubiquitin chain is recognized and degraded by the 26S proteasome complex. The active proteasome is formed by of a central unit (20S) and a regulatory subunit (19S). The 19S recognizes the polyubiquitylated substrate and mediates deubiquitination. The central subunit 20S is normally found as inactive form and require binding of 20S activators such as 19S regulatory protein. After substrate is recognized and enter into 20S complex, the substrate is cleaved into small peptides. The UPS is important regulator for several cellular functions such as stress response, signal transduction.

1.2.2) The Alterations of Ubiquitin-Proteasome system activity during aging

Stability of protein homeostasis is a key determinant in the regulation of aging and lifespan. Regulation of proteostasis englobes protein refolding capacity, regulation of protein stability, cellular localization of proteins, protein degradation. Impairment in proteostasis leads to the accumulation of damaged, misfolded and aggregated protein which compromises cell viability (Saez and Vilchez 2014). One of the key components in proteostasis is the UPS, which is the major protein clearance mechanism and is essential for removing damaged, unneeded and aggregated proteins as well as short lived proteins. Thus, the progressive decline in UPS function and activity has been correlated with aging and senescence. This impairment in activity and function could be due to several reasons such as structural alterations or the replacement of proteasome subunits, declined amount of proteasome, disassembly of proteasomes, activity alteration due to interaction with protein aggregates and decline in energy source (ATP) from malfunction of mitochondria (Grune, Jung et al. 2004, Ferrington, Husom et al. 2005, Chondrogianni, Petropoulos et al. 2014). An age-related decline in proteasome activity has been reported in different human tissues such as muscle, skin, kidney and in several other mammals, such as rats and mice (Bulteau, Szweda et al. 2002, Chondrogianni and Gonos 2005, Kapphahn, Giwa et al. 2006, Dasuri, Zhang et al. 2011, Chondrogianni, Petropoulos et al. 2014). Moreover, human senescent fibroblasts show a reduction in proteasome activity and expression of proteasome subunits compared to lower-passage counterparts (Chondrogianni, Stratford et al. 2003). The role of proteasome activity in senescence is also supported by the fact that fibroblasts treated with an inhibitor of the proteasome inhibitor show senescence-like phenotypes and a decreased replicative lifespan (Torres, Lewis et al. 2006). The role of proteasome in aging has also been supported with gain-of-function experiments. Proteasome activation by genetic manipulation or chemicals endorse lifespan and healthspan extension in organisms and cellular models and prevents the formation of aggregates, a process associated with distinct age-related diseases (Chondrogianni, Voutetakis et al. 2015, Krahn, Kaschani et al. 2017). The treatment of human embryonic fibroblasts with chemical compounds such as IMP20 and WI-38, which enhance proteasome activity reduces protein carbonyl levels and promotes lifespan extension (Katsiki, Chondrogianni et al. 2007). In *Drosophila melanogaster*, the activation of the proteasome activity via overexpression of Rpn11 (a subunit of 19S regulator) promotes lifespan extension (Tonoki, Kuranaga et al. 2009). Different E2 and E3 ligases have a role in UPS activation as well as lifespan extension. For example, RLE-1, an E3 ligase, is responsible for ubiquitination of DAF-16, which is the ortholog of FoxO family of transcription factors in *C. elegans*, and leads to its degradation (Li, Gao et al. 2007). Moreover,

UPS is also involved in the regulation of insulin signaling. Insulin/ IGF-1 regulates aging in several organisms and inhibits the forkhead transcription factor, FoxO. Suppression of FoxO transcription mediates the inhibition of proteasomal degradation. Notably, activation of FoxO through reduced insulin/IGF-1 signaling increases lifespan (Saez and Vilchez 2014).

On the other hand, deficiency in proteasome activity worsens the phenotype of several aging-related diseases such as neurodegenerative diseases (e.g. HD, PD and AD), skin aging, cardiovascular diseases and cancer through a decrease in the degradation of damaged and oxidized proteins (Saez and Vilchez 2014). Notably, the accumulation of oxidized proteins due to an age-related impairment in the proteasome activity is one of the major factor that promotes skin aging (Koziel, Greussing et al. 2011). A decline in proteasome activity in AD patients compared with controls has been shown (Keck, Nitsch et al. 2003). Furthermore, in the neurodegenerative disease HD, the overexpression of the proteasome subunit PSMD11/RPN6 in a *C. elegans* model of HD ameliorates the pathology of the disease (Vilchez, Morantte et al. 2012). In summary, proteasome dysfunction is tightly associated with aging and aging-associated diseases. Therapeutic approaches for regulating the proteasome activity may improve cellular homeostasis and promote lifespan extension.

1.2.3) The role of Ubiquitin-Proteasome system in stem cell identity

One of the roles of the UPS is to regulate pluripotency and self-renewal of hESC and induced pluripotent stem cell (iPSC), as well as cellular reprogramming (Okita and Nakayama 2012, Vilchez, Boyer et al. 2012, Strikoudis, Guillaumot et al. 2014, koyuncu 2015). ESCs are derived from the inner cell mass of blastocysts and are pluripotent. Therefore, they have the capacity to differentiate into the three different germ layers: endoderm, ectoderm and mesoderm (Thomson, Itskovitz-Eldor et al. 1998). Like ESCs, iPSCs are also pluripotent and can differentiate into the three germ layers. iPSCs are derived from somatic cells that are reprogrammed by a set of transcription factor into epigenetic and transcriptional state to embryonic-like pluripotency (Takahashi, Tanabe et al. 2007, Kaye and Finkbeiner 2013). This major breakthrough in stem cells area by generation of iPSC came in 2006 by generation of iPSC from fibroblasts cells by using combination of four transcription factor (Oct4, Sox2, Klf4, and, c-Myc).

Regulation of the levels of some pluripotency factors such as Oct-4, Nanog through polyubiquitylation is a key determinant of hESC/iPSC function (Strikoudis, Guillaumot et al. 2014). Furthermore, the UPS is also essential for cell reprogramming (Buckley, Aranda-Orgilles et al. 2012). Proteomics analysis based on three different hESC lines (H2, H3, H5)

have indicated that the proteins which are enriched in hESCs include components of UPS when compared with differentiated counterparts (Baharvand, Hajheidari et al. 2006). Moreover, microarray-based transcriptional network analysis based on RNAi dependent depletion of OCT4 function in hESCs has uncovered 18 genes related with the UPS pathway (Babaie, Herwig et al. 2007). Strikingly, hESCs are more sensitive to proteasome inhibition compared with differentiated cells (Assou, Cerecedo et al. 2009, Vilchez, Boyer et al. 2012). Pluripotent stem cells treated with the proteasome inhibitor MG132 exhibit strong downregulation of pluripotency-associated genes such as *OCT4*, *c-MYC* and *SOX-2* (Assou, Cerecedo et al. 2009, Vilchez, Boyer et al. 2012). Furthermore, it has been reported that the non-ATPase subunit PSMD11/RPN6 is required for pluripotency in hESC by increasing proteasome activity (Vilchez, Boyer et al. 2012, Vilchez, Boyer et al. 2013). PSMD11/RPN6 is highly expressed in both hESCs and iPSC and this expression decreases during neuronal differentiation. Decrease in PSMD11/RPN6 leads to a reduction in the proteasome activity. Notably, this enhanced levels of PSMD11/RPN6 are regulated by FOXO4, a pro-longevity transcription factor (Vilchez, Boyer et al. 2013). Moreover, comparison between hESCs with either hESCs-derived cells or somatic cells such as fibroblasts, indicate a decline in proteasome activity with differentiation (Vilchez, Boyer et al. 2012, Vilchez, Boyer et al. 2013). Another way the UPS regulates pluripotency is based on the immunoproteasome, which is upregulated in response to cytokines (Ferrington and Gregerson 2012). Inhibition of the two immunoproteasome subunits PSMB9 and PSMB8 results in downregulation of the pluripotency markers in hESCs (Atkinson, Collin et al. 2012). In embryonic-body mediated differentiation of hESCs, it has been observed a decline in PSMD9/ β 1i and PSMB8/ β 5i expression (Atkinson, Collin et al. 2012). Similar to the 26S/30S proteasome, the immunoproteasome is highly assembled in hESCs compared with differentiated counterparts (Atkinson, Collin et al. 2012).

Although the UPS has a specific role in maintenance of pluripotency and cell-fate decisions by controlling the half-life of proteins as well as removing damaged proteins, it is still not clear which are the underlying mechanisms for this regulation. The regulation of pluripotency by the proteasome might be based not only on controlling protein degradation rates both also on other functions such as increased global translational. As such, the proteasome also prevents the nonspecific assembly of the preinitiation complex by targeting cryptic promoter elements for degradation (Szutorisz, Georgiou et al. 2006). In summary, the UPS is key for regulating cell-fate and pluripotency although the mechanisms underlying this regulation are yet not well-understood.

CHAPTER 2) Proteostasis of Huntingtin

2.1) Huntington's Disease (HD)

Huntington's Disease (HD) is a fatal autosomal dominant neurodegenerative disease characterized by motor dysfunction, cognitive decline and psychosis (Mendez 1994, Ross and Tabrizi 2011). HD is caused by abnormal expansion of a CAG triplet repeats in the *Huntingtin* (*HTT*) gene which translates into a polyglutamine (polyQ) stretch of the N-terminal domain of the huntingtin (HTT) protein and leads to protein aggregation and proteotoxicity (Davies, Turmaine et al. 1997, Scherzinger, Lurz et al. 1997, Finkbeiner 2011). In unaffected individuals, *HTT* gene encodes for HTT protein which contains 6–35 polyQ repeats, while in HD patients HTT protein contains more than 35 polyQ repeats (Finkbeiner 2011). Although HTT protein is ubiquitously expressed, expanded- polyQ mutations leads to selective neurodegeneration which affects preferentially neurons of the striatum essential for cognition, motor control and sensory pathways (Vonsattel, Myers et al. 1985). This selective neurodegeneration is associated with the age-dependent aggregation of mutant HTT protein in the striatum (Vonsattel and DiFiglia 1998). The age of onset and disease progression inversely correlates with the length of polyQ repeats (Ross and Tabrizi 2011).

HTT protein is involved in several biological processes such as embryonic development, transcriptional regulation, apoptosis, microtubule-based transport, ciliogenesis and autophagy (Saudou and Humbert 2016). Although polyQ-expansions could also lead to a loss of normal HTT function and contribute to the pathology of HD, extensive experimental data and the dominant inheritance pattern of the disease indicate that a gain-of-function HTT is toxic. As a result of a gain-of-function, mutant HTT impairs cellular homeostasis by overwhelming the cellular proteostasis machinery and triggers neurodegeneration (Bates 2003, Kratter and Finkbeiner 2010, Zuccato, Valenza et al. 2010). (Figure III). The function, folding and clearance of HTT are regulated by different proteostatic mechanisms including chaperones, the UPS and autophagy-lysosome pathways (Wytenbach, Carmichael et al. 2000, Rubinsztein 2006, Li, Li et al. 2010, Vilchez, Saez et al. 2014).

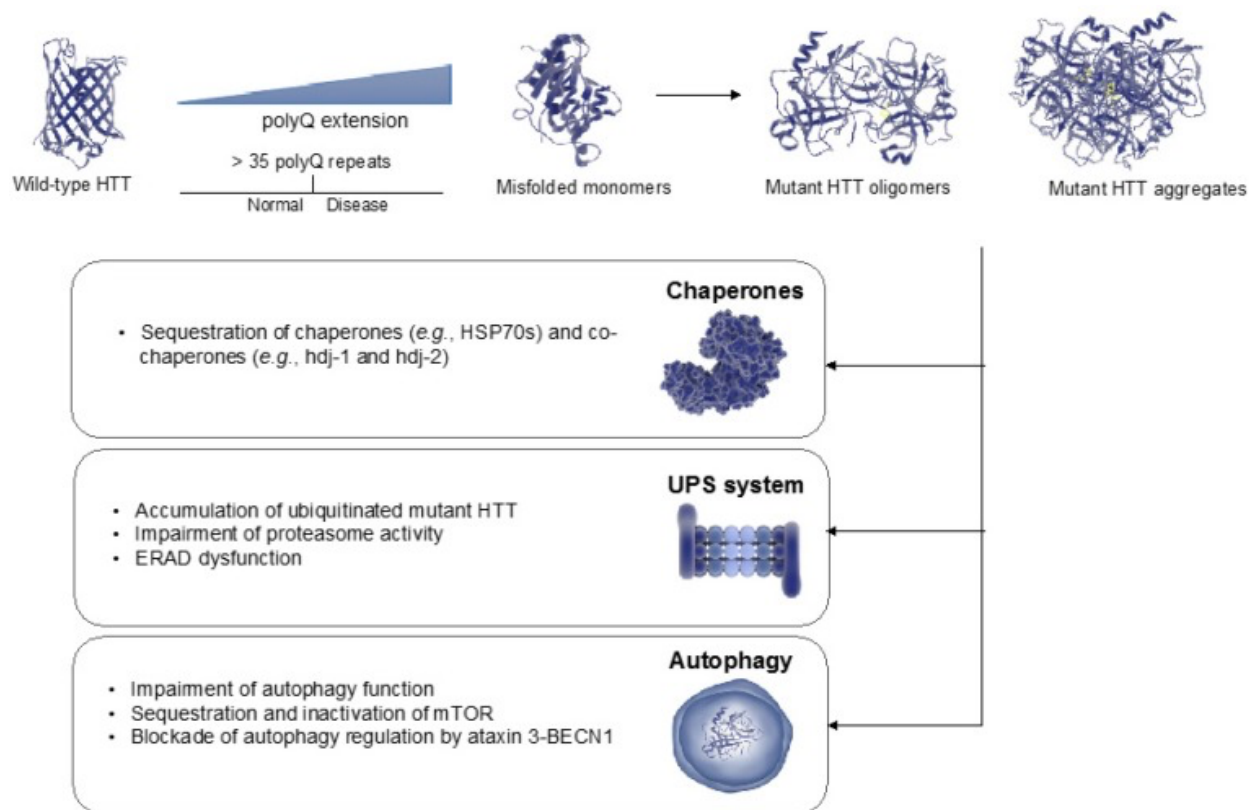


Figure III) The collapse in different proteostasis network upon accumulation of mHTT aggregation. The abnormal polyQ expansion in HTT protein leads its aggregation and also formation of toxic oligomers. The accumulation of polyQ-expanded aggregates and oligomers causes impairment in distinct proteostasis nodes such as the chaperome, the ubiquitin-proteasome system (UPS) and autophagy. Image reprinted from (Koyuncu, Fatima et al. 2017), with permission from Int J Mol Sci.

2.2) The chaperone node in Huntington's Disease

Protein quality control is crucial for maintaining a proper folding and conformation of newly- synthesized proteins. Moreover, cells must regulate the concentration and localization of proteins in response to cellular stimuli (Balch, Morimoto et al. 2008). Chaperones are key players in protein quality control system by assisting correct folding into the native conformation and assembly of newly synthesized proteins (Chen, Retzlaff et al. 2011). In addition to their folding activity, they also regulate proper translocation, aggregation and degradation of proteins (Hartl, Bracher et al. 2011, Cortez and Sim 2014). In humans, there are 88 chaperones and 244 co-chaperones forming a chaperome network (Brehme, Voisine et al. 2014). Chaperone families are classified according to their molecular weight and homology into several classes: 40 kilodalton heat shock proteins (HSP40s), HSP60, HSP70, HSP90, HSP100 and the small HSPs (sHSPs) (Li and Srivastava 2004). Each class includes multiple members which have equivalent functional domains and similar sequence identity. They are

mainly divided into two groups according to their source of energy required for their activity: ATP-dependent chaperones such as HSP90s and HSP100s, and ATP-independent chaperones such as small HSPs (Saibil 2013, Brehme, Voisine et al. 2014, Haslbeck and Vierling 2015). Chaperones prevent the formation of protein aggregation through preventing aberrant protein interactions (Balchin, Hayer-Hartl et al. 2016). Moreover, several co-chaperones such as CHIP, parkin, the BAG-domain-containing family (BAG1–BAG6) assist in the proteostatic roles of chaperones (Hartl and Hayer-Hartl 2002, Brehme, Voisine et al. 2014).

Recent studies have suggested that an impairment in chaperone function is associated with HD (Tam, Geller et al. 2006, Brehme, Voisine et al. 2014, Kakkar, Meister-Broekema et al. 2014, Labbadia and Morimoto 2015). Proteomic analyses have shown that mutant HTT (mHTT) interacts with members of the HSP90, HSP70, HSP40 (DNAJ chaperones) and TCP-1 ring complex (TRiC) chaperone families (Shirasaki, Greiner et al. 2012). Moreover, the reduction in HSP70 and HSP40 levels in HD mice brain tissues has also evidenced the essential role of chaperones in HD (Hay, Sathasivam et al. 2004, Yamanaka, Miyazaki et al. 2008). These data have suggested that expression of aggregate-prone mHTT may lead to impaired global disruption of the proteome through affecting the chaperome network. Furthermore, overexpression of HSP40s and HSP70s in multiple models of HD enhances suppression of mHTT toxicity and polyQ-mediated neurodegeneration (Warrick, Chan et al. 1999, Kazemi-Esfarjani and Benzer 2000, Muchowski and Wacker 2005). Multiple HSP40s and HSP70s co-chaperones are also determinant for polyQ-expanded aggregation and toxicity. The co-chaperones BAG1 and CHIP regulate mHTT aggregation through the interaction with HSP70s (Jana, Dikshit et al. 2005, Jana and Nukina 2005, Katsuno, Sang et al. 2005). HSP70 is upregulated in cerebellar neurons in HD but not in striatal neurons. This suggests that the differential induction of HSP70 could also contribute to the selective neurodegeneration in striatal neurons (Tagawa, Marubuchi et al. 2007). In addition, a mammalian cell- based screen of HSP70 and DNAJ chaperones in regulating polyglutamine aggregation indicated that a DNAJB subclass of molecular chaperones, such as DNAJB2a, DNAJB8, have an essential role in suppressing mHTT aggregation (Hageman, Rujano et al. 2010). Besides, the TRiC/CCT complex (T-complex protein-1 ring complex, also called CCT for chaperonin containing TCP1) has also a key role in the regulation of mHTT aggregation. Mutation or loss of a single subunits-mediated loss of function leads to the acceleration of mHTT deposition and disease-associated changes (Kitamura, Kubota et al. 2006, Tam, Geller et al. 2006, Brehme, Voisine et al. 2014). Conversely, overexpression of subunits of CCT complex leads to a reduction of mHTT aggregates and neurotoxicity (Kitamura, Kubota et al. 2006, Noormohammadi, Khodakarami

et al. 2016). Altogether, the chaperome network is an essential regulator of mutant HTT aggregation and toxicity. mHTT could cause decrease the levels of molecular chaperones which could lead to a proteostasis collapse and neurodegeneration (Cummings, Mancini et al. 1998, Perez, Paulson et al. 1998, Suhr, Senut et al. 2001).

2.3) The UPS in Huntington's Disease

As previously described in section 1.2.1, the UPS is necessary to maintain the proper proteome composition by determining the half-life of numerous proteins and also preventing the accumulation of damaged, misfolded and aggregated proteins (Powers, Morimoto et al. 2009). The importance of the UPS in the regulation of mHTT has been highlighted in several studies. Several mutations in components of UPS have been described in HD (van Leeuwen, de Kleijn et al. 1998). For example, mutant ubiquitin (UBB⁺¹) have been detected in inclusion bodies (IB) formed by mHTT (van Leeuwen, de Kleijn et al. 1998). Furthermore, upregulation of UPS-associated proteins in the striatum of HD mice R6/2 model is another important indicator for the requirement of the UPS in HD (Liu, Miller et al. 2007). Another study also proves that IB are disassembled in a proteasome-dependent manner in a conditional mouse model of HD (Yamamoto, Lucas et al. 2000). Co-staining of mutant HTT- aggregates with ubiquitin and proteasome subunits in human HD postmodern brains and in mouse models also points to a role of the proteasome in the regulation of mHTT (Mangiarini, Sathasivam et al. 1996, Davies, Turmaine et al. 1997, DiFiglia, Sapp et al. 1997). Moreover, pharmacological data indicates that inhibition of the proteasome by specific inhibitors increases aggregation of mHTT (Waelter, Boeddrich et al. 2001, McNaught, Perl et al. 2004).

One of the main features of HD is an impairment of the proteasome (Ciechanover and Brundin 2003). In transient cells transfected with mHTT fragments the UPS was inhibited, suggesting that mHTT- aggregation could directly impair UPS function (Bence, Sampat et al. 2001). Furthermore, a decline in the activity of the proteasome has been observed in both HD patients and HD mouse models (Finkbeiner and Mitra 2008). Incubation of ubiquitylated, aggregated mHtt with 26S proteasome results in the inhibition of the 26S proteasome in HD mouse model (Diaz-Hernandez, Valera et al. 2006).

Although several studies have suggested a proteasome impairment in HD, there are some contradictory results. In the mHtt-Q150 expressing neuronal cells, increased proteasome activity has been reported (Jana, Zemskov et al. 2001). Besides, one *in vitro* study in which they aimed to test whether 26S activity is affected by IBs, indicates that there is a no clear

effect of IB on 26S activity (Bennett, Bence et al. 2005). However, whether proteasome impairment is a consequence of IB or it is rather the triggering factor is unknown. These data suggest that a possible reason of the proteasome impairment may be due to a general proteostasis collapse in HD disease (Hipp, Patel et al. 2012). Remarkably, mHTT also affects endoplasmic reticulum-associated degradation (ERAD) which targets misfolded proteins of the endoplasmic reticulum for proteasomal degradation. Impairment in ERAD is caused by the sequestration of p97/Npl4/Ufd1 chaperone and mHTT could cause sequestration of this chaperone complex (Leitman, Ulrich Hartl et al. 2013).

On the other hand, enhanced proteasome machinery is also beneficial in HD disease models. Ectopic expression of PSMD11/RPN6 in a HD nematode model helps in the amelioration of the disease-related symptoms (Vilchez, Morantte et al. 2012). Overexpression of ubiquilin-1 delays Htt aggregate formation and extends lifespan in HD mice (Safren, El Ayadi et al. 2014). Moreover, overexpression of PA28 γ activator improves survival of neurons (Seo, Sonntag et al. 2007). Also, the overexpression of specific E3 ligases such as Hrd1, Parkin and CHIP improved the clearance of mHtt and reduced cell death (Tsai, Fishman et al. 2003, Jana, Dikshit et al. 2005, Yang, Zhong et al. 2007). Activation of proteasome with sulforaphane equally enhanced the elimination of mHtt in cells (Liu, Hettinger et al. 2014). Taken together, these studies evidence an important role of the UPS and suggest that an activation of the UPS could be an effective approach for the treatment of HD.

2.4) The Autophagy-Lysosome system in Huntington's Disease

Autophagy is a catabolic process that delivers cytosolic fractions, macromolecules such as long-lived proteins and organelles to the lysosomes for degradation (Rubinsztein, Gestwicki et al. 2007). Autophagy is classified into three different types; macroautophagy, microautophagy and chaperone mediated autophagy (Chen and Klionsky 2011). Macroautophagy is a clearance process which is characterized by the formation of a double-membrane structure vesicle called autophagosome. The autophagosomes fuse with lysosomes, which contain nucleotidases, lipases, hydrolases, glycosidases and proteases, and form autolysosomes (Rubinsztein, Gestwicki et al. 2007). After the degradation of the sequestered cellular material in autolysosomes, the degradation products are transported into the cytosol for their reuse (Chen and Klionsky 2011). In the chaperone-mediated autophagy (CMA), chaperone proteins such as HSP70 bind to specific client proteins and promote that these proteins are located to a complex surrounded by a lysosomal membrane. This complex is recognized by the lysosomal membrane proteins LAMP-2A and the targeted proteins are unfolded and degraded (Saftig,

Beertsen et al. 2008). In microautophagy, the cytosol is directly sequestered to the lysosomal membrane or vacuole (Li, Li et al. 2012). Although microautophagy is generally a non-selective process, it has been reported that certain organelles are selectively removed by microautophagy, as it is the case with micropexophagy (autophagy for peroxisomes) (Sakai, Koller et al. 1998).

Autophagy is involved in multiple cellular processes such as development, cell growth and cell death. Moreover, regulation and impairment in autophagy is associated with many neurodegenerative disease such as HD (Martinez-Vicente and Cuervo 2007, Glick, Barth et al. 2010). Impairment in autophagy hastens HD-associated phenotypes such as increase in vulnerability to cell death due to mHTT (Bjorkoy, Lamark et al. 2005). Conversely, activation of autophagy ameliorates proteotoxicity in HD (Ravikumar, Vacher et al. 2004, Sarkar, Perlstein et al. 2007). For instance, the mTOR inhibitor rapamycin activates autophagy in *Drosophila* and mouse models of HD and consequently ameliorates mHTT toxicity (Ravikumar, Vacher et al. 2004). Moreover, small molecules which activate autophagy promote the removal of mHTT in different HD models including yeast, fly and mammals (Sarkar, Perlstein et al. 2007).

On the other hand, different studies indicate that mHTT impairs autophagy formation. For example, the expression of Omi/HtrA2, a mitochondrial chaperone and protease which is important for the regulation of autophagy and mitophagy, is decreased in human HD striatum and cultured striatal neurons (Inagaki, Tagawa et al. 2008). Therefore, a reduction in the expression of autophagy-lysosome related proteins as well as in the autophagy flux could make neurons more vulnerable to mHTT. Moreover, HTT has a scaffolding role in selective autophagy. HTT interacts with p62, which is an autophagy receptor and involved in sequestration of cargos into autophagosomes. HTT also interacts with ULK1, a key regulator of autophagy (Rui, Xu et al. 2015). In HD, the scaffolding function of HTT in autophagy is impaired. Evidence based on human cells from HD patients and mouse models of HD have also suggested that there is an impairment in the recognition of the cytosolic cargo by autophagosomes in HD, possibly due to an interaction of mHTT with p62 (Martinez-Vicente, Tallochy et al. 2010). In conclusion, these results have shown the fundamental role of autophagy in HD either as a mechanism to regulate degradation of mHTT or an important biological process regulated by HTT.

2.5) Modeling Huntington's Disease in Pluripotent Stem Cells

Due to the multiple function of HTT in the cellular processes, the understanding of the mechanisms of HD pathologies should be based on multiple levels by using different approaches to recapitulate the disease. The knowledge about the progress and mechanism of

HD is based on the studies from model systems, including cellular and animal models (Vonsattel 2008, Carter and Chan 2012, Pouladi, Morton et al. 2013). Until recently, murine neuronal cells and transgenic animals were the primary models. However, the therapies which are helpful in these models have been not beneficial in human patients. One of the main problem about the rodent transgenic model for HD is the functional differences of human and rodent proteins (Kaye and Finkbeiner 2013). Secondly, the human brain is more complex than rodents and the development of the subventricular zones and cerebral cortex are significantly different (Dolmetsch and Geschwind 2011). Therefore, recapitulate the physiologically same phenomena in rodent models is complicated. Moreover, studies in human tissue have been also limited with blood samples, immortalized cell lines and fixed post-mortem tissues. Although they promote valuable information about the disease pathology and progress, these models also present limitations. For example, post-mortem tissues are vulnerable to DNA and RNA degradation. Immortalized cells have different biological characteristics than brain cells. Though blood samples give valuable information about variations in gene expression which may be used as biomarkers of disease, these changes are just one part of the disease pathology and progress (Borovecki, Lovrecic et al. 2005, Lovrecic, Kastrin et al. 2009).

Recent advances in the stem cell area and the discovery of reprogramming of fibroblasts into pluripotent cells which sharing many of the properties of embryonic stem cells open a new area to study the development and progression of human disease. These advances may also provide to identify potential drug targets and to investigate alternative cell sources for cell replacement therapy (Takahashi, Tanabe et al. 2007). Moreover, the possibility to differentiate these iPSCs into neurons open new doors for the investigation of the impact of mHTT. Currently, distinct stem cell systems are used for a better understanding of pathology and disease progress, including such as iPSCs, ESCs, as well as neural stem cells/neural progenitor cells (NSCs/NPCs) (Schwarz and Schwarz 2010, Maucksch, Vazey et al. 2013, Hargus, Ehrlich et al. 2014).

ESCs are capable to self-renew and they can be used to study the pathology and progress of HD *in vitro* (Ben-David, Kopper et al. 2012). Some of the HD lines are established from donated embryos which have 40-51 polyQ repeats in HTT (Verlinsky, Strelchenko et al. 2005, Glick, Barth et al. 2010, Bradley, Scott et al. 2011). Established ESCs lines are able to differentiate into terminally differentiated neurons carrying mHTT (Niclis, Trounson et al. 2009, Bradley, Scott et al. 2011). However, these HD-ESCs and their differentiated counterparts have not revealed HD-related phenotypes (Kaye and Finkbeiner 2013). On the other hand, murine HD-ESCs can show HD-related phenotypes. The established murine HD-

ESCs have either 150 or 77 polyglutamine repeats in HTT and have similar neural proliferative characteristics with human subventricular zone cells in HD brains (Kaye and Finkbeiner 2013). The transcriptional profiling of murine HD-ESCs exhibit changes in gene expression of pathways involved in regulating axonal growth and neuronal differentiation, processes also observed in HD patients' brains (Cha 2007). These results reveal that murine ESCs can recapitulate key aspects of HD. On the other hand, iPSC derived from HD patients may be used as invaluable source for studying HD and identification of novel therapeutic approaches without the ethical limitations posed by ESCs. The first HD iPSCs were derived from patients with 54 expansion of CAG and 72 CAG in *HTT* by reprogramming from fibroblast using retroviral induction with a combination of four pluripotency factors: Oct4, Sox2, Klf4 and cMyc (Park, Arora et al. 2008). Recently, the generation and characterization of 14 different iPSCs lines from somatic cells of HD patients and control individuals have been reported by the HD iPSC Consortium (Consortium 2012). Notably, studies have suggested that HD iPSCs reveal HD-related phenotypes such as the impairment in mitochondrial function, signaling by brain-derived neurotrophic factor (BDNF), and caspase activity (Consortium 2012, Hargus, Ehrlich et al. 2014). Furthermore, neurons derived from HD-iPSCs are more vulnerable to oxidative stress, cellular excitotoxic factors and deprivation of growth factors. They have also increased caspase activity and basal lysosomal activity (Consortium 2012, Hargus, Ehrlich et al. 2014). Finally, transcriptome analysis of NPCs derived from iPSCs reveals that 1,601 genes were differentially regulated in HD-NPCs compared with control NPCs (Consortium 2012). Besides, pathways involved in cell cycle regulation, proliferation, axonal guidance and cell signaling are dysregulated in NPCs derived from HD-iPSC (Consortium 2012).

Taken together, modeling HD using pluripotent stem cells, especially iPSCs derived from HD patients, holds great promise for understanding the progress and pathology of HD. Research in HD-iPSCs and derived neurons may fill the gaps in knowledge from the rodent models. In addition, they are an invaluable source for drug screening to uncover potential novel therapies.

2) OBJECTIVES AND RATIONALITIES

Maintenance of cellular homeostasis is essential for controlling the aging process and it is determined by several mechanisms including proteostasis. Proteostasis is required for organismal development and function (Carmona and Michan 2016). Accumulation of damaged proteins or aggregates by a demise in proteostasis can disrupt cellular function and cause cell malfunction (Taylor and Dillin 2011). Moreover, the decline in proteostasis has been associated with multiple age-related diseases such as HD (Labbadia and Morimoto 2015). Recent studies have also suggested that proteostasis is required to maintain the function and identity of embryonic and many of adult stem cells (Moreno-Gonzalez and Soto 2011, Taylor and Dillin 2011). A decline in proteostasis is considered a hallmark of aging (Lopez-Otin, Blasco et al. 2013). Strikingly, hESCs are immortal and replicate in the absence of senescence (Buckley, Aranda-Orgilles et al. 2012, Lopez-Otin, Blasco et al. 2013). It has been shown that hESCs have high proteasome activity compared with their differentiated counterparts (Vilchez, Boyer et al. 2012). In addition, it has been uncovered that PSMD11/Rpn-6, a key proteasome subunit, is required for stem cell identity as well as regulation of longevity and healthspan in *C. elegans*. Furthermore, FOXO4 modulates proteasome activity and is required for pluripotency through the regulation of PSDM11 expression in hESCs (Vilchez, Boyer et al. 2012, Vilchez, Morante et al. 2012). These studies highlight the importance of the proteasome for both hESCs and aging. However, the mechanism(s) by which proteasome activity regulates hESC function remains unknown. Therefore, we proposed that understanding the regulation of the proteostasis network for self-renewal and identity of hESCs may provide valuable information for better understanding of hESC identity and aging process. For this purpose, we first aimed to define which E3 ubiquitin ligases are essential for pluripotency and differentiation capacity of hESCs. Our proteomics data have shown that 35 E3 enzymes are upregulated in hESC compared with their differentiated counterparts. Then, we focused on several of these enzymes after validation of our proteomics data by western blot. Among these up-regulated E3 ligases, there are HECT-domain E3 ligases such as HERC2 and UBE3A and RING-domain E3 ligases such as UBR7 and RNF181. We then sought to define possible substrates of these E3 ligases which could have a role in stemness and differentiation capacity of hESCs. Moreover, we also manipulated proteasome activity in hESCs to assess possible endogenous targets of the proteasome in these cells. Our systemic characterization of interactome of these E3 ligases suggests a link with hESCs identity. Moreover, the loss of function experiment for these E3 ligases reveals significant change in transcriptome and proteome level of hESCs. However, the loss of these

E3 ligases do not alter pluripotency or differentiation capacity of hESCs. On the contrary, we show that global proteasome inhibition impairs diverse biological processes required for hESCs identity, including telomere maintenance, protein synthesis, rRNA maturation and glycolytic metabolism. Thus, our data suggest that enhanced proteasome activity is linked with other determinant processes of hESCs identity.

In the second part of this study, our goal was to understand how enhanced proteasome activity determines the proteostasis of mHTT in pluripotent stem cells by specifically focusing on the intrinsic E3 ubiquitin ligase network. The decline in folding capacity and clearance of proteins is associated with the onset of age-related neurodegenerative disease such as HD (Lopez-Otin, Blasco et al. 2013). HD is an autosomal neurodegenerative disorder caused by expansion in CAG in *HTT*. This abnormal expansion of polyQ repeats in HTT protein causes its aggregation and neurodegeneration (Bates 2003). The onset of the disease is related to expansion number and patients affected by HD contains mHTT with greater than 35 polyQ repeats (Ross and Tabrizi 2011). Although the loss of normal HTT function could be a determinant in the pathology and progress of the disease, it has been shown that the gain of function of mHTT is toxic and causes neurodegeneration (Saudou and Humbert 2016). Interestingly, the length of pathological polyQ does not influence pluripotency, survival, and self-renewal of HD-iPSCs (Consortium 2012). Besides, HD-iPSCs do not exhibit accumulation of polyQ-expanded aggregates (Consortium 2012, Jeon, Lee et al. 2012, Noormohammadi, Khodakarami et al. 2016). Strikingly, during cell reprogramming from somatic cells to iPSCs, the proteostasis network is rewired and they acquire high levels of proteasome activity similar to hESCs (Vilchez, Boyer et al. 2012, Noormohammadi, Khodakarami et al. 2016, Noormohammadi, Calculli et al. 2018). These results suggest that iPSCs have enhanced mechanisms to maintain proteostasis of mHTT. Although several studies revealed a strong link between proteasomal impairment and HD, the underlying mechanisms by which proteasome regulates polyQ-expanded HTT are poorly understood (Koyuncu, Fatima et al. 2017). Therefore, in this study, we wanted to answer whether these cells have an intrinsic E3 ubiquitin ligase network to regulate proteostasis of mHTT. We observed that proteasome activity regulates HTT levels and prevents the accumulation of polyQ-expanded aggregates in HD-iPSCs. Remarkably, iPSCs have enhanced levels of the E3 ubiquitin ligase UBR5. We found that UBR5 interacts with HTT and modulates the degradation of both mutant and wild-type HTT protein levels. Besides, the knockdown of UBR5 leads to accumulation of HTT protein as well as polyQ-expanded aggregates in HD-iPSCs. Interestingly, the loss of the orthologue of UBR5 hastens polyQ-expanded aggregation and neurotoxicity in a *C. elegans* model of HD.

Moreover, we also observed that ectopic expression of UBR5 induces polyubiquitination and degradation of mHTT, decreasing mHTT aggregates in HD cell models. Furthermore, increased UBR5 expression determines global proteostasis of iPSCs preventing the aggregation of misfolded proteins ensued from normal metabolism. Therefore, we suggested that UBR5 is a novel regulator of super-vigilant proteostasis of iPSCs.

3) PUBLICATIONS

1) I. Saez^{*}, **S. Koyuncu**^{*}, R. Gutierrez-Garcia, C. Dieterich and D. Vilchez (2018). Insights into the ubiquitin-proteasome system of human embryonic stem cells. *Scientific Reports* 8: 4092.

2) **Koyuncu, S^{*}**, Saez, I^{*}, Lee, H.J., Gutierrez Garcia, Pokrzywa, W., Fatima, A., Hoppe, T. and Vilchez, D. (2018) The ubiquitin ligase UBR5 suppresses proteostasis collapse in pluripotent stem cells from Huntington's disease patients. *Nat. Commun.*, 9, 2886.

3) A. Noormohammadi, A. Khodokarami, R. Gutierrez-Garcia, H.J. Lee, **S. Koyuncu**, T. Konig, C. Schindler, I. Saez, A. Fatima, C. Dieterich and **D. Vilchez** (2016). Somatic increase of CCT8 mimics proteostasis of human pluripotent stem cells and extends *C. elegans* lifespan. *Nature Communications* 7: 13649.

SCIENTIFIC REPORTS

OPEN

Insights into the ubiquitin-proteasome system of human embryonic stem cells

Isabel Saez¹, Seda Koyuncu¹, Ricardo Gutierrez-Garcia¹, Christoph Dieterich² & David Vilchez¹ 

Human embryonic stem cells (hESCs) exhibit high levels of proteasome activity, an intrinsic characteristic required for their self-renewal, pluripotency and differentiation. However, the mechanisms by which enhanced proteasome activity maintains hESC identity are only partially understood. Besides its essential role for the ability of hESCs to suppress misfolded protein aggregation, we hypothesize that enhanced proteasome activity could also be important to degrade endogenous regulatory factors. Since E3 ubiquitin ligases are responsible for substrate selection, we first define which E3 enzymes are increased in hESCs compared with their differentiated counterparts. Among them, we find HECT-domain E3 ligases such as HERC2 and UBE3A as well as several RING-domain E3s, including UBR7 and RNF181. Systematic characterization of their interactome suggests a link with hESC identity. Moreover, loss of distinct up-regulated E3s triggers significant changes at the transcriptome and proteome level of hESCs. However, these alterations do not dysregulate pluripotency markers and differentiation ability. On the contrary, global proteasome inhibition impairs diverse processes required for hESC identity, including protein synthesis, rRNA maturation, telomere maintenance and glycolytic metabolism. Thus, our data indicate that high proteasome activity is coupled with other determinant biological processes of hESC identity.

Pluripotent stem cells can replicate indefinitely in an undifferentiated state while retaining their potential to differentiate into all cell lineages^{1,2}. Embryonic stem cells (ESCs) derived from blastocysts are the gold standard of pluripotency. Moreover, somatic cells can be reprogrammed into induced pluripotent stem cells (iPSCs) that share similar characteristics with ESCs^{3,4}. Given their intrinsic abilities, pluripotent stem cells represent an invaluable resource to investigate development and disease, holding great promise for regenerative medicine. As the origin of multicellular organisms, a series of regulatory and quality control mechanisms must operate at high fidelity in these cells⁵. As such, protein homeostasis (proteostasis) is central for self-renewal, pluripotency and cell fate decisions^{6–9}.

A key node of the proteostasis network is the ubiquitin proteasome system (UPS), the major selective proteolytic mechanism in eukaryotic cells^{10,11}. Notably, human ESCs (hESCs) and iPSCs have increased proteasome activity compared with their differentiated counterparts¹². This enhanced activity is induced by PSMD11/RPN6¹³, a scaffolding subunit that promotes proteasome assembly¹⁴. Besides PSMD11, other proteasome regulators (*e.g.*, Psmd14, POMP) are up-regulated in mouse and human pluripotent stem cells^{6,15,16}. Conversely, a mild down-regulation of proteasome activity induces a demise of hESC identity, characterized by decreased mRNA and protein levels of pluripotency markers^{13,15,17}. Concomitantly, pluripotent stem cells with reduced proteasome activity lose their ability to differentiate into neural cells while expressing high levels of markers of endoderm, mesoderm and fibroblast differentiation¹³.

These findings raise the intriguing question of why ESC function needs enhanced proteasome activity. The proteasome terminates damaged, misfolded and aggregated proteins ensued from stress conditions and misfolding-prone mutations^{11,18}. The accumulation of damaged proteins could alter the immortality of pluripotent stem cells⁵. Notably, growing evidence indicates that increased proteasome activity prevents the aggregation

¹Institute for Genetics and Cologne Excellence Cluster for Cellular Stress Responses in Aging-Associated Diseases (CECAD), University of Cologne, Joseph-Stelzmann-Strasse 26, 50931, Cologne, Germany. ²Department of Internal Medicine III and Klaus Tschira Institute for Computational Cardiology, Section of Bioinformatics and Systems Cardiology, Neuenheimer Feld 669, University Hospital, 69120, Heidelberg, Germany. Isabel Saez and Seda Koyuncu contributed equally to this work. Correspondence and requests for materials should be addressed to D.V. (email: dvilchez@uni-koeln.de)

of damaged proteins such as mutant huntingtin, which underlies Huntington's disease^{9,12,13,19}. Moreover, the passage of altered proteins to progenitor cells could compromise organismal development and aging. In this regard, enhanced proteasome activity participates in the degradation of damaged proteins in the early steps of mouse ESC differentiation, a key step to generate daughter cells with an intact proteome^{20,21}.

The UPS also modulates half-life of a myriad of regulatory proteins^{22,23}, in a dynamic process adjusted to the specific requirements of a particular cell type and status^{24,25}. Since the differentiation process triggers numerous changes in the cellular proteome, the UPS determines successful organismal development⁵. In these lines, the proteasome modulates the abundance of key pluripotency factors such as OCT4 or NANOG^{26–29}. A chain of at least four 48-linked ubiquitins is the primary signal for recognition and degradation by the proteasome^{30,31}. E3 ligases transfer ubiquitin to a target protein, providing specificity to the proteolytic process. Accordingly, over 600 E3 ubiquitin ligases have been identified in humans so far. To prevent proteolysis, deubiquitinating enzymes (DUBs) perform the opposite action. Thus, both E3 and DUBs must operate in a balanced manner to maintain hESC function or activate differentiation^{26,27}. Remarkably, the levels of distinct E3 and DUB enzymes undergo dramatic changes during differentiation of mouse ESCs and cell reprogramming^{6,9}. Recent studies have revealed that distinct proteins with DUB activity such as USP22^{32,33}, USP44^{34,35} or the proteasome component Psmd14⁶ regulate the levels of core pluripotency transcription factors. Likewise, specific E3 enzymes modulate pluripotency and differentiation²⁹. For instance, Huwe1 polyubiquitinates the pluripotency transcription factor N-myc, promoting its degradation by the proteasome and allowing for neural differentiation of mouse ESCs³⁶.

To obtain further insights into the mechanisms by which increased proteasome activity sustain hESC identity, here we determine the interactome of highly-expressed E3 ligases in these cells (*i.e.*, HERC2, UBE3A or RNF181). Moreover, we perform loss-of-function experiments of these E3s enzymes to examine their impact on hESC identity. Besides its role in the regulation of damaged proteins and endogenous substrates, increased proteasome activity could also be coupled to intrinsic characteristics of pluripotent stem cells. For instance, ESC and iPSCs exhibit up-regulated global translational rates³⁷. To assess this hypothesis, we define the alterations induced by proteasome dysregulation using a shot label-free proteomic approach. Notably, we find changes in key biological processes of hESC identity such as RNA biogenesis, protein synthesis and telomere function, establishing the proteasome as a central regulator of hESCs.

Results

The levels of specific E3 enzymes decrease during differentiation. To obtain insights into the role of the UPS in hESC function, we examined changes in the expression of E3 ubiquitin ligases and DUBs during differentiation. For this purpose, we analysed available proteomics data comparing hESCs with their differentiated neuronal counterparts⁹ (Supplementary Data 1). We identified 31 DUBs in both hESCs and neurons. Among them, 10 were upregulated and 15 were downregulated during differentiation into neurons. We found that 44 out of 99 identified E3 enzymes increase during neuronal differentiation. In contrast, 35 E3 enzymes were decreased during differentiation into neurons (Supplementary Data 1 and Supplementary Table 1). To identify potential substrates of the UPS in hESCs, we further examined their up-regulated E3 ubiquitin ligases. Our approach was supported by the fact that three of these E3 enzymes were previously reported as regulators of ESC identity (*i.e.*, HUWE1³⁶, TRIM33³⁸ and RNF40)³⁴.

Among the 35 E3 enzymes significantly increased in hESCs, we found 6 ubiquitin ligases with HECT domain while the other E3 enzymes belonged to the RING-domain family³⁹ (Supplementary Table 1). To validate these proteomics data, we performed western blot analysis of representative E3s of both families comparing hESCs with their neural progenitor cell (NPC) and neuronal counterparts. As a control, we also examined the levels of STUB1, an E3 enzyme which slightly increased during neuronal differentiation (Fig. 1a and Supplementary Data 1). At early neural stages, we already observed a downregulation in HECTD1, HERC2, HUWE1, UBE3A, KCMF1, RNF40, RNF181 and UBR7 levels (Fig. 1a). We corroborated the downregulation of distinct E3 ligases during neural differentiation in an independent hESC line (Supplementary Fig. 1). Moreover, these E3 enzymes were also decreased in terminally differentiated neurons validating our proteomics analysis (Fig. 1a and Supplementary Table 1). However, we could not confirm a decrease of TRIM33 levels during neurogenesis as we obtained inconsistent results among independent differentiation experiments (Fig. 1a and Supplementary Fig. 2).

The downregulation in the protein amount of the E3 ubiquitin ligases did not correlate with a reduction in their mRNA levels during neuronal differentiation (Fig. 1b), suggesting a post transcriptional or post-translational regulation of these enzymes. Since multiple E3 ligases are regulated by autoubiquitination rates⁴⁰, decreased levels of E3s may also indicate their potential activation during differentiation. In hESCs, proteasome inhibition did not result in higher levels of the tested E3 enzymes (Supplementary Fig. 3a). Most importantly, proteasome inhibition did not up-regulate the levels of these E3 enzymes in neurons (Supplementary Fig. 3b). Thus, these data discard a faster turnover of our target E3 enzymes in differentiated cells induced by higher autoubiquitination activity.

With the exception of RNF40, the protein levels of most of our target E3 enzymes were also decreased with differentiation into endoderm, indicating that this is not a specific phenomenon associated with the neural lineage (Fig. 1c). Among them, HECTD1, HERC2, HUWE1, UBE3A, RNF181 and TRIM33 were dramatically downregulated while KCMF1 and UBR7 were reduced to a lesser extent (Fig. 1c). In contrast to neuronal differentiation, we also observed a downregulation at the mRNA level (Fig. 1d). Moreover, the gene expression of many of these E3 enzymes (*e.g.*, HECTD1, HERC2, KCMF1) was also downregulated when hESCs differentiated into mesodermal lineages (Fig. 1e). Overall, our results indicate that specific E3 enzymes such as HERC2, UBE3A and RNF181 are highly abundant in hESCs and decrease during differentiation.

HECTD1 interacts with regulators of WNT signaling and glycolysis. To examine the role of up-regulated E3 enzymes in hESCs, we characterized their interactome. For this purpose, we performed co-immunoprecipitation experiments from hESCs followed by a single shot label-free proteomic approach. Our

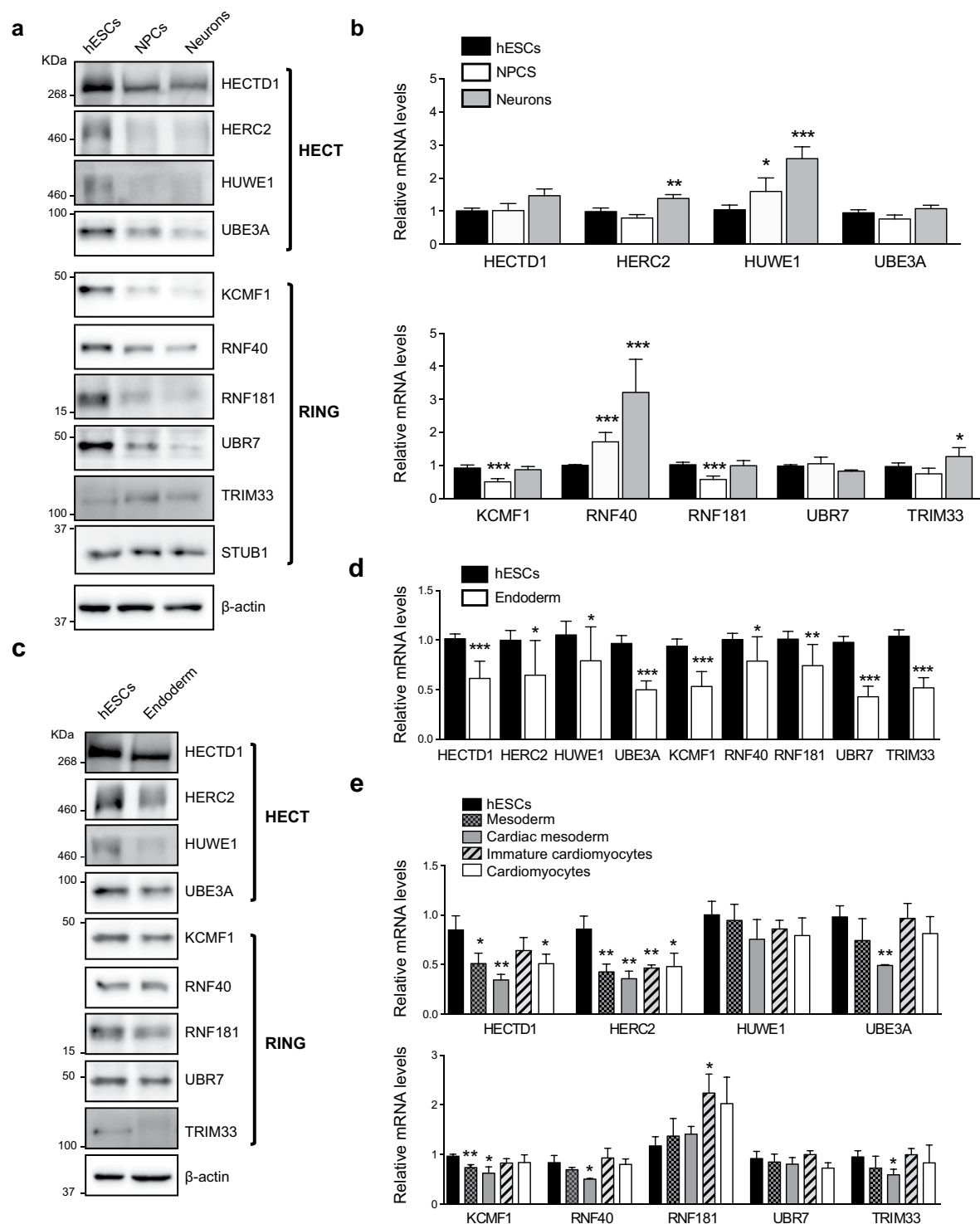


Figure 1. The levels of distinct E3 ubiquitin ligases decrease during differentiation. (a) Western blot analysis of H9 hESCs compared with their neural and neuronal counterparts (*i.e.*, neural precursor cells (NPCs) and terminally differentiated neurons, respectively) with antibodies against distinct E3 ubiquitin ligases. β -actin is the loading control. E3 enzymes are shown following their classification into HECT and RING-domain families. The images are representative of at least two independent experiments. (b) Quantitative PCR (qPCR) of E3 ubiquitin ligases mRNA levels. Graphs represent the mean \pm s.e.m. (relative expression to H9 hESCs) of three independent cells. (c) Western blot analysis of E3 ubiquitin ligases comparing H9 hESCs with their differentiated endoderm precursors counterparts. β -actin is the loading control. The images are representative of two independent experiments. All cropped blots were run under the same experimental conditions. Uncropped versions of western blots are presented in Supplementary Fig. 13. (d) qPCR analysis of E3 ubiquitin ligases transcript levels upon definitive endodermal differentiation of H9 hESCs. Graphs represent the mean \pm s.e.m. (relative expression to H9 hESCs) of four independent cells. (e) mRNA levels of E3 enzymes in H1 hESCs and their differentiated

mesoderm and cardiomyocyte counterparts. qPCR data represents the mean \pm s.e.m. of three independent experiments. All the statistical comparisons were made by Student's t-test for unpaired samples. P-value: * ($P < 0.05$), ** ($P < 0.01$), *** ($P < 0.001$).

first target was HECTD1, a HECT E3 ubiquitin ligase involved in the negative regulation of β -catenin (CTNNB1). β -catenin is the main effector of WNT signaling⁴¹, one of the regulatory nodes of ESC pluripotency and neural differentiation^{42,43}. We successfully immunoprecipitated significant levels of endogenous HECTD1 (Fig. 2a and Supplementary Fig. 4). Notably, interactome analysis indicated that HECTD1 binds β -catenin and GSK3B, a negative regulator of WNT signaling (Fig. 2b–c and Supplementary Data 2). We also found a strong interaction with subunits of the pyruvate dehydrogenase complex (PDC) (*i.e.*, DLAT, PDHA1, PDHB, PDHX) (Fig. 2b–c). PDC catalyses the mitochondrial conversion of pyruvate into acetyl-CoA, which will be further metabolized through the tricarboxylic acid cycle and electron chain⁴⁴. The metabolism of ESCs relies on glycolysis rather than mitochondrial respiration for energy production, a process achieved through an inactive PDC complex⁴⁵. Thus, HECTD1 could participate in maintaining the glycolytic state of hESCs via modulation of PDC activity. In these lines, gene ontology biological process (GOBP) term analysis of the HECTD1 interactome indicated the strongest enrichment for proteins involved in the regulation of Acetyl-CoA biosynthetic process (Fig. 2d and Supplementary Data 2). Interestingly, SIN3A, a transcriptional regulatory protein required for both survival and pluripotency of ESCs^{46,47}, also strongly interacted with HECTD1 (Fig. 2b–c), providing an additional putative link between HECTD1 and ESC function.

To determine whether HECTD1 binds these proteins specifically in hESCs, we performed co-immunoprecipitation experiments from NPCs and neurons. Among the 63 HECTD1 interactors identified in hESCs, 39.7% and 28.6% were also significant interactors in NPCs and neurons, respectively (Fig. 2e and Supplementary Data 3). These common interactors included GSK3B, PDC subunits (*i.e.*, DLAT, PDHA1, PDHB, PDHX) and SIN3A in the three cell types tested. Thus, cell-type differences in HECTD1 abundance or activity could determine its regulatory impact on distinct pathways such as WNT signaling or Acetyl-CoA biosynthetic process. Our data also indicate a high percentage of specific interactions of HECTD1 depending on the cell type. Remarkably, 34 proteins interacted with HECTD1 in hESCs while we did not find a significant interaction in NPCs or neurons (Supplementary Data 3). Among these specific interactors, we found β -catenin as well as several regulators of cell cycle and proliferation (*e.g.*, BIRC6, CCNK, CDH1, DDX41, PRPF40A, SRPK2, TAF1), providing a potential link of HECTD1 with the high division rates of these cells. We also identified a hESC-specific interaction of HECTD1 with AURKB, a regulator of telomerase activity in ESCs⁴⁸. Moreover, HECTD1 specifically interacted in hESCs with proteins involved in gastrulation (*i.e.*, DLD⁴⁹) and embryonic cell differentiation (*e.g.*, PAXBP1⁵⁰, SRGAP2⁵¹ and THOC6⁵²). Thus, our data suggest that cell-specific interactions can also determine endogenous roles of up-regulated E3 enzymes in hESCs.

Knockout of HERC2 alters the transcriptome of hESCs. HERC2 is one of the most up-regulated E3 enzymes in hESCs when compared with their differentiated counterparts (Fig. 1a,c). HERC2 belongs to the HERC gene family, that contains a HECT domain and at least one RCC1-like domain (RLD). HERC2 interacts with chromatin via the RLD domain and participates in DNA repair, DNA replication as well as checkpoint control⁵³. As such, HERC2 is located in a chromosomal region associated with neurodevelopmental disorders, including Prader-Willi and Angelman syndromes⁵⁴. We immunoprecipitated endogenous HERC2 in hESCs (Fig. 3a and Supplementary Fig. 4) and identified 113 potential interactors (Supplementary Data 4). The three strongest interacting partners were SEC23IP, SRGAP2 and NEURL4 (Supplementary Fig. 5a), which are linked to development^{51,55,56}. These proteins are already reported to interact with HERC2 in human cell lines, validating our data⁵⁷. In differentiated cells, HERC2 has also been reported to interact with UBE3A, the primary E3 involved in Angelman syndrome⁵⁸. Moreover, HERC2 has been recently associated with the kinase LRRK2, which plays a role in the familial Parkinson's disease⁵⁹. However, we did not observe these interactions in our proteomic data from hESCs, suggesting cell-type differences. On the other hand, the HERC2 interactome was strongly enriched for RNA-binding proteins (Supplementary Data 4). In addition, the most enriched GOBP pathways were related with RNA metabolism (Supplementary Fig. 5b and Supplementary Data 4). The high enrichment for pathways involved in RNA metabolism could indicate indirect interactions mediated by RNA and, therefore, ensuing from immunoprecipitation of RNA-protein complexes rather than direct protein-protein interactions⁶⁰. To assess whether HERC2 directly interacted with these RBPs, we repeated the interactome analysis treating the samples with RNase A prior to immunoprecipitation with HERC2 antibody⁶⁰. Whereas the interactions with SEC23IP, SRGAP2 and NEURL4 remained upon RNase treatment, the number of total significant interactors was reduced to 33 proteins (Fig. 3b and Supplementary Data 5). We found a significant interaction with centrosomal proteins (*i.e.*, CENPF, CEP97) as well as RNA-binding proteins such as translation factors (*i.e.*, EIF3A, EIF3C) and the helicase DDX20 (Supplementary Data 5). However, most of the interactions with RNA-binding proteins were lost upon RNase treatment. Moreover, GOBP analysis did not show an enrichment of RNA-related processes among these proteins (Fig. 3c and Supplementary Data 5). These data suggest that the previously identified RNA-binding proteins were immunoprecipitated due to secondary, RNA-mediated interactions.

With the high levels of HERC2 in hESCs and the role of one of its main interactors, SRGAP2, in neurogenesis and spine maturation⁶¹, we asked whether HERC2 regulates hESC function or differentiation. For this purpose, we generated a knockout hESC line by CRISPR/Cas9 genome editing (*HERC2*^{-/-}) and performed transcriptome analysis. We found 1494 transcripts significantly changed in *HERC2*^{-/-} hESCs (Supplementary Data 6). Interestingly, GOBP analysis indicated strong enrichment for genes involved in the regulation of dendritic spine maintenance and regulation of glial cell proliferation (Fig. 3d and Supplementary Data 6). We also found an

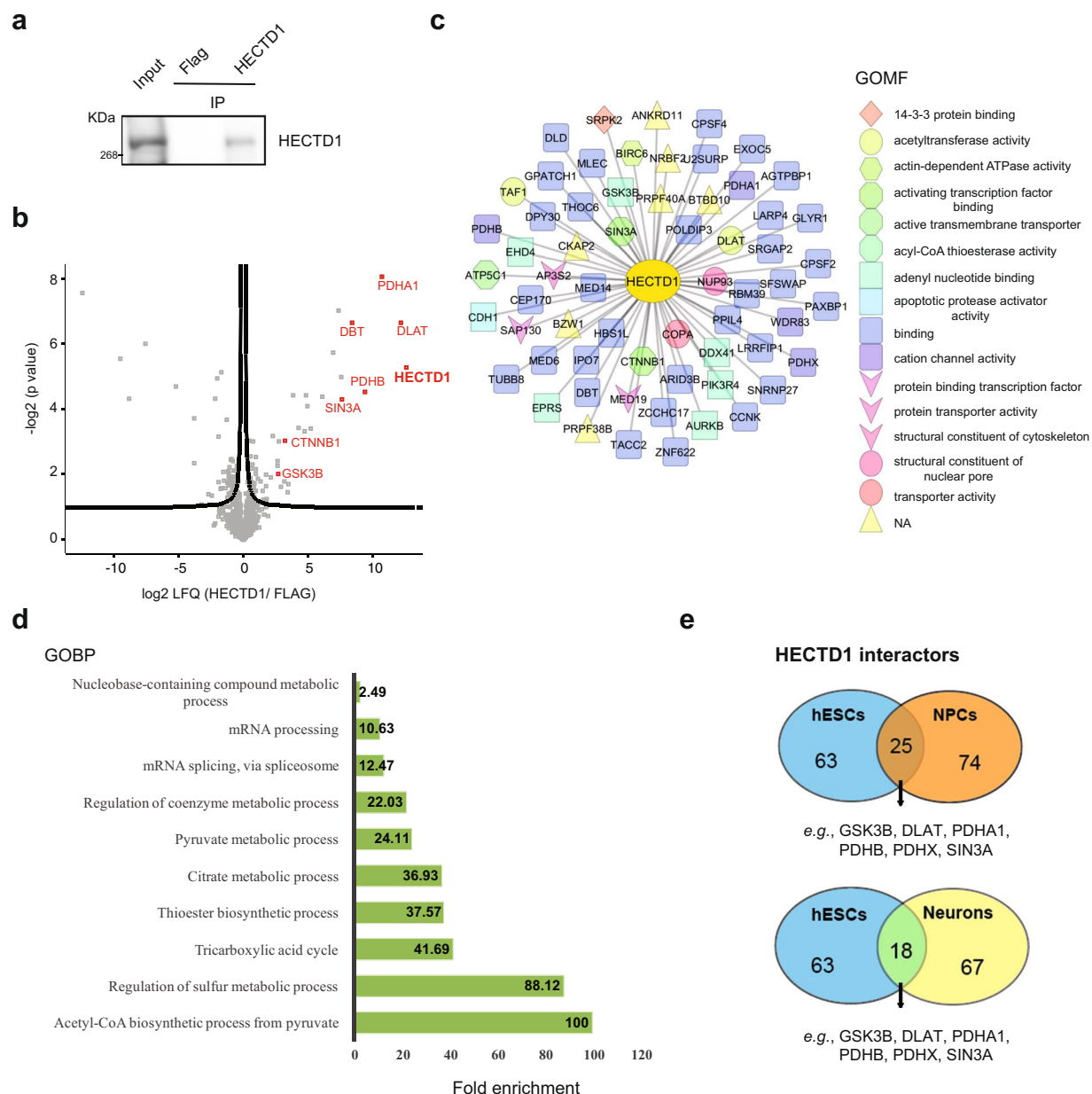


Figure 2. HECTD1 interacts with regulators of WNT signaling and glycolysis. **(a)** Co-immunoprecipitation (co-IP) with HECTD1 and FLAG antibodies in H9 hESCs followed by western blot against HECTD1. We loaded 13.3% of total input and 20% of total immunoprecipitated sample. The images are representative of three independent experiments. All cropped blots were run under the same experimental conditions. The original blots are included in Supplementary Fig. 13. **(b)** Volcano plot of the interactome of HECTD1 in H9 hESCs ($n = 4$). Graph represents the $-\log(p\text{-value})$ of a two-tailed t -test plotted against the \log_2 ratio of protein label-free quantification (LFQ) values from co-IP experiments with HECTD1 antibody compared to control co-IP with FLAG antibody. Red colored dots beyond the curved lines indicate some of the most enriched interacting proteins after correction for multiple testing (False Discovery Rate (FDR) adjusted p -value (q -value) < 0.2 , $s_0 = 0.1$). **(c)** Scheme indicating the Gene Ontology Molecular Function (GOMF) of HECTD1 interactors (Analysis tool: Cytoscape 3.6.0)¹³⁷. **(d)** Bar graph representing the top GOBPs of HECTD1 interactome ($P < 0.05$) (Analysis tool: PANTHER¹³⁸ and Gene Ontology Consortium). **(e)** Venn diagram represents total number and common significant interactors in hESCs, NPCs and neurons (FDR < 0.2 was considered significant, hESCs ($n = 4$), NPCs ($n = 3$) and neurons ($n = 3$)).

alteration in regulators of other developmental process, including nephron and placenta morphogenesis (Fig. 3d). Prompted by these findings, we examined whether these changes in the transcriptome impaired the levels of pluripotency markers. However, *HERC2*^{-/-} hESCs did not exhibit alterations in the levels of pluripotency markers when compared to control hESCs (Fig. 3e–g), indicating that the sole deletion of *HERC2* does not majorly impact on hESCs function. In addition, we did not find an increase in the expression of markers of the distinct

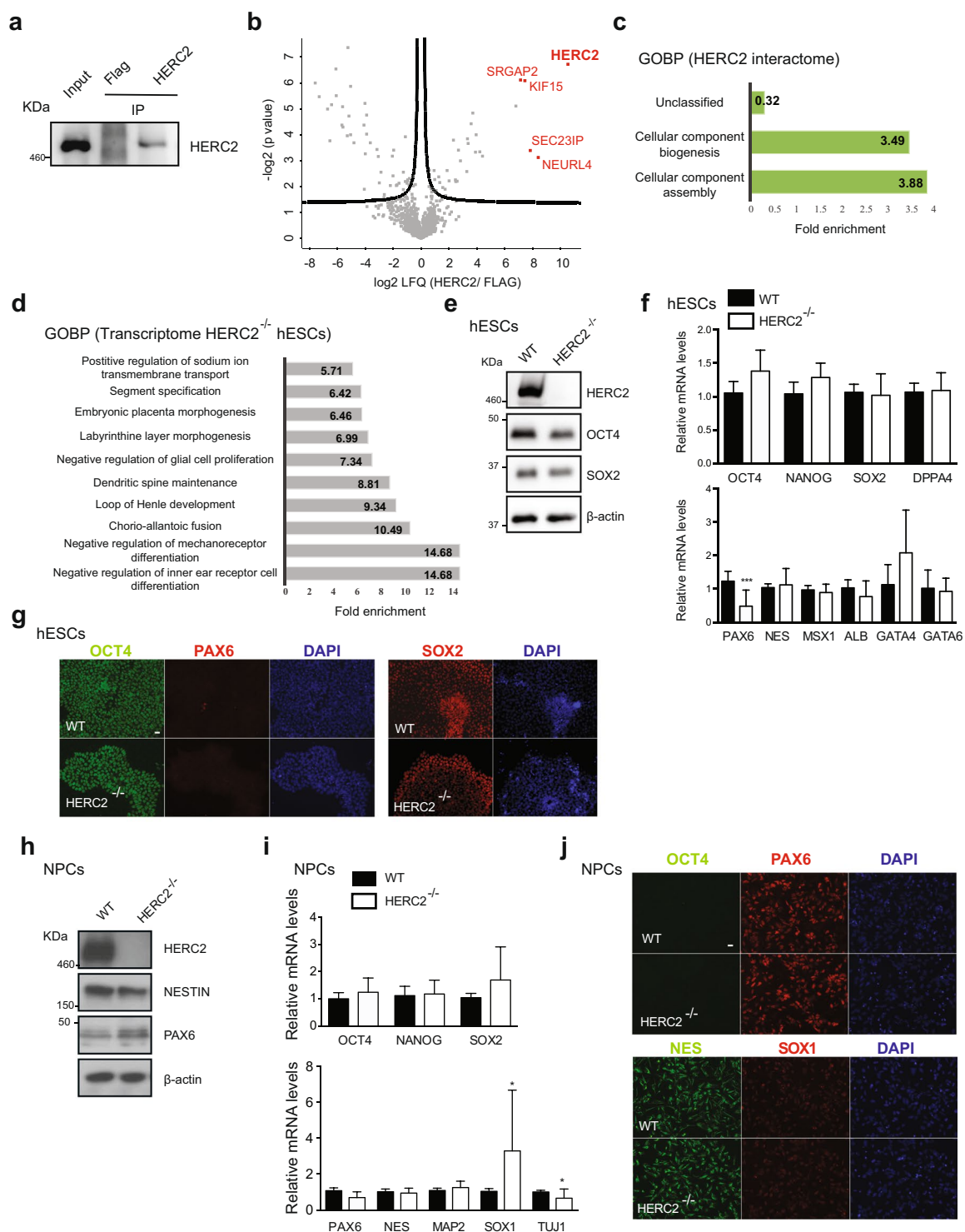


Figure 3. Knockout of HERC2 does not impair neural differentiation of hESCs. **(a)** co-IP with HERC2 and FLAG antibodies in H9 hESCs followed by western blot against HERC2. We loaded 13.3% of input and 20% of immunoprecipitated sample. The images are representative of three independent experiments. All cropped blots were run under the same experimental conditions. The original blots are included in Supplementary Fig. 13. **(b)** Volcano plot of the interactome of HERC2 treating H9 hESC samples with RNase A prior to immunoprecipitation (n = 4). Graph represents the -log₂ (p-value) of a two-tailed *t*-test plotted against the log₂ ratio of LFQ values from co-IP experiments with HERC2 antibody compared to control co-IP with FLAG antibody. Red colored dots indicate some of the most enriched interacting proteins after correction for multiple testing (FDR < 0.2, s₀ = 0.1). **(c)** Bar graph representing the top GOBPs of HERC2 interactome (P < 0.05). **(d)** Bar graph representing the top GOBPs of the differentially expressed transcripts in *HERC2*^{-/-} H9 hESCs (P < 0.05). Transcripts showing a log₂-fold change at a FDR < 0.05 were retained as significantly differentially expressed. **(e)** Western blot analysis with antibodies to HERC2, OCT4 and SOX2 comparing

wild-type H9 (WT) with *HERC2*^{-/-} H9 hESCs. β -actin is the loading control. The images are representative of two independent experiments. All cropped blots were run under the same experimental conditions. The original blots are included in Supplementary Fig. 13. (f) Real-time PCR analysis of pluripotency (upper panel) and germ-layer markers (lower panel) in *HERC2*^{-/-} H9 hESCs. Graphs (relative expression to wild-type H9 hESCs (WT)) represent the mean \pm s.e.m. of four independent experiments. Statistical comparisons were made by Student's *t*-test for unpaired samples. P-value: *** ($P < 0.001$). (g) Immunocytochemistry of H9 hESC with antibodies against OCT4 and SOX2 (markers for pluripotency) and PAX6 (neuroectodermal marker). DAPI staining was used as a marker of nuclei. Scale bar represents 20 μ m. (h) Western blot analysis with antibodies to *HERC2*, *NESTIN* and *PAX6* after 10 days of neural induction. β -actin is the loading control. The images are representative of three independent experiments. (i) Real-time PCR analysis of pluripotency (upper panel) and neuroectodermal markers (lower panel) in H9 cells after 10 days of neural induction. Graphs (relative expression to WT) represent the mean \pm s.e.m. of four independent experiments. Statistical comparisons were made by Student's *t*-test for unpaired samples. P-value: * $P < 0.05$. (j) Immunocytochemistry after 10 days of neural differentiation of *HERC2*^{-/-} hESCs using antibodies against OCT4, *PAX6*, *NES* and *SOX1*. DAPI was used as a marker of nuclei. Scale bar represents 20 μ m.

germ layers (Fig. 3f), suggesting that loss of *HERC2* does not induce differentiation. We only observe a decrease in the mRNA levels of *PAX6*, an early marker of neuroectodermal differentiation⁶² (Fig. 3f). At the pluripotent state, hESCs express marginal amounts of *PAX6*⁶³ making these results difficult to interpret. Nevertheless, a decrease in *PAX6* levels at the hESC stage could indicate a dysfunction in their ability to differentiate into NPCs. To assess this hypothesis, we induced neural differentiation. Besides a mild decrease in the mRNA levels of *TUJ1*, we did not find a significant downregulation in the induction of NPC markers at both protein and transcript levels (Fig. 3h,i). Most importantly, both control and *HERC2*^{-/-} cultures consisted mostly of *PAX6*-positive cells at the end of the neural induction treatment (Fig. 3j). Taken together, these results suggest that *HERC2* has not a big impact in neural differentiation of hESCs.

Highly abundant E3s interact with stem cell regulators in hESCs. We continued our interactome analysis of up-regulated E3 enzymes focusing on KCMF1, UBR7, UBE3A and RNF181 (Fig. 4a and Supplementary Fig. 4). We excluded HUWE1, TRIM33 and RNF40 as their role and targets have been previously defined in the context of hESC function^{34,36,38}. KCMF1 is a poorly characterized RING finger-domain E3 enzyme⁶⁴. In *Drosophila melanogaster*, KCMF1 orthologue regulates MAPK levels through its interaction with UBR4⁶⁵, another E3 ubiquitin ligase. Moreover, the complex KCMF1-UBR4 promotes lysosomal degradation of the E2 ubiquitin protein RAD6⁶⁶. We identified 23 significant KCMF1 interactors in hESCs, including UBR4 (Fig. 4b,c and Supplementary Data 7). One of the most enriched proteins was HMMR (Fig. 4b,c), an important regulator of stemness in murine ESCs through its role in signal transduction at microtubules⁶⁷. TAF15, another significant KCMF1 interactor, has been previously reported as an epigenetic regulator of ESC pluripotency⁶⁸. Among the most enriched GOBPs of KCMF1 interactors, we found processes involved in cotranslational protein targeting to the endoplasmic reticulum (Fig. 4d).

UBR7 belongs to the UBR-box family of E3 ligases. The UBR-box domain contains three zinc finger sites to bind proteins with modified N-terminal amino acid residues based on the N-end rule pathway⁶⁹. In contrast to other members of the UBR-box family, little is known about UBR7. It was discovered in mammalian sperm, where it was shown to exhibit E3 ligase activity and suggested to be involved in spermiogenesis⁷⁰. We identified 18 significant interactors of UBR7 in hESCs (Fig. 4e,f and Supplementary Data 8). The most enriched interactor was A2M, a regulator of cytokine availability in the local environment of hESCs and, thus, having a direct impact on pluripotency⁷¹ (Fig. 4e,f). Another strong UBR7 interactor was ZSCAN10, which is key for mouse ESC identity⁷². Similar to HECTD1, UBR7 interacted with distinct PDC subunits (*i.e.*, DLAT, PDHA1 and PDHB) (Supplementary Data 8). Accordingly, GOBP analysis of UBR7 interactors indicated an enrichment in acetyl-CoA biosynthetic pathways (Fig. 4g).

UBE3A, also known as E6-AP, belongs to the family of HECT E3 ubiquitin ligases and was initially discovered as a modulator of p53 degradation⁷³. Genetic abnormalities in the maternally inherited UBE3A are responsible for Angelman syndrome^{74,75}. Conversely, duplication or increased expression of *UBE3A* is linked to autism spectrum disorders⁷⁶. UBE3A plays a role in dendritic arborization and synapse maturation^{77–79}, as well as cell cycle progression⁸⁰. Additionally, UBE3A participates in the clearance of several aggregated proteins^{81,82}. Among the UBE3A interactors in hESCs, the most enriched protein was SAE1, an important regulator for reprogramming of human somatic cells⁸³ (Fig. 5a–c and Supplementary Data 9). Another interactor of UBE3A was BCCIP, whose deficiency in mouse leads to impaired neural progenitor self-renewal and differentiation capabilities⁸⁴. AHNK, which was also significantly enriched in the UBE3A pull-down, is necessary for proper iPSC generation⁸⁵. GOBP analysis of UBE3A interactors indicated enrichment for proteins involved in metabolic processes of cellular macromolecules, aromatic and nitrogen compounds as well as mRNAs (Fig. 5d and Supplementary 9). However, we cannot rule out that these interactions with RBPs involved in mRNA stability ensue from indirect RNA-mediated binding and further experiments will be required to assess direct interaction (*e.g.*, RNase A prior to immunoprecipitation).

The interactome of RNF181 was highly enriched for subunits of dynactin (specifically, DCTN2, ACTR1A, ACTR1B, DCTN4, DCTN1) (Fig. 5e,f and Supplementary Data 10), a macromolecular complex that regulates not only intracellular transport but also chromosome alignment and spindle organization during cell division⁸⁶. Dynactin is necessary for proper asymmetric division of embryonic skin progenitors⁸⁷ and thus may also play a role in the asymmetric divisions invoked by ESCs. Furthermore, RNF181 interacts with DZIP3, an E3 enzyme

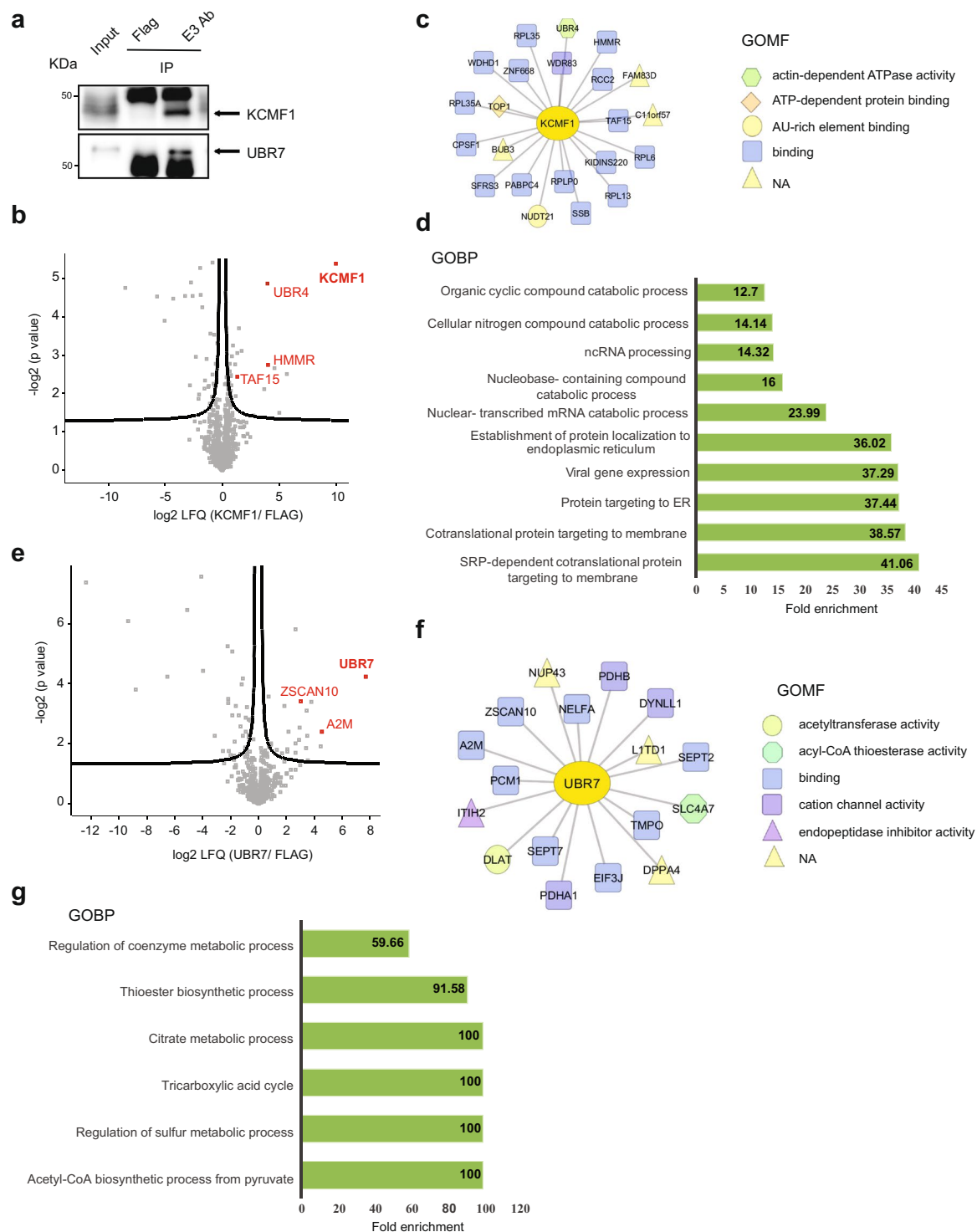


Figure 4. Analysis of the interactome of KCMF1 and UBR7 in H9 hESCs. **(a)** Co-IP with KCMF1, UBR7 and FLAG antibodies in H9 hESCs followed by western blot against the respective E3 ubiquitin ligases. We loaded 13.3% of input and 20% of immunoprecipitated sample. Arrows indicate the specific bands for KCMF1 and UBR7. The images are representative of three independent experiments. All cropped blots were run under the same experimental conditions. The original blots are included in Supplementary Fig. 13. **(b)** Volcano plot of the KCMF1 interactome ($n = 4$, $FDR < 0.2$). Red colored dots indicate some of the most enriched interacting proteins after correction for multiple testing. **(c)** Scheme indicating the Gene Ontology Molecular Function (GOMF) of KCMF1 interactors **(d)** Bar graph representing the top GOBPs of KCMF1 interactome ($P < 0.05$). **(e)** Volcano plot of the UBR7 interactome ($n = 4$, $FDR < 0.2$). **(f)** Scheme indicating the GOMF of UBR7 interactors **(g)** Bar graph representing the top GOBPs of UBR7 interactome ($P < 0.05$).

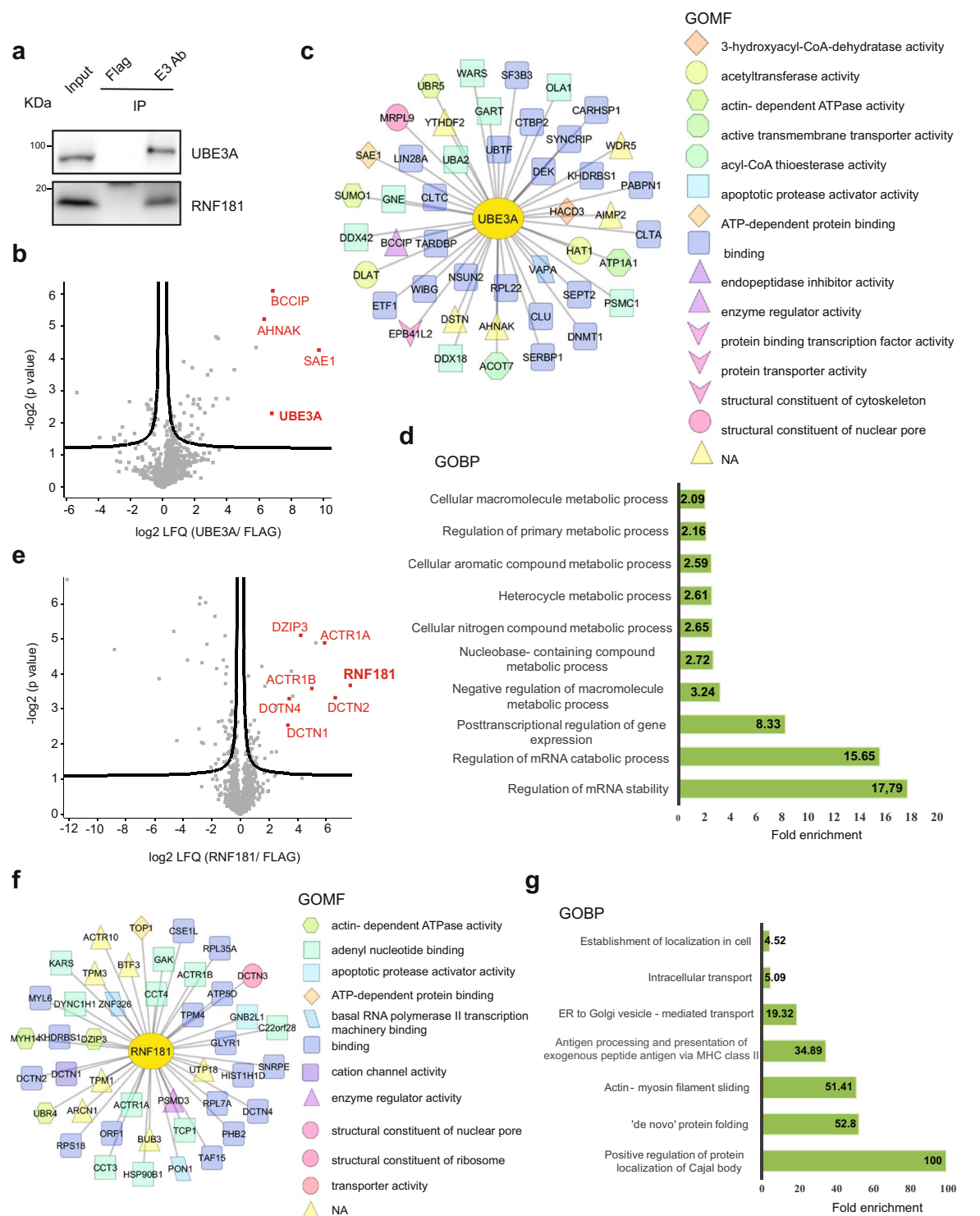


Figure 5. Highly abundant E3s interact with stem cell regulators in hESCs. **(a)** Co-IP with UBE3A, RNF181 and FLAG antibodies in H9 hESCs followed by western blot against the respective E3 ubiquitin ligases. We loaded 13.3% of input and 20% of immunoprecipitated sample. The images are representative of three independent experiments. All cropped blots were run under the same experimental conditions. The original blots are included in Supplementary Fig. 13. **(b)** Volcano plot of the UBE3A interactome ($n = 3$, $FDR < 0.2$). Red colored dots indicate some of the most enriched interacting proteins after correction for multiple testing. **(c)** Scheme indicating the Gene Ontology Molecular Function (GOMF) of UBE3A interactors **(d)** Bar graph representing the top GOBPs of UBE3A interactome ($P < 0.05$). **(e)** Volcano plot of the RNF181 interactome ($n = 4$, $FDR < 0.2$). **(f)** Scheme indicating the GOMF of RNF181 interactors **(g)** Bar graph representing the top GOBPs of RNF181 interactome ($P < 0.05$).

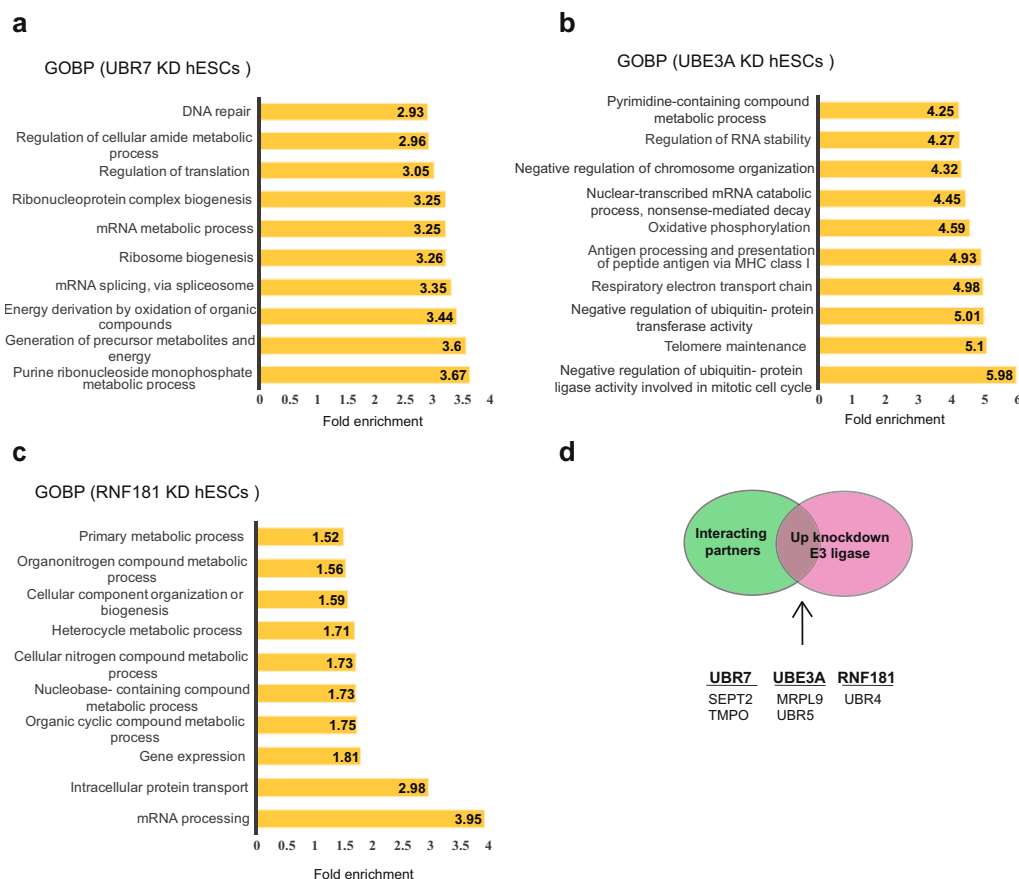


Figure 6. Loss of distinct up-regulated E3 enzymes induces changes in the hESC proteome. **(a)** Loss of UBR7 changed the levels of 506 proteins in H9 hESCs (FDR < 0.2 was considered significant, $n = 3$). GOBP analysis ($P < 0.05$) revealed a strong enrichment for regulators of the purine metabolic process as well as generation of energy and metabolites. **(b)** Loss of UBE3A changed the levels of 661 proteins in H9 hESCs (FDR < 0.2 was considered significant, $n = 3$). Bar graph representing the top GOBPs changed upon UBE3A KD ($P < 0.05$). **(c)** Loss of RNF181 changed the levels of 202 proteins in H9 hESCs (FDR < 0.2, $n = 3$). Bar graph representing the top GOBPs changed upon RNF181 KD ($P < 0.05$). **(d)** Common proteins between interacting partners of E3 ubiquitin ligases and proteins up-regulated in hESCs with knockdown of the respective E3 enzymes.

which regulates developmental genes in mouse ESCs by reorganizing 3D chromatin conformation⁸⁸. Further experiments will be required to determine whether this interaction is direct or DNA-mediated. Besides the proteasome subunit PSMD3, RNF181 also interacted with distinct subunits of the TRiC/CCT chaperonin complex which is critical for hESC proliferation and differentiation⁹ (Fig. 5f). The TRiC/CCT complex facilitates the folding of ~10% of the eukaryotic proteome and mediates protein localization to Cajal bodies, a sub-organelle found in the nucleus of highly proliferative cells, such as hESCs^{89,90}. Accordingly, the most enriched GOBP of RNF181 interactors was the positive regulation of protein localization to Cajal bodies (Fig. 5g and Supplementary Data 10). Prompted by these findings, we examined whether RNF181 also interacts with these proteins in post-mitotic neuronal cells. Among the 46 RNF181 interactors found in hESCs, only 17% were also significant interactors in neurons (Supplementary Fig. 6 and Supplementary Data 11). Although RNF181 bound some of the dynactin subunits in neurons (*i.e.*, DCTN2, ACTR1A, DCTN1), the interaction with DZIP3 as well as TRiC/CCT subunits was lost (Supplementary Fig. 6 and Supplementary Data 11). Taken together, the role of the interacting partners of up-regulated E3 ubiquitin ligases in hESCs indicated that these enzymes might be important for stem cell identity.

Loss of distinct up-regulated E3 enzymes induces changes in the proteome of hESCs. To assess the role of up-regulated E3 ligases in hESC function, we generated stable knockdown (KD) lines for UBR7, UBE3A and RNF181 and analysed their proteome by quantitative proteomics (Supplementary Data 12). We identified the significantly changed proteins upon E3 knockdown and performed GOBP analysis (Supplementary Data 12). Loss of UBR7 changed the levels of 506 proteins, which were enriched for regulators of the generation of energy and metabolites as well as the purine metabolic process (Fig. 6a and Supplementary Data 12). These changes could have an impact on hESCs, which rely on highly active nucleotide synthesis rates for sustaining their rapid proliferation rates and *de novo* DNA and RNA production^{91,92}. Among the 661 proteins changed upon UBE3A knockdown, GOBP analysis indicated the strongest enrichment for factors involved in the negative regulation of ubiquitin-ligase activity (Fig. 6b and Supplementary Data 12). This is consistent with previous studies,

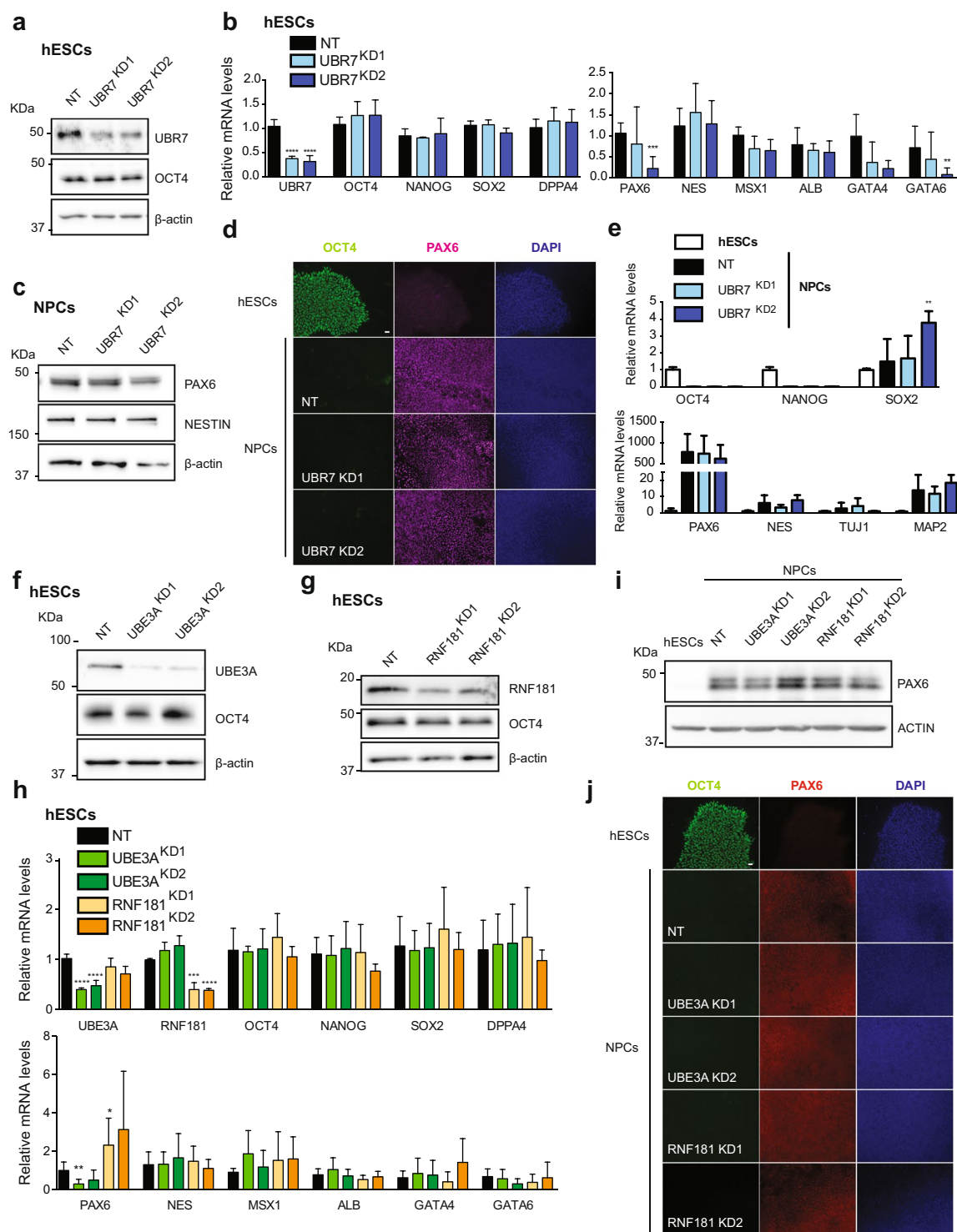


Figure 7. Loss of UBR7, UBE3A and RNF181 does not affect the expression of pluripotency markers and neural differentiation. **(a)** Western blot analysis with antibodies to UBR7 and OCT4 comparing non-targeting shRNA (NT) with UBR7 knockdown (KD) H9 hESCs. We used two independent shRNAs to UBR7 (KD1 and KD2, respectively). β-actin is the loading control. The images are representative of two independent experiments. All cropped blots were run under the same experimental conditions. The original blots are included in Supplementary Fig. 13. **(b)** Real-time PCR analysis of pluripotency (left panel) and germ-layer markers (right panel) in UBR7 KD H9 hESCs. Graphs (relative expression to NT shRNA) represent the mean ± s.e.m. of four independent experiments. **(c)** Western blot analysis after 10 days of neural induction of UBR7 KD H9 hESCs. β-actin is the loading control. The images are representative of two independent experiments. **(d)** Immunocytochemistry after 10 days of neural differentiation. OCT4, PAX6, and DAPI staining were used as markers of pluripotency, neuroectodermal differentiation, and nuclei, respectively. Scale bar represents 20 μm. **(e)** Real-time PCR analysis of pluripotency (upper panel) and neuroectodermal markers

(lower panel) in UBR7 KD H9 hESCs after 10 days of neural differentiation. Graphs (relative expression to NT) represent the mean \pm s.e.m. of three independent experiments. (f,g) Western blots of UBE3A and OCT4 (f) and RNF181 and OCT4 (g) protein levels. β -actin is the loading control. The images are representative of two independent experiments. (h) Real-time PCR analysis of pluripotency (upper panel) and germ-layer markers (lower panel) in UBE3A and RNF181 KD H9 hESCs. Graphs (relative expression to NT shRNA) represent the mean \pm s.e.m. of three independent experiments. (i) Western blot analysis after 10 days of neural induction of UBE3A and RNF181 KD H9 hESCs. β -actin is the loading control. The images are representative of two independent experiments. (j) Immunocytochemistry after 10 days of neural differentiation. OCT4, PAX6, and DAPI staining were used as markers of pluripotency, neuroectodermal differentiation, and nuclei, respectively. Scale bar represents 20 μ m. All the statistical comparisons were made by Student's t-test for unpaired samples. P-value: *($P < 0.05$), **($P < 0.01$), ***($P < 0.001$), ****($P < 0.0001$).

that showed that UBE3A interacts and ubiquitinates several proteasome subunits^{93,94} and regulates the activity of the proteasome in a ligase-dependent way^{95,96}. Thus, UBE3A could be involved in the regulation of hESC identity through modulation of the proteasome, which is central for maintaining pluripotency¹³. Loss of RNF181 changed the hESC proteome to a lesser extent (202 proteins) compared with UBR7 and UBE3A KD (Supplementary Data 12). Proteins dysregulated in RNF181 KD hESCs were involved mainly in mRNA processing-related pathways (Fig. 6c). Transcription hyperactivity has been proposed as a hallmark of pluripotent stem cells, as the transcription rates markedly decline during differentiation⁹⁷. In these lines, mRNA-related proteins deregulated in RNF181 KD lines -such as SNRPD1, SRSF5 or HNRNPK- have been proven necessary for stemness in pluripotent cells^{98–100}. If E3 interactors are activated for proteasomal degradation by the respective E3 enzyme, we would expect them to increase upon loss of the ubiquitin ligase. However, only a marginal number of the interacting partners were up-regulated upon E3 knockdown despite the numerous changes in the proteome induced by loss of E3 ligases (Fig. 6d).

One step further was to examine whether loss of UBR7, UBE3A or RNF181 alters hESC identity and differentiation. Loss of UBR7 did not result in significant differences in pluripotency markers compared with control hESCs (Fig. 7a,b). Furthermore, the expression of markers of the distinct germ layers was not impaired (Fig. 7b). We induced neural differentiation of UBR7 KD hESCs and monitored the expression of PAX6. After 10 days of neural induction, PAX6 levels were increased at the same extent in control and UBR7 KD lines (Fig. 7c–e). We also analysed the levels of other neural and neuronal markers and found no differences at this stage (Fig. 7e). To assess whether UBR7 was required for proper differentiation into other germ lineages, we differentiated UBR7 KD hESCs into endoderm (Supplementary Fig. 7). The induction of distinct endoderm markers was similar between control and UBR7 KD lines, suggesting no major role of UBR7 in cell fate decisions towards the endodermal lineage (Supplementary Fig. 7).

We observed similar results in UBE3A and RNF181 KD hESCs, as pluripotency and differentiation markers remained unchanged after reducing the expression of these E3 enzymes (Fig. 7f–h). We also performed neural (Fig. 7i–j and Supplementary Fig. 8) and endodermal differentiation (Supplementary Fig. 9) from UBE3A and RNF181 KD hESCs and found no differences compared with control cells. Altogether, these results indicate that loss of UBR7, UBE3A or RNF181 alone does not alter the commitment of hESCs to a neuroectodermal or endodermal fate.

Proteasome inhibition induces numerous changes in the proteome of hESCs. To assess whether E3 enzymes potentially regulate proteasomal degradation of specific interactors, we induced acute proteasome dysfunction with the potent MG-132 proteasome inhibitor followed by a shot label-free proteomic approach (Fig. 8a,b). We identified 2735 proteins and hierarchical clustering indicated a clear separation of MG-132-treated hESCs compared with control hESCs based on global protein expression profiles (Supplementary Fig. 10). Quantitative analysis revealed that 899 proteins were significantly changed in MG-132-treated hESCs as compared to control hESCs (Fig. 8b and Supplementary Data 13). Among them, 552 proteins were down-regulated whereas 347 were up-regulated upon proteasome inhibition (Fig. 8b and Supplementary Data 13). Since the latter group could be putative proteasome targets, we integrated these data with the statistically significant E3 interactors. We identified several interactors of each E3 which were also up-regulated upon proteasome inhibitor (Fig. 8c). Among them, we confirmed by western blot the interactions of HECTD1 with EXOC5 and RNF181 with PSMD3 (Fig. 8d). Proteasome inhibition induced a slight increase in both EXOC5 and PSMD3 as we observed by proteomics and western blot (Fig. 8e, Supplementary Fig. 11 and Supplementary Data 13). Thus, a detailed analysis and validation of other E3 interacting partners could reveal novel proteasome targets in hESCs. However, it is also important to note the low number of up-regulated proteins commonly identified in E3 KD lines and proteasome inhibitor-treated hESCs (Fig. 8f). Among the 256 proteins up-regulated in UBR7 KD hESC, only 11 proteins were also increased upon proteasome inhibition (Fig. 8f). Loss of UBE3A resulted in 407 up-regulated proteins. Among them, 22 were also increased upon MG-132 treatment, including TRIOBP and MFGE8, both important for ESC function^{101,102} (Fig. 8f). Knockdown of RNF181 only induced an increase in 4 proteins that were also up-regulated under proteasome inhibition (Fig. 8f). Thus, although a E3-based approach could lead to the discovery of potential proteasomal targets in hESCs, our results indicate that E3s are regulating multiple processes in a proteasome-independent manner that can complicate our analysis. Moreover, we cannot discard compensatory mechanisms or potential functional redundancies among different E3 enzymes^{103–106} as suggested by the lack of strong phenotypes in our loss-of-function experiments. In these lines, we have observed multiple common interactors between distinct E3 enzymes (Supplementary Fig. 12).

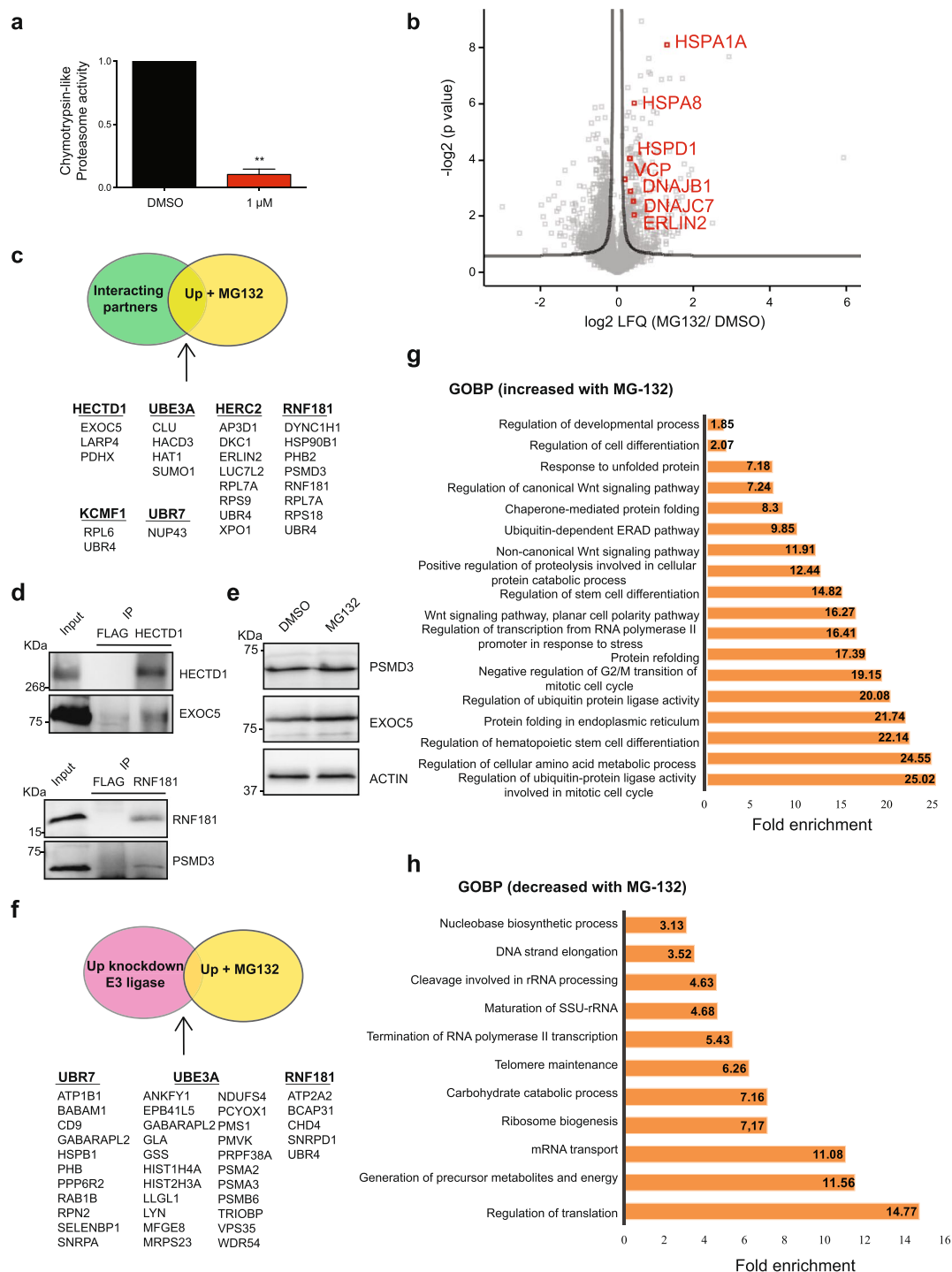


Figure 8. Proteasome inhibition induces profound changes in the proteome of ESCs. **(a)** Chymotrypsin-like proteasome activity in H9 hESCs treated with 1 μ M MG-132 for 24h (relative slope to H9 hESCs treated with DMSO). Graph represents the mean \pm s.d. of two independent experiments. Statistical comparisons were made by Student's *t*-test for unpaired samples. *P*-value: **(*P* < 0.01). **(b)** Volcano plot of LFQ intensities in MG-132-treated hESCs. The significance of a two-tailed *t*-test is plotted against the log₂ fold change of LFQs (FDR = 0.2, *s*₀ = 1). Proteasome inhibitor: 1 μ M MG-132 for 24h. **(c)** Common proteins between interacting partners of the E3 ubiquitin ligases and proteins up-regulated in hESCs upon proteasome inhibition. **(d)** Co-IP with HECTD1, RNF181 and FLAG antibodies in H9 hESCs followed by western blot against EXOC5 and PSMD3. **(e)** Western blot analysis with antibodies to EXOC5 and PSMD3 of MG-132-treated H9 hESCs. β -actin is the loading control. The images are representative of three independent experiments. All cropped blots were run under the same experimental conditions. The original blots are included in Supplementary Fig. 13. **(f)** Common up-regulated proteins between E3 knockdown hESCs and MG-132-treated hESCs. **(g)** Bar graph representing the top GOBPs of the up-regulated proteins upon proteasome inhibitor treatment (*P* < 0.05). **(h)** Bar graph representing the top GOBPs of the down-regulated proteins upon proteasome inhibitor treatment (*P* < 0.05).

Another potential hypothesis is that enhanced proteasome activity of hESCs is not directly linked to the degradation of endogenous substrates. In this model, increased proteasome activity could be coupled with intrinsic characteristics of pluripotent stem cells. In support of this hypothesis, we observed a higher number of down-regulated proteins than increased proteins under proteasome inhibition (552 down-regulated *versus* 347 up-regulated). To gain insight into the effects of proteasome dysfunction in hESCs, we performed GOBP term analysis of these altered proteins. Analysis of up-regulated proteins indicated strong enrichment for genes involved in proteasomal-mediated ubiquitin degradation, including numerous proteasome subunits (Fig. 8g and Supplementary Data 13). Among them, we found an up-regulation of the proteasome activator PSMD11/RPN6¹³. Thus, these data suggest that hESCs trigger the expression of proteasome subunits as a compensatory mechanism to ameliorate the proteostasis decline induced by proteasome inhibition. In line with these results, we also found a marked up-regulation of proteins involved in chaperone-mediated protein folding and refolding (*e.g.*, HSPA1A, DNAJ7, DNAJB1, HSPA8, HSPD1 and the stress-induced HSP90AA1), protein folding in the endoplasmic reticulum (ER) and ubiquitin-dependent ER-associated degradation (ERAD) (*e.g.*, ERLIN2, VCP). Moreover, we found GOBP enrichment for regulators of stem cell differentiation, cell cycle and WNT signalling pathway (Fig. 8g and Supplementary Data 13). However, this enrichment was essentially due to increased levels of proteasome subunits, which are well-known regulators of the aforementioned biological processes.

On the other hand, GOBP term analysis of down-regulated proteins upon MG-132 treatment revealed a strong enrichment for factors involved in different pathways linked with hESC maintenance (Fig. 8h and Supplementary Data 13). For instance, proteasome dysfunction induced downregulation of activators of ribosome biogenesis and translation (Fig. 8h), a process that may compensate the decline in proteolytic ability. However, these changes could also trigger differentiation as ESCs rely on enhanced expression of ribosomal subunits and global translational rates to sustain their self-renewal and pluripotency^{37,107}. Moreover, ESCs produce high levels of pre-rRNA¹⁰⁸ and we found a down-regulation of proteins involved in maturation of rRNA (TSR1, HEATR1, EMG1) (Fig. 8h). In addition, proteasome dysfunction decreased the levels of distinct modulators of mRNA transport such as the nuclear pore complex protein NUP153, which is required for ESC pluripotency¹⁰⁹.

Notably, proteasome inhibition also induced the down-regulation of factors involved in telomere maintenance and organization (*e.g.*, RIF1, NOP10) (Fig. 8h), a key process for hESC maintenance^{110,111}. Besides these changes, we found a decrease in the levels of multiple proteins involved in catabolic carbohydrate process (*e.g.*, the glycogen phosphorylases PYGL/PYGB) as well as generation of precursor metabolites and energy (Fig. 8h). Remarkably, we observed a downregulation of hexokinase II (HK2), which is required for the high glycolytic rates of hESCs⁹². We also found a decrease in LIN28A (Supplementary Data 13), a core component of hESC identity that regulates the translation and stability of numerous mRNAs^{112–115}, modulating key biological processes such as metabolism¹¹⁶. Thus, proteasome dysfunction impairs the protein levels of multiple factors involved in biological processes required for hESC function, suggesting a potential link between enhanced proteasome and other determinants of hESC identity such as metabolism, RNA biogenesis and telomere maintenance.

Discussion

Pluripotent stem cells exhibit intrinsic high levels of proteasome activity¹². Recent work demonstrates that this enhanced proteasome activity is essential for the striking ability of hESCs to maintain their proteostasis^{9,12,13,19}. Besides this role in protein quality control, here we aimed to uncover additional molecular mechanisms by which proteasome activity regulates hESC function. First, we assessed whether increased proteasome is also required to regulate the concentration of endogenous targets in these cells by identifying highly-expressed E3 enzymes. Then, we characterized the interactome of the up-regulated E3 ligases and integrated these data with our proteomics experiments in E3-knockdown and proteasome inhibitor-treated hESCs. Unexpectedly, we identified a relatively low number of potential E3 substrates which were also increased upon proteasome inhibition. The difficulties in the identification of E3 substrates have been previously shown to be notoriously challenging^{117,118}. First, protein ubiquitination is a highly dynamic process modulated by the coordinated action of E3 ligases and DUBs, which can remove the ubiquitin chains of E3 substrates. The balanced regulation of both competing processes could determine the fate of specific targets depending on the cellular status and environment. In this context, changes in the activity of specific DUBs could compensate the silencing of E3 enzymes. In a further level of complexity, DUBs can directly modulate the activity and turnover of E3 ligases¹¹⁹. Thus, a further understanding of the equilibrium between DUB and E3 activities in proteasomal degradation of pluripotency factors is of central importance. Secondly, the interaction between the E3 ligases and the substrates is rapid and weak. Hence, this transient interaction will make it especially challenging to isolate the complex E3-substrate¹²⁰. Finally, we believe that significant degrees of redundancy and compensatory mechanisms among the E3 enzymes could be particularly relevant for our study. A substrate may be ubiquitinated by multiple E3s in the same or different lysines and even one single protein might be ubiquitinated by distinct enzymes under different conditions or even within single cellular compartments¹²¹. E3 substrates can be modified with a single ubiquitin or chains of ubiquitin at one or multiple sites. This variety in the ubiquitination generates a highly diverse topology of poly-ubiquitin chains, which not always targets the substrate towards degradation through the proteasome, but will have several different functions (*i.e.*, intracellular signalling events)¹²². Thus, the interacting partners found in our proteomic analysis could not be substrates of the proteasome, but rather have their activity/function modified upon ubiquitination or simply be interacting proteins which might participate in an E3-containing protein complex. Nevertheless, our interactome analysis in hESCs may contribute to the understanding of the role of these E3 ubiquitin ligases.

In order to establish whether the E3 ubiquitin ligases have an impact on hESC identity, we silenced their expression and analysed stem cell pluripotency and differentiation capacities. However, we did not find a major effect on stem cell markers and their differentiation capacity upon loss of single E3 ubiquitin ligases. As mentioned above, that could be explained by potential functional redundancies between E3 ligases, as it has been previously shown for distinct E3s¹⁰⁵. One example is the yeast transcriptional repressor alpha2, which can be

independently marked for proteasomal degradation by the E3 enzymes Doa10 and Slx5/Slx8¹⁰⁶. Moreover, the E3 ligases SAN1 and UBR1 can independently regulate the chaperone-dependant ubiquitination of misfolded proteins in yeast¹⁰³. In mammalian cells, the tumour suppressor p53 can be degraded through the action of many E3 ligases, such as COP1, WWP1, E4F1 and PIRH2, which provides an additional layer of complexity in the regulation of the UPS¹⁰⁴. These redundant mechanisms could ensure proper degradation of a particular substrate, even when one of the E3s might not be functional or overloaded by the number of targets to ubiquitinate. Furthermore, the different E3s might show subtle differences depending on their distinct subcellular localizations to enable intracellular-specific ubiquitination of the same substrate. Given the complex roles of E3s in maintaining cellular homeostasis and development, pluripotent stem cells likely rely on a tight coordination of redundant and compensatory mechanisms to maintain their function. Thus, simultaneous deletion of distinct E3 ligases might be necessary to induce a strong demise in their pluripotency. In addition, we cannot discard that the lack of phenotype of E3-depleted hESCs ensues from the activation of other proteostatic pathways that counterbalance UPS disturbances. For instance, it has been demonstrated that inhibition of proteasome induces autophagy as a compensatory response, in a p62-mediated manner^{123,124}.

In parallel to this approach, we also performed quantitative proteomic analysis of hESCs treated with proteasome inhibitor. By integrating these data with our interactome and loss of function experiments for distinct E3 ligases, we identified potential targets of the proteasome in hESCs. Most importantly, global proteasome inhibition experiments showed that besides its key role in maintaining proteostasis in hESCs, the proteasome is also coupled to other determinant biological processes of hESC identity, such as their intrinsic metabolism, RNA biogenesis and telomere maintenance. Overall, here we provide a comprehensive characterization of the UPS system in hESCs that could have important implications for a further understanding of these cells.

Experimental Procedures

hESCs culture and differentiation. The human H9 (WA09) and H1 (WA01) lines were obtained from WiCell Research Institute. H9 and H1 were maintained on Geltrex (ThermoFisher Scientific) using mTeSR1 (Stem Cell Technologies). Undifferentiated hESCs colonies were passaged using a solution of dispase (2 mg ml⁻¹) and scraping the colonies with a glass pipette. All the cell lines used in this study were tested for mycoplasma contamination at least once every three weeks and no mycoplasma contamination was detected. All research involving hESCs lines was performed with approval of the German Federal competent authority (Robert Koch Institute) and in accordance with the relevant guidelines and regulations.

Neural differentiation of H9 cell line was performed following the monolayer culture method as described previously¹²⁵ with STEMdiff Neural Induction Medium (Stem Cell Technologies) on polyornithine (15 µg ml⁻¹)/laminin (10 µg ml⁻¹)-coated plates. Undifferentiated hESCs were rinsed once with PBS and then we added 1 ml Gentle Dissociation Reagent (Stem Cell Technologies) for 5 min. After incubation at 5 min, we gently collected hESCs and 2 ml of Dulbecco's Modified Eagle Medium (DMEM)-F12 + 10 µM ROCK inhibitor (Abcam). Afterward, we centrifuged cells at 300 g for 10 min. Cells were resuspended on STEMdiff Neural Induction Medium + 10 µM ROCK inhibitor and plated on polyornithine (15 µg ml⁻¹)/laminin (10 µg ml⁻¹)-coated plates. For neuronal differentiation, NPC at passage 4 were dissociated with Accutase (Stem Cell Technologies) and plated into neuronal differentiation medium (DMEM/ F12, N2, B27 (ThermoFisher Scientific), 1 mg ml⁻¹ laminin (ThermoFisher Scientific), 20 ng ml⁻¹ brain-derived neurotrophic factor (BDNF) (Peprotech), 20 ng ml⁻¹ glial cell-derived neurotrophic factor (GDNF) (Peprotech), 1 mM dibutyryl-cyclic AMP (Sigma) and 200 nM ascorbic acid (Sigma)) onto polyornithine/laminin-coated plates. Cells were differentiated for 1 month, with weekly feeding of neuronal differentiation medium. Endoderm differentiation of H9 hESCs was performed using STEMdiff Definitive Endoderm Kit (Stem Cell Technologies).

Cardiomyocyte differentiation of H1 hESCs was performed as described in ref.¹²⁶. Confluent H1 hESCs were dissociated into single cells with Accutase at 37 °C for 10 min followed by inactivation using two volumes of F12/DMEM. Cells were counted and 230,000 cells cm² were plated in ITS medium (Corning), containing 1.25 mM CHIR 99021 (AxonMedchem) and 1.25 ng ml⁻¹ BMP4 (R&D), and seeded on Matrigel-coated 24-well plates. After 24 h, medium was changed to TS (transferrin/selenium) medium. After 48 h, medium was changed to TS medium supplemented with 10 mM canonical Wnt-Inhibitor IWP-2 (Santa Cruz) for 48 h. Then, medium was changed to fresh TS until beating cells were observed at days 8–10. Finally, medium was changed to Knockout DMEM (ThermoFisher Scientific) supplemented with 2% FCS, L-Glutamine and Penicillin/Streptomycin until cells were used for downstream analysis.

Lentiviral infection of H9 hESCs. Lentivirus (LV)-non-targeting shRNA control, LV-UBR7 shRNA #1 (TRCN0000037025), LV-UBR7 shRNA #2 (TRCN0000037026), LV-UBE3A shRNA #1 (TRCN0000419838), LV-UBE3A shRNA #2 (TRCN000003368), LV-RNF181 shRNA #1 (TRCN0000364405) and LV-RNF181 shRNA #2 (TRCN0000022389) in pLKO.1-puro vector were obtained from Mission shRNA (Sigma). For generation of stable hESCs transfected lines, H9 hESCs growing on Geltrex were incubated with 10 µM ROCK inhibitor for one hour and then individualized using Accutase. Fifty thousand cells were infected in suspension with 25 µL of concentrated virus in the presence of 10 µM ROCK inhibitor. Cell suspension was centrifuged to remove the virus and plated back on a feeder layer of mitotically inactivated MEF in CDF12 media containing ROCK inhibitor (DMEM/F12 plus 20% Knock-out Serum Replacement, β-mercaptoethanol (0.1%), 0.1 mM non-essential-aminoacids, Glutamax (1%), and 10 ng/ml bFGF). After few days in culture, cells were selected for lentiviral integration with 2 µg ml⁻¹ puromycin (ThermoFisher Scientific) and remaining colonies were manually passaged onto fresh MEFs to establish new hESC lines.

Generation of *HERC2*^{-/-} hESCs by CRISPR/Cas9 system and colony analysis. *HERC2* genomic sequence was obtained from ENSEMBL Genome browser. Two guide sequences (Guide A, targeting the intron 4–5, F: CCTCAGTTTCTTCATCCATAAAAC, and R: CAGCACTGCTTGACAGTGCTGGG; Guide B, targeting the fifth exon, F: CCGTCCAGTCAGCCACCACCACC, and R: CAGCCCTGCGACTCAAGCAGAGG), were generated using the Zinc Finger Consortium online resource (<http://zifit.partners.org/ZiFit/>). Guide-carrying plasmid were designed as previously described in refs^{127,128} using Cas9-puromycin selection plasmid (pX335-U6-Chimeric_BB-CBh-hSpCas9n(D10A) was a gift from Feng Zhang (Addgene plasmid # 42335)). H9 hESCs were plated on MEF-containing plates and transfected with 1 µg of each of the guide-carrying plasmids using FuGene HD (Promega). 24 h after the transfection, 0.5 µg ml⁻¹ puromycin selection was performed for 24 h followed by maintenance of hESCs with CDF12 media. Single cell split was performed prior to colony pick for genotyping. Genomic DNA isolation was done using QuickExtract (Epicentre). PCR using primer pairs surrounding *HERC2* fifth exon was performed (Forward: TAGAGAGAGGCAGTGTGCCA, and Reverse: TGGCTGGCTTCCACAGTTAC) to identify *HERC2*^{-/-} hESCs.

Immunoprecipitation of *HERC2*, *HECTD1*, *RNF181*, *KCMF1* and *UBR7* for interaction analysis.

hESCs were lysed in RIPA buffer (50 mM Tris-HCl (pH 6.7), 150 mM NaCl, 1% Triton x-100, 1% sodium deoxycholate, 1 mM EDTA, 1 mM PMSF) and supplemented with protease inhibitor (Roche). Lysates were homogenized through syringe needle (27 G) and centrifuged at 13,000 g for 15 min at 4 °C. For RNase A-treated samples, the supernatant was incubated with 125 µl ml⁻¹ RNase A (ThermoFischer) for one hour on ice. Otherwise, incubation with the antibody was performed. 330 µg of protein-containing samples were incubated for 30 minutes with *HERC2* antibody (Abcam, # ab85832, 4 µg) or *UBR7* antibody (Thermo Scientific, # PA5-31559, 4 µg) or *KCMF1* antibody (Abcam, # ab80287, 4 µg) or *RNF181* antibody (Thermo Scientific, PA5-31008, 4 µg) or *HECTD1* antibody (Abcam, #ab101992, 4 µg) on ice. As a control, the same amount of protein was incubated with anti-FLAG antibody (SIGMA, F7425, 4 µg). Subsequently samples were incubated with 100 µl of µMACS Micro Beads for 1 h at 4 °C with overhead shaking. After incubation, samples were loaded to precleared µMACS column (# 130-042-701). Beads were washed three times with 50 mM Tris (pH 7.5), 150 mM NaCl, 5% glycerol, 0.05% Triton and then five times with 50 mM Tris (pH 7.5) and 150 mM NaCl. For elution of the proteins for further Western Blot analysis, the beads were incubated with 50 µl of pre-heated (95 °C) 1X Laemmli Buffer for 5 minutes and collected into eppendorf tubes. The samples were boiled for 5 minutes at 95 °C and loaded in a SDS-PAGE gel. In Supplementary Fig. 4, we also show flow-through controls, that correspond to the supernatant that remains after centrifuging the tubes containing the antibody as well as the beads. For proteomics analysis, after the washes we performed partial digestion on the beads using 25 µl of 2 M Urea in 25 mM Tris, 7.5 mM ammonium bicarbonate, 1 mM DTT and 5 ng/ml trypsin, pH = 8.0 for 30 minutes at room temperature. The samples were then eluted twice with 50 µl of 2 M Urea, 25 mM Tris, 7.5 mM ammonium bicarbonate, 5 mM Iodoacetamide and left for fully digestion overnight at room temperature in the dark. For stopping the digestion, 5 µl of 100% formic acid was added to samples. Peptides were cleaned up using stage tip extraction¹²⁹.

Immunoprecipitation of *UBE3A* for interaction analysis. hESCs were lysed in RIPA buffer (50 mM Tris-HCl (pH 7.4), 150 mM NaCl, 1% Triton x-100, 1% sodium deoxycholate, 0.1% SDS, 1 mM EDTA, 1 mM PMSF) supplemented with protease inhibitor (Roche). Lysates were homogenized through syringe needle (27 G) and centrifuged at 13,000 g for 15 min at 4 °C. After pre-clearing the supernatant with Protein A agarose beads (Pierce), the samples were incubated overnight with *UBE3A* antibody (Cell Signaling, # 7526 1:50) on the overhead shaker at 4 °C. As a control, the same amount of protein was incubated with anti-FLAG antibody (SIGMA, F7425, 1:50) in parallel. Subsequently, samples were incubated with 30 µl of Protein A beads for 1 h at room temperature. After this incubation, samples were centrifuged 5 minutes at 5,000 g at room temperature and the pellet was washed three times with the RIPA buffer. For elution of the proteins for further western blot analysis, the pellet was incubated with pre-heated (95 °C) 2X Laemmli Buffer, boiled for 5 minutes and centrifuged 5 minutes at maximum speed. The supernatant was taken and loaded in a SDS-PAGE gel. For further proteomics analysis, after the washing steps, partial digestion of the proteins was performed on the agarose beads using 25 µl of 2 M Urea in 25 mM Tris, 7.5 mM ammonium bicarbonate, 1 mM DTT and 5 ng/ml trypsin, pH = 8.0 for 30 minutes at room temperature. Then, the samples were eluted 2 times with 50 µl of 2 M Urea, 25 mM Tris, 7.5 mM AmBic 5 mM Iodoacetamide and were fully digested overnight at room temperature in the dark. For stopping the digestion, 5 µl of 100% formic acid was added to the samples. Peptides were cleaned up using stage tip extraction¹²⁹.

Sample preparation for quantitative proteomics and analysis. For analysis of MG132 inhibited cells and hESCs, NPC and neurons we performed tandem mass tag (TMT) proteomics. Cells were collected in 8 M urea buffer, 50 mM ammonium bicarbonate, homogenized with a syringe and cleared using centrifugation (16,000 g, 20 min). Supernatants were reduced by addition of DTT to a final concentration of 5 mM and incubated at room temperature for 30 minutes. Iodoacetamide was added to the samples to a final concentration of 5 mM to alkylate the cysteines and incubated in the dark for 45 minutes. Lys-C (Wako, Richmond, VA) was added for digestion at a ratio 1:100 enzyme/substrate and incubated for three hours at room temperatures. Then, lysates were diluted to 2 M Urea with 50 mM ammonium bicarbonate, after which 10 ng µl⁻¹ Trypsin was added and incubated overnight at room temperature. Trypsin digestion was stopped by addition of formic acid and peptides were cleaned up using stage tip extraction¹²⁹. The liquid chromatography tandem mass spectrometry (LC-MS/MS) equipment consisted out of an EASY nLC 1000 coupled to the quadrupole based QExactive instrument (Thermo Scientific) via a nano-spray electroionization source. Peptides were separated on an in-house packed 50 cm column (1.9 µm C18 beads, Dr. Maisch) using a binary buffer system: A) 0.1% formic acid and B) 0.1% formic acid in ACN. The content of buffer B was raised from 7% to 23% within 120 min and followed by an increase to 45% within 10 min. Then, within 5 min buffer B fraction was raised to 80% and held for further 5 min after which it was decreased

to 5% within 2 min and held there for further 3 min before the next sample was loaded on the column. Eluting peptides were ionized by an applied voltage of 2.2 kV. The capillary temperature was 275 °C and the S-lens RF level was set to 60. MS1 spectra were acquired using a resolution of 70,000 (at 200 m/z), an Automatic Gain Control (AGC) target of 3e6 and a maximum injection time of 20 ms in a scan range of 300–1750 Th. In a data dependent mode, the 10 most intense peaks were selected for isolation and fragmentation in the HCD cell using a normalized collision energy of 25 at an isolation window of 2.1 Th. Dynamic exclusion was enabled and set to 20 s. The MS/MS scan properties were: 17,500 resolution at 200 m/z, an AGC target of 5e5 and a maximum injection time of 60 ms. All label-free proteomics data sets were analysed with the MaxQuant software¹³⁰ (release 1.5.3.8). We employed the LFQ mode¹³¹ and used MaxQuant default settings for protein identification and LFQ quantification. All downstream analyses were carried out on LFQ values with Perseus (v. 1.5.2.4)¹³².

Quantitative proteomics analysis of E3 enzymes. For the characterization of protein expression differences in E3 enzymes comparing H9 hESCs with their neuronal counterparts, we analysed the quantitative proteomics data published in ref.⁹. Statistical comparisons were made by Student's t-test. Discovery Rate (FDR) adjusted p-value (q-value) was calculated using the Benjamini–Hochberg procedure. All the proteins at a FDR level below 0.2 were retained as significantly differentially expressed (Supplementary Data 1). Then, we intersected the human E3 network annotated in¹³³ with this proteomics dataset (Supplementary Table 1).

RNA sequencing. Total RNA was extracted using RNeasy (Tel-Test Inc.). Libraries were prepared using the TruSeq Stranded mRNA Library Prep Kit. Library preparation started with 1 µg total RNA. After selection (using poly-T oligo-attached magnetic beads), mRNA was purified and fragmented using divalent cations under elevated temperature. The RNA fragments underwent reverse transcription using random primers followed by second strand cDNA synthesis with DNA Polymerase I and RNase H. After end repair and A-tailing, indexing adapters were ligated. The products were then purified and amplified (20 µl template, 14 PCR cycles) to create the final cDNA libraries. After library validation and quantification (Agilent 2100 Bioanalyzer), equimolar amounts of library were pooled. The pool was quantified by using the Peqlab KAPA Library Quantification Kit and the Applied Biosystems 7900HT Sequence Detection System. The pool was sequenced on an Illumina HiSeq. 4000 sequencer with a paired-end (2 × 75 bp) protocol. We used the human genome sequence and annotation (Ensembl 79) together with the splice-aware STAR read aligner¹³⁴ (release 2.5.1b) to map and assemble our reference transcriptome. Subsequent transcriptome analyses on differential gene and transcript abundance were carried out with the cufflinks package¹³⁵.

Western Blot. Cells were scraped from tissue culture plates and lysed in non-denaturing lysis buffer (10 mM Tris-HCl, pH 7.4, 10 mM EDTA, 50 mM NaCl, 50 mM NaF, 1% Triton X-100, 0.1% SDS, supplemented with 2 mM sodium orthovanadate, 1 mM PMSF and protease inhibitor (Roche)) and homogenized through a syringe needle (27 G). Cell lysates were centrifuged at 15,000 g for 15 min at 4 °C and protein concentration was measured from the supernatant using BCA protein assay (Thermo Scientific). Approximately 30 µg of total protein was separated by SDS-PAGE, transferred to PVDF membranes (Millipore) and subjected to immunoblot. Western blot analysis was performed with anti-HERC2 antibody (Abcam, # ab85832 1:2000), anti-UBR7 antibody (Thermo Scientific, # PA5-31559 1:2000), anti-KCMF1 antibody (Abcam, # ab80287, 1:3000), anti-RNF181 antibody (Thermo Scientific, PA5-31008, 1:2000), anti-HECTD1 antibody (Abcam, #ab101992, 1:1000), anti-UBE3A antibody (Cell Signaling, # 7526 1:1000), anti-RNF40 (Cell Signaling, #12187, 1:1000), anti-HUWE1 (Cell Signaling, #5695, 1:1000) anti-TRIM33 (Cell Signaling, #13387, 1:1000), anti-STUB1 (Cell Signaling, #2080, 1:1000), anti-OCT4 (Abcam, #ab19857, 1:5000), anti-SOX2 (Abcam, #97959, 1:1000), anti-PAX6 (Stem Cell Technologies, #60094, 1:1000), anti-NESTIN (Stem Cell Technologies, # 60091, 1:1000), anti-PSMD3 (Proteintech, # 12054-1-AP, 1:1000), anti-EXOC5 (Proteintech, # 17593-1-AP, 1:1000) and anti-β-actin (Abcam, #8226, 1:10000). Uncropped versions of western blots are presented in Supplementary Fig. 13.

Immunocytochemistry. Cells were fixed with paraformaldehyde (4% in PBS) for 20 min, followed by permeabilization (0.2% Triton X-100 in PBS for 10 min) and blocking (3% BSA in 0.2% Triton X-100 in PBS for 10 min). Human cells were incubated in primary antibody for 1.5 h at room temperature with anti-OCT4 (Stem Cell Technology, #60093, 1:200), anti-PAX6 (Stem Cell Technology, #60094, 1:300) or anti-SOX1 (Stem Cell Technology, #60095, 1:100). Then, cells were washed with PBS and incubated with secondary antibody (Alexa Fluor 488 goat anti-mouse (Thermo Fisher Scientific, A-11029), Alexa Fluor 568 F(ab')₂ Fragment of Goat Anti-Rabbit IgG (H + L) (Life Technologies, #A21069) and DAPI (Life Technologies, #1306) for 45 minutes at room temperature. PBS and distilled water wash were followed before the cover slips were mounted on Mowiol (Sigma, #324590).

RNA isolation and quantitative RT-PCR. Total RNA was isolated using RNeasy (Tel-Test Inc.). cDNA was generated from 1 µg of RNA using qScript Flex cDNA synthesis kit (Quantabio). SybrGreen real-time qPCR experiments were performed with a 1:20 dilution of cDNA using a CFC384 Real-Time System (Bio-Rad) following the manufacturer's instructions. Data were analysed with the comparative 2 $\Delta\Delta C_t$ method using the geometric mean of *ACTB* and *GAPDH* as housekeeping genes. See Supplementary Information for details about the primers used for this assay.

26S proteasome fluorogenic peptidase assays. The *in vitro* assay of 26S proteasome activities was performed as previously described¹³⁶. Cells were collected in proteasome activity assay buffer (50 mM Tris-HCl, pH7.5, 250 mM sucrose, 5 mM MgCl₂, 0.5 mM EDTA, 2 mM ATP and 1 mM DTT) and lysed by passing ten times through syringe needle (27 G). Then, lysate was centrifuged at 10,000 g for 10 min at 4 °C. 25 µg of total protein of

cell lysates were transferred to a 96-well microtiter plate (BD Falcon) and incubated with the fluorogenic substrate Z-Gly-Gly-Leu-AMC (Enzo Lifescience). Fluorescence (380 nm excitation, 460 nm emission) was monitored on a microplate fluorometer (EnSpire, Perkin Elmer) every 5 min for 2 h at 37 °C.

Data availability. All the mass spectrometry proteomics data as well as the transcriptomic data are available in the Supplementary Information. All the other data are also available from the corresponding author upon request.

References

- Jaenisch, R. & Young, R. Stem cells, the molecular circuitry of pluripotency and nuclear reprogramming. *Cell* **132**, 567–582 (2008).
- Miura, T., Mattson, M. P. & Rao, M. S. Cellular lifespan and senescence signaling in embryonic stem cells. *Aging Cell* **3**, 333–343 (2004).
- Takahashi, K. *et al.* Induction of pluripotent stem cells from adult human fibroblasts by defined factors. *Cell* **131**, 861–872 (2007).
- Weinberger, L., Ayyash, M., Noverstern, N. & Hanna, J. H. Dynamic stem cell states: naive to primed pluripotency in rodents and humans. *Nat Rev Mol Cell Biol* **17**, 155–169 (2016).
- Lee, H. J., Gutierrez-Garcia, R. & Vilchez, D. Embryonic stem cells: a novel paradigm to study proteostasis? *FEBS J* **284**, 391–398 (2017).
- Buckley, S. M. *et al.* Regulation of pluripotency and cellular reprogramming by the ubiquitin-proteasome system. *Cell Stem Cell* **11**, 783–798 (2012).
- Garcia-Prat, L., Sousa-Victor, P. & Munoz-Canoves, P. Proteostatic and Metabolic Control of Stemness. *Cell Stem Cell* **20**, 593–608 (2017).
- Noormohammadi, A. *et al.* Mechanisms of protein homeostasis (proteostasis) maintain stem cell identity in mammalian pluripotent stem cells. *Cell Mol Life Sci* (2017).
- Noormohammadi, A. *et al.* Somatic increase of CCT8 mimics proteostasis of human pluripotent stem cells and extends *C. elegans* lifespan. *Nat Commun* **7**, 13649 (2016).
- Schmidt, M. & Finley, D. Regulation of proteasome activity in health and disease. *Biochim Biophys Acta* **1843**, 13–25 (2014).
- Vilchez, D., Saez, I. & Dillin, A. The role of protein clearance mechanisms in organismal ageing and age-related diseases. *Nat Commun* **5**, 5659 (2014).
- Vilchez, D. *et al.* RPN-6 determines *C. elegans* longevity under proteotoxic stress conditions. *Nature* **489**, 263–268 (2012).
- Vilchez, D. *et al.* Increased proteasome activity in human embryonic stem cells is regulated by PSMD11. *Nature* **489**, 304–308 (2012).
- Pathare, G. R. *et al.* The proteasomal subunit Rpn6 is a molecular clamp holding the core and regulatory subcomplexes together. *Proc Natl Acad Sci USA* **109**, 149–154 (2012).
- Assou, S. *et al.* A gene expression signature shared by human mature oocytes and embryonic stem cells. *BMC Genomics* **10**, 10 (2009).
- Jang, J., Wang, Y., Kim, H. S., Lalli, M. A. & Kosik, K. S. Nrf2, a regulator of the proteasome, controls self-renewal and pluripotency in human embryonic stem cells. *Stem Cells* **32**, 2616–2625 (2014).
- Schroter, F. & Adjaye, J. The proteasome complex and the maintenance of pluripotency: sustain the fate by mopping up? *Stem Cell Res Ther* **5**, 24 (2014).
- Labbadia, J. & Morimoto, R. I. The biology of proteostasis in aging and disease. *Annu Rev Biochem* **84**, 435–464 (2015).
- Jeon, I. *et al.* Neuronal properties, *in vivo* effects, and pathology of a Huntington's disease patient-derived induced pluripotent stem cells. *Stem Cells* **30**, 2054–2062 (2012).
- Hernebring, M., Brolén, G., Aguilaniu, H., Semb, H. & Nystrom, T. Elimination of damaged proteins during differentiation of embryonic stem cells. *Proc Natl Acad Sci USA* **103**, 7700–7705 (2006).
- Hernebring, M. *et al.* Removal of damaged proteins during ES cell fate specification requires the proteasome activator PA28. *Sci Rep* **3**, 1381 (2013).
- Okita, Y. & Nakayama, K. I. UPS delivers pluripotency. *Cell Stem Cell* **11**, 728–730 (2012).
- Tanaka, K. The proteasome: from basic mechanisms to emerging roles. *Keio J Med* **62**, 1–12 (2013).
- Balch, W. E., Morimoto, R. I., Dillin, A. & Kelly, J. W. Adapting proteostasis for disease intervention. *Science* **319**, 916–919 (2008).
- Powers, E. T., Morimoto, R. I., Dillin, A., Kelly, J. W. & Balch, W. E. Biological and chemical approaches to diseases of proteostasis deficiency. *Annu Rev Biochem* **78**, 959–991 (2009).
- Strikoudis, A., Guillamot, M. & Aifantis, I. Regulation of stem cell function by protein ubiquitylation. *EMBO Rep* **15**, 365–382 (2014).
- Suresh, B., Lee, J., Kim, K. S. & Ramakrishna, S. The Importance of Ubiquitination and Deubiquitination in Cellular Reprogramming. *Stem Cells Int* **2016**, 6705927 (2016).
- Vilchez, D., Simic, M. S. & Dillin, A. Proteostasis and aging of stem cells. *Trends Cell Biol* **24**, 161–170 (2014).
- Werner, A., Manford, A. G. & Rape, M. Ubiquitin-Dependent Regulation of Stem Cell Biology. *Trends Cell Biol* (2017).
- Adams, J. The proteasome: structure, function, and role in the cell. *Cancer Treat Rev* **29**(Suppl 1), 3–9 (2003).
- Finley, D. Recognition and processing of ubiquitin-protein conjugates by the proteasome. *Annu Rev Biochem* **78**, 477–513 (2009).
- Sussman, R. T. *et al.* The epigenetic modifier ubiquitin-specific protease 22 (USP22) regulates embryonic stem cell differentiation via transcriptional repression of sex-determining region Y-box 2 (SOX2). *J Biol Chem* **288**, 24234–24246 (2013).
- Zhang, X. Y. *et al.* The putative cancer stem cell marker USP22 is a subunit of the human SAGA complex required for activated transcription and cell-cycle progression. *Mol Cell* **29**, 102–111 (2008).
- Fuchs, G. *et al.* RNF20 and USP44 regulate stem cell differentiation by modulating H2B monoubiquitylation. *Mol Cell* **46**, 662–673 (2012).
- Huang, Z. *et al.* Deubiquitylase HAUSP stabilizes REST and promotes maintenance of neural progenitor cells. *Nat Cell Biol* **13**, 142–152 (2011).
- Zhao, X. *et al.* The HECT-domain ubiquitin ligase Huwe1 controls neural differentiation and proliferation by destabilizing the N-Myc oncoprotein. *Nat Cell Biol* **10**, 643–653 (2008).
- You, K. T., Park, J. & Kim, V. N. Role of the small subunit processome in the maintenance of pluripotent stem cells. *Genes Dev* **29**, 2004–2009 (2015).
- Dupont, S. *et al.* FAM/USP9x, a deubiquitinating enzyme essential for TGFβ signaling, controls Smad4 monoubiquitination. *Cell* **136**, 123–135 (2009).
- Metzger, M. B., Hristova, V. A. & Weissman, A. M. HECT and RING finger families of E3 ubiquitin ligases at a glance. *J Cell Sci* **125**, 531–537 (2012).
- de Bie, P. & Ciechanover, A. Ubiquitination of E3 ligases: self-regulation of the ubiquitin system via proteolytic and non-proteolytic mechanisms. *Cell Death Differ* **18**, 1393–1402 (2011).
- Tran, H. *et al.* HectD1 E3 ligase modifies adenomatous polyposis coli (APC) with polyubiquitin to promote the APC-axin interaction. *J Biol Chem* **288**, 3753–3767 (2013).

42. Chuang, J. H., Tung, L. C. & Lin, Y. Neural differentiation from embryonic stem cells *in vitro*: An overview of the signaling pathways. *World J Stem Cells* **7**, 437–447 (2015).
43. Fernandez, A. *et al.* The WNT receptor FZD7 is required for maintenance of the pluripotent state in human embryonic stem cells. *Proc Natl Acad Sci USA* **111**, 1409–1414 (2014).
44. Patel, M. S. & Roche, T. E. Molecular biology and biochemistry of pyruvate dehydrogenase complexes. *FASEB J* **4**, 3224–3233 (1990).
45. Zhang, J., Nuebel, E., Daley, G. Q., Koehler, C. M. & Teitell, M. A. Metabolic regulation in pluripotent stem cells during reprogramming and self-renewal. *Cell Stem Cell* **11**, 589–595 (2012).
46. Kadamb, R., Mittal, S., Bansal, N., Batra, H. & Saluja, D. Sin3: insight into its transcription regulatory functions. *Eur J Cell Biol* **92**, 237–246 (2013).
47. Saunders, A. *et al.* The SIN3A/HDAC Corepressor Complex Functionally Cooperates with NANOG to Promote Pluripotency. *Cell Rep* **18**, 1713–1726 (2017).
48. Mallm, J. P. & Rippe, K. Aurora Kinase B Regulates Telomerase Activity via a Centromeric RNA in Stem Cells. *Cell Rep* **11**, 1667–1678 (2015).
49. Johnson, M. T., Yang, H. S., Magnuson, T. & Patel, M. S. Targeted disruption of the murine dihydrolipoamide dehydrogenase gene (Dld) results in perigastrulation lethality. *Proc Natl Acad Sci USA* **94**, 14512–14517 (1997).
50. Dia, Y. *et al.* Pax3/7BP is a Pax7- and Pax3-binding protein that regulates the proliferation of muscle precursor cells by an epigenetic mechanism. *Cell Stem Cell* **11**, 231–241 (2012).
51. Guerrier, S. *et al.* The F-BAR domain of srGAP2 induces membrane protrusions required for neuronal migration and morphogenesis. *Cell* **138**, 990–1004 (2009).
52. Beaulieu, C. L. *et al.* Intellectual disability associated with a homozygous missense mutation in THOC6. *Orphanet J Rare Dis* **8**, 62 (2013).
53. Sanchez-Tena, S., Cubillos-Rojas, M., Schneider, T. & Rosa, J. L. Functional and pathological relevance of HERC family proteins: a decade later. *Cell Mol Life Sci* **73**, 1955–1968 (2016).
54. Ji, Y. *et al.* The ancestral gene for transcribed, low-copy repeats in the Prader-Willi/Angelman region encodes a large protein implicated in protein trafficking, which is deficient in mice with neuromuscular and spermiogenic abnormalities. *Hum Mol Genet* **8**, 533–542 (1999).
55. Arimitsu, N. *et al.* p125/Sec. 23-interacting protein (Sec. 23ip) is required for spermiogenesis. *FEBS Lett* **585**, 2171–2176 (2011).
56. Jones, J. & Macdonald, P. M. Neurl4 contributes to germ cell formation and integrity in Drosophila. *Biol Open* **4**, 937–946 (2015).
57. Al-Hakim, A. K., Bashkurov, M., Gingras, A. C., Durocher, D. & Pelletier, L. Interaction proteomics identify NEURL4 and the HECT E3 ligase HERC2 as novel modulators of centrosome architecture. *Mol Cell Proteomics* **11**(M111), 014233 (2012).
58. Kuhnle, S. *et al.* Physical and functional interaction of the HECT ubiquitin-protein ligases E6AP and HERC2. *J Biol Chem* **286**, 19410–19416 (2011).
59. Imai, Y. *et al.* The Parkinson's Disease-Associated Protein Kinase LRRK2 Modulates Notch Signaling through the Endosomal Pathway. *PLoS Genet* **11**, e1005503 (2015).
60. Emmott, E. & Goodfellow, I. Identification of protein interaction partners in mammalian cells using SILAC-immunoprecipitation quantitative proteomics. *J Vis Exp* (2014).
61. Charrier, C. *et al.* Inhibition of SRGAP2 function by its human-specific paralogs induces neoteny during spine maturation. *Cell* **149**, 923–935 (2012).
62. Callaerts, P., Halder, G. & Gehring, W. J. PAX-6 in development and evolution. *Annu Rev Neurosci* **20**, 483–532 (1997).
63. Lee, H. J. *et al.* A post-transcriptional program coordinated by CSDE1 prevents intrinsic neural differentiation of human embryonic stem cells. *Nat Commun* **8**, 1456 (2017).
64. Jang, J. H. FIGC, a novel FGF-induced ubiquitin-protein ligase in gastric cancers. *FEBS Lett* **578**, 21–25 (2004).
65. Ashton-Beaucage, D. *et al.* The Deubiquitinase USP47 Stabilizes MAPK by Counteracting the Function of the N-end Rule ligase POE/UBR4 in Drosophila. *PLoS Biol* **14**, e1002539 (2016).
66. Hong, J. H. *et al.* KCMF1 (potassium channel modulatory factor 1) Links RAD6 to UBR4 (ubiquitin N-recognition domain-containing E3 ligase 4) and lysosome-mediated degradation. *Mol Cell Proteomics* **14**, 674–685 (2015).
67. Jiang, J., Mohan, P. & Maxwell, C. A. The cytoskeletal protein RHAMM and ERK1/2 activity maintain the pluripotency of murine embryonic stem cells. *PLoS One* **8**, e73548 (2013).
68. Luzzani, C. *et al.* Modulation of chromatin modifying factors' gene expression in embryonic and induced pluripotent stem cells. *Biochem Biophys Res Commun* **410**, 816–822 (2011).
69. Tasaki, T., Sriram, S. M., Park, K. S. & Kwon, Y. T. The N-end rule pathway. *Annu Rev Biochem* **81**, 261–289 (2012).
70. Zimmerman, S. W. *et al.* Identification and characterization of RING-finger ubiquitin ligase UBR7 in mammalian spermatozoa. *Cell Tissue Res* **356**, 261–278 (2014).
71. Zhong, J. F. *et al.* Gene regulation networks related to neural differentiation of hESC. *Gene Expr* **14**, 23–34 (2007).
72. Yamane, M., Fujii, S., Ohtsuka, S. & Niwa, H. Zscan10 is dispensable for maintenance of pluripotency in mouse embryonic stem cells. *Biochem Biophys Res Commun* **468**, 826–831 (2015).
73. Huijbregtse, J. M., Scheffner, M. & Howley, P. M. Cloning and expression of the cDNA for E6-AP, a protein that mediates the interaction of the human papillomavirus E6 oncoprotein with p53. *Mol Cell Biol* **13**, 775–784 (1993).
74. Williams, C. A. *et al.* Angelman syndrome. *Curr Probl Pediatr* **25**, 216–231 (1995).
75. Buiting, K. Prader-Willi syndrome and Angelman syndrome. *Am J Med Genet C Semin Med Genet* **154C**, 365–376 (2010).
76. Bolton, P. F. *et al.* The phenotypic manifestations of interstitial duplications of proximal 15q with special reference to the autistic spectrum disorders. *Am J Med Genet* **105**, 675–685 (2001).
77. Khatri, N. *et al.* The autism protein Ube3A/E6AP remodels neuronal dendritic arborization via caspase-dependent microtubule destabilization. *J Neurosci* (2017).
78. Kuhnle, S., Mothes, B., Matentzoglou, K. & Scheffner, M. Role of the ubiquitin ligase E6AP/UBE3A in controlling levels of the synaptic protein Arc. *Proc Natl Acad Sci USA* **110**, 8888–8893 (2013).
79. Miura, K. *et al.* Neurobehavioral and electroencephalographic abnormalities in Ube3a maternal-deficient mice. *Neurobiol Dis* **9**, 149–159 (2002).
80. Mishra, A., Godavarthi, S. K. & Jana, N. R. UBE3A/E6-AP regulates cell proliferation by promoting proteasomal degradation of p27. *Neurobiol Dis* **36**, 26–34 (2009).
81. Mishra, A. *et al.* E6-AP association promotes SOD1 aggregates degradation and suppresses toxicity. *Neurobiol Aging* **34**(1310), e1311–1323 (2013).
82. Mishra, A., Godavarthi, S. K., Maheshwari, M., Goswami, A. & Jana, N. R. The ubiquitin ligase E6-AP is induced and recruited to aggregates in response to proteasome inhibition and may be involved in the ubiquitination of Hsp70-bound misfolded proteins. *J Biol Chem* **284**, 10537–10545 (2009).
83. Toh, C. X. *et al.* RNAi Reveals Phase-Specific Global Regulators of Human Somatic Cell Reprogramming. *Cell Rep* **15**, 2597–2607 (2016).
84. Huang, Y. Y., Lu, H., Liu, S., Droz-Rosario, R. & Shen, Z. Requirement of mouse BCCIP for neural development and progenitor proliferation. *PLoS One* **7**, e30638 (2012).

85. Lim, H. J. *et al.* Regulation of c-Myc Expression by Ahnak Promotes Induced Pluripotent Stem Cell Generation. *J Biol Chem* **291**, 752–761 (2016).
86. Schroer, T. A. Dynactin. *Annu Rev Cell Dev Biol* **20**, 759–779 (2004).
87. Williams, S. E., Beronja, S., Pasolli, H. A. & Fuchs, E. Asymmetric cell divisions promote Notch-dependent epidermal differentiation. *Nature* **470**, 353–358 (2011).
88. Inoue, D. *et al.* Dzip3 regulates developmental genes in mouse embryonic stem cells by reorganizing 3D chromatin conformation. *Sci Rep* **5**, 16567 (2015).
89. Freund, A. *et al.* Proteostatic control of telomerase function through TRiC-mediated folding of TCAB1. *Cell* **159**, 1389–1403 (2014).
90. Lopez, T., Dalton, K. & Frydman, J. The Mechanism and Function of Group II Chaperonins. *J Mol Biol* **427**, 2919–2930 (2015).
91. Vander Heiden, M. G., Cantley, L. C. & Thompson, C. B. Understanding the Warburg effect: the metabolic requirements of cell proliferation. *Science* **324**, 1029–1033 (2009).
92. Varum, S. *et al.* Energy metabolism in human pluripotent stem cells and their differentiated counterparts. *PLoS One* **6**, e20914 (2011).
93. Uchiki, T. *et al.* The ubiquitin-interacting motif protein, S5a, is ubiquitinated by all types of ubiquitin ligases by a mechanism different from typical substrate recognition. *J Biol Chem* **284**, 12622–12632 (2009).
94. Kleijnen, M. F. *et al.* The hPLIC proteins may provide a link between the ubiquitination machinery and the proteasome. *Mol Cell* **6**, 409–419 (2000).
95. Lee, S. Y. *et al.* Ube3a, the E3 ubiquitin ligase causing Angelman syndrome and linked to autism, regulates protein homeostasis through the proteasomal shuttle Rpn10. *Cell Mol Life Sci* **71**, 2747–2758 (2014).
96. Tomaic, V. & Banks, L. Angelman syndrome-associated ubiquitin ligase UBE3A/E6AP mutants interfere with the proteolytic activity of the proteasome. *Cell Death Dis* **6**, e1625 (2015).
97. Efroni, S. *et al.* Global transcription in pluripotent embryonic stem cells. *Cell Stem Cell* **2**, 437–447 (2008).
98. Kim, Y. D. *et al.* The unique spliceosome signature of human pluripotent stem cells is mediated by SNRPA1, SNRPD1, and PNN. *Stem Cell Res* **22**, 43–53 (2017).
99. Botti, V. *et al.* Cellular differentiation state modulates the mRNA export activity of SR proteins. *J Cell Biol* **216**, 1993–2009 (2017).
100. Fang, X. *et al.* Landscape of the SOX2 protein-protein interactome. *Proteomics* **11**, 921–934 (2011).
101. Tan, Y. *et al.* MFG-E8 Is Critical for Embryonic Stem Cell-Mediated T Cell Immunomodulation. *Stem Cell Reports* **5**, 741–752 (2015).
102. Lee, S. H., Lee, Y. J., Park, S. W., Kim, H. S. & Han, H. J. Caveolin-1 and integrin beta1 regulate embryonic stem cell proliferation via p38 MAPK and FAK in high glucose. *J Cell Physiol* **226**, 1850–1859 (2011).
103. Heck, J. W., Cheung, S. K. & Hampton, R. Y. Cytoplasmic protein quality control degradation mediated by parallel actions of the E3 ubiquitin ligases Ubr1 and San1. *Proc Natl Acad Sci USA* **107**, 1106–1111 (2010).
104. Lee, J. T. & Gu, W. The multiple levels of regulation by p53 ubiquitination. *Cell Death Differ* **17**, 86–92 (2010).
105. Rubenstein, E. M. & Hochstrasser, M. Redundancy and variation in the ubiquitin-mediated proteolytic targeting of a transcription factor. *Cell Cycle* **9**, 4282–4285 (2010).
106. Xie, Y., Rubenstein, E. M., Matt, T. & Hochstrasser, M. SUMO-independent *in vivo* activity of a SUMO-targeted ubiquitin ligase toward a short-lived transcription factor. *Genes Dev* **24**, 893–903 (2010).
107. Ingolia, N. T., Lareau, L. F. & Weissman, J. S. Ribosome profiling of mouse embryonic stem cells reveals the complexity and dynamics of mammalian proteomes. *Cell* **147**, 789–802 (2011).
108. Savic, N. *et al.* lncRNA maturation to initiate heterochromatin formation in the nucleolus is required for exit from pluripotency in ESCs. *Cell Stem Cell* **15**, 720–734 (2014).
109. Jacinto, F. V., Benner, C. & Hetzer, M. W. The nucleoporin Nup153 regulates embryonic stem cell pluripotency through gene silencing. *Genes Dev* **29**, 1224–1238 (2015).
110. Allen, N. D. & Baird, D. M. Telomere length maintenance in stem cell populations. *Biochim Biophys Acta* **1792**, 324–328 (2009).
111. Zeng, S. *et al.* Telomerase-mediated telomere elongation from human blastocysts to embryonic stem cells. *J Cell Sci* **127**, 752–762 (2014).
112. Cho, J. *et al.* LIN28A is a suppressor of ER-associated translation in embryonic stem cells. *Cell* **151**, 765–777 (2012).
113. Peng, S. *et al.* Genome-wide studies reveal that Lin28 enhances the translation of genes important for growth and survival of human embryonic stem cells. *Stem Cells* **29**, 496–504 (2011).
114. Wilbert, M. L. *et al.* LIN28 binds messenger RNAs at GGAGA motifs and regulates splicing factor abundance. *Mol Cell* **48**, 195–206 (2012).
115. Xu, B., Zhang, K. & Huang, Y. Lin28 modulates cell growth and associates with a subset of cell cycle regulator mRNAs in mouse embryonic stem cells. *RNA* **15**, 357–361 (2009).
116. Zhang, J. *et al.* LIN28 Regulates Stem Cell Metabolism and Conversion to Primed Pluripotency. *Cell Stem Cell* **19**, 66–80 (2016).
117. Iconomou, M. & Saunders, D. N. Systematic approaches to identify E3 ligase substrates. *Biochem J* **473**, 4083–4101 (2016).
118. O'Connor, H. F. & Huibregtse, J. M. Enzyme-substrate relationships in the ubiquitin system: approaches for identifying substrates of ubiquitin ligases. *Cell Mol Life Sci* **74**, 3363–3375 (2017).
119. Sheng, Y. *et al.* Molecular recognition of p53 and MDM2 by USP7/HAUSP. *Nat Struct Mol Biol* **13**, 285–291 (2006).
120. Pierce, N. W., Kleiger, G., Shan, S. O. & Deshaies, R. J. Detection of sequential polyubiquitylation on a millisecond timescale. *Nature* **462**, 615–619 (2009).
121. Jain, A. K. & Barton, M. C. Regulation of p53: TRIM24 enters the RING. *Cell Cycle* **8**, 3668–3674 (2009).
122. Xu, P. *et al.* Quantitative proteomics reveals the function of unconventional ubiquitin chains in proteasomal degradation. *Cell* **137**, 133–145 (2009).
123. Ding, W. X. *et al.* Linking of autophagy to ubiquitin-proteasome system is important for the regulation of endoplasmic reticulum stress and cell viability. *Am J Pathol* **171**, 513–524 (2007).
124. Pandey, U. B. *et al.* HDAC6 rescues neurodegeneration and provides an essential link between autophagy and the UPS. *Nature* **447**, 859–863 (2007).
125. Chambers, S. M. *et al.* Highly efficient neural conversion of human ES and iPS cells by dual inhibition of SMAD signaling. *Nat Biotechnol* **27**, 275–280 (2009).
126. Rao, J. *et al.* Stepwise Clearance of Repressive Roadblocks Drives Cardiac Induction in Human ESCs. *Cell Stem Cell* **18**, 554–556 (2016).
127. Cong, L. *et al.* Multiplex genome engineering using CRISPR/Cas systems. *Science* **339**, 819–823 (2013).
128. Ran, F. A. *et al.* Double nicking by RNA-guided CRISPR Cas9 for enhanced genome editing specificity. *Cell* **154**, 1380–1389 (2013).
129. Rappsilber, J., Ishihama, Y. & Mann, M. Stop and go extraction tips for matrix-assisted laser desorption/ionization, nanoelectrospray, and LC/MS sample pretreatment in proteomics. *Anal Chem* **75**, 663–670 (2003).
130. Cox, J. & Mann, M. MaxQuant enables high peptide identification rates, individualized p.p.b.-range mass accuracies and proteome-wide protein quantification. *Nat Biotechnol* **26**, 1367–1372 (2008).
131. Cox, J. *et al.* Accurate proteome-wide label-free quantification by delayed normalization and maximal peptide ratio extraction, termed MaxLFQ. *Mol Cell Proteomics* **13**, 2513–2526 (2014).

132. Cox, J. & Mann, M. 1D and 2D annotation enrichment: a statistical method integrating quantitative proteomics with complementary high-throughput data. *BMC Bioinformatics* **13**(Suppl 16), S12 (2012).
133. Li, W. *et al.* Genome-wide and functional annotation of human E3 ubiquitin ligases identifies MULAN, a mitochondrial E3 that regulates the organelle's dynamics and signaling. *PLoS One* **3**, e1487 (2008).
134. Dobin, A. *et al.* STAR: ultrafast universal RNA-seq aligner. *Bioinformatics* **29**, 15–21 (2013).
135. Trapnell, C. *et al.* Differential gene and transcript expression analysis of RNA-seq experiments with TopHat and Cufflinks. *Nat Protoc* **7**, 562–578 (2012).
136. Kisselev, A. F. & Goldberg, A. L. Monitoring activity and inhibition of 26S proteasomes with fluorogenic peptide substrates. *Methods Enzymol* **398**, 364–378 (2005).
137. Shannon, P. *et al.* Cytoscape: a software environment for integrated models of biomolecular interaction networks. *Genome Res* **13**, 2498–2504 (2003).
138. Mi, H., Muruganujan, A., Casagrande, J. T. & Thomas, P. D. Large-scale gene function analysis with the PANTHER classification system. *Nat Protoc* **8**, 1551–1566 (2013).

Acknowledgements

This work was supported by the European Research Council (ERC Starting Grant-677427 StemProteostasis), the Deutsche Forschungsgemeinschaft (DFG) (CECAD), and the Alexander von Humboldt Stiftung. We thank Christina Schindler for her technical support. We thank the CECAD Proteomics Facility and the Cologne Center for Genomics (CCG) for their advice and contribution in proteomics and RNA sequencing experiments, respectively.

Author Contributions

I.S. and S.K. performed all of the experiments, most of the data analysis and interpretation through discussions with D.V. R.G. performed the Cytoscape analysis. C.D. performed bioinformatic analysis of transcriptomics data and some proteomics data. D.V. planned and supervised the project. The manuscript was written by I.S. and D.V. All the authors discussed the results and commented on the manuscript.

Additional Information

Supplementary information accompanies this paper at <https://doi.org/10.1038/s41598-018-22384-9>.

Competing Interests: The authors declare no competing interests.

Publisher's note: Springer Nature remains neutral with regard to jurisdictional claims in published maps and institutional affiliations.



Open Access This article is licensed under a Creative Commons Attribution 4.0 International License, which permits use, sharing, adaptation, distribution and reproduction in any medium or format, as long as you give appropriate credit to the original author(s) and the source, provide a link to the Creative Commons license, and indicate if changes were made. The images or other third party material in this article are included in the article's Creative Commons license, unless indicated otherwise in a credit line to the material. If material is not included in the article's Creative Commons license and your intended use is not permitted by statutory regulation or exceeds the permitted use, you will need to obtain permission directly from the copyright holder. To view a copy of this license, visit <http://creativecommons.org/licenses/by/4.0/>.

© The Author(s) 2018

Supplementary Information

Insights into the ubiquitin-proteasome system of human embryonic stem cells

Isabel Saez^{1#}, Seda Koyuncu^{1#}, Ricardo Gutierrez-Garcia¹, Christoph Dieterich² and David Vilchez¹

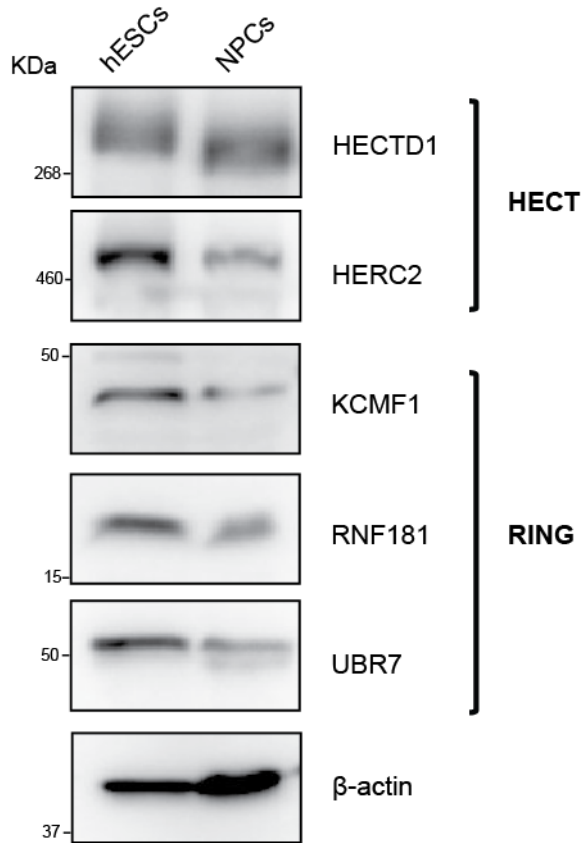
¹ Institute for Genetics and Cologne Excellence Cluster for Cellular Stress Responses in Aging-Associated Diseases (CECAD), University of Cologne, Joseph-Stelzmann-Strasse 26, 50931 Cologne, Germany.

² Section of Bioinformatics and Systems Cardiology, Department of Internal Medicine III and Klaus Tschira Institute for Computational Cardiology, Neuenheimer Feld 669, University Hospital, 69120 Heidelberg, Germany.

[#] These authors contributed equally to this work.

Supplementary Figure 1

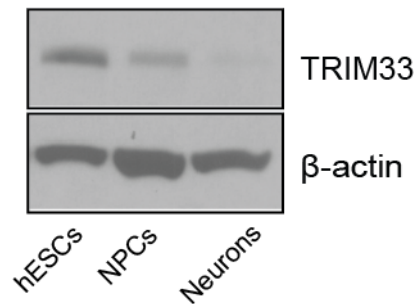
H1 hESCs



Supplementary Figure 1. Analysis of E3 protein levels in H1 hESCs. Western blot with antibodies against HECTD1, HERC2, KCMF1, RNF181 and UBR7 comparing H1 hESCs with their neural (NPC) counterparts. β -actin is the loading control.

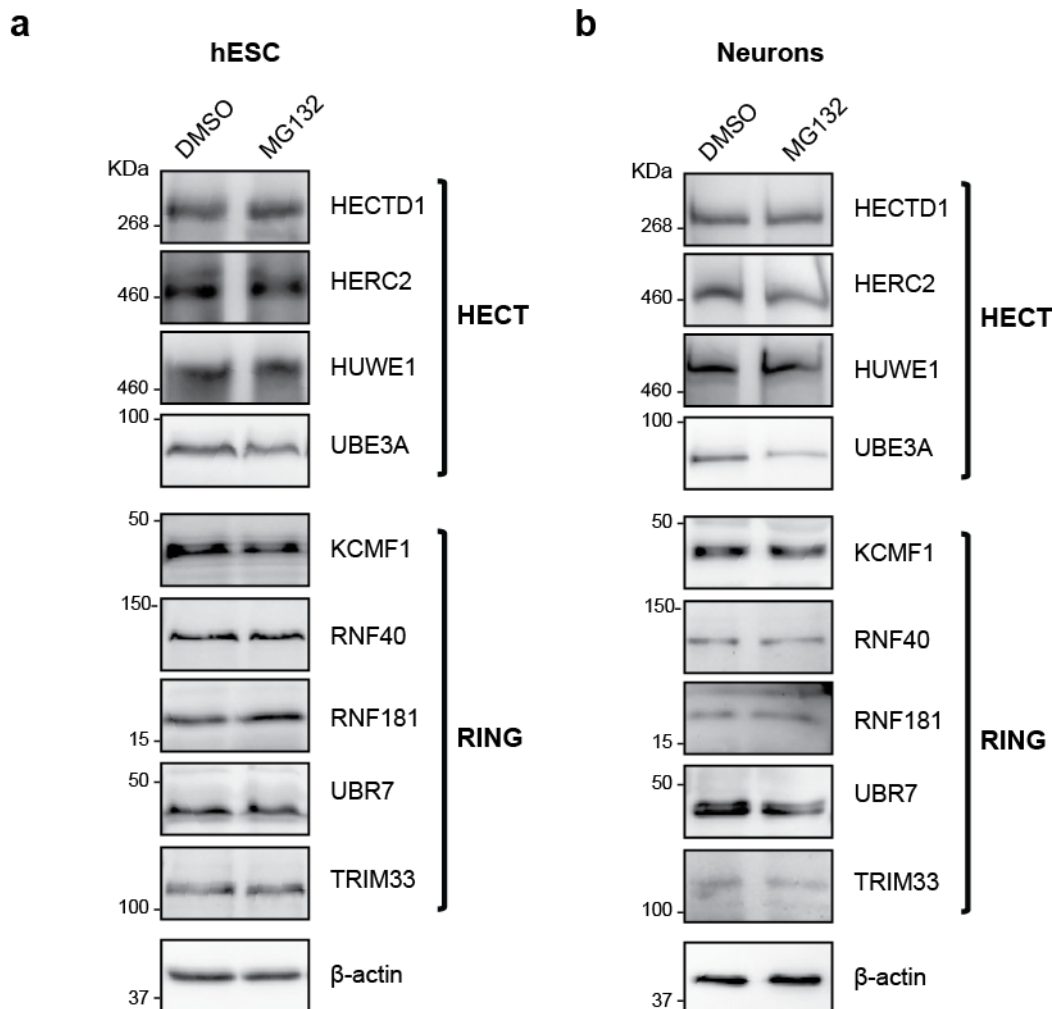
Supplementary Figure 2

H9 hESCs



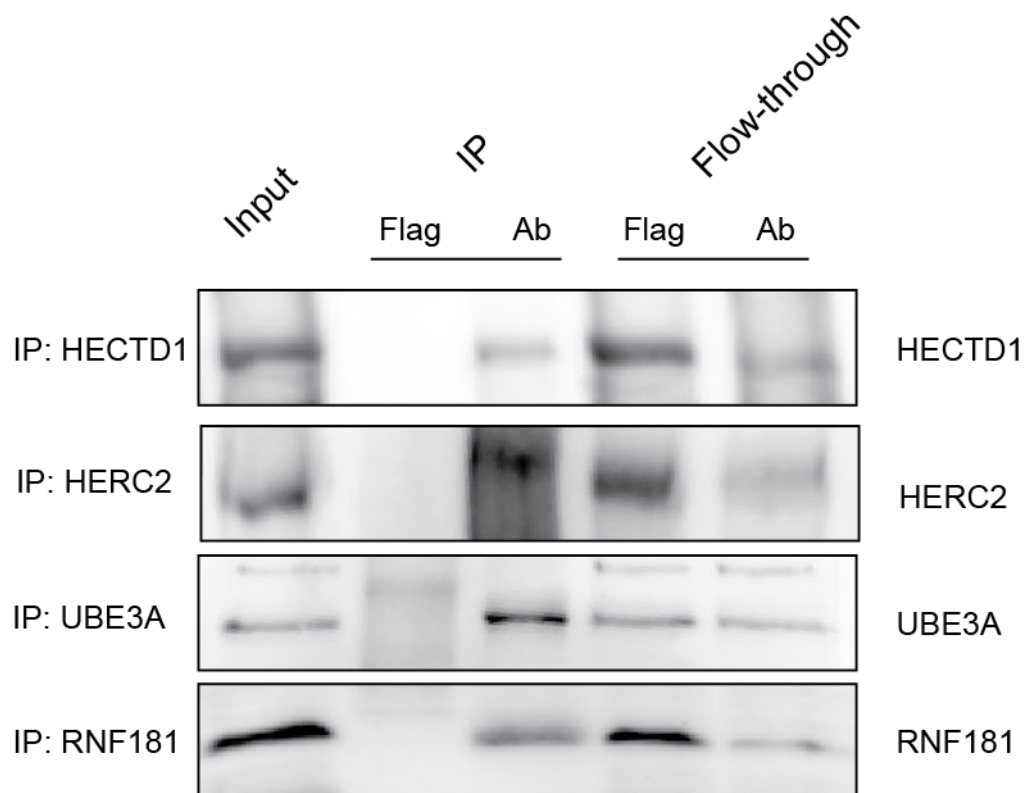
Supplementary Figure 2. Analysis of TRIM33 protein levels in H9 hESCs. Western blot with antibody against TRIM33 comparing H9 hESCs with their differentiated neural (NPC) and neuronal counterparts. β -actin is the loading control. Although two independent experiments showed a decrease in TRIM33 levels during neuronal differentiation as we observed in our proteomics analysis, this downregulation was not consistent in other neural differentiation experiments (please see **Fig. 1a**).

Supplementary Figure 3



Supplementary Figure 3. Proteasome inhibition does not change protein levels of the tested E3 ligases. Western Blot analysis with antibodies against the indicated E3 enzymes of (a) H9 hESCs and (b) terminally differentiated neurons upon proteasome inhibition. Cells were treated with 1 μ M MG132 for 16 h. β -actin is the loading control. The images are representative of at least two independent experiments. All cropped blots were run under the same experimental conditions.

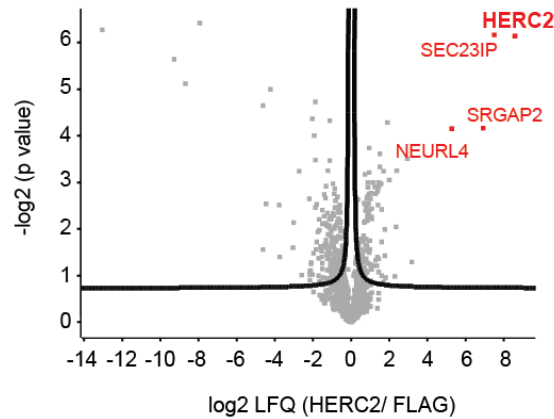
Supplementary Figure 4



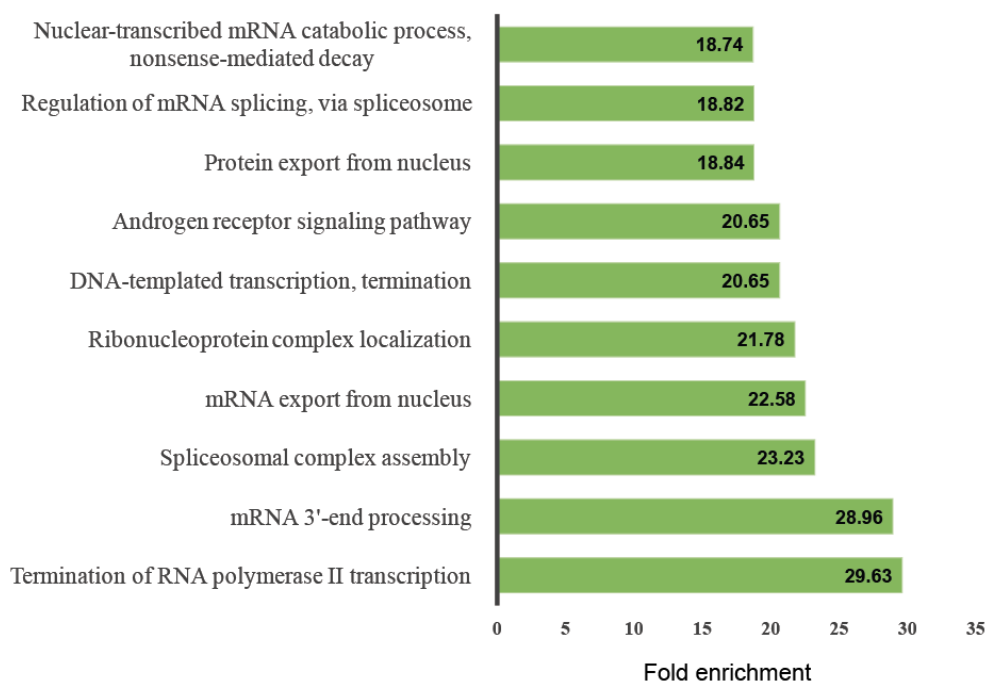
Supplementary Figure 4. Flow-through controls indicate significant immunoprecipitation of endogenous E3 enzymes. Co-immunoprecipitation (co-IP) with HERC2, HECTD1, UBE3A, RNF181 and FLAG antibodies from H9 hESCs followed by western blot against the respective E3 ubiquitin ligases. We loaded the same amount of total input and flow-through (8% of the sample) for direct comparison. We loaded 20% of total immunoprecipitated sample. The images are representative of two independent experiments.

Supplementary Figure 5

a

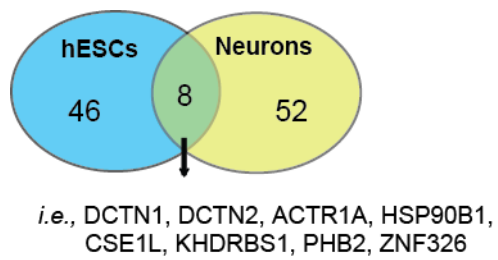


b



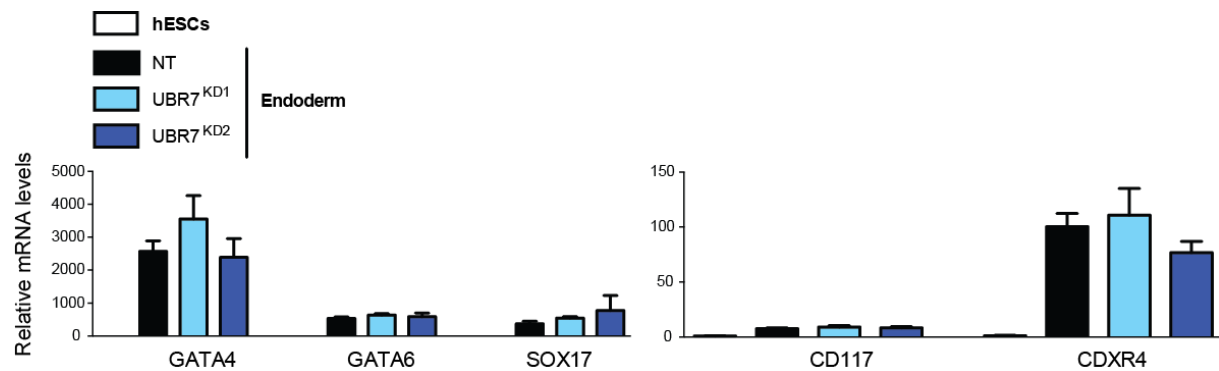
Supplementary Figure 5. Significant enriched proteins upon co-immunoprecipitation with HERC2 antibody under standard conditions (no RNase treatment). (a) Volcano plot of the interactome of HERC2 in H9 hESCs under standard immunoprecipitation conditions ($n = 4$). Graph represents the $-\log_2(p\text{-value})$ of a two-tailed t -test plotted against the \log_2 ratio of protein label-free quantification (LFQ) values from co-IP experiments with HERC2 antibody compared to control co-IP with FLAG antibody. Red colored dots indicate the most enriched interacting proteins after correction for multiple testing (FDR < 0.2, $s_0 = 0.1$). (b) Bar graph representing the top GOBPs of HECTD1 interactome ($P < 0.05$).

Supplementary Figure 6



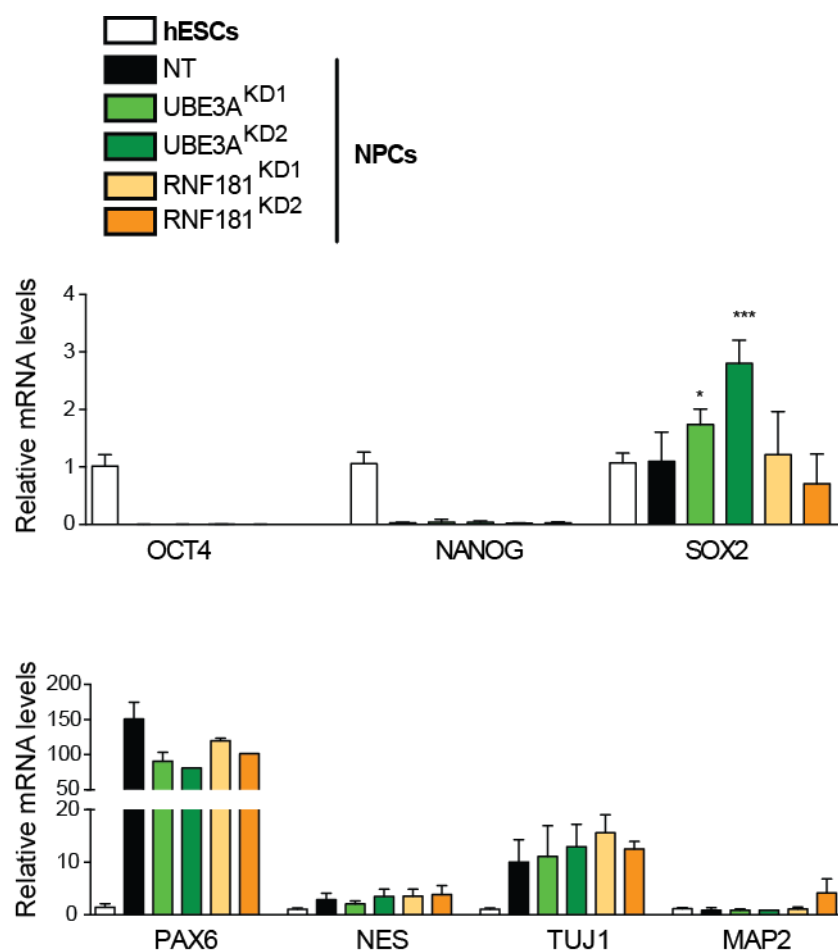
Supplementary Figure 6. Venn diagram represents total number and common significant interactors in hESCs and their differentiated neuronal counterparts (FDR <0.2 was considered significant, hESCs (n= 4) and neurons (n= 3)).

Supplementary Figure 7



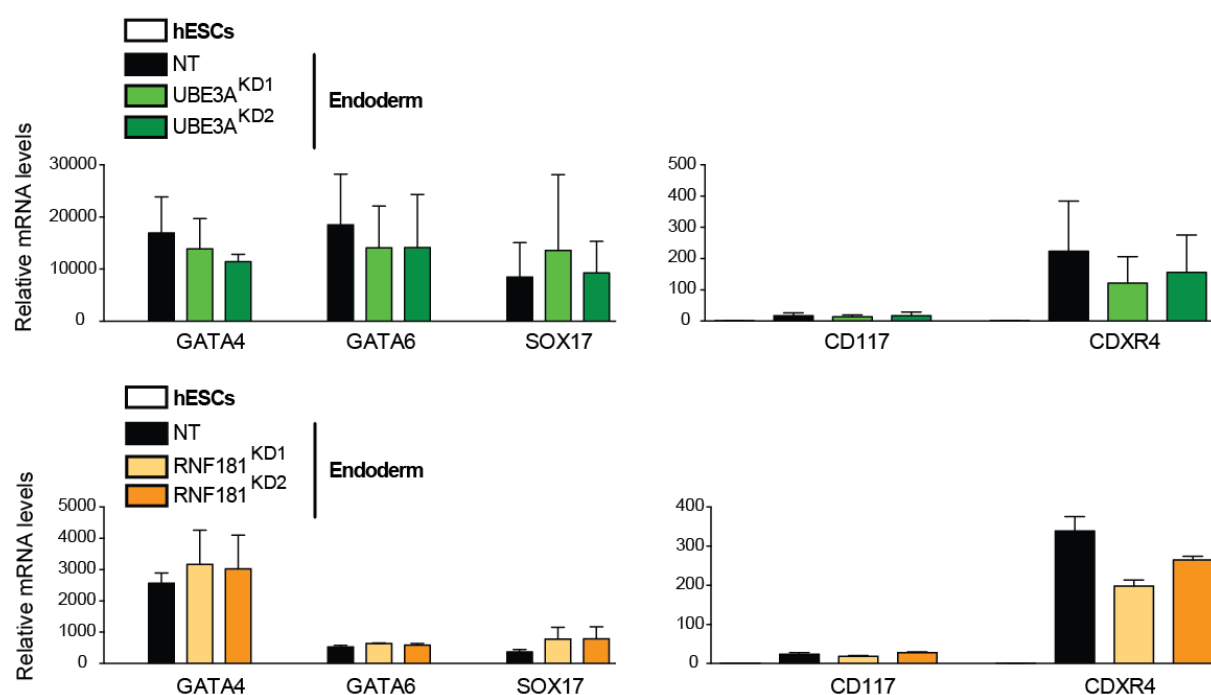
Supplementary Figure 7. Loss of UBR7 does not affect differentiation of hESCs into definitive endoderm. Real-time PCR analysis of endodermal markers in UBR7 KD H9 hESCs after definitive endodermal differentiation. Graphs (relative expression to NT) represent the mean \pm s.e.m. of two independent experiments. Statistical comparisons were made by Student's *t*-test for unpaired samples.

Supplementary Figure 8



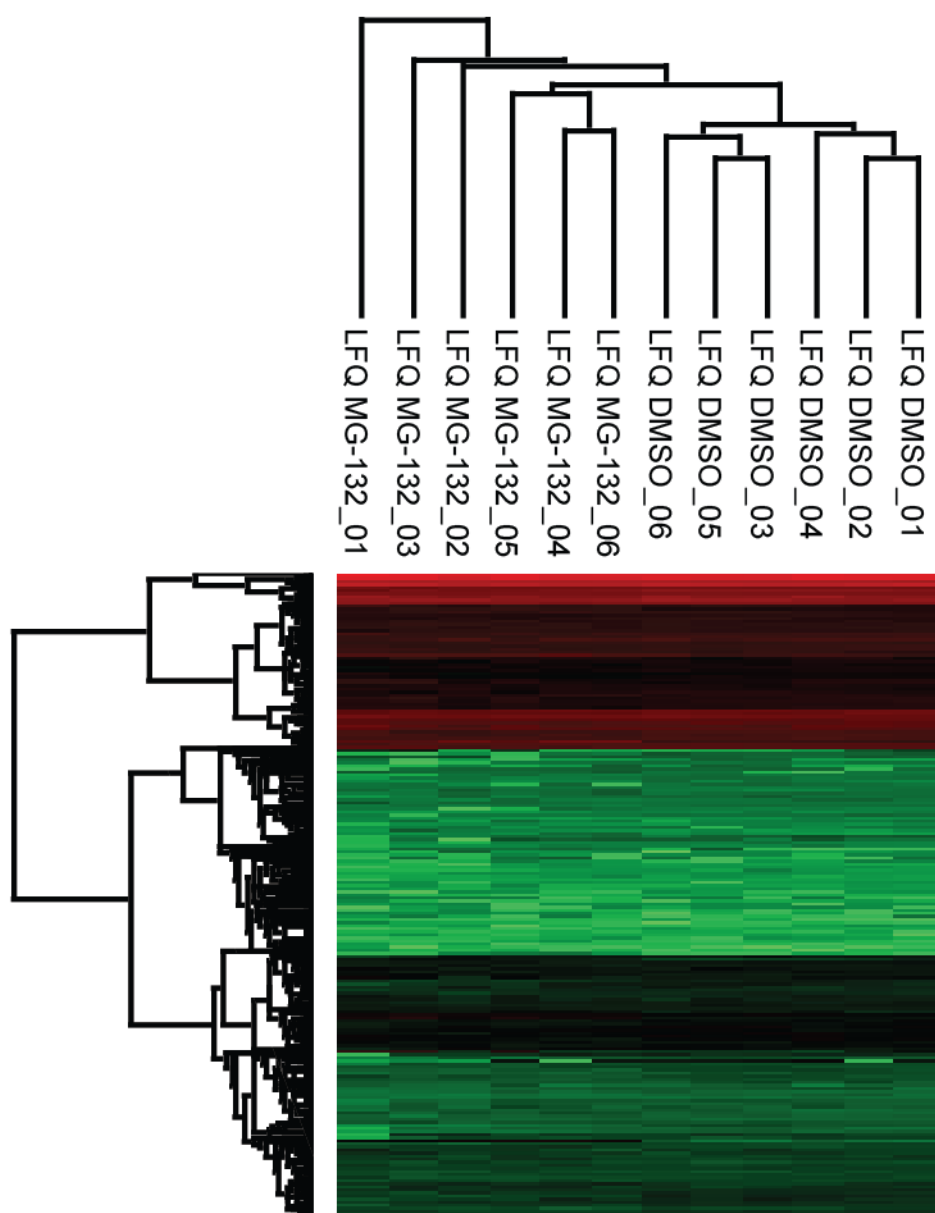
Supplementary Figure 8. Analysis of neural markers upon differentiation of UBE3A and RNF181 KD hESCs. Real-time PCR analysis of pluripotency (upper panel) and neuroectodermal markers (lower panel) in UBE3A and RNF181 KD H9 hESCs after 10 days of neural differentiation. Graphs (relative expression to NT) represent the mean \pm s.e.m. of two independent experiments. Statistical comparisons were made by Student's t-test for unpaired samples. P-value: *P<0.05, ***P<0.001.

Supplementary Figure 9



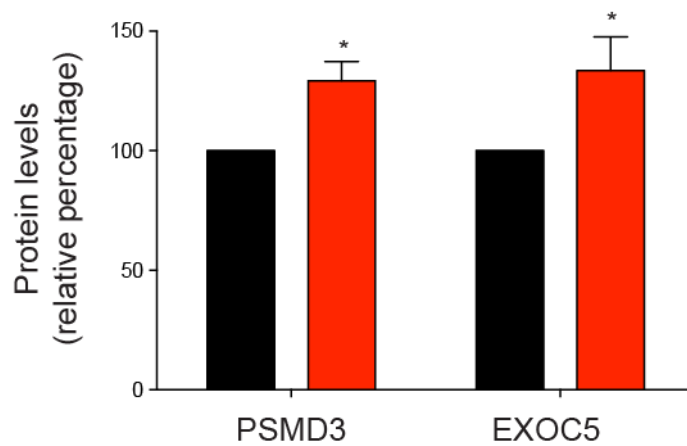
Supplementary Figure 9. Loss of UBE3A and RNF181 does not affect differentiation of hESCs into definitive endoderm. Real-time PCR analysis of endodermal markers in UBE3A (upper panel) and RNF181 (lower panel) KD H9 hESCs after definitive endodermal differentiation. Graphs (relative expression to NT) represent the mean \pm s.e.m. of two independent experiments. Statistical comparisons were made by Student's *t*-test for unpaired samples.

Supplementary Figure 10



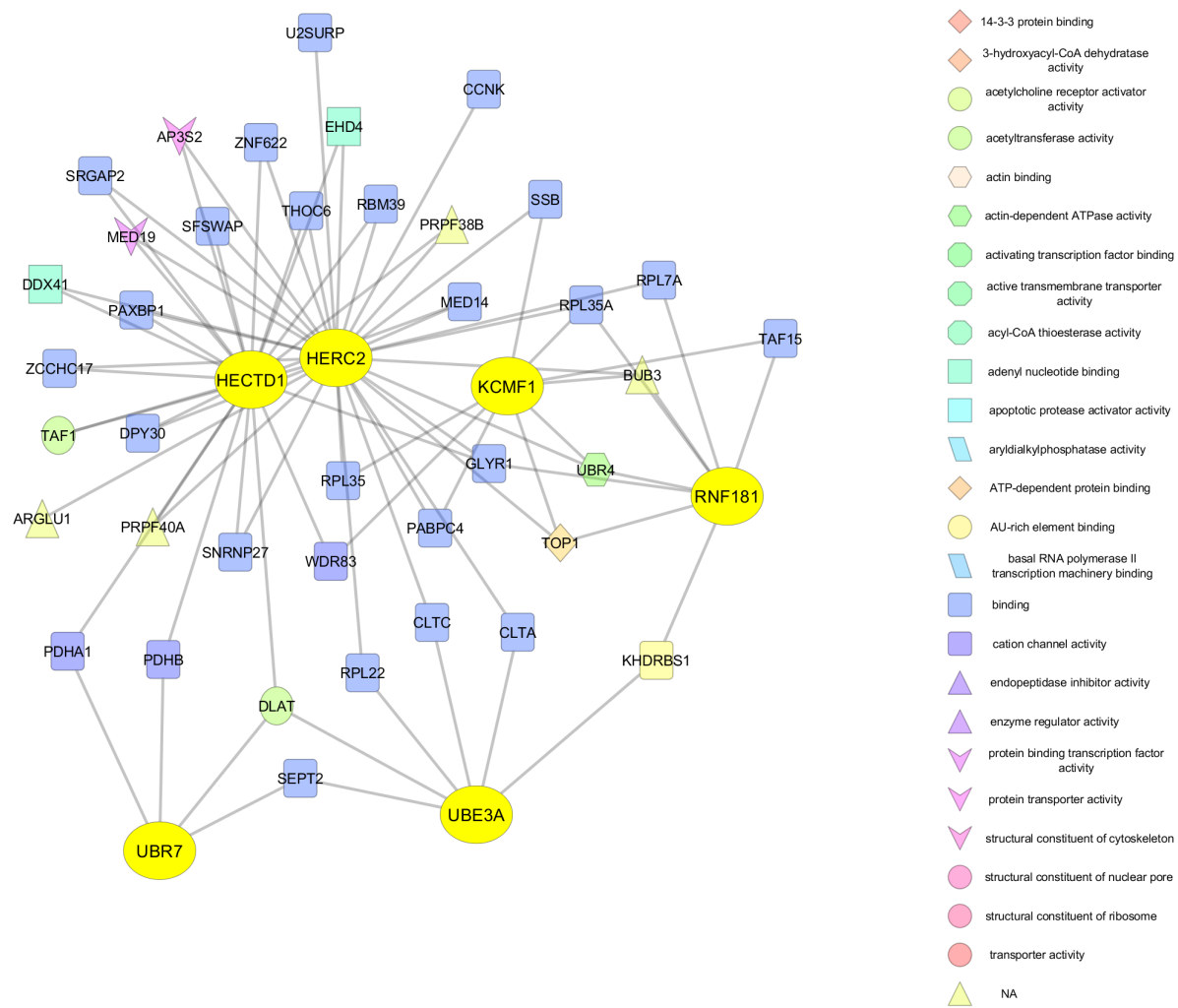
Supplementary Figure 10. Label-free quantification (LFQ) of 2735 proteins reveals partial separation of MG-132-treated H9 hESCs and control DMSO-treated H9 hESCs (n= 6). Proteins (rows) and samples (columns) are clustered according to euclidean distance (red= low, green= high abundance). Proteasome inhibitor: 1 μ M MG-132 for 24 h.

Supplementary Figure 11



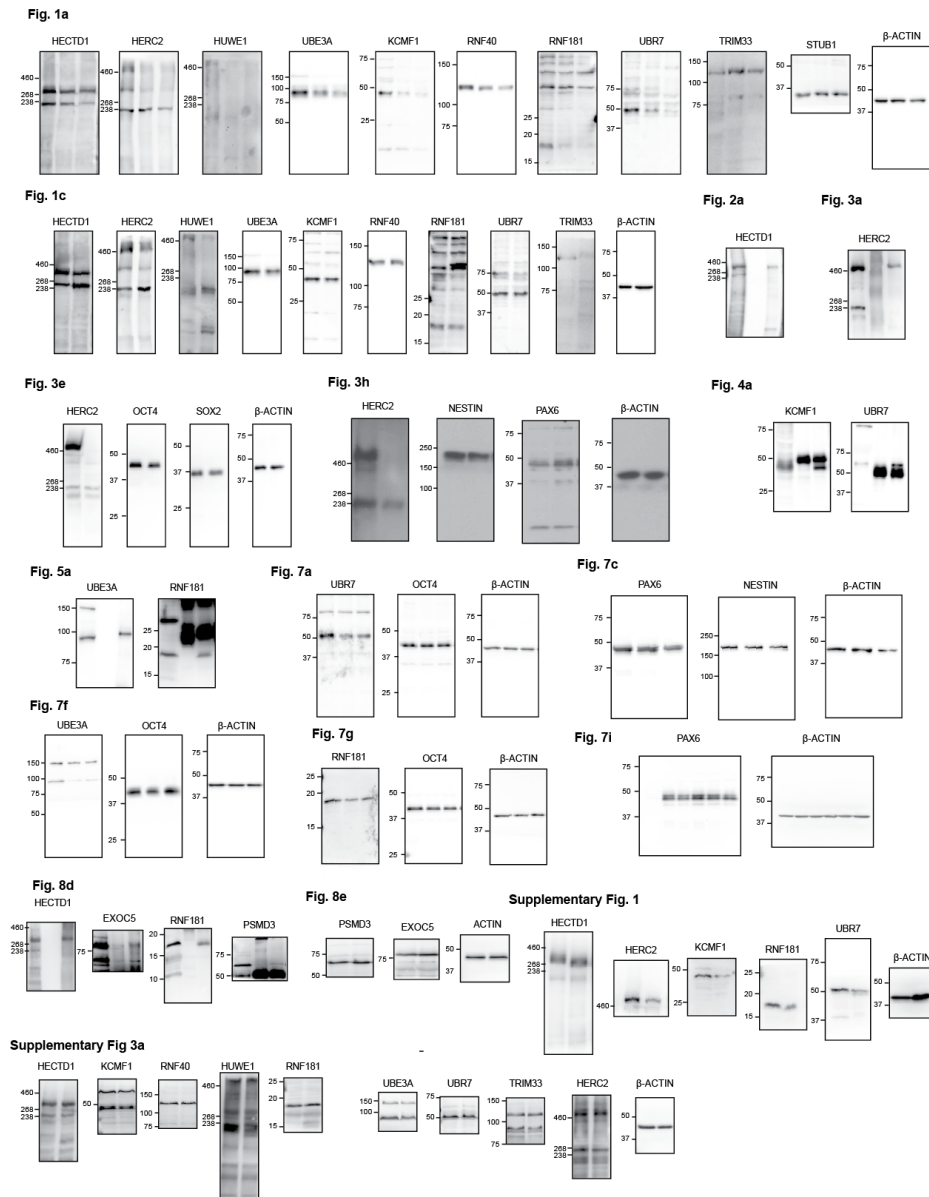
Supplementary Figure 11. Proteasome inhibition results in increased levels of PSMD3 and EXOC5. Quantification of the western blots presented in Figure 8e. The graph represents the relative percentage values to DMSO-treated H9 of PSMD3 and EXOC5 corrected for β -actin loading control (mean \pm s.e.m. of three independent experiments). Statistical comparisons were made by Student's *t*-test for unpaired samples. P-value: *P<0.05.

Supplementary Figure 12



Supplementary Figure 12. Schematic network showing proteins that interact with at least two of the tested E3 enzymes.

Supplementary Figure 13



Supplementary Figure 13. Uncropped images of western blots experiments. Uncropped images are presented with molecular weight ladders.

Protein names	Domain	hESCs vs Neurons (fold enrichment)	-Log p-value	q-value	Differences supported by Western blot
FBXO22	RING	1.85	5.43	0	Not tested
KLHL4	RING	2.22	5.69	0	Not tested
TRIM24	RING	1.42	8.01	0	Not tested
TRIM28	RING	1.26	11.20	0	Not tested
TRIP12	HECT	2.08	7.,20	0	Not tested
UBR5	HECT	2.98	6.99	0	Not tested
IVNS1ABP	RING	3.20	4.01	0.0000124	Not tested
KLHL7	RING	1.72	4.26	0.0000136	Not tested
RBX1	RING	1.01	5.54	0.0000138	Not tested
TRIM33	RING	1.31	4.81	0.0000139	NO
PPIL2	RING	1.96	4.28	0.0000145	Not tested
UHRF1	RING	2.42	3.71	0.0000180	Not tested
SKP2	RING	1.77	3.86	0.0000242	Not tested
KEAP1	RING	2.69	3.31	0.0000380	Not tested
ARIH2	RING	0.79	4.94	0.0000506	Not tested
UBR7	RING	2.28	3.08	0.0000536	YES
RBBP6	RING	2.81	2.66	0.0000964	Not tested
ZNF598	RING	1.55	2.80	0.000143	Not tested
UBE4B	RING	0.89	3.33	0.000191	Not tested
TRIM65	RING	1.46	2.51	0.000283	Not tested
UBE3A	HECT	0.63	3.64	0.000345	YES
RNF2	RING	0.67	3.07	0.000645	Not tested
NOSIP	RING	0.69	2.96	0.000680	Not tested
TRIM56	RING	1.21	1.96	0.00139	Not tested
RNF40	RING	0.43	3.48	0.00166	YES
RNF20	RING	0.38	3.37	0.00285	Not tested
HERC2	HECT	0.79	1.91	0.00288	YES
RNF181	RING	1.53	1.53	0.00307	YES
HECTD1	HECT	0.55	2.61	0.00367	YES
KCMF1	RING	0.73	1.83	0.00379	YES
RNF138	RING	1.15	0.77	0.0468	Not tested
KCTD15	RING	0.59	0.79	0.0645	Not tested
BRAP	RING	0.78	0.71	0.0702	Not tested
TRAF2	RING	0.25	1.08	0.0934	Not tested
HUWE1	HECT	0.12	2.45	0.162	YES

Supplementary Table 1. List of E3 ubiquitin ligases increased in hESCs compared with their neuronal counterparts. Statistical comparisons were made by Student's t-test (n= 6). False Discovery Rate (FDR) adjusted p-value (q-value) <0.2 was considered significant. Up-regulated E3s in hESCs are ranked according to the q-value.

Primers for Real Time PCR used in this study

Gene	Primer sequence
HERC2 F	GCCTTACACGCAGCCATTACT
HERC2 R	TTCCTTCTGTGCTTCTTTTTTGG
UBE3A F	GACTCAAAGTTAGACGTGACCATATCA
UBE3A R	CTTCAAGTCTGCAGGATTTTCCA
UBR7 F	TGCCGGCTCTAGTTCTGAATC
UBR7 R	TTCTGCGTTGAGGCTTTCATT
KCMF1 F	GCCCCTAGAGATTTAGATGAATCG
KCMF1 R	CCCGGCCAGGGTGAAA
RNF181 F	CCTTGCCATCACCTTTTCCA
RNF181 R	GGACAGGAATTTGTCTTGCTTAGC
HECTD1 F	CAACAATTGTAAGTCTGCTCTCAACA
HECTD1 R	TCACCCTGCAATGCACTTTC
TRIM33 F	CACAGCCTACAAGCACCATGA
TRIM33 R	TGTGAGAATTGGATAAACCTGATGA
RNF40 F	CTCCCACCTGCGACACATC
RNF40 R	CCTCTGTGCGTAGCTTCTTCTG
HUWE1 F	CACAAGAAGGAGAGGAAATGGAA
HUWE1 R	AGTGCTGCTCGTTGTGGAATAC
GAPDH F	GCACCGTCAAGGCTGAGAAC
GAPDH R	GGATCTCGCTCCTGGAAGATG
ACTIN F	CTGGCACCCAGCACAAATG
ACTIN R	CCGATCCACACGGAGTACTTG
OCT4 F	GGAGGAAGCTGACAACAATGAAA
OCT4 R	GGCCTGCACGAGGGTTT
NANOG F	AAATCTAAGAGGTGGCAGAAAAACA
NANOG R	GCCTTCTGCGTCACACCATT
SOX 2 F	TGCGAGCGCTGCACAT
SOX 2 R	TCATGAGCGTCTTGGTTTTCC
DPPA4 F	CTGGTGCCAACAATTGAAGCT
DPPA4 R	AGGCACACAGGCGCTTATATG




MSX1 F	CTCCGCAAACACAAGACGAAC
MSX1 R	CACATGGGCCGTGTAGAGTC
GATA4 F	TCCGTGTCCCAGACGTTCTC
GATA4 R	GAGAGGACAGGGTGGATGGA
GATA6 F	AGCGCGTGCCTTCATCA
GATA6 R	GTGGTAGTTGTGGTGTGACAGTTG
ALBUMIN F	TGAGGTTGCTCATCGGTTTAAA
ALBUMIN R	GCAATCAACACCAAGGCTTTG
PAX6 F	CATACCAAGCGTGTCATCAATAAAC
PAX6 R	TGCGCCCATCTGTTGCT
NESTIN F	TGAAGGGCAATCACAACAGG
NESTIN R	TGACCCCAACATGACCTCTG
MAP2 F	AAAGAAGCTCAACATAAAGACCAGACT
MAP2 R	GTGGAGAAGGAGGCAGATTAGC
SOX1 F	GCTGACACCAGACTTGGGTT
SOX1 R	GTGCTTGGACCTGCCTTACT
TUJ1 F	GGCCAAGTTCTGGGAAGTCA
TUJ1 R	CGAGTCGCCCACGTAGTTG
SOX17 F	TGGCGCAGCAGAATCCA
SOX17 R	CGACTTGCCCAGCATCTTG
CD117 F	CCAAGGCCGACAAAAGGA
CD117 R	GGCGGGAGTCACATCTCTTTC
CDXR4 F	GGCCGACCTCCTCTTTGTC
CDXR4 R	TTGCCACGGCATCAACTG

ARTICLE

DOI: 10.1038/s41467-018-05320-3

OPEN

The ubiquitin ligase UBR5 suppresses proteostasis collapse in pluripotent stem cells from Huntington's disease patients

Seda Koyuncu ¹, Isabel Saez¹, Hyun Ju Lee¹, Ricardo Gutierrez-Garcia¹, Wojciech Pokrzywa^{1,2}, Azra Fatima¹, Thorsten Hoppe ¹ & David Vilchez ¹

Induced pluripotent stem cells (iPSCs) undergo unlimited self-renewal while maintaining their potential to differentiate into post-mitotic cells with an intact proteome. As such, iPSCs suppress the aggregation of polyQ-expanded huntingtin (HTT), the mutant protein underlying Huntington's disease (HD). Here we show that proteasome activity determines HTT levels, preventing polyQ-expanded aggregation in iPSCs from HD patients (HD-iPSCs). iPSCs exhibit high levels of UBR5, a ubiquitin ligase required for proteasomal degradation of both normal and mutant HTT. Conversely, loss of UBR5 increases HTT levels and triggers polyQ-expanded aggregation in HD-iPSCs. Moreover, UBR5 knockdown hastens polyQ-expanded aggregation and neurotoxicity in invertebrate models. Notably, UBR5 overexpression induces polyubiquitination and degradation of mutant HTT, reducing polyQ-expanded aggregates in HD-cell models. Besides HTT levels, intrinsic enhanced UBR5 expression determines global proteostasis of iPSCs preventing the aggregation of misfolded proteins ensued from normal metabolism. Thus, our findings indicate UBR5 as a modulator of super-vigilant proteostasis of iPSCs.

¹Institute for Genetics and Cologne Excellence Cluster for Cellular Stress Responses in Aging-Associated Diseases (CECAD), University of Cologne, Joseph Stelzmann Strasse 26, 50931 Cologne, Germany. ²Laboratory of Protein Metabolism in Development and Aging, International Institute of Molecular and Cell Biology, Trojdena Street 4, 02-109 Warsaw, Poland. These authors contributed equally: Seda Koyuncu, Isabel Saez. Correspondence and requests for materials should be addressed to D.V. (email: dvilchez@uni-koeln.de)

As the origin of multicellular organisms, a series of cellular quality control mechanisms must operate at high fidelity in pluripotent stem cells¹. In culture, embryonic stem cells (ESCs) derived from blastocysts do not undergo senescence and can replicate indefinitely while maintaining their capacity to differentiate into all cell lineages². Alternatively, somatic cells can be reprogrammed to generate induced pluripotent stem cells (iPSCs), which are similar to ESCs in many respects, such as their gene expression, potential for differentiation and ability to replicate continuously³. This unlimited self-renewal capacity requires stringent quality control mechanisms, including increased DNA damage responses and antioxidant defense systems^{1,4–7}. Growing evidence indicates that pluripotent stem cells also have intrinsic mechanisms to maintain the integrity of the proteome, a critical process for organismal development and cell function^{7–9}. Hence, defining the mechanisms of super-vigilant proteostasis in these cells is of central importance.

The proteostasis network is formed by multiple integrated processes that control the concentration, folding, location and interactions of proteins from their synthesis through their degradation¹⁰. Defects in proteostasis lead to the accumulation of damaged, misfolded and aggregated proteins that may alter the immortality of pluripotent stem cells. During the asymmetric divisions invoked by these cells, the passage of damaged proteins to progenitor cells could compromise organismal development and aging. Thus, pluripotent stem cells have a tightly regulated proteostasis network linked with their intrinsic characteristics and biological function^{1,7}. While ESC identity requires enhanced global translational rates¹¹, these cells also exhibit high levels of distinct chaperones to assure proper protein folding^{5,9}. For instance, ESCs have increased assembly of the TRiC/CCT (T-complex protein-1 (TCP-1) ring complex)/(chaperonin containing TCP-1) complex¹², a chaperonin that facilitates the folding of approximately 15% of the proteome and reduces the aggregation of disease-related mutant proteins¹³. To terminate damaged proteins, ESCs possess a powerful proteolytic machinery induced by high levels of PSMD11/RPN6^{14–16}, a scaffolding subunit that promotes the assembly of active proteasomes^{16,17}.

Remarkably, pluripotent stem cells are able to maintain enhanced proteostasis while proliferating indefinitely in their undifferentiated state^{1,7,8}. However, the differentiation process triggers a rewiring of the proteostasis network that reduces their ability to sustain proteome integrity^{7–9}. In addition, post-mitotic and progenitor cells as well as somatic stem cells undergo a progressive decline in their protein folding and clearance activities with age^{8,18,19}. This demise of proteostasis is linked with the onset of age-related disorders such as Alzheimer's, Parkinson's and Huntington's disease (HD)^{10,18}. On the other hand, the proteostasis network of somatic cells is rewired during cell reprogramming to generate iPSCs with high assembly of active TRiC/CCT and proteasome complexes, resembling ESCs^{9,12,16,20}.

HD is a fatal neurodegenerative disorder characterized by cognitive deficits, psychosis and motor dysfunction. The disease is inherited in a dominant manner and caused by mutations in the *huntingtin* (*HTT*) gene, which translates into an expanded polyglutamine stretch (polyQ)²¹. The wild-type *HTT* gene encodes a large protein of approximately 350 kDa that contains 6–35 polyQ repeats. In individuals affected by HD, *HTT* contains greater than 35 polyQ repeats²¹. Although loss of normal *HTT* function could also be a determinant of HD²², the dominant inheritance pattern of the disease and numerous experiments in model organisms indicate that gain of function of mutant *HTT* is toxic and induces neurodegeneration^{21,23,24}. PolyQ-expanded *HTT* is prone to aggregation, and the accumulation of mutant *HTT* fibrils as well as intermediate oligomers formed during the aggregation/disaggregation process contributes to neurodegeneration^{21,23,24}. The longer

the polyQ-expanded repeat, the earlier HD symptoms (e.g., neurodegeneration) typically appear²¹. However, the length of the pathological polyQ does not affect survival, self-renewal and pluripotency of iPSCs derived from HD patients (HD-iPSCs), which can proliferate indefinitely as control iPSCs^{25,26}. Moreover, HD-iPSCs do not accumulate polyQ-expanded inclusions^{12,25,27}. These findings indicate that iPSCs have increased mechanisms to maintain proteostasis of mutant *HTT*. Once differentiated into neural progenitors and neurons, these cells exhibit HD-associated phenotypes such as altered gene expression, increased vulnerability to excitotoxic stressors and cumulative risk of death over time^{25,28}. However, HD neurons lack polyQ aggregates and robust neurodegeneration phenotype^{12,25,27}, supporting a proteostasis-rejuvenating process during cell reprogramming that allows for HD-iPSC differentiation into neurons with an intact proteome.

Although cumulative evidence indicates a strong link between HD-related changes and proteasomal dysfunction²⁹, the mechanisms by which the proteasome recognizes polyQ-expanded *HTT* are poorly understood. With the high levels of proteasome activity exhibited by iPSCs¹⁶, we ask whether these cells have an intrinsic E3 ubiquitin ligase network to regulate proteostasis of polyQ-expanded *HTT*. We find that iPSCs have increased levels of UBR5, a HECT domain E3 enzyme that promotes proteasomal degradation of both mutant and wild-type *HTT*. Notably, an impairment of mutant *HTT* levels induced by UBR5 downregulation triggers the accumulation of polyQ-expanded aggregates in HD-iPSCs. Prompted by these findings, we examine whether modulation of UBR5 impinges on polyQ-expanded aggregation in distinct models. Since HD iPSC-derived neurons lack aggregates even upon proteasome inhibition, we assess *Caenorhabditis elegans* and human cell lines that accumulate polyQ-expanded aggregates. We find that loss of UBR5 worsens polyQ-expanded aggregation and neurotoxicity in *C. elegans* models. Notably, ectopic expression of UBR5 is sufficient to promote polyubiquitination of *HTT*, resulting in decreased levels and aggregation of mutant *HTT* in human cell models. Thus, we identify UBR5 as a potential modulator of *HTT* proteostasis by studying immortal pluripotent stem cells.

Results

The proteasome suppresses mutant *HTT* aggregation in iPSCs.

iPSCs derived from HD patients do not accumulate polyQ-expanded *HTT* aggregates^{12,27}. Since pluripotent stem cells exhibit high proteasome activity¹⁶, we assessed whether this activity is required to prevent mutant *HTT* aggregation in iPSCs generated from two individuals with juvenile-onset HD (i.e., Q71 and Q180)²⁵ (Supplementary Table 1). Indeed, downregulation of proteasome activity triggered accumulation of mutant *HTT* aggregates, which were mostly located in the cytoplasm (Fig. 1a and Supplementary Fig. 1a–b). Although the size of aggregates was generally smaller in iPSCs that express longer polyQ repeats (Q180), these cultures exhibited a higher percentage of aggregate-containing cells (Fig. 1a). Moreover, proteasome inhibition also induced a high percentage of mutant *HTT* aggregation in iPSCs derived from an individual with adult-onset HD (Q57) (Supplementary Fig. 1c–d). On the contrary, we did not detect accumulation of polyQ aggregates in three distinct control iPSCs upon proteasome inhibition (Fig. 1a and Supplementary Fig. 1e). Likewise, proteasome inhibition did not induce *HTT* aggregation in two isogenic counterparts of the Q180-iPSC line (Supplementary Fig. 2), in which the 180 CAG expansion was corrected to a nonpathological repeat length³⁰.

To further examine the link between proteasome activity and polyQ-expanded aggregation in iPSCs, we tested different concentrations of proteasome inhibitor. Lower concentrations

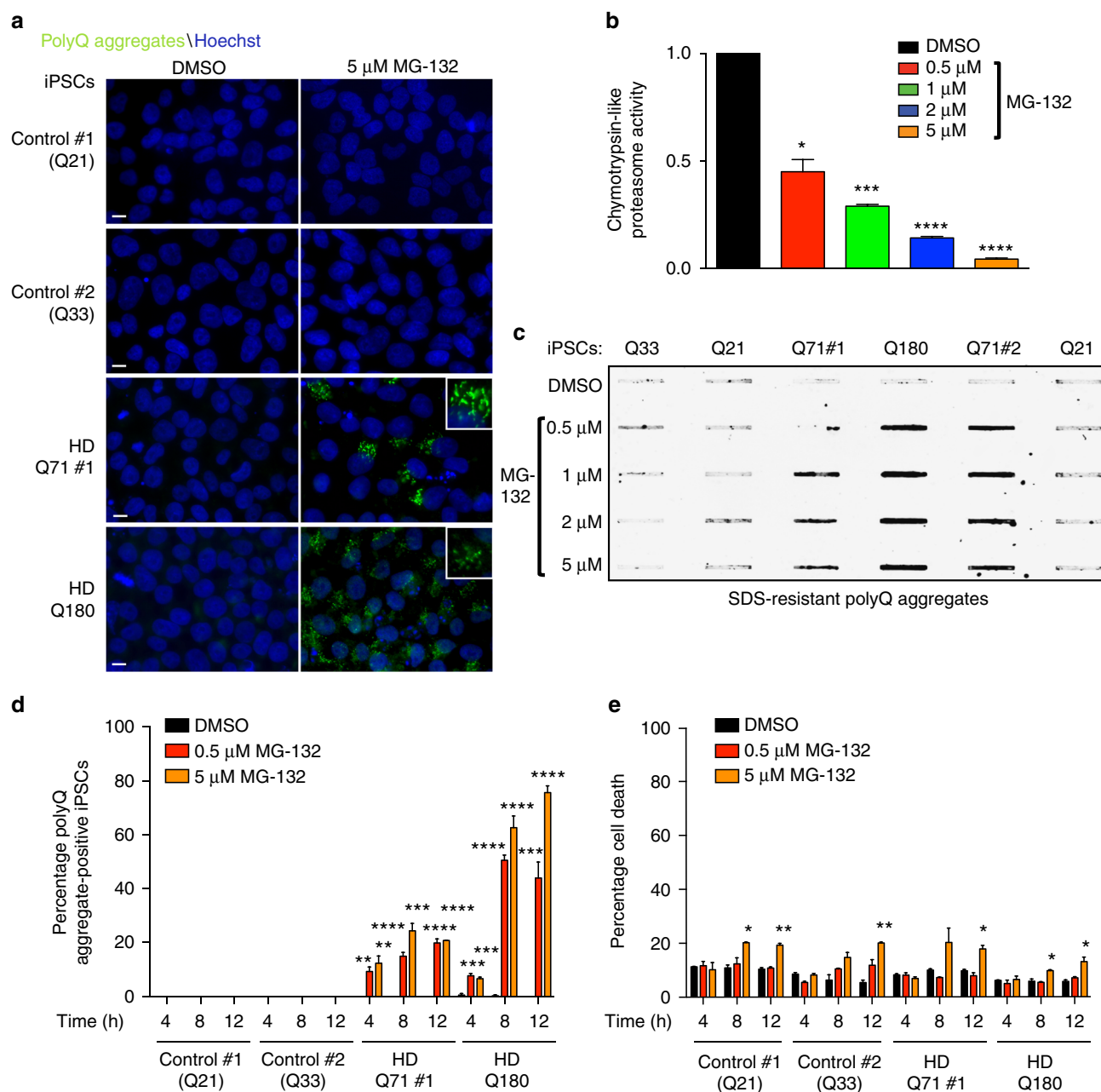


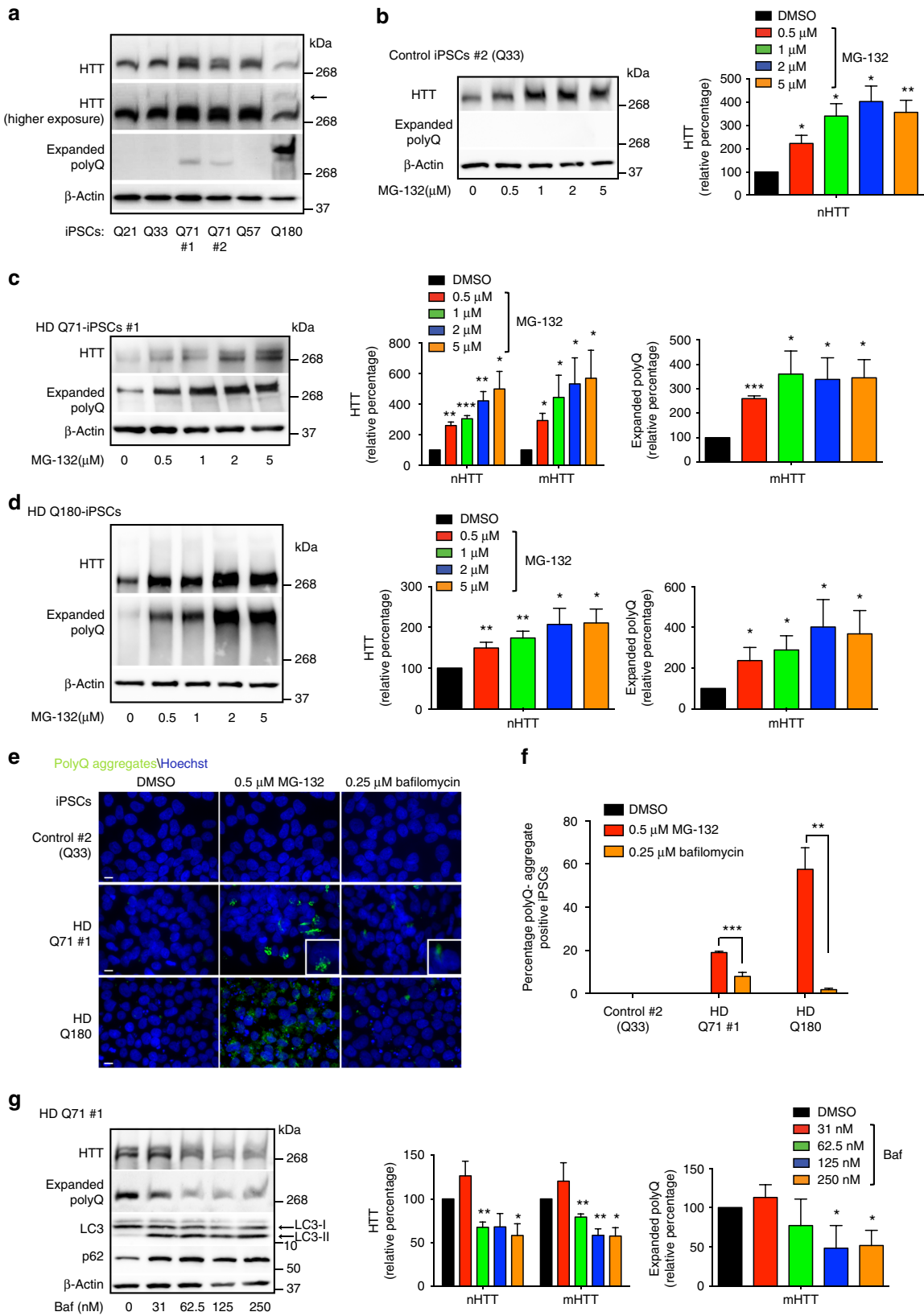
Fig. 1 Proteasome inhibition triggers mutant HTT aggregation in HD-iPSCs. **a** Immunocytochemistry of control and HD-iPSC lines treated with 5 μM MG-132 for 12 h. We used an antibody against polyQ-expanded protein to detect mutant HTT aggregates. Cell nuclei were stained with Hoechst 33342. Scale bar represents 10 μm. The images are representative of six independent experiments. **b** Chymotrypsin-like proteasome activity in HD Q180-iPSC line treated with MG-132 for 12 h (relative slope to Q180-iPSCs treated with DMSO). Graph represents the mean \pm s.e.m. of three independent experiments. **c** Filter trap analysis of the indicated control and HD-iPSCs. Proteasome inhibition with MG-132 for 12 h results in increased levels of polyQ aggregates in HD-iPSCs lines (detected by anti-polyQ-expanded diseases marker antibody). However, proteasome inhibition does not induce accumulation of polyQ aggregates in control iPSC lines. The images are representative of five independent experiments. **d** Graph represents the percentage of polyQ aggregate-positive cells/total nuclei in the indicated iPSC lines (mean \pm s.e.m., 3 independent experiments, 300–350 total cells per treatment for each line). **e** Graph represents the percentage of propidium iodide-positive cells/total nuclei in the indicated iPSC lines (mean \pm s.e.m., 3 independent experiments, 500–600 total cells per treatment for each line). For each time point, MG-132-treated lines were statistically compared with their respective DMSO-treated line. All the statistical comparisons were made by Student's *t*-test for unpaired samples. **P* < 0.05, ***P* < 0.01, ****P* < 0.001, *****P* < 0.0001

reduced approximately 50% of the proteasome activity, which was sufficient to induce mutant HTT aggregation as assessed by both filter trap and immunofluorescence experiments (Fig. 1b–d and Supplementary Fig. 3). Since these analyses were performed in iPSCs treated with proteasome inhibitor for 12 h, we examined whether this treatment reduces cell viability, a process that could trigger proteostasis collapse and, in turn, dysregulation of protein

aggregation. Whereas different concentrations of proteasome inhibitor resulted in polyQ-expanded aggregation (Fig. 1c, d), only higher concentrations induced a mild increase (~8%) in cell death (Fig. 1e). In addition, we found accumulation of mutant HTT aggregates at an earlier time point (4 h) of the proteasome inhibition treatment when higher concentrations did not trigger cell death (Fig. 1d, e). Thus, these results indicate that a decline in

proteasome activity promotes mutant HTT aggregation in HD-iPSCs, a process that cannot only be explained by impairment of cell viability. Remarkably, control and HD-iPSCs exhibited similar sensitivity to proteasome inhibition (Fig. 1e), suggesting that mutant HTT aggregation does not induce cell death in iPSCs.

Proteasome dysfunction impairs HTT levels in iPSCs. With the link between proteasome inhibition and mutant HTT aggregation, we asked whether HTT levels are regulated by the proteasome in HD-iPSCs. For this purpose, we characterized in our model two antibodies that recognize HTT and polyQ-expanded proteins, respectively^{12,31}. First, we validated that these antibodies



detect endogenous levels of HTT in iPSCs (Supplementary Fig. 4a–c). The HD-iPSCs used in this study express one mutant allele of HTT but also one normal copy (Supplementary Table 1)^{12,25,32–34}. Since the length of the polyQ stretch diminishes the electrophoretic mobility of proteins³¹, we could discriminate normal HTT and mutant HTT in both HD Q71 and Q180-iPSC lines by western blot using anti-HTT antibody (Fig. 2a and Supplementary Fig. 4a). In HD Q57-iPSCs, the differences in the electrophoretic mobilities of both alleles were marginal and they were not efficiently separated on western blot assays (Fig. 2a). We also observed that anti-HTT antibody was less immunoreactive to mutant HTT (Fig. 2a and Supplementary Fig. 4d). These differences were more pronounced in HD-iPSCs that express longer polyQ repeats (Q180), as mutant HTT was only detected after high exposure times in these cells (Fig. 2a). Thus, we used the antibody to polyQ-expanded proteins to examine the expression of mutant HTT in these cells (Fig. 2a). We confirmed that this antibody only recognizes mutant HTT on western blots and the intensity of the signal correlates with the length of the polyQ expansion (Fig. 2a and Supplementary Fig. 4d), as previously reported³¹. Although Q57 expansion was not detected with anti-polyQ-expanded proteins by western blot, this antibody strongly detected mutant HTT in Q71 and Q180 lines (Fig. 2a).

Once we characterized these antibodies in iPSCs, we assessed whether proteasome dysfunction impairs HTT levels. In control iPSCs, proteasome inhibition resulted in upregulated HTT protein levels (Fig. 2b and Supplementary Fig. 5a, b). In HD-iPSCs, proteasome dysregulation not only increased the amounts of normal HTT but also aggregation-prone HTT (Fig. 2c, d and Supplementary Fig. 5c, d). Although these results suggest a direct link between proteasome activity with HTT levels and aggregation, another possibility is that HTT dysregulation ensues from a global proteostasis collapse induced by proteasome inhibition. To assess this hypothesis, we inhibited the autophagy–lysosome system, which also modulates proteostasis of HTT through its proteolytic activity²⁹. Although autophagy inhibition induced mutant HTT aggregation in HD Q71-iPSCs, these aggregates were less compact and the percentage of aggregate-containing cells were lower when compared to proteasome inhibition treatment (Fig. 2e, f and Supplementary Fig. 7a, b). In HD Q180-iPSCs, autophagy inhibition only induced aggregation in a low percentage of cells (Fig. 2e, f). Whereas proteasome inhibition increased HTT levels, autophagy downregulation resulted in decreased amounts of HTT protein (Fig. 2g and Supplementary Fig. 8a–c). This decrease in HTT levels was not associated with potential changes in cell viability or a compensatory upregulation of the proteasome, as we did not find significant changes in

these parameters upon autophagy inhibition (Supplementary Fig. 8d–e). The differences between autophagy and proteasome inhibition supported a direct role of the proteasome in HTT degradation of iPSCs. In these lines, proteasome dysfunction results in increased levels of both normal HTT and aggregation-prone HTT. Since the impairment of clearance of misfolded proteins is key to their accumulation¹⁹, the increase in mutant HTT levels upon proteasome inhibition could contribute to diminish the ability of HD-iPSCs to suppress HTT aggregation.

UBR5 prevents mutant HTT aggregation in HD-iPSCs. To assess whether pluripotent stem cells have an intrinsic proteostasis to regulate HTT levels, we examined their E3 ubiquitin ligase network. For this purpose, we analyzed available quantitative proteomics data³⁵ and found 26 E3 ligases significantly increased in hESCs compared with their differentiated neuronal counterparts (Supplementary Table 2). Notably, UBR5 was one of the most upregulated E3 enzymes (Supplementary Table 2). UBR5 shows a striking preference for Lys48 linkages of ubiquitin³⁶, which is the primary signal for proteasomal degradation¹⁹. Under proteotoxic stress, UBR5 cooperates with Lys11-specific ligases to produce K11/K48 heterotypic chains, promoting proteasomal clearance of misfolded nascent polypeptides³⁶. Recently, a genome-wide association analysis has identified that genetic variations in the chromosome region containing *UBR5* gene hasten the clinical onset of HD³⁷. Remarkably, loss of UBR5 reduces the modification of overexpressed HTT protein with K11/K48-linked ubiquitin chains in a human cell line³⁶. Thus, increased endogenous expression of UBR5 could provide a link between proteostasis and regulation of HTT levels in pluripotent stem cells.

Besides its downregulation during differentiation of hESCs (Supplementary Fig. 9a and Supplementary Table 2), we confirmed that UBR5 protein levels are also increased in both control and HD-iPSC compared with their neuronal counterparts (Fig. 3a–c and Supplementary Fig. 10). In all the lines tested, we observed that UBR5 downregulation is already significant when iPSCs differentiate into neural progenitor cells (NPCs) (Fig. 3a–c and Supplementary Fig. 10). The decrease in UBR5 protein levels correlated with a downregulation of messenger RNA (mRNA) amounts during differentiation (Fig. 3d–f and Supplementary Fig. 9b).

Since UBR5 promotes microRNA-mediated transcript destabilization in mouse ESCs³⁸ and may be involved in transcriptional repression during development³⁹, we examined whether UBR5 downregulation during differentiation correlates with

Fig. 2 Loss of proteasome activity increases HTT levels in iPSCs. **a** Western blot of iPSCs with antibodies to total HTT, polyQ-expanded proteins and β -actin. Arrow indicates mutant HTT detected with total HTT antibody in HD Q180-iPSCs. The images are representative of three independent experiments. **b** Western blot of control iPSCs #2 treated with MG-132 (12 h). The graph represents the relative percentage values to DMSO-treated iPSCs of normal huntingtin (nHTT) detected with total HTT antibody and corrected for β -actin loading control (mean \pm s.e.m., three independent experiments). **c** Western blot of HD Q71-iPSC line #1 treated with MG-132 (12 h). Graphs represent the relative percentage values to DMSO-treated iPSCs (corrected for β -actin) of nHTT and mutant HTT (mHTT) detected with antibodies to total HTT and polyQ-expanded proteins (mean \pm s.e.m., three independent experiments). **d** Western blot of HD Q180-iPSCs treated with MG-132 (12 h). The graphs represent the relative percentage values to DMSO-treated iPSCs (corrected for β -actin) of nHTT and mHTT detected with antibodies to total HTT and polyQ-expanded proteins, respectively (mean \pm s.e.m., four independent experiments). Supplementary Fig. 6 presents a higher exposure time of the same membrane for a better comparison of mHTT levels detected with HTT antibody. **e** Immunocytochemistry of control and HD-iPSCs treated with 0.5 μ M MG-132 or 0.25 μ M bafilomycin for 12 h. PolyQ-expanded and Hoechst 33342 staining were used as markers of mutant HTT aggregates and nuclei, respectively. Scale bar represents 10 μ m. The images are representative of three independent experiments. **f** Graph represents the percentage of polyQ aggregate-positive cells/total nuclei in the indicated iPSC lines treated with MG-132 or bafilomycin for 12 h (mean \pm s.e.m., four independent experiments, 300–350 total cells per treatment for each line). **g** Western blot of HD Q71-iPSCs #1 treated with bafilomycin (12 h) using antibodies to total HTT, polyQ-expanded proteins, LC3 and P62. Graphs represent the relative percentage values to DMSO-treated iPSCs (corrected for β -actin) of nHTT and mHTT (mean \pm s.e.m., three independent experiments). Statistical comparisons were made by Student's *t*-test for unpaired samples. **P* < 0.05, ***P* < 0.01, ****P* < 0.001

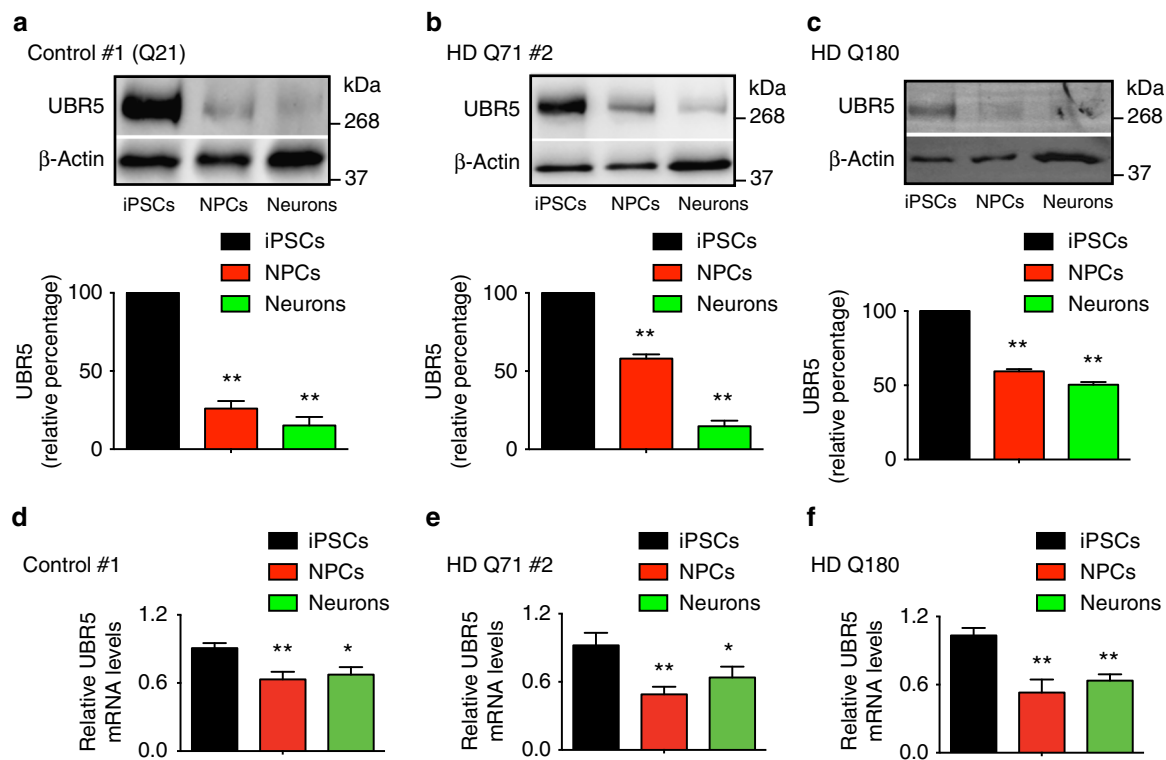


Fig. 3 The levels of UBR5 decrease during differentiation of iPSCs. **a–c** Western blot of UBR5 levels in control #1 (**a**), HD Q71 #2 (**b**) and HD Q180 (**c**) iPSC lines compared with their neural progenitor cell (NPC) and striatal neuron counterparts. The graphs represent the UBR5 relative percentage values to the respective iPSCs corrected for β -actin loading control (mean \pm s.e.m. of three independent experiments for each cell line). **d–f** Quantitative PCR (qPCR) analysis of UBR5 mRNA levels in control #1 (**d**), HD Q71 #2 (**e**) and HD Q180 (**f**) iPSC lines compared with their differentiated counterparts. Graphs (UBR5 relative expression to iPSCs) represent the mean \pm s.e.m. of three independent experiments for each line. * $P < 0.05$, ** $P < 0.01$

increased HTT mRNA levels. However, the amounts of HTT mRNA were either downregulated or not significantly changed with iPSC differentiation (Supplementary Fig. 11). As a more formal test, we assessed whether knockdown of UBR5 alters the transcript levels of HTT in distinct iPSC/hESC lines and found no differences (Fig. 4a and Supplementary Fig. 12). On the contrary, knockdown of UBR5 induced an increase in the protein levels of HTT in human pluripotent stem cells (Fig. 4b–e and Supplementary Fig. 13). We assessed three independent control iPSCs as well as two hESC lines and obtained similar results (Fig. 4b, c and Supplementary Fig. 13a–c). In HD Q71 and Q180-iPSC lines, the loss of UBR5 not only impaired the levels of normal HTT but also mutant HTT at a similar extent (Fig. 4d, e and Supplementary Fig. 13d). Although we could not discriminate normal and polyQ-expanded HTT in HD Q57-iPSCs, we confirmed an upregulation of total HTT protein levels in these cells upon UBR5 knockdown (Supplementary Fig. 13e). Since loss of UBR5 did not impair HTT mRNA levels (Fig. 4a and Supplementary Fig. 12), our data supported a role of this E3 enzyme in post-translational regulation of HTT. To examine whether UBR5 modulates HTT levels in a proteasome-dependent manner, we blocked proteasomal degradation in iPSCs. Notably, UBR5 knockdown and MG-132-treated cells exhibited similar levels of HTT (Fig. 4b–e). Most importantly, UBR5 downregulation did not further increase the levels of HTT in both control and HD-iPSCs with reduced proteasome activity (Fig. 4b–e), indicating a role of UBR5 in proteasomal degradation of HTT. Given that pluripotent stem cells exhibit high levels of proteasome activity compared with their differentiated counterparts¹⁶, we assessed whether UBR5 is required for this activity. However, loss of UBR5 did not affect global proteasome activities in iPSCs (Fig. 4f and Supplementary Fig. 14), suggesting a specific link between UBR5 and HTT

modulation. Besides UBR5, other E3 ligases are also increased in pluripotent stem cells (Supplementary Table 2 and Supplementary Fig. 15a). We knocked down four of these upregulated enzymes (i.e., UBE3A, RNF181, UBR7, TRIM71) and found no differences in HTT levels of HD-iPSCs (Supplementary Fig. 15b–g). Moreover, UBR5 interacted with both normal and polyQ-expanded HTT in HD-iPSCs, whereas we were not able to detect this interaction with a distinct upregulated E3 enzyme (Fig. 4g and Supplementary Fig. 16).

Taken together, these results suggest that intrinsic high expression of UBR5 determines HTT levels in iPSCs, a process that could contribute to the remarkable ability of these cells to maintain proteostasis of mutant HTT. In support of this hypothesis, loss of UBR5 triggered the accumulation of mutant HTT aggregates in all the HD-iPSCs tested as we confirmed by immunocytochemistry and filter trap experiments (Fig. 5a–e and Supplementary Fig. 17a). In contrast, we did not observe accumulation of polyQ aggregates in control iPSCs as well as corrected isogenic counterparts of HD Q180-iPSCs despite the upregulation of normal HTT levels (Fig. 5a, b, f, g and Supplementary Figs. 17b, 18).

Notably, proteasome inhibition did not further increase the accumulation of aggregates induced by loss of UBR5 in HD-iPSCs (Fig. 5h–l and Supplementary Fig. 19), indicating that UBR5 regulates proteostasis of mutant HTT via its proteasomal degradation. To further determine the impact of UBR5 on HTT levels and aggregation, we examined other components of the ubiquitin–proteasome system (UPS) network previously associated with HTT regulation. In particular, we focused on UBE3A, an E3 enzyme that promotes proteasomal degradation of polyQ-expanded HTT in cell lines⁴⁰. In addition, we examined UBE2K, an E2 enzyme that was found to interact with HTT in a yeast two-

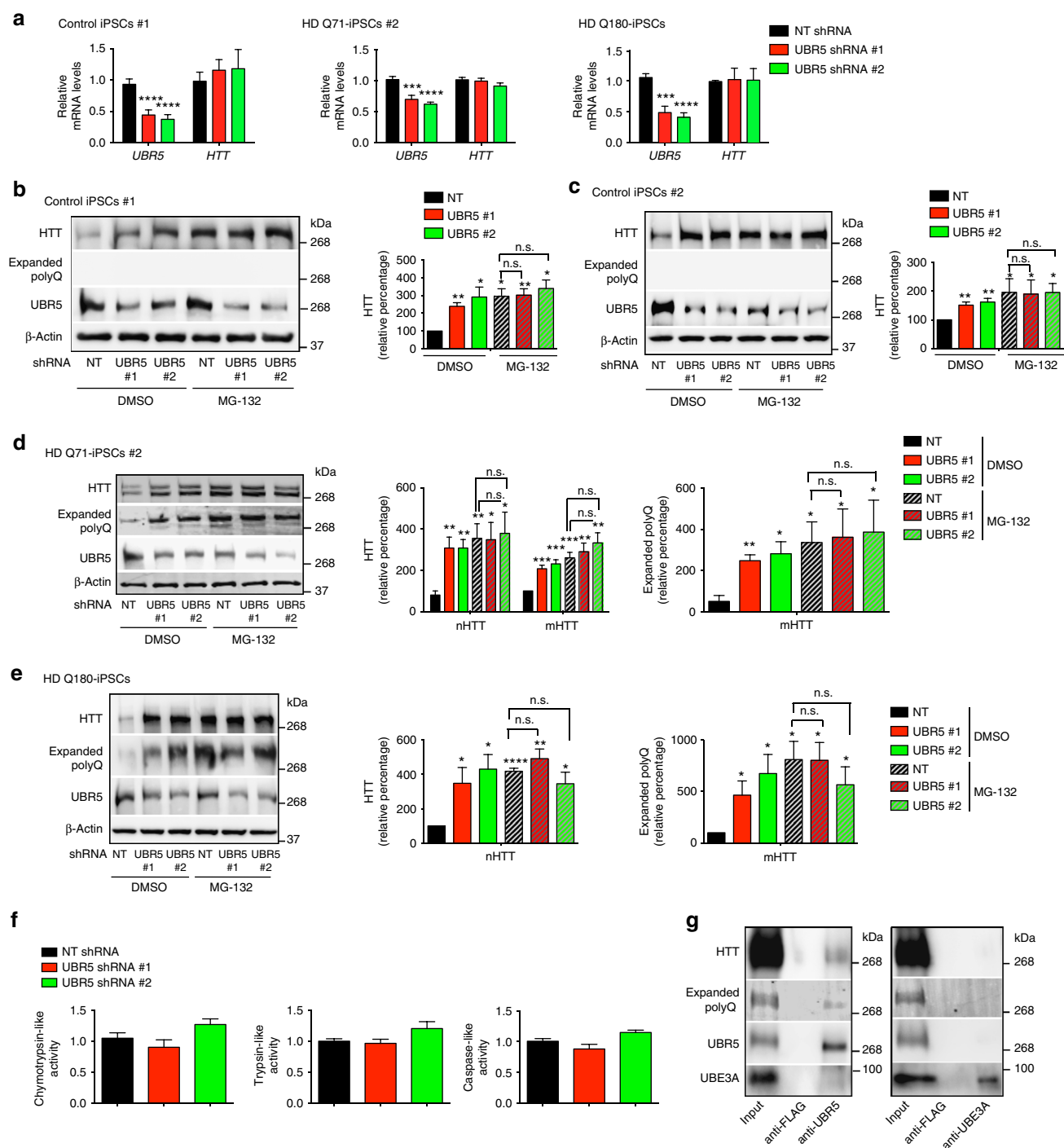
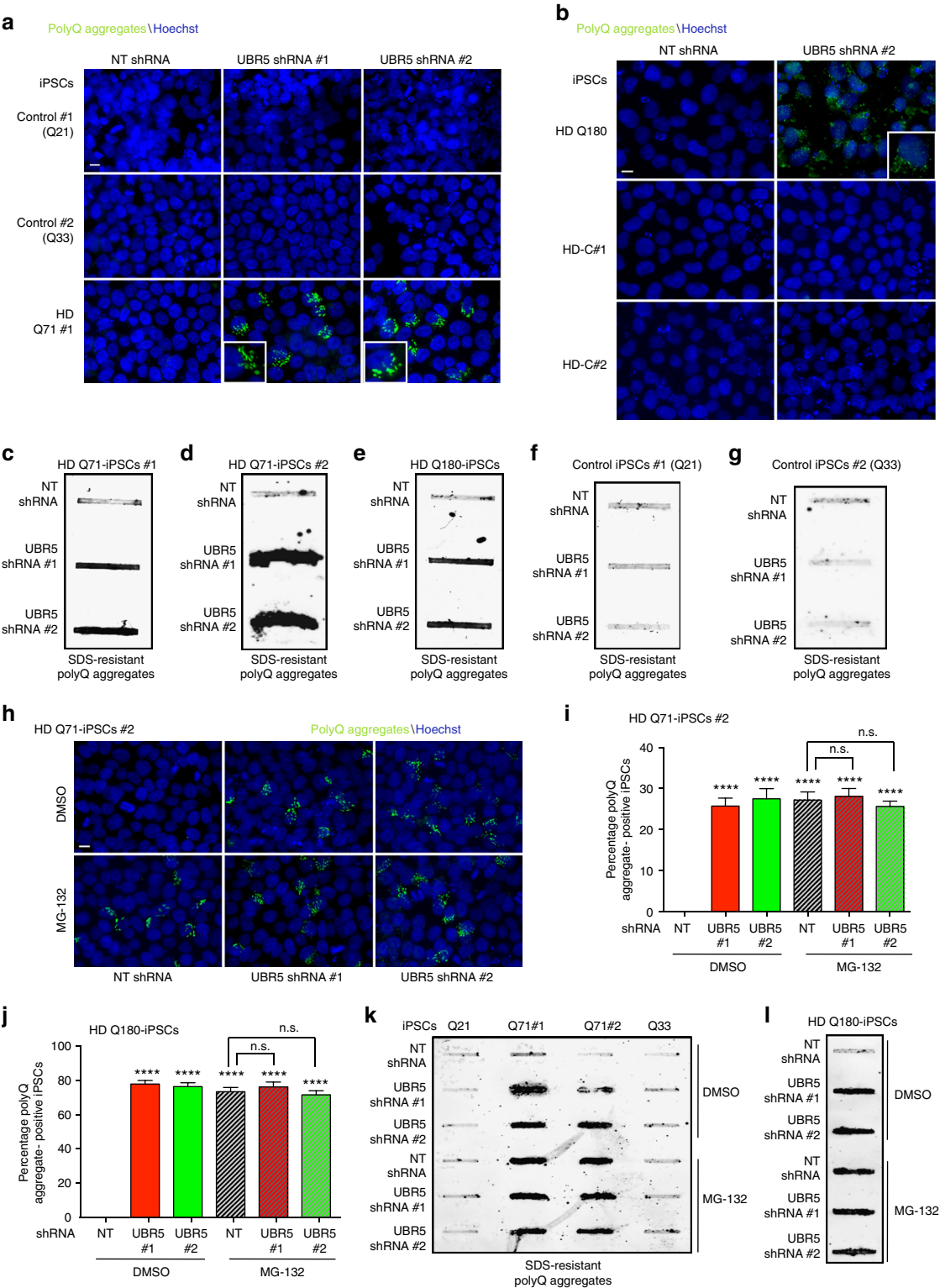


Fig. 4 Loss of UBR5 impairs HTT protein levels in iPSCs. **a** qPCR analysis of UBR5 and HTT mRNA levels in control iPSCs #1 ($n = 4$ independent experiments), HD Q71-iPSCs #2 ($n = 3$) and HD Q180-iPSCs ($n = 3$). Graphs (relative expression to non-targeting (NT) shRNA) represent the mean \pm s.e. m. **b, c** Western blot analysis of the indicated control iPSC lines with antibodies to HTT and polyQ-expanded proteins. Proteasome inhibitor treatment: 5 μ M MG-132 for 12 h. The graphs represent the HTT relative percentage values to DMSO-treated NT shRNA iPSCs corrected for β -actin loading control (mean \pm s.e.m. of three independent experiments). **d** Western blot analysis of HD Q71-iPSC line #2 upon UBR5 knockdown. The graphs represent the relative percentage values to DMSO-treated NT shRNA iPSCs (corrected for β -actin) of nHTT and mHTT detected with antibodies to total HTT and polyQ-expanded proteins (mean \pm s.e.m. of four independent experiments). Proteasome inhibitor treatment: 5 μ M MG-132 for 12 h. **e** Western blot analysis of HD Q180-iPSCs upon UBR5 knockdown. Proteasome inhibitor treatment: 5 μ M MG-132 for 12 h. The graphs represent the relative percentage values to DMSO-treated NT shRNA iPSCs (corrected for β -actin) of nHTT and mHTT detected with antibodies to total HTT and polyQ-expanded proteins, respectively (mean \pm s.e.m. of three independent experiments). **f** Proteasome activities in HD Q71-iPSCs #1 upon UBR5 knockdown (relative slope to NT shRNA iPSCs). Graphs represent the mean \pm s.e.m. of three independent experiments. **g** Co-immunoprecipitation with UBR5, UBE3A and FLAG antibodies in HD Q71-iPSC line #1 followed by western blot with HTT, polyQ-expanded HTT, UBR5 and UBE3A antibodies. The images are representative of three independent experiments. All the statistical comparisons were made by Student's t -test for unpaired samples. * $P < 0.05$, ** $P < 0.01$, *** $P < 0.001$, **** $P < 0.0001$

hybrid screen and reduce polyQ aggregation in cell lines^{41,42}. Although both UBE3A and UBE2K are upregulated in pluripotent stem cells³⁵, their knockdown did not increase mutant HTT levels and aggregation in HD-iPSCs (Fig. 6a, b and Supplementary Fig. 20). Thus, these results further support a specific role of UBR5 as a key determinant of HTT levels in iPSCs. Whereas the UPS regulates HTT degradation facilitating its proteostasis, the chaperone network is essential to modulate different steps of the aggregation process²⁹. Remarkably, pluripotent stem cells exhibit an intrinsic chaperone network that could contribute to

preventing mutant HTT aggregation¹². For instance, these cells have increased levels of HTT-interacting protein K (HYPK)³⁵, a chaperone that reduces polyQ-expanded HTT aggregates in mouse neuroblastoma cell lines⁴³. However, loss of HYPK did not trigger aggregation of mutant HTT in HD-iPSCs (Fig. 6b). Pluripotent stem cells also exhibit increased assembly of the TRiC/CCT complex¹², a chaperonin that suppresses mutant HTT aggregation^{44,45}. In hESCs/iPSCs, increased assembly of the TRiC/CCT complex is induced by high levels of CCT8 subunit¹². As UBR5 knockdown, loss of CCT8 triggers aggregation of



mutant HTT in HD-iPSCs (Fig. 6b)¹². In contrast, CCT8 downregulation did not affect HTT protein levels in HD-iPSCs (Fig. 6a), supporting a direct role of the TRiC/CCT complex in mutant HTT aggregation rather than degradation. Altogether, our results indicate a key role of UBR5 in monitoring HTT levels, a process that could facilitate mutant HTT regulation by other proteostasis nodes such as enhanced TRiC/CCT complex.

Loss of UBR5 triggers aggresome formation in hESCs/iPSCs.

Besides its role in HTT regulation, we asked whether UBR5 modulates other disease-associated proteins. To assess this hypothesis, we first examined ataxin-3 (ATXN3), a distinct polyQ-containing protein. An abnormal expansion of CAG triplets (>52) in the ATXN3 gene causes Machado–Joseph disease (MJD), a neurodegenerative disorder characterized by neuronal loss in the cerebellum and progressive ataxia^{46,47}. Here we used iPSCs derived from two individuals with MJD (MJD-iPSCs) (Supplementary Table 1), both expressing one normal copy of ATXN3 and one mutant allele with 74 CAG repeats (Fig. 6c). As previously reported⁴⁸, these MJD-iPSCs did not accumulate polyQ-expanded aggregates (Fig. 6d). To examine whether the UPS regulates proteostasis of ATXN3 in iPSCs, we downregulated proteasome activity by using MG-132 proteasome inhibitor. In contrast with HD-iPSC lines, the treatment with proteasome inhibitor for 12 h induced acute cell death and detachment of MJD-iPSCs. To reduce these effects, we performed our analysis at an earlier time point of the treatment (6 h) (Supplementary Fig. 21). Notably, proteasome inhibition did not change the levels of normal and mutant ATXN3, whereas the amounts of HTT were upregulated in these cells (Fig. 6c). Thus, our results suggest that the UPS does not modulate the levels of ATXN3 in iPSCs. However, proteasome inhibition triggered polyQ-expanded ATXN3 aggregation (Fig. 6d), a process that could be linked with the global proteostasis collapse induced by this treatment. Although loss of UBR5 increased HTT levels in MJD-iPSCs, we did not find changes in either normal or mutant ATXN3 (Fig. 6e, f). Moreover, we found that UBR5 binds HTT but it does not interact with wild-type or mutant ATXN3 in MJD-iPSCs (Supplementary Fig. 22a). In contrast to global proteasome inhibition, UBR5 downregulation did not induce aggregation of polyQ-expanded ATXN3 (Fig. 6g). This phenotype differed from HD-iPSCs lines, where upregulation of mHTT levels upon UBR5 knockdown was sufficient to trigger polyQ-expanded HTT aggregation (Fig. 5). Thus, these data indicate that not all polyQ-containing proteins are modulated by UBR5.

To further assess the role of UBR5 in the proteostasis of aggregation-prone proteins, we used iPSCs carrying mutations in

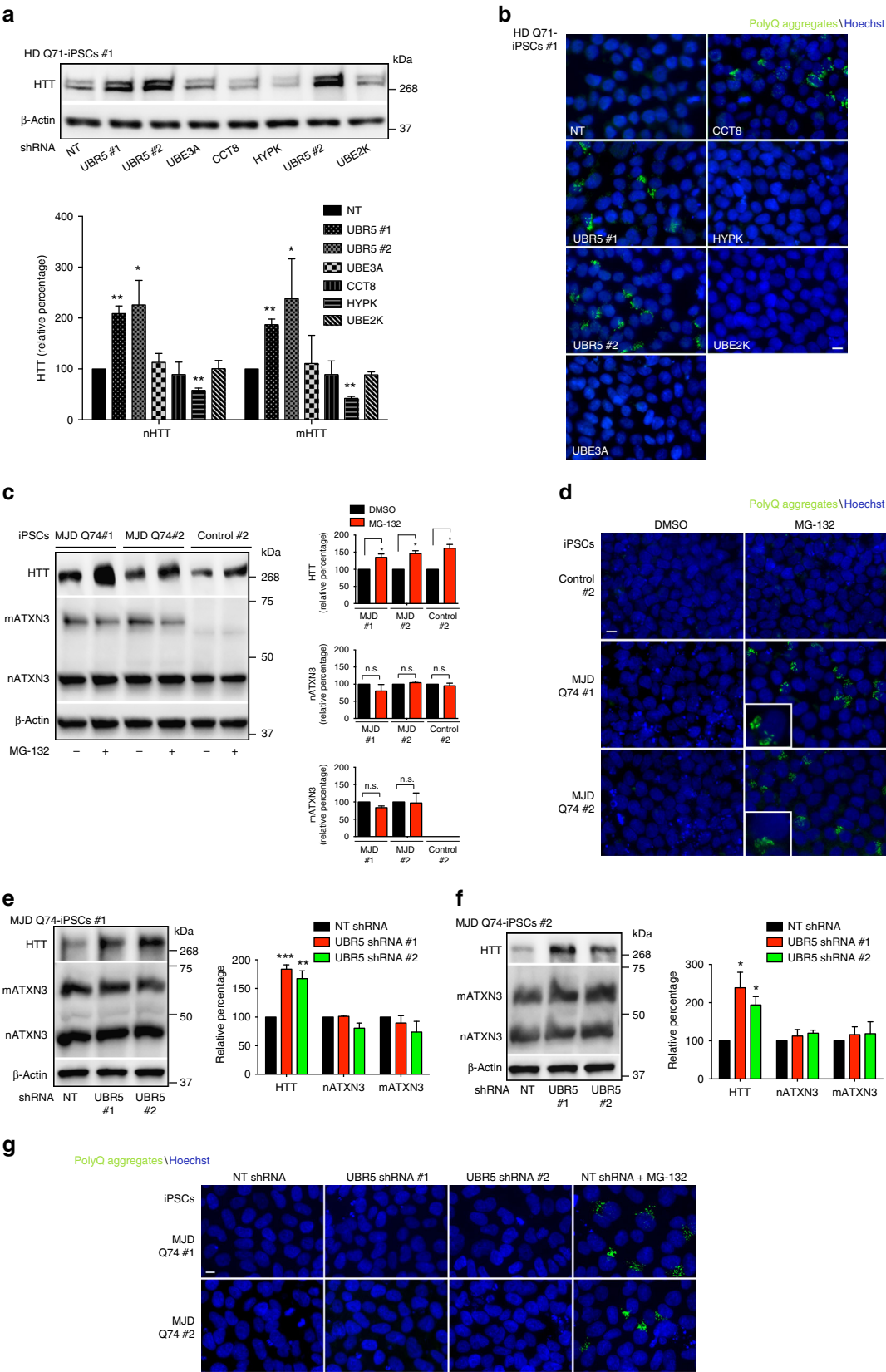
the RNA-binding protein FUS⁴⁹. These mutations are linked with amyotrophic lateral sclerosis (ALS), a fatal neurodegenerative disorder characterized by loss of motor neurons and concomitant progressive muscle atrophy^{49,50}. Although wild-type FUS shuttles between the nucleus and cytoplasm, it is mostly localized in the nucleus in normal conditions⁵¹. However, many of the ALS-related FUS mutations disrupt the nuclear import of the protein, resulting in aberrant localization and aggregation of FUS in the cytoplasm^{52,53}. As previously reported⁴⁹, wild-type FUS was essentially located in the nucleus of iPSCs (Fig. 7a). Likewise, FUS was predominantly detected in the nucleus of iPSCs (FUS^{R521C/wt}) derived from a patient affected by ALS in mid-late age^{49,50} (Fig. 7a). In iPSCs expressing a FUS variant linked with severe and juvenile ALS (FUS^{P525L/P525L}), the protein was mostly located in the cytoplasm⁴⁹ (Fig. 7a). Under oxidative stress, the cells form stress granules (SGs) where mutant variants of FUS are recruited⁵⁴. Despite the induction of cytoplasmic SGs, wild-type FUS remains in the nucleus in iPSCs under oxidative stress⁴⁹. On the contrary, mutant variants of FUS colocalize with SGs⁴⁹. Similar to oxidative stress, proteasome inhibition induced the accumulation of SGs in iPSCs (Fig. 7a). In control iPSCs, FUS remained in the nucleus upon proteasome dysfunction (Fig. 7a). Although FUS signal was mostly nuclear in FUS^{R521C}-iPSCs upon proteasome inhibition, we also found cytoplasmic FUS speckles co-localizing with SGs as reported for oxidative stress⁴⁹ (Fig. 7a). On the other hand, FUS^{P525L} variant showed a strong co-localization with SGs under proteasome inhibition (Fig. 7a). Remarkably, loss of UBR5 did not stimulate SG formation or FUS delocalization in control or ALS-iPSC lines (Fig. 7a). In addition, UBR5 knockdown did not impair wild-type or mutant FUS levels, whereas HTT was upregulated in these cells (Fig. 7b). Accordingly, UBR5 interacted with HTT in both control and ALS-iPSC lines, but we could not detect interaction with wild-type or mutant FUS in these cells (Supplementary Fig. 22b, c). Thus, these results indicate a specific role of UBR5 on HTT regulation. Although UBR5 was dispensable for ATXN3 and FUS proteostasis, we cannot discard a role of UBR5 in the control of other aggregation-prone proteins associated with disease.

Besides its role in HTT modulation, we asked whether UBR5 also determines the global proteostatic ability of pluripotent cells. Under normal conditions, misfolded proteins are refolded by chaperones or terminated via proteolytic systems¹⁰. Metabolic and environmental conditions (e.g., heat stress) challenge the structure of proteins, increasing the load of misfolded and damaged proteins. When proteolytic systems are overwhelmed, misfolded proteins accumulate into aggresomes. In these lines, we observed that heat stress induces the accumulation of aggresomes in pluripotent stem cells despite their increased proteolytic ability

Fig. 5 UBR5 suppresses mutant HTT aggregation in HD-iPSCs. **a** Immunocytochemistry of control iPSC line #1 (Q21), control iPSC line #2 (Q33) and HD Q71-iPSC line #1 upon UBR5 knockdown. PolyQ-expanded and Hoechst 33342 staining were used as markers of aggregates and nuclei, respectively. Scale bar represents 10 μ m. The images are representative of four independent experiments. **b** Immunocytochemistry of Q180-iPSCs and two isogenic counterparts (i.e., HD-C#1 and HD-C#2), in which the 180 CAG expansion was corrected to a nonpathological repeat length. Scale bar represents 10 μ m. The images are representative of three independent experiments. **c–g** Filter trap analysis of the indicated control and HD-iPSC lines upon UBR5 knockdown with anti-polyQ-expansion diseases marker antibody. The images are representative of at least three independent experiments for each cell line. **h** Immunocytochemistry of HD Q71-iPSC line #2 upon knockdown of UBR5. PolyQ-expanded and Hoechst 33342 staining were used as markers of aggregates and nuclei, respectively. Scale bar represents 10 μ m. Proteasome inhibitor treatment: 5 μ M MG-132 for 12 h. The images are representative of four independent experiments. **i** Graph represents the percentage of polyQ aggregate-positive cells/total nuclei in HD Q71-iPSC line #2 (mean \pm s.e.m., 3 independent experiments, 500–600 total cells per condition). Proteasome inhibitor treatment: 5 μ M MG-132 for 12 h. **j** Graph represents the percentage of polyQ aggregate-positive cells/total nuclei in HD Q180-iPSCs (mean \pm s.e.m., 3 independent experiments, 300–400 total cells per condition). Proteasome inhibitor treatment: 5 μ M MG-132 for 12 h. **k** Filter trap analysis of the indicated control and HD-iPSC lines with anti-polyQ-expansion diseases marker antibody. Proteasome inhibitor treatment: 5 μ M MG-132 for 12 h. The images are representative of three independent experiments. **l** Filter trap analysis of HD Q180-iPSCs with anti-polyQ-expansion diseases marker antibody. Proteasome inhibitor treatment: 5 μ M MG-132 for 12 h. The images are representative of three independent experiments. All the statistical comparisons were made by Student's *t*-test for unpaired samples. *****P* < 0.0001

(Fig. 7c). Notably, loss of UBR5 was sufficient to induce the accumulation of aggresomes in these cells (Fig. 7c). Thus, our data suggest that UBR5 not only regulates the levels of specific proteins such as HTT, but is also involved in the degradation of misfolded proteins ensued during normal metabolism.

Mutant HTT aggregates do not affect neural differentiation. Loss of UBR5 did not impair the levels of pluripotency and germ layer markers in control iPSCs (Supplementary Fig. 23a–c). With the pronounced accumulation of mutant HTT aggregates induced by UBR5 knockdown in HD-iPSCs (Fig. 5), we asked whether



these inclusions alter iPSC identity. However, the accumulation of aggregates did not result in decreased expression of pluripotency markers in HD-iPSCs (Fig. 8a and Supplementary Fig. 24). Likewise, we did not observe increased levels of markers of the distinct germ layers (Fig. 8a), indicating that polyQ-expanded HTT aggregates do not induce differentiation. Accordingly, we did not find a decrease in the number of cells expressing the pluripotency marker OCT4 (Fig. 8b and Supplementary Fig. 25). Most importantly, UBR5 knockdown HD-iPSCs could differentiate into neural cells (Fig. 8c and Supplementary Fig. 26). Under neural induction treatment, naive HD-iPSCs differentiated into NPCs with no detectable amounts of polyQ-expanded-HTT aggregates (Fig. 8d and Supplementary Fig. 27). However, neural cells derived from HD-iPSCs with impaired expression of UBR5 exhibited increased levels of mutant HTT and accumulation of aggregates (Fig. 8d–h and Supplementary Figs. 27–29). Overall, our results indicate that intrinsic high levels of UBR5 are essential to suppress mutant HTT aggregation in iPSCs, contributing to their ability to generate neural progenitor cells with no detectable polyQ-expanded aggregates. One step further was to determine whether these cells are able to generate terminally differentiated neurons. Since GABAergic medium spiny neurons (MSNs) undergo the greatest neurodegeneration in HD⁵⁵, we differentiated iPSCs into striatal neurons⁵⁶. Among those cells expressing the neuronal marker microtubule-associated protein-2 (MAP2), ~30–60% also expressed GABA depending on the cell line (Supplementary Fig. 30a, b). As previously reported²⁵, these differences were not associated with the expression of mutant HTT (Supplementary Fig. 30a, b). Knockdown of UBR5 at the iPSC stage did not reduce their ability to differentiate into striatal neurons (Supplementary Fig. 30a–g). In contrast to NPCs, terminally differentiated neurons derived from HD-iPSCs with downregulated UBR5 levels did not accumulate polyQ-expanded aggregates (Supplementary Fig. 31). Thus, the lack of defects in neurogenesis and aggregates in these cells indicate that other mechanisms activate during neuronal differentiation to facilitate proteostasis of mutant HTT.

UBR5 loss hastens neurotoxicity in polyQ nematode models.

Although HD-iPSCs can terminally differentiate into MSNs, these cells do not exhibit mutant HTT aggregates even after the addition of proteasome and autophagy inhibitors or the induction of oxidative stress^{12,20,25,27}. Thus, these findings support a rejuvenation process during cell reprogramming that prevents aberrant aggregation in differentiated neurons. In addition, the lack of polyQ-expanded aggregates in these cells could reflect the long period of time before aggregates accumulate in HD²⁵. In these

lines, HD-MSNs derived from iPSCs do not accumulate detectable polyQ-expanded inclusions at 12 weeks after transplantation into HD rat models. However, they accumulate aggregates after 33 weeks of transplantation²⁷. Proteasome inhibition did not induce upregulation of HTT protein levels or aggregation in HD-MSNs differentiated from iPSCs (Supplementary Fig. 32a–d). Likewise, knockdown of UBR5 in differentiated HD-MSNs was not sufficient to induce mutant HTT aggregation and upregulated HTT levels (Supplementary Fig. 33, 34). In addition, UBR5 knockdown did not reduce cell viability of HD-MSNs (Supplementary Fig. 35).

Given the challenges presented by MSNs derived from HD-iPSCs to study the role of UBR5 in polyQ-expanded aggregation and toxicity, we used a distinct model. Remarkably, a RNA interference (RNAi) screen against E3 ubiquitin ligases found that knockdown of the worm *UBR5* ortholog (*ubr-5*) accelerates paralysis in a *C. elegans* model expressing 35 polyQ repeats fused to yellow fluorescent protein (YFP) in body wall muscle cells⁵⁷. To assess the requirement of *ubr-5* for resistance to polyQ neurotoxicity, we examined a *C. elegans* model that expresses polyQ-expanded YFP in the nervous system⁵⁸. In these worms, polyQ aggregation and neurotoxicity correlates with the age and length of the polyQ repeat, with a pathogenic threshold of 40 glutamine repeats⁵⁸. Notably, loss of *ubr-5* resulted in increased levels of polyQ67-expanded protein with concomitant aggregation (Fig. 9a, b). Knockdown of *ubr-5* had a strong effect in the aggregation propensity of head neurons, resulting in more aggregates in the circumpharyngeal nerve ring and chemosensory processes (Fig. 9c). We also observed more propensity aggregation in the neurons of the animal mid-body (Fig. 9c and Supplementary Fig. 36). To assess whether the polyQ67-YFP foci were immobile protein aggregates, we performed a quantitative fluorescence recovery after photobleaching analysis of head neurons. In both empty vector and *ubr-5* RNAi-treated worms, most of the polyQ67-YFP foci signal could not be recovered, indicating an immobile state (Supplementary Fig. 37a). However, *ubr-5* RNAi induced a faster incorporation of new polyQ67-YFP peptides into the aggregates (Supplementary Fig. 37b).

Although *ubr-5* RNAi was sufficient to induce a pronounced increase of polyQ-expanded aggregates (Fig. 9b), it is important to note that neurons are less sensitive to RNAi when compared with other tissues⁵⁹. For this reason, we introduced a *rrf-3* mutation in the polyQ-YFP neuronal models, which confers hypersensitivity to RNAi in all the tissues, including neurons⁶⁰. Accordingly, we found that *ubr-5* RNAi treatment induced a strong increase in polyQ67-YFP aggregation of *rrf-3* mutants (Fig. 9d). On the contrary, *ubr-5* knockdown did not induce

Fig. 6 UBR5 maintains proteostasis of HTT but not ATXN3 in iPSCs. **a** Western blot analysis of HD Q71-iPSC line #1 with antibody to HTT. The graph represents the nHTT and mHTT relative percentage values (corrected for β -actin loading control) to NT shRNA iPSCs (mean \pm s.e.m. of three independent experiments). **b** Immunocytochemistry of HD Q71-iPSC line #1 upon knockdown of the indicated proteostasis components. PolyQ-expanded and Hoechst 33342 staining were used as markers of aggregates and nuclei, respectively. Scale bar represents 10 μ m. The images are representative of three independent experiments. **c** Western blot analysis with antibodies to HTT and ATXN3 of iPSCs derived from two individuals with MJD (MJD-iPSC lines #1 and #2) and control iPSCs. Anti-ATXN3 antibody detects both normal (nATXN3) and mutant ATXN3 (mATXN3). Proteasome inhibitor treatment: 5 μ M MG-132 for 6 h. The graphs represent the HTT, nATXN3, mATXN3 relative percentage values to the respective DMSO-treated iPSCs corrected for β -actin loading control (mean \pm s.e.m. of three independent experiments). **d** Immunocytochemistry of control iPSCs #2, MJD-iPSC lines #1 and #2 upon proteasome inhibition (5 μ M MG-132 for 6 h). PolyQ-expanded and Hoechst 33342 staining were used as markers of aggregates and nuclei, respectively. Scale bar represents 10 μ m. The images are representative of three independent experiments. **e, f** Western blot analysis with antibodies to HTT and ATXN3 of MJD-iPSC lines #1 and #2 upon UBR5 knockdown. The graphs represent the relative percentage values of HTT, nATXN3 and mATXN3 to the respective NT shRNA iPSCs corrected for β -actin loading control (mean \pm s.e.m. of three independent experiments for each line). **g** Immunocytochemistry of MJD-iPSC lines #1 and #2 upon UBR5 knockdown. Proteasome inhibitor: 5 μ M MG-132 for 6 h. PolyQ-expanded and Hoechst 33342 staining were used as markers of aggregates and nuclei, respectively. Scale bar represents 10 μ m. The images are representative of three independent experiments. All the statistical comparisons were made by Student's *t*-test for unpaired samples. **P* < 0.05, ***P* < 0.01, ****P* < 0.001

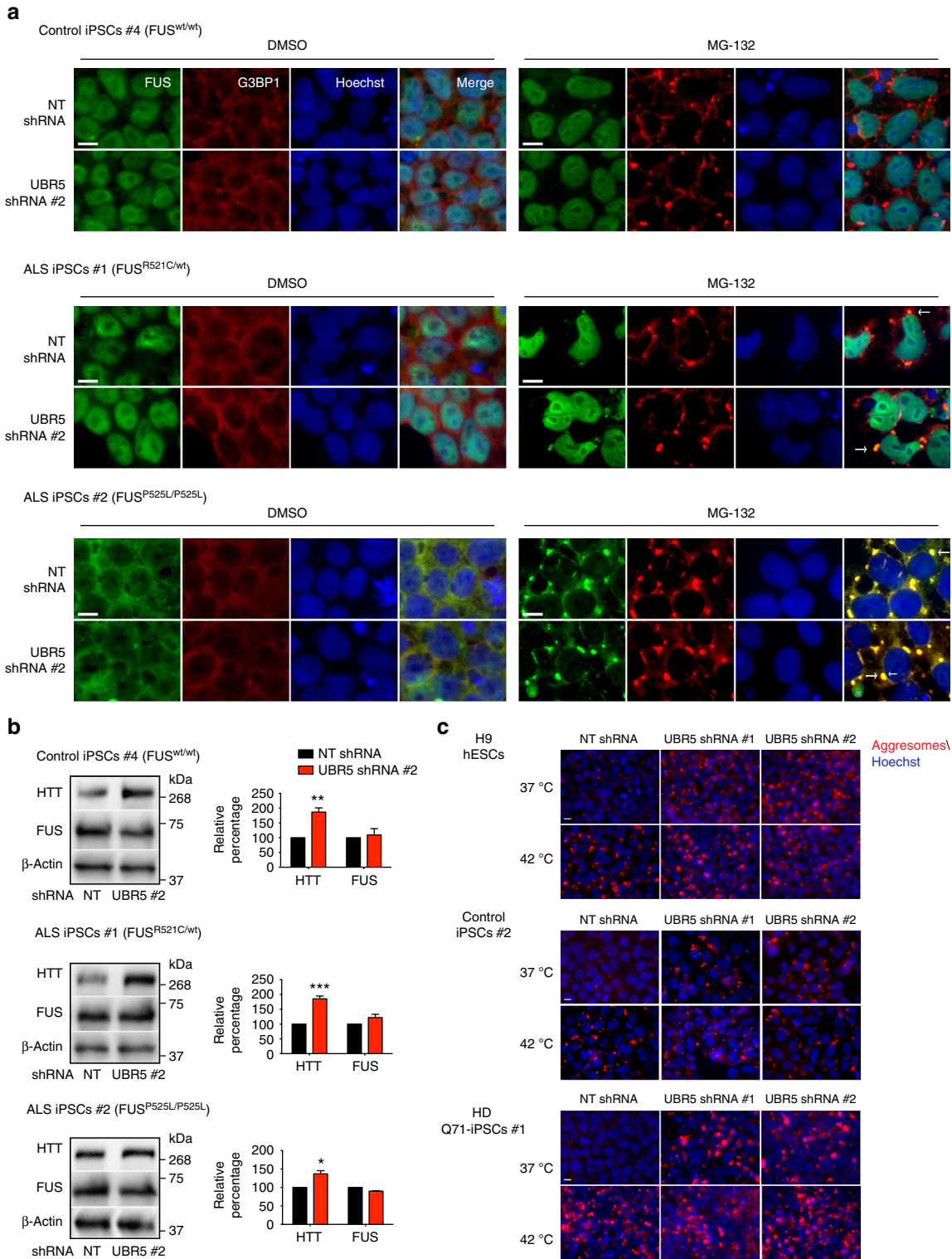
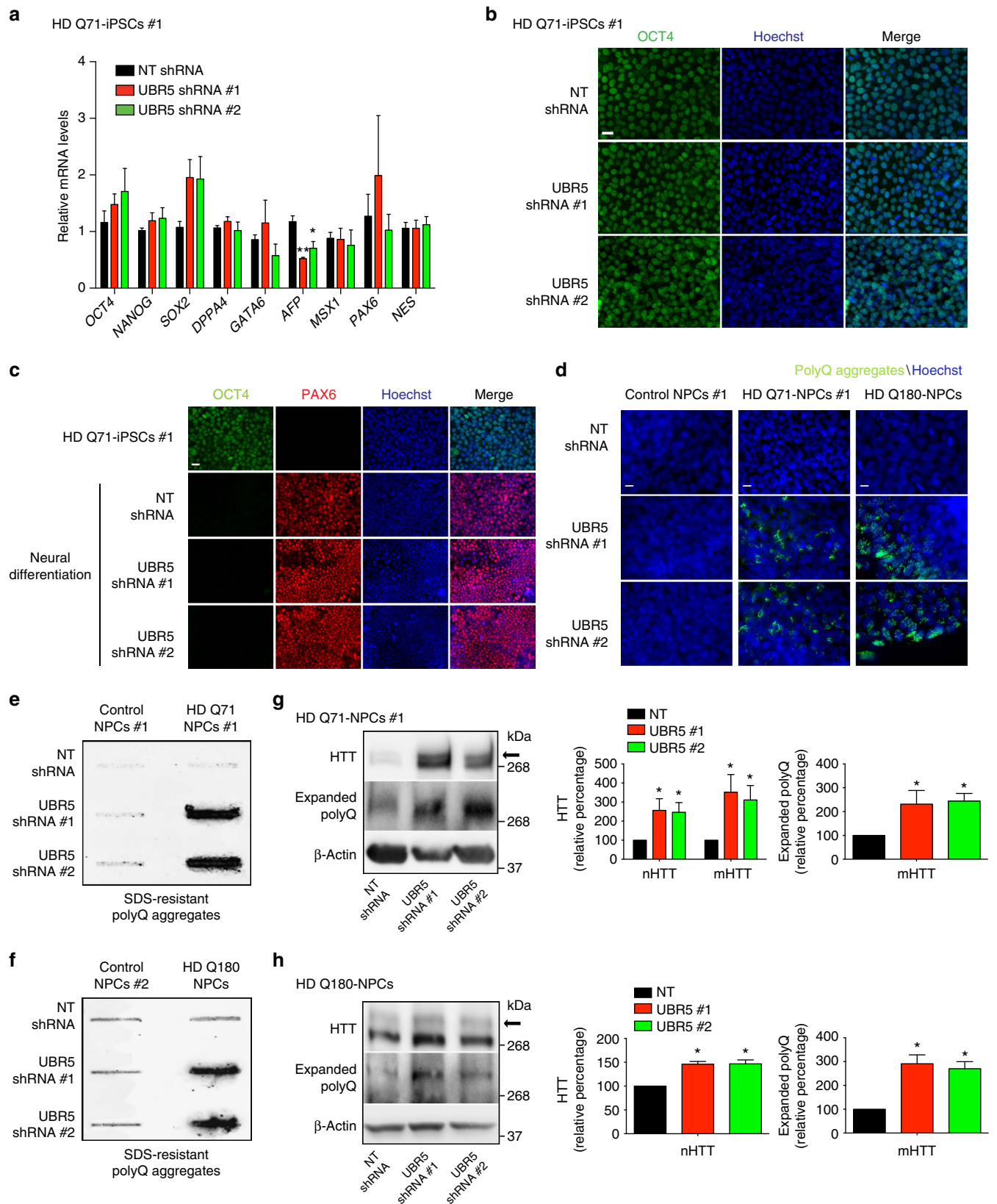


Fig. 7 Loss of UBR5 triggers aggresome formation in pluripotent stem cells. **a** Immunocytochemistry of control iPSCs #4 (FUS^{wt/wt}), ALS-iPSCs #1 (FUS^{R521C/wt}) and ALS-iPSCs #2 (FUS^{P525L/P525L}) with anti-FUS antibody. G3BP1 and Hoechst 33342 staining were used as markers of stress granules (SGs) and nuclei, respectively. Proteasome inhibition: 5 μM MG-132 for 6 h. Scale bar represents 10 μm. Arrows indicate examples of co-localization of FUS with SGs. The images are representative of three independent experiments. **b** Western blot analysis with antibodies to HTT and FUS of ALS-iPSC lines upon UBR5 knockdown. The graphs represent the relative percentage values of HTT and FUS to the respective NT shRNA iPSCs corrected for β-actin loading control (mean ± s.e.m. of three independent experiments for each line). All the statistical comparisons were made by Student's *t*-test for unpaired samples. **P* < 0.05, ***P* < 0.01, ****P* < 0.001. **c** Staining of aggresomes in H9 hESCs, control iPSCs #2 and HD Q71-iPSCs #1. Hoechst 33342 staining was used as a marker of nuclei. Heat stress: 42 °C for 4 h. Scale bar represents 10 μm. The images are representative of two independent experiments for each line

aggregation of polyQ19-peptides, even in the RNAi-hypersensitive mutant strain (Fig. 9d). Since the neurotoxic effects of polyQ-expanded aggregation correlate with impairment of coordinated movement⁵⁸, we performed motility assays to quantify the role of *ubr-5* in the resistance to polyQ-toxicity. Notably, loss of *ubr-5* hastened the

detrimental effects on motility induced by polyQ67 repeats (Fig. 9e), correlating with increased polyQ aggregation. On the contrary, knockdown of *ubr-5* did not affect the motility of polyQ19-expressing worms (Fig. 9e). Altogether, these results provide a direct link between UBR5 function and polyQ-expanded aggregation with age.



Ectopic expression of UBR5 suppresses mutant HTT aggregation. Since loss of UBR5 hastened polyQ-expanded aggregation, we asked whether ectopic expression of this HECT E3 enzyme is sufficient to ameliorate the accumulation of polyQ aggregates. To assess this hypothesis, we generated human cell models that express either control (Q23) or polyQ-expanded (Q100) HTT protein. In these cells, overexpression of mutant HTT resulted in the accumulation of polyQ-expanded aggregates, whereas control HTT did not form aggregates (Fig. 10a). Notably, ectopic expression of UBR5 ameliorated polyQ-expanded aggregation in Q100-HTT cells (Fig. 10a), a process blocked by proteasome inhibition (Fig. 10b). In contrast, UBR5 overexpression did not reduce the insolubility of aggregation-prone β -amyloid protein (Supplementary Fig. 38).

In support of a direct role of UBR5 in modulation of HTT, we found that UBR5 overexpression decreases the protein levels of mutant HTT (Fig. 10c). To further determine the role of UBR5, we overexpressed a UBR5 mutant with two point mutations that causes a change in an amino acid (C2769A) located in the HECT domain, resulting in ubiquitin ligase-dead UBR5⁶¹. Remarkably, similar overexpression levels of this catalytic inactive UBR5 mutant did not diminish polyQ-expanded HTT protein levels and aggregation (Fig. 10a–c). Given that our results in iPSCs indicate that UBR5 regulates HTT levels via the proteasome, we tested whether UBR5 overexpression promotes proteasomal degradation of Q100-HTT. Indeed, proteasome inhibition blocked the reduction of Q100-HTT levels induced by enhanced wild-type UBR5 expression (Fig. 10d). To further assess the link between UBR5 and HTT regulation, we performed immunoprecipitation experiments and examined polyubiquitination of HTT. Prior to immunoprecipitation, we treated the cells with proteasome inhibitor to block the degradation of HTT induced by UBR5. Under these conditions, we immunoprecipitated similar amounts of HTT in cells overexpressing wild-type UBR5 when compared with cells expressing empty vector or catalytic inactive UBR5 (Fig. 10e). Notably, we found that ectopic expression of UBR5 induces a dramatic increase in polyubiquitination of mutant HTT (Fig. 10e). In contrast, overexpression of the catalytic inactive UBR5 mutant did not promote polyubiquitination of Q100-HTT protein (Fig. 10e). In support of our findings, a recent study reported that UBR5 downregulation decreases the modification of overexpressed HTT protein with K11/K48-linked polyubiquitin chains in HeLa human cells³⁶. Moreover, this study revealed K11/K48-linked polyubiquitin modifications at Lys337 of HTT by proteomics experiments³⁶. We performed proteomics analysis of immunoprecipitated HTT in Q100-HTT-overexpressing cells to determine potential lysine sites modified by UBR5

(Supplementary Fig. 39a, b). Although we did not detect ubiquitination at Lys337 of HTT in our assays, we identified two other ubiquitinated lysine sites: Lys631 and Lys2097. However, only Lys631 shows a small but significant higher ubiquitination in cells overexpressing wild-type UBR5 when compared to catalytic inactive UBR5 (Supplementary Fig. 39b), suggesting that this site could be ubiquitinated by UBR5. Taken together, our data indicate that the ubiquitin ligase activity of UBR5 modulates proteasomal degradation of mutant HTT, a process that ameliorates polyQ-expanded aggregation.

Discussion

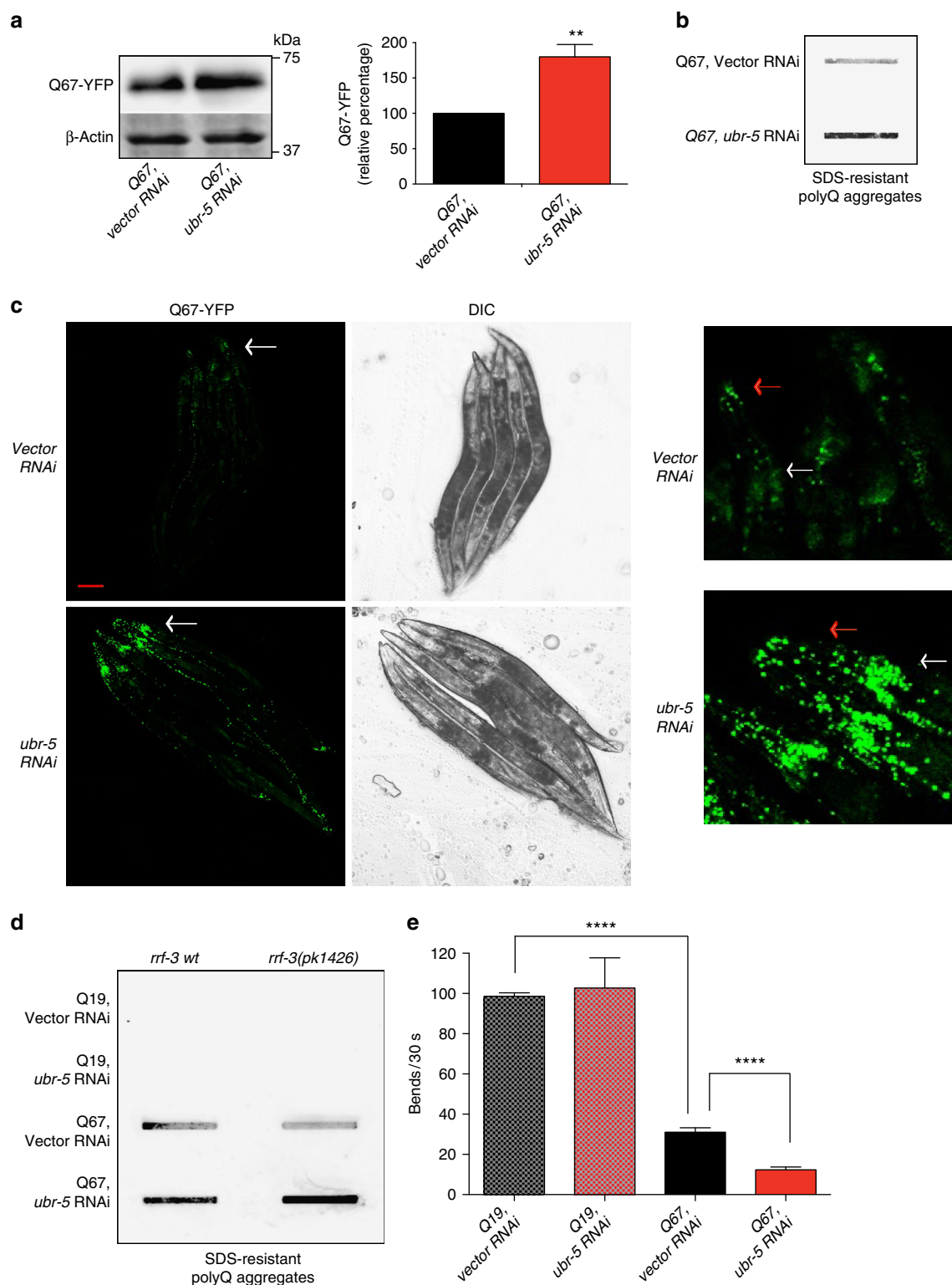
While the transcriptional, epigenetic and signaling networks of pluripotency have been a primary focus of research efforts, emerging evidence indicates that pluripotent stem cells also exhibit intrinsic proteostasis mechanisms^{8,12,14,17}. Thus, a comprehensive understanding of this proteostasis network could be necessary for pluripotent stem cells to hold a great promise for regenerative medicine. As an invaluable resource to generate terminally differentiated cells, pluripotent stem cells can facilitate the study of human diseases and drug screening. This is particularly fascinating in the context of proteostasis-related disorders. At least 30 different human diseases are directly associated with aberrant protein folding protein and aggregation⁶². Whereas a collapse in proteostasis of somatic cells could underlie these diseases, pluripotent stem cells exhibit a striking ability to correct and suppress proteostatic deficiencies. Thus, investigating pluripotent stem cells from patients could contribute to identifying super-vigilant proteostasis mechanisms that could be mimicked in somatic tissues to ameliorate disease.

Despite expressing significant amounts of mutant HTT²⁵, several studies have demonstrated that HD-iPSCs do not accumulate polyQ-expanded HTT aggregates even after multiple passages^{12,25,27}. In addition, HD-iPSCs can terminally differentiate into neurons lacking the aggregation phenotype characteristic of HD^{12,25,27}, indicating a rejuvenation process during reprogramming that prevents polyQ-expanded aggregation in neurons prior to proteostasis collapse with age. Here we show that increased proteasome activity of iPSCs regulates the levels of both normal and mutant HTT, contributing to suppressing polyQ-expanded HTT aggregation in HD-iPSCs. Conversely, a dysfunction in proteasome activity results in impaired HTT levels, leading to aggregation of mutant HTT in HD-iPSCs. Importantly, we have uncovered that intrinsic high expression of UBR5 is a key component of the UPS to regulate HTT levels in iPSCs. This E3 enzyme interacts with HTT and promotes

Fig. 8 UBR5 determines HD-iPSC differentiation into NPCs with no aggregates. **a** qPCR of pluripotency (*OCT4*, *NANOG*, *SOX2*, *DPPA4*), endodermal (*GATA6*, *AFP*), mesodermal (*MSX1*) and ectodermal markers (*PAX6*, *NES*) in HD Q71-iPSC line #1. The graph represents the relative expression to NT shRNA HD-iPSCs (mean \pm s.e.m. (n = four independent experiments)). **b** Immunocytochemistry of HD Q71-iPSC line #1. *OCT4* and Hoechst 33342 staining were used as markers of pluripotency and nuclei, respectively. Scale bar represents 20 μ m. The images are representative of four independent experiments. **c** After neural induction of HD Q71-iPSC line #1 with downregulated levels of UBR5, we observed similar numbers of *PAX6*-positive cells compared to NT shRNA control. Scale bar represents 20 μ m. **d** Upon neural induction of HD-iPSCs with downregulated levels of UBR5, NPCs accumulate mutant HTT aggregates. PolyQ-expanded and Hoechst 33342 staining were used as markers of aggregates and nuclei, respectively. Scale bar represents 10 μ m. The images are representative of three independent experiments. **e** Filter trap analysis of polyQ-expanded aggregates in NPCs derived from HD Q71-iPSCs #1 with downregulated levels of UBR5. The images are representative of four independent experiments. **f** Filter trap of control NPCs #2 and HD Q180-NPCs derived from iPSCs with downregulated levels of UBR5. The images are representative of three independent experiments. **g** HD Q71-iPSCs #1 with downregulated UBR5 levels were differentiated into NPCs and analyzed by western blot. Graphs represent the relative percentage values to NT shRNA NPCs (corrected for β -actin) of nHTT and mHTT detected with antibodies to total HTT and polyQ-expanded proteins (mean \pm s.e.m. of three independent experiments). **h** Western blot analysis of NPCs derived from HD Q180-iPSCs with downregulated levels of UBR5. Graphs represent the relative percentage values to NT shRNA NPCs (corrected for β -actin) of nHTT and mHTT detected with antibodies to total HTT and polyQ-expanded proteins (mean \pm s.e.m. of three independent experiments), respectively. In **g**, **h** arrow indicates polyQ-expanded HTT detected with total HTT antibody. Statistical comparisons were made by Student's *t*-test for unpaired samples. * P < 0.05, ** P < 0.01

proteasomal degradation of both normal and polyQ-expanded HTT. Since the clearance of misfolded and aggregation-prone proteins is key to their aggregation, the impairment of HTT levels could be particularly relevant in iPSCs expressing mutant HTT. Accordingly, UBR5 downregulation and concomitant dysregulation of HTT levels results in polyQ-expanded HTT aggregation in HD-iPSCs. Thus, our results suggest that UBR5 monitors HTT levels, facilitating the regulation of mutant HTT by other proteostasis nodes. For instance, pluripotent stem cells

also exhibit increased activity of the TRiC/CCT chaperone complex to tightly suppress the aggregation of mutant HTT¹². We found that the HECT domain containing the E3 ligase activity of UBR5 is required for HTT degradation, providing a further link between increased proteasome activity and stringent control of mutant HTT. It is important to note that pluripotent stem cells also express high levels of other E3 ligases. Although our results discard a direct role of several of these E3s (i.e., UBR7, UBE3A, RNF181) in modulation of HTT levels in



iPSCs, it will be fascinating to examine the impact of the other upregulated E3s.

Whereas our data highlight the importance of UBR5 in proteostasis of iPSCs, the intrinsic high levels of this enzyme could also suggest a role in pluripotency via the ubiquitination of endogenous substrates. Interestingly, a study has reported that Ubr5 knockdown results in significant loss of pluripotency markers in mouse ESCs¹⁴. However, a different study did not find impairment of pluripotency markers in murine ESCs upon Ubr5 RNAi treatment⁶³. Likewise, we did not find changes in the expression of pluripotency or germ layer markers in control hESCs/iPSCs upon loss of UBR5. Interestingly, knockdown of Ubr5 reduces the induction of *Sonic hedgehog* (Shh) in murine pluripotent stem cells upon retinoic-acid treatment⁶³. In these lines, a conditional *Ubr5* mutant mouse presents decreased hedgehog signaling during embryogenesis⁶³. Although this model exhibits shorter limbs, the differences were not significant and the mutants do not have other obvious morphological defects⁶³. Since our striatal neuronal differentiation protocol is based on the induction of hedgehog signaling, we tested whether UBR5 is necessary for the generation of MSNs from human iPSCs. However, loss of UBR5 did not affect their differentiation into MSNs, indicating that these cells conserved their ability to induce the hedgehog signaling. The distinct impact of UBR5 in pluripotency and differentiation could be associated with genetic differences between mouse and human species. Moreover, it is important to note the distinct pluripotent states exhibited by murine ESCs and hESCs/iPSCs³. Mouse ESCs are cultured in the presence of serum and leukemia inhibitory factor (LIF), and exhibit a naive state resembling the pluripotent state observed in the inner cell mass of the pre-implantation embryo³. On the other hand, hESCs as well as human iPSCs do not require LIF signaling and exhibit a more primed state that resembles post-implantation embryonic configurations³.

Although loss of UBR5 did not impair pluripotency markers in human control iPSCs, it induced the formation of misfolded protein aggregates (i.e., aggresomes). However, we found that the accumulation of polyQ-expanded aggregates in HD-iPSCs does not impair pluripotency markers or induce their differentiation. Most importantly, these cells retain the ability to differentiate into neural cells that also accumulate polyQ-expanded aggregates. With these results, we speculate that increased proteostasis of pluripotent stem cells may be required to avoid the generation of precursor cells that accumulate protein aggregates at early organismal stages, a process that could be detrimental to organismal survival and healthspan. However, it is important to remark that most of our studies were performed in iPSCs, and further evidence in hESCs as well as in vivo experiments using mouse models are necessary to assess this intriguing possibility. On the other hand, HD-iPSCs with decreased levels of UBR5 can be further differentiated into MSNs with no aggregates. These results

could imply the activation of additional proteostatic control mechanisms to scavenge aggregates during terminal neuronal differentiation. It will be fascinating to define these mechanisms due to its implications for development and organismal aging.

Notably, genetic variations in a region of the chromosome 8 that contains the *UBR5* gene, among others (i.e., *RRM2B*, *MIR5680*, *NCALD*), have been associated with an early onset of HD by genome-wide association analysis³⁷. Whereas our results demonstrate that UBR5 levels decrease during differentiation, an intriguing possibility is that a further dysfunction of UBR5 activity with age could contribute to the onset of diseases such as HD. However, modeling HD as well as other neurodegenerative disorders using patient-specific neurons is challenging, as neurons differentiated from iPSCs lack aggregates and strong cell death phenotype^{12,20,25,27}. Moreover, iPSC-derived neurons do not exhibit HTT mutant aggregates even after the addition of cellular stressors such as proteasome inhibitors. Although the relevance of UBR5 in HD pathology remains unclear due to these limitations, we find that ectopic expression of UBR5 is sufficient to reduce the protein levels of polyQ-expanded HTT and its aggregation in mutant HTT-overexpressing cell models. Moreover, UBR5 knockdown hastens the deleterious changes induced by polyQ-expanded expression in *C. elegans* models, providing direct evidence of a link between UBR5 activity and polyQ-expanded aggregation with age. It is important to note that these *C. elegans* models express polyQ-expanded fused to YFP but not HTT protein. Thus, these results suggest that UBR5 could also have a role in the proteostasis of other polyQ-containing proteins related with disease. However, we found that UBR5 knockdown does not impair polyQ-expanded ATXN3 levels and aggregation in MJD-iPSCs. Thus, we conclude that not all polyQ-containing proteins are regulated via UBR5 activity. In these lines, we observed that UBR5 does not impinge upon cellular localization and aggregation of FUS variants linked with ALS. Although these results suggest specificity of UBR5 for HTT regulation, we cannot discard a role in the proteostasis of other aggregation-prone proteins associated with disease. Notably, UBR5 downregulation is sufficient to induce the accumulation of aggresomes in control hESCs/iPSCs. Since aggresomes form from the accumulation of misfolded proteins when proteolytic systems are overwhelmed, UBR5 may also be involved in the degradation of misfolded proteins ensued from normal metabolism. Taken together, our studies in immortal pluripotent stem cells identified UBR5 as a determinant of their super-vigilant proteostasis.

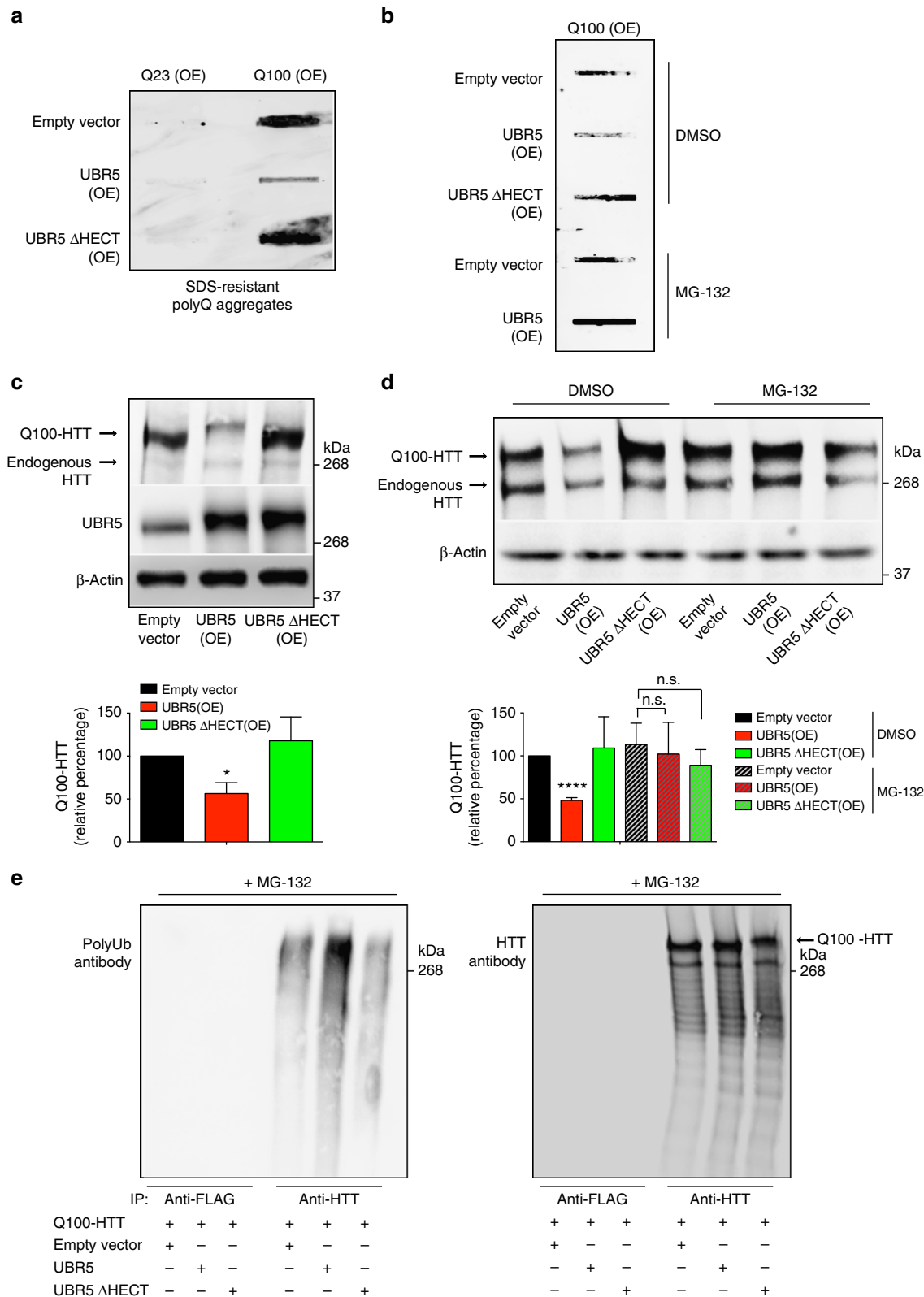
Methods

hESC/iPSC lines and culture. The H9 (WA09) and H1 (WA01) hESC lines were obtained from the WiCell Research Institute. The H9 and H1 hESCs used in our study matches exactly the known short tandem repeat (STR) profile of these cells across the 8 STR loci analyzed (Supplementary Table 3a). No STR polymorphisms other than those corresponding to H9 and H1¹² were found in the respective cell

Fig. 9 UBR5 loss hastens aggregation and neurotoxicity in HD *C. elegans* models. **a** Western blot analysis of *C. elegans* with antibodies to GFP and β -actin loading control. The graph represents the Q67-YFP relative percentage values to Q67, vector RNAi-*C. elegans* corrected for β -actin loading control (mean \pm s.e.m. of three independent experiments). **b** Filter trap analysis indicates that *ubr-5* knockdown increases polyQ aggregates (detected by anti-GFP antibody) in *C. elegans*. The images are representative of four independent experiments. **c** Representative images of Q67-YFP aggregation under *ubr-5* knockdown in whole adult worms. On the right, a higher magnification of head neurons is presented. For higher magnification of *C. elegans* mid-body, please see Supplementary Fig. 36. The images are representative of five independent experiments. Scale bar represents 100 μ m. White arrows and red arrows indicate nerve ring and chemosensory processes, respectively. DIC, differential interference contrast. **d** Filter trap analysis with anti-GFP antibody of polyQ-expressing neuronal models in wild-type and *rff-3(pk1426)* background. The images are representative of five independent experiments. **e** Loss of *ubr-5* hastens the motility defects of polyQ67 worms. Bar graphs represent average (\pm s.e.m.) thrashing movements over a 30 s period on day 3 of adulthood (Q19 fed vector RNAi ($n = 62$) versus Q19 fed *ubr-5* RNAi ($n = 64$), $P = 0.11$; Q19 fed vector RNAi versus Q67 fed vector RNAi ($n = 65$), $P < 0.0001$; Q67 fed vector RNAi versus Q67 fed *ubr-5* RNAi ($n = 65$), $P < 0.0001$). All the statistical comparisons were made by Student's *t*-test for unpaired samples. $^{**}P < 0.01$, $^{***}P < 0.0001$

lines, indicating correct hESC identity and no contamination with any other human cell line. The control iPSCs #3 and HD Q71-iPSC lines #1 were a gift from G.Q. Daley. These cells were generated using retroviral induction of c-Myc, Klf4, Oct4 and Sox2 and fully characterized for pluripotency in refs.^{26,64}. HD Q71-iPSC line #2 (ND42230) was obtained from NINDS Human Cell and Data Repository (NHCDR) through Coriell Institute. These cells were generated from the same parental fibroblast as HD Q71-iPSC line #1 via episomal expression of l-Myc, Klf4, Oct4, Sox2 and LIN28 reprogramming factors. Likewise, ND42242 (control iPSC

line #1, Q21), ND36997 (control iPSC line #2, Q33), ND41656 (HD Q57-iPSC) and ND36999 (HD Q180-iPSC) were also obtained from NHCDR through Coriell Institute. Corrected isogenic counterparts of Q180-iPSCs (i.e., HD-C#1 and HD-C#2) were a gift from M.A. Pouladi³⁰. By STR analysis, we confirmed correct genetic identity of the control and HD-iPSCs used in our study with the corresponding parental fibroblast lines when fibroblasts were available (that is, control iPSCs #1, control iPSCs #2, HD Q71-iPSCs, HD Q57-iPSCs and HD Q180-iPSCs; Supplementary Table 4). Parental fibroblasts GM02183 (control #2), GM04281



(HD Q71) and GM09197 (HD Q180) were obtained from Coriell Institute, whereas ND30014 (control #1) and ND33392 (HD Q57) fibroblasts were obtained from NHCDR through RUCDR Infinite Biologicals at Rutgers University.

UKBi001-B (MJD Q74-iPSC line #1) and UKBi003-A (MJD Q74-iPSC line #2) were obtained from the European Bank for induced pluripotent Stem Cells (EBiSC). These MJD-iPSC lines were generated using retroviral expression of reprogramming factors (i.e., c-Myc, Klf4, Oct4 and Sox2) and fully characterized for pluripotency in ref.⁴⁸. The MJD-iPSCs used in our study matches exactly the STR profile of the parental fibroblasts provided by the depositor of the lines (Supplementary Table 3b).

Control iPSCs #4 (FUS^{wt/wt}), ALS-iPSCs #1 (FUS^{R521C/wt}) and ALS-iPSCs #2 (FUS^{P525L/P525L}) were kindly provided by A. Rosa and I. Bozzoni. All of them were produced and characterized for pluripotency in ref.⁴⁹. Briefly, control iPSCs #4 were derived from a control donor and checked for absence of mutation in FUS⁴⁹ whereas ALS-iPSCs #1 were generated from a patient affected by ALS in mid-late age⁵⁰. Both iPSCs lines were established via lentiviral expression of c-Myc, Klf4, Oct4 and Sox2. ALS-iPSCs #2 were raised from control iPSCs #4 by TALEN (transcription activator-like effector nucleases)-directed mutagenesis and are homozygote for a FUS mutation (P525L) linked with severe and juvenile ALS⁴⁹. We confirmed that the STR profile of the ALS-iPSCs #2 used in our experiments matches with the profile of control iPSCs #4 (Supplementary Table 4).

The hESCs and iPSCs were maintained on Geltrex (ThermoFisher Scientific) using mTeSR1 (Stem Cell Technologies). Undifferentiated hESC/iPSC colonies were passaged using a solution of dispase (2 mg ml⁻¹), and scraping the colonies with a glass pipette. Alternatively, cells were individualized with Accutase (1 unit ml⁻¹, Invitrogen) and seeded into Geltrex-coated plates for experiments with proteasome and autophagy inhibitors to facilitate homogenous treatment of cultures. All the hESC and iPSC lines used in our experiments had a normal diploid karyotype as assessed by single nucleotide polymorphism (SNP) genotyping (Supplementary Fig. 40). Moreover, all the cell lines used in this study were tested for mycoplasma contamination at least once every 3 weeks. No mycoplasma contamination was detected. Research involving hESC lines was performed with approval of the German Federal competent authority (Robert Koch Institute).

SNP genotyping. The molecular karyotype was analyzed by SNP genotyping with Illumina's HumanOmniExpressExome-8-v1.2 BeadArray (Illumina, Inc., San Diego, USA) at the Institute for Human Genetics (Department of Genomics, Life & Brain Center, University of Bonn, Germany). Processing was performed on genomic DNA following the manufacturer's procedures. Copy number regions were detected using the cnvPartition version 3.1.6.

STR analysis. STR analysis of H9 and H1 hESCs was conducted using the Promega PowerPlex 21 system (Promega Corporation) by Eurofins Genomics (Germany). We analyzed loci D5S818, D13S317, D7S820, D16S539, vWA, TH01, TP0X and CSF1P0 to compare with the known STR profile of these hESC lines¹². The STR analysis of MJD-iPSC lines was also performed by Eurofins Genomics using the Promega PowerPlex 21 system.

Genotype comparison of control and HD-iPSCs lines with their parental fibroblasts was performed using the following microsatellite markers: D17S1303, D16S539, vWA, TH01, CSF1P0 and TP0X. Fluorescently labeled PCR products were electrophoresed and detected on an automated 3730 DNA Analyzer and data were analyzed using Genemapper software version 3.0 to compare allele sizes between iPSCs and their parental fibroblasts (Applied Biosystems).

Neural differentiation. To obtain NPC cultures, we induced neural differentiation of iPSCs with STEMdiff Neural Induction Medium (Stem Cell Technologies)

following the monolayer culture method⁶⁵. Undifferentiated iPSCs were rinsed once with phosphate-buffered saline (PBS) and then we added 1 ml of Gentle Dissociation Reagent (Stem Cell Technologies) for 10 min. After the incubation period, we gently dislodged pluripotent cells and added 2 ml of Dulbecco's Modified Eagle Medium (DMEM)/F12 (ThermoFisher Scientific)+10 μ M ROCK inhibitor (Abcam). Then, we centrifuged cells at 300 \times g for 10 min. Cells were resuspended on STEMdiff Neural Induction Medium+10 μ M ROCK inhibitor and plated on poly-ornithine (15 μ g ml⁻¹)/laminin (10 μ g ml⁻¹)-coated plates at a density of 200,000 cells cm⁻².

Striatal neuron differentiation. iPSCs were differentiated into striatal neurons by induction of hedgehog signaling pathway⁵⁶. iPSCs were detached by incubating with dispase (1 mg ml⁻¹) for 20 min. The detached colonies were cultured in suspension as free-floating embryoid bodies (EBs) in the differentiation medium consisting of DMEM/F12, 20% knockout serum replacement, 100 μ M β -Mercaptoethanol (Sigma), 1 \times minimum essential medium (MEM) non-essential amino acids and 2 mM l-glutamine. On day 4, the medium was replaced with a neural induction medium consisting of DMEM/F12, N2 supplement (ThermoFisher Scientific), 1 \times MEM non-essential amino acids, 2 mM glutamine and 2 μ g ml⁻¹ heparin. On day 7, the EBs were attached to the laminin (ThermoFisher Scientific)-coated substrate in a 35 mm culture Petri dish and cultured in the neural induction medium. In the next week, the EBs flattened and columnar neuroepithelia organized into rosette appeared in the center of individual colonies. On day 12, 0.65 μ M purmorphamine (Stem Cell Technologies) was added for 14 days (until day 25). From day 26, neuroepithelial spheres were dissociated with Accutase (1 unit ml⁻¹, Invitrogen) at 37 °C for 5 min and placed onto poly-ornithine/laminin-coated cover slips in Neurobasal medium containing a set of trophic factors, including brain-derived neurotrophic factor (20 ng ml⁻¹), glial-derived neurotrophic factor (10 ng ml⁻¹), insulin-like growth factor-1 (10 ng ml⁻¹), and cAMP (1 μ M) (all from R&D Systems). DARPP32-expressing neurons appeared by day 32 as assessed by immunohistochemistry using Rabbit anti-DARPP32 (Abcam, ab40801, 1:50). We performed the experiments between days 32 and 35 of the differentiation protocol.

Lentiviral infection of iPSCs. Lentivirus (LV)-non-targeting small hairpin RNA (shRNA) control, LV-HTT shRNA (TRCN0000322961), LV-UBR5 shRNA #1 (TRCN0000003411), LV-UBR5 shRNA #2 (TRCN0000226458), LV-UBE3A shRNA (TRCN0000419838), LV-UBR7 shRNA (TRCN0000037025), LV-RNF181 shRNA #1 (TRCN0000364405), LV-RNF181 shRNA #2 (TRCN0000022389), LV-TRIM71 shRNA #1 (TRCN0000245956) and LV-TRIM71 shRNA #2 (TRCN0000245959) in pLKO.1-puro vector were obtained from Mission shRNA (Sigma). Transient infection experiments were performed as follows. iPSCs colonies growing on Geltrex were individualized using Accutase. Hundred thousand cells were plated on Geltrex plates and incubated with mTeSR1 medium containing 10 μ M ROCK inhibitor for 1 day. Then, cells were infected with 5 μ l of concentrated lentivirus. Plates were centrifuged at 800 \times g for 1 h at 30 °C. Cells were fed with fresh media the day after to remove the virus. After 1 day, cells were selected for lentiviral integration using 2 μ g ml⁻¹ puromycin (ThermoFisher Scientific). Cells were split for further experiments and collected after 5–7 days of infection.

Transfection of HEK293T cells. HEK293T cells (ATCC) were plated on 0.1% gelatin-coated plates and grown in DMEM supplemented with 10% fetal bovine serum and 1% MEM non-essential amino acids (ThermoFisher Scientific) at 37 °C, 5% CO₂ conditions. Cells were transfected once they reached 80–90% confluency. Then, 1 μ g GFP-UBR5 wild-type or GFP-UBR5 Δ HECT overexpression plasmid

Fig. 10 Upregulation of UBR5 suppresses polyQ-expanded HTT aggregation. **a** Filter trap analysis with anti-polyQ-expansion diseases marker antibody of HEK293 human cells overexpressing (OE) Q23-HTT or Q100-HTT. Ectopic expression of UBR5 reduces the accumulation of aggregates in Q100-HTT(OE) cells. On the contrary, overexpression of a catalytic inactive UBR5 mutant (UBR5 Δ HECT) does not ameliorate polyQ-expanded aggregation. The images are representative of three independent experiments. **b** Filter trap analysis of Q100-HTT(OE) HEK293 cells. Proteasome inhibition with 0.5 μ M MG-132 for 16 h blocks the reduction of polyQ-expanded aggregation induced by ectopic expression of wild-type UBR5. The images are representative of three independent experiments. **c** Western blot analysis of Q100-HTT(OE) HEK293 cells with antibodies to HTT and UBR5. Overexpression of wild-type UBR5 reduces the levels of Q100-HTT, whereas similar levels of UBR5 Δ HECT do not decrease mutant HTT levels. The graph represents the relative percentage values of Q100-HTT to empty vector cells corrected for β -actin loading control (mean \pm s.e.m. of three independent experiments). **d** Western blot analysis of whole cell lysates from Q100-HTT(OE) HEK293 cultures with antibodies to HTT and β -actin loading control. Proteasome inhibition with 0.5 μ M MG-132 for 16 h blocks proteasomal degradation of Q100-HTT levels induced by wild-type UBR5 overexpression. The graph represents the relative percentage values of Q100-HTT to DMSO-empty vector cells corrected for β -actin loading control (mean \pm s.e.m. of three independent experiments). **e** Immunoprecipitation with anti-HTT and anti-FLAG antibodies in Q100-HTT(OE) HEK293. Immunoprecipitation was followed by western blot with antibodies to HTT and polyubiquitinated proteins (polyUb) to detect immunoprecipitated total HTT protein and polyUb-HTT, respectively. Prior to immunoprecipitation, cells were treated with proteasome inhibitor (0.5 μ M MG-132, 16 h) to block the degradation of HTT induced by UBR5 so we could immunoprecipitate similar amounts of HTT for direct comparison of polyubiquitination among the distinct conditions. The images are representative of three independent experiments. All the statistical comparisons were made by Student's *t*-test for unpaired samples. **P* < 0.05, *****P* < 0.0001

and 0.5 µg pARIS-mCherry-httQ23-GFP or pARIS-mCherry-httQ100-GFP were used for transfection, using Eugene HD (Promega) following the manufacturer's instructions. After 36 h of incubation in normal medium, the cells were harvested for further experiments. GFP-UBR5 wild-type and GFP-UBR5 ΔHECT overexpression plasmids (Addgene plasmids #52050 and #52051, respectively) were a gift from D. Saunders and were first published in ref.⁶¹. The pARIS-mCherry-httQ23-GFP and pARIS-mCherry-httQ100-GFP⁶⁶ plasmids were a gift from F. Saudou.

Analysis of β-amyloid aggregation. N-terminal c-Myc-tagged β23 protein construct was a gift from F.U. Hartl⁶⁷. For mammalian expression, c-Myc-tagged β23 sequence was cloned into pCDH-CMV-MCS-EF1 from pcDNA3.1 using *Xba*I and *Bam*HI enzymes. Cell fractionation was performed following the protocol described in ref.⁶⁷. Briefly, cells were collected and resuspended in lysis buffer (50 mM Tris (pH 7.8), 150 mM NaCl, 1% (v/v) NP40, 0.25% sodium deoxycholate, 1 mM EDTA and 1 tablet protease inhibitor cocktail (Roche) per 10 ml). The cell lysate was then centrifuged at 20,000 × g for 30 min at 4 °C. The supernatant was applied for analyzing soluble fraction and pellets were dissolved in SDT buffer (4% (w/v) sodium dodecyl sulfate (SDS), 100 mM Tris-HCl (pH 7.6) and 0.1 M dithiothreitol (DTT)). Anti-Myc antibody (Proteintech, #66004-1-Ig, 1:2000) was used for western blot to detect c-Myc-tagged β23 protein.

Protein immunoprecipitation for interaction analysis. iPSCs were lysed in RIPA buffer (50 mM Tris-HCl (pH 7.4), 150 mM NaCl, 1% Triton X-100, 1% sodium deoxycholate, 0.1% SDS, 1 mM EDTA, 1 mM phenylmethylsulfonyl fluoride (PMSF)) supplemented with protease inhibitor cocktail (Roche). Lysates were homogenized by passing 10 times through a 27-gauge (27 G) needle attached to a 1 ml syringe and centrifuged at 13,000 × g for 15 min at 4 °C. After pre-clearing the supernatant with Protein A agarose beads (Pierce), the samples were incubated overnight with UBR5 antibody (Cell Signaling, #8755, 1:50) on the overhead shaker at 4 °C. As a control, the same amount of protein was incubated with anti-FLAG (SIGMA, F7425, 1:50) or anti-UBE3A antibody (Cell Signaling, #7526, 1:50) in parallel. Subsequently, samples were incubated with 30 µl of Protein A beads for 1 h at room temperature. After this incubation, samples were centrifuged for 5 min at 5,000 × g and the pellet was washed three times with RIPA buffer. For elution of the proteins, the pellet was incubated with 2× Laemmli Buffer, boiled for 5 min and centrifuged for 5 min at maximum speed. The supernatant was taken and loaded onto a sodium dodecyl sulfate–polyacrylamide gel electrophoresis (SDS–PAGE) gel for western blot analysis.

Protein immunoprecipitation for assessing polyubiquitination. HEK293 cells were lysed in protein lysis buffer (50 mM Tris-HCl (pH 6.7), 150 mM NaCl, 1% NP40, 0.25% sodium deoxycholate, 1 mM EDTA, 1 mM PMSF, 1 mM Na₃VO₄, 1 mM NaF) supplemented with protease inhibitor cocktail. Lysates were homogenized through a syringe needle (27 G) and centrifuged at 13,000 × g for 15 min at 4 °C. The samples were incubated for 30 min with HTT antibody (Cell Signaling, ab#5656, 1:1000) on ice. As a negative control, the same amount of protein was incubated with anti-FLAG antibody (SIGMA, F7425) in parallel. Subsequently, samples were incubated with 50 µl of µMACS Micro Beads for 1 h at 4 °C with overhead shaking. After this incubation, samples were loaded to pre-cleared µMACS column (#130-042-701). Beads were washed three times with 50 mM Tris (pH 7.5) buffer containing 150 mM NaCl, 5% glycerol and 0.05% Triton and then washed five times with 50 mM Tris (pH 7.5) and 150 mM NaCl. For protein elution, the beads were incubated with 1× Laemmli Buffer for 5 min and collected into tubes. The samples were boiled for 5 min at 95 °C and loaded in a SDS–PAGE gel for western blot analysis.

Proteomics analysis of HTT ubiquitination sites. HEK293 cells were lysed in protein lysis buffer (50 mM Tris-HCl (pH 6.7), 150 mM NaCl, 1% NP40, 0.25% sodium deoxycholate, 1 mM EDTA, 1 mM NaF) supplemented with protease inhibitor cocktail. Lysates were homogenized through syringe needle (27 G) and centrifuged at 13,000 × g for 15 min at 4 °C. The samples were incubated for 30 min with HTT antibody (Cell Signaling, ab#5656, 1:1000) on ice. Subsequently, samples were incubated with 50 µl of µMACS Micro Beads for 1 h at 4 °C with overhead shaking. After this incubation, samples were loaded to pre-cleared µMACS column (#130-042-701). Beads were washed three times with 50 mM Tris (pH 7.5) buffer containing 150 mM NaCl, 5% glycerol and 0.05% Triton and then washed five times with 50 mM Tris (pH 7.5) and 150 mM NaCl. Then, columns were subjected to in-column tryptic digestion containing 7.5 mM ammonium bicarbonate, 2 M urea, 1 mM DTT and 5 ng ml^{−1} trypsin. Digested peptides were eluted using two times 50 µl of elution buffer 1 containing 2 M urea, 7.5 mM Ambic, and 5 mM iodoacetamide. Digests were incubated overnight at room temperature with mild shaking in the dark. Samples were stage-tipped the next day for label-free quantitative proteomics. All samples were analyzed on a Q-Exactive Plus (Thermo Scientific) mass spectrometer that was coupled to an EASY nLC 1200 UPLC (Thermo Scientific)⁶⁸. Peptides were loaded with solvent A (0.1% formic acid in water) onto an in-house packed analytical column (50 cm × 75 µm I.D., filled with 2.7 µm Poroshell EC120 C18, Agilent). Peptides were chromatographically separated at a constant flow rate of 250 nl min^{−1} using 150 min methods: 5–30%

solvent B (0.1% formic acid in 80% acetonitrile) within 119 min, 30–50% solvent B within 19 min, followed by washing and column equilibration. The mass spectrometer was operated in data-dependent acquisition mode. The MS1 survey scan was acquired from 300 to 1750 *m/z* at a resolution of 70,000. The top 10 most abundant peptides were subjected to higher collisional dissociation fragmentation at a normalized collision energy of 27%. The AGC (automatic gain control) target was set to 5e5 charges. Product ions were detected in the Orbitrap at a resolution of 17,500.

All mass spectrometric raw data were processed with Maxquant (version 1.5.3.8) using default parameters. Briefly, MS2 spectra were searched against the human Uniprot database, including a list of common contaminants. False discovery rates (FDRs) on protein and peptide–spectrum match (PSM) level were estimated by the target-decoy approach to 0.01% (Protein FDR) and 0.01% (PSM FDR) respectively. The minimal peptide length was set to 7 amino acids and carbamidomethylation at cysteine residues was considered as a fixed modification. Oxidation (M), GlyGly (K) and Acetyl (Protein N-term) were included as variable modifications. The match-between runs option was enabled. Label-free quantification (LFQ) was enabled using default settings. The resulting output was processed using Perseus as follows: protein groups flagged as “reverse”, “potential contaminant” or “only identified by site” were removed from the proteinGroups.txt. LFQ values were log2 transformed. Missing values were replaced using an imputation-based approach (random sampling from a normal distribution using a down shift of 1.8 and a width of 0.3). Significant differences between the groups were assessed using Student's *t*-test. A permutation-based FDR approach was applied to correct for multiple testing.

Western blot. Cells were scraped from tissue culture plates by cell scraping and lysed in protein cell lysis buffer (50 mM Hepes pH 7.4, 150 mM NaCl, 1 mM EDTA, 1% Triton X-100) supplemented with 2 mM sodium orthovanadate, 1 mM PMSF and protease inhibitor mix). Lysates were homogenized through syringe needle (27 G) followed by centrifugation at 8000 × g for 5 min at 4 °C and then supernatants were collected (with the exception of the western blots showed in Fig. 6d, where we loaded whole cell lysates without centrifugation because protease inhibition induced high concentration of Q100-HTT (OE) in the pellet fraction). Protein concentrations were determined with a standard BCA protein assay (ThermoFisher Scientific). Approximately 30 µg of total protein was separated by SDS–PAGE, transferred to polyvinylidene difluoride membranes (Millipore) and subjected to immunoblotting. Western blot analysis was performed with anti-UBR5 (Stem Cell Technologies, #60094, 1:1000), anti-UBE3A (Cell Signaling, ab#7526, 1:1000), anti-RNF181 (ThermoFisher Scientific, PA5-31008, 1:2000), anti-UBR7 (ThermoFisher Scientific, PA5-31559, 1:1000), anti-ATXN3 (Merck, MAB5360, 1:500), anti-FUS (Abcam, #154141, 1:1000), anti-GFP (Immuno-kontakt, 210-PS-1GF, 1:5000), anti-polyubiquitylated conjugates (Enzo, PW8805-0500, 1:1000), anti-p62 (Progen, GP62-C, 1:1000), anti-LC3 (Sigma, L7543, 1:1000), anti-DARPP32 (Abcam, #40801, 1:1000) and anti-β-actin (Abcam, #8226, 1:5000). To detect HTT protein, we used anti-HTT (Cell Signaling, ab#5656, 1:1000), a monoclonal antibody produced by immunizing animals with a synthetic peptide corresponding to residues surrounding Pro1220 of human HTT protein. To detect mutant HTT, we used anti-polyQ-expansion diseases marker (Millipore, MAB1574, 1:1000), a monoclonal antibody raised against TATA-binding protein that recognizes peptides overlapping the polyQ stretch of this protein. This antibody also recognizes polyQ-containing proteins such as HTT and ATXN3 with the remarkable property of detecting much better the polyQ-expanded pathological proteins than the wild-type proteins^{12,31}. Uncropped versions of all important western blots are presented in Supplementary Fig. 41.

Immunocytochemistry. Cells were fixed with paraformaldehyde (4% in PBS) for 20 min, followed by permeabilization (0.2% Triton X-100 in PBS for 10 min) and blocking (3% bovine serum albumin in 0.2% Triton X-100 in PBS for 10 min). Human iPSCs/NPCs were incubated in primary antibody for 2 h at room temperature (Mouse anti-polyQ (Millipore, MAB1574, 1:50), Mouse anti-OCT4 (Stem Cell Technologies, #60093, 1:200), Rabbit anti-PAX6 (Stem Cell Technologies, #60094, 1:300), Mouse anti-FUS (Abcam, #154141, 1:500), Rabbit anti-G3BP1 (MBL, #RN048PW, 1:500), Rabbit anti-DARPP32 (Abcam, #40801, 1:50), Rabbit anti-GABA (Sigma, #A2052, 1:100) and Chicken anti-MAP2 (Abcam, #5392, 1:500). Then, cells were washed with 0.2% Triton-X/PBS and incubated with secondary antibody (Alexa Fluor 488 Goat anti-Mouse (ThermoFisher Scientific, #A-11029, 1:500), Alexa Fluor 568F(ab')₂ Fragment of Goat Anti-Rabbit IgG (H+L) (ThermoFisher Scientific, #A-21069, 1:500)), Alexa Fluor 647 Donkey anti-Chicken (Jackson ImmunoResearch, #A-703-605-155, 1:500) and Hoechst 33342 (Life Technologies, #1656104) for 1 h at room temperature. PBS and distilled water wash were followed before the cover slips were mounted on Mowiol (Sigma, #324590).

Aggresome detection. Pluripotent stem cells were cultured at 37 °C or under heat stress conditions at 42 °C for 4 h. Aggresome formation was detected by PROTEOSTAT Aggresome Detection Kit (ENZO, #ENZ-51035), following the manufacturer's instructions. Briefly, the cells were fixed in 4% formaldehyde solution and permeabilized with 0.5% Triton X-100, 3 mM EDTA, pH 8.0, in 1× assay buffer from the detection kit. Then, aggresomes were stained with PROTEOSTAT

Aggresome Detection reagent, including Hoechst 33342 for nuclear staining. Imaging of aggresomes was performed using a standard rhodamine filter set.

Propidium iodide staining. Cells were incubated with 2 $\mu\text{g ml}^{-1}$ propidium iodide (Sigma, #81845) and Hoechst 33342 (Life Technologies, #1656104) for 1.5 h. Then, cover slips were mounted using FluorSave Reagent (Calbiochem, #345789).

TUNEL staining. TUNEL (terminal deoxynucleotidyl transferase dUTP nick end labeling) measurement was performed with the In situ BrdU-Red DNA Fragmentation (TUNEL) Assay Kit (Abcam, #66110) according to the manufacturer's protocol. Briefly, cells were washed twice and stained with TdT enzyme and BrdUTP for 1 h at 37 °C. A second incubation with an Anti-BrdU-Red antibody was performed at room temperature for 30 min. Nuclei were stained with Hoechst 33342 (Life Technologies, #1656104).

RNA isolation and quantitative reverse transcription-PCR. Total RNA was extracted using RNeasy (Tel-Test Inc.). Complementary DNA (cDNA) was generated using qScript Flex cDNA synthesis kit (Quantabio). SybrGreen real-time quantitative PCR (qPCR) experiments were performed with a 1:20 dilution of cDNA using a CFC384 Real-Time System (Bio-Rad) following the manufacturer's instructions. Data were analyzed with the comparative $2\Delta\Delta C_t$ method using the geometric mean of *ACTB* and *GAPDH* as housekeeping genes. See Supplementary Table 5 for details about the primers used for this assay.

26S proteasome fluorogenic peptidase assays. Cells were collected in proteasome activity assay buffer (50 mM Tris-HCl, pH 7.5, 250 mM sucrose, 5 mM MgCl_2 , 0.5 mM EDTA, 2 mM ATP and 1 mM DTT) and lysed by passing 10 times through a 27 G needle attached to a 1 ml syringe needle. Lysates were centrifuged at $10,000 \times g$ for 10 min at 4 °C. Then, 25 μg of total protein of cell lysates were transferred to a 96-well microtiter plate (BD Falcon) and incubated with the fluorogenic proteasome substrate. To measure the chymotrypsin-like activity of the proteasome we used either Z-Gly-Gly-Leu-AMC (Enzo) or Suc-Leu-Leu-Val-Tyr-AMC (Enzo). We used Z-Leu-Leu-Glu-AMC (Enzo) to measure the caspase-like activity of the proteasome, and Ac-Arg-Leu-Arg-AMC (Enzo) for the proteasome trypsin-like activity. Fluorescence (380 nm excitation, 460 nm emission) was monitored on a microplate fluorometer (EnSpire, Perkin Elmer) every 5 min for 1 h at 37 °C.

Quantitative proteomics analysis of E3 enzymes. For the characterization of protein expression differences in E3 enzymes comparing H9 hESCs with their neuronal counterparts, we analyzed quantitative proteomics data³⁵ available via ProteomeXchange with identifier PXD007738. Then, we intersected the annotated human E3 network from KEGG (Kyoto Encyclopedia of Genes and Genomes) database⁶⁹ with this proteomics dataset. Statistical comparisons were made by Student's *t*-test. FDR-adjusted *P* value (*q* value) was calculated using the Benjamini–Hochberg procedure.

C. elegans strains and maintenance. *C. elegans* strains were maintained at 20 °C using standard methods¹⁷. AM23 (*rmls298[pF25B3.3::Q19::CFP]*) and AM716 (*rmls284[pF25B3.3::Q67::YFP]*) strains were a gift from R. I. Morimoto. For the generation of the strains DVG144 (*rmls298[pF25B3.3::Q19::CFP]; rrf-3(pk1426)*) and DVG145 (*rmls284[pF25B3.3::Q67::YFP]; rrf-3(pk1426)*), NL2099 strain (*rrf-3(pk1426)*) was crossed to AM23 and AM716, respectively. Screening of *rrf-3(pk1426)* worms was done by PCR using the forward primer F: GTTTTGACGC CAAACGGTGA and two reverse primers: TGCAGCATGTCCAGACACAA, which outflanks the deleted region in *rrf-3(pk1426)*, and CCATTCTGTGCACGT TTCCA, which binds inside the deletion.

RNAi experiments in C. elegans. RNAi-treated strains were fed *Escherichia coli* (HT115) containing an empty control vector (L4440) or expressing double-stranded *ubr-5* RNAi. *ubr-5* RNAi construct was obtained from the Ahringer RNAi library and sequence verified.

Imaging of polyQ aggregates in C. elegans. AM716 and AM23 strains were grown at 20 °C until L4 stage and then grown at 25 °C on *E. coli* (HT115) containing either empty control vector or *ubr-5* RNAi until day 3. Day 3 adult worms were immobilized following the protocol described in ref.⁷⁰. Briefly, worms were placed on 5% agarose-containing pads on a suspension of polystyrene beads (Polyscience, 2.5% by volume). For imaging, we used a Meta 710 confocal microscope (Zeiss) at the CECAD Imaging Facility.

Quantitative fluorescence recovery after photobleaching. Q67-YFP day 3 adult worms were immobilized on 5% agarose pads using 0.1% sodium azide. After three prebleaching scans, a constant region of interest (ROI) ($44.29 \times 30.09 \mu\text{m}$) was bleached for 20 scans (860 ms per iteration) in a SP8 Confocal Microscope (Leica). Directly after bleaching, the fluorescence recovery was sampled once every 2 s for 90 times. Average fluorescence intensities within ROIs were measured under the

same condition for empty vector and *ubr-5* RNAi-treated worms using ImageJ software. The half-life of fluorescence recovery ($t_{1/2}$) was determined by curve fitting of experimental data using the following exponential equation: $I(t) = a(1 - e^{-(\tau \times t)})$.

Motility assay. Animals were grown on *E. coli* (OP50) bacteria at 20 °C until L4 stage and then transferred to 25 °C and fed with *E. coli* (HT115) bacteria containing empty control vector or *ubr-5* RNAi for the rest of the experiment. At day 3 of adulthood, worms were transferred to a drop of M9 buffer and after 30 s of adaptation the number of body bends was counted for 30 s. A body bend was defined as change in direction of the bend at the mid-body⁵⁸.

Filter trap. AM716, AM23, DVG144 and DVG145 *C. elegans* strains were grown at 20 °C until L4 stage and then grown at 25 °C on *E. coli* (HT115) bacteria containing either empty control vector or *ubr-5* RNAi for the rest of the experiment. Day 3 adult worms were collected with M9 buffer and worm pellets were frozen with liquid N₂. Frozen worm pellets were thawed on ice and worm extracts were generated by glass bead disruption on ice in non-denaturing lysis buffer (50 mM Hepes pH 7.4, 150 mM NaCl, 1 mM EDTA, 1% Triton X-100) supplemented with EDTA-free protease inhibitor cocktail (Roche). Worm and cellular debris was removed with $8000 \times g$ spin for 5 min. Approximately 100 μg of protein extract was supplemented with SDS at a final concentration of 0.5% and loaded onto a cellulose acetate membrane assembled in a slot blot apparatus (Bio-Rad). The membrane was washed with 0.2% SDS and retained Q67-GFP was assessed by immunoblotting for green fluorescent protein (GFP; ImmunoKontakt, 210-PS-1GFP, 1:5000). Extracts were also analyzed by SDS–PAGE with GFP antibody to determine protein expression levels.

iPSCs were collected in non-denaturing lysis buffer supplemented with EDTA-free protease inhibitor cocktail and lysed by passing 10 times through a 27 G needle attached to a 1 ml syringe. Then, we followed the filter trap protocol described above. Cell pellet lysates were loaded after solubilization with 2% SDS. The membrane was washed with 0.2% SDS and retained polyQ proteins were assessed by immunoblotting for anti-polyQ-expansion diseases marker antibody (Millipore, MAB1574, 1:5000). Extracts were also analyzed by SDS–PAGE to determine HTT protein expression levels.

Data availability. Proteomics data of HTT ubiquitination sites have been deposited to the ProteomeXchange Consortium via the PRIDE partner repository with the dataset identifier PXD009803. To define E3 enzymes significantly increased in hESC, we analyzed available quantitative proteomics data from PRIDE: PXD007738³⁵. All the other data are also available from the corresponding author upon reasonable request.

Received: 27 September 2017 Accepted: 29 June 2018

Published online: 23 July 2018

References

- Lee, H. J., Gutierrez-Garcia, R. & Vilchez, D. Embryonic stem cells: a novel paradigm to study proteostasis? *FEBS J.* **284**, 391–398 (2017).
- Miura, T., Mattson, M. P. & Rao, M. S. Cellular lifespan and senescence signaling in embryonic stem cells. *Aging Cell* **3**, 333–343 (2004).
- Weinberger, L., Ayyash, M., Novershtern, N. & Hanna, J. H. Dynamic stem cell states: naive to primed pluripotency in rodents and humans. *Nat. Rev. Mol. Cell Biol.* **17**, 155–169 (2016).
- Nagaria, P., Robert, C. & Rassool, F. V. DNA double-strand break response in stem cells: mechanisms to maintain genomic integrity. *Biochim. Biophys. Acta* **1830**, 2345–2353 (2013).
- Saretzki, G. et al. Downregulation of multiple stress defense mechanisms during differentiation of human embryonic stem cells. *Stem Cells* **26**, 455–464 (2008).
- Tichy, E. D. & Stambrook, P. J. DNA repair in murine embryonic stem cells and differentiated cells. *Exp. Cell Res.* **314**, 1929–1936 (2008).
- Vilchez, D., Simic, M. S. & Dillin, A. Proteostasis and aging of stem cells. *Trends Cell Biol.* **24**, 161–170 (2014).
- Garcia-Prat, L., Sousa-Victor, P. & Munoz-Canoves, P. Proteostatic and metabolic control of stemness. *Cell Stem Cell* **20**, 593–608 (2017).
- Noormohammadi, A. et al. Mechanisms of protein homeostasis (proteostasis) maintain stem cell identity in mammalian pluripotent stem cells. *Cell. Mol. Life Sci.* **75**, 275–290 (2018).
- Powers, E. T., Morimoto, R. I., Dillin, A., Kelly, J. W. & Balch, W. E. Biological and chemical approaches to diseases of proteostasis deficiency. *Annu. Rev. Biochem.* **78**, 959–991 (2009).
- You, K. T., Park, J. & Kim, V. N. Role of the small subunit processome in the maintenance of pluripotent stem cells. *Genes Dev.* **29**, 2004–2009 (2015).

12. Noormohammadi, A. et al. Somatic increase of CCT8 mimics proteostasis of human pluripotent stem cells and extends *C. elegans* lifespan. *Nat. Commun.* **7**, 13649 (2016).
13. Lopez, T., Dalton, K. & Frydman, J. The mechanism and function of group II chaperonins. *J. Mol. Biol.* **427**, 2919–2930 (2015).
14. Buckley, S. M. et al. Regulation of pluripotency and cellular reprogramming by the ubiquitin-proteasome system. *Cell Stem Cell* **11**, 783–798 (2012).
15. Liu, P. et al. High autophagic flux guards ESC identity through coordinating autophagy machinery gene program by FOXO1. *Cell Death Differ.* **24**, 1672–1680 (2017).
16. Vilchez, D. et al. Increased proteasome activity in human embryonic stem cells is regulated by PSMD11. *Nature* **489**, 304–308 (2012).
17. Vilchez, D. et al. RPN-6 determines *C. elegans* longevity under proteotoxic stress conditions. *Nature* **489**, 263–268 (2012).
18. Lopez-Otin, C., Blasco, M. A., Partridge, L., Serrano, M. & Kroemer, G. The hallmarks of aging. *Cell* **153**, 1194–1217 (2013).
19. Vilchez, D., Saez, I. & Dillin, A. The role of protein clearance mechanisms in organismal ageing and age-related diseases. *Nat. Commun.* **5**, 5659 (2014).
20. Victor, M. B. et al. Striatal neurons directly converted from Huntington's disease patient fibroblasts recapitulate age-associated disease phenotypes. *Nat. Neurosci.* **21**, 341–352 (2018).
21. Finkbeiner, S. Huntington's Disease. *Cold Spring Harb. Perspect. Biol.* **3**, a007476 (2011).
22. Saudou, F. & Humbert, S. The biology of Huntingtin. *Neuron* **89**, 910–926 (2016).
23. Bates, G. Huntingtin aggregation and toxicity in Huntington's disease. *Lancet* **361**, 1642–1644 (2003).
24. Zuccato, C., Valenza, M. & Cattaneo, E. Molecular mechanisms and potential therapeutic targets in Huntington's disease. *Physiol. Rev.* **90**, 905–981 (2010).
25. Consortium, H. Di Induced pluripotent stem cells from patients with Huntington's disease show CAG-repeat-expansion-associated phenotypes. *Cell Stem Cell* **11**, 264–278 (2012).
26. Park, I. H. et al. Disease-specific induced pluripotent stem cells. *Cell* **134**, 877–886 (2008).
27. Jeon, I. et al. Neuronal properties, in vivo effects, and pathology of a Huntington's disease patient-derived induced pluripotent stem cells. *Stem Cells* **30**, 2054–2062 (2012).
28. Consortium, H. Di Developmental alterations in Huntington's disease neural cells and pharmacological rescue in cells and mice. *Nat. Neurosci.* **20**, 648–660 (2017).
29. Koyuncu, S., Fatima, A., Gutierrez-Garcia, R. & Vilchez, D. Proteostasis of Huntingtin in health and disease. *Int. J. Mol. Sci.* **18**, E1568 (2017).
30. Xu, X. et al. Reversal of phenotypic abnormalities by CRISPR/Cas9-mediated gene correction in Huntington Disease patient-derived induced pluripotent stem cells. *Stem Cell Rep.* **8**, 619–633 (2017).
31. Trotter, Y. et al. Polyglutamine expansion as a pathological epitope in Huntington's disease and four dominant cerebellar ataxias. *Nature* **378**, 403–406 (1995).
32. An, M. C. et al. Genetic correction of Huntington's disease phenotypes in induced pluripotent stem cells. *Cell Stem Cell* **11**, 253–263 (2012).
33. Monteys, A. M., Ebanks, S. A., Keiser, M. S. & Davidson, B. L. CRISPR/Cas9 editing of the mutant Huntingtin allele in vitro and in vivo. *Mol. Ther.* **25**, 12–23 (2017).
34. Zhao, M. et al. Improved high sensitivity screen for Huntington disease using a one-step triplet-primed PCR and melting curve assay. *PLoS ONE* **12**, e0180984 (2017).
35. Lee, H. J. et al. A post-transcriptional program coordinated by CSDE1 prevents intrinsic neural differentiation of human embryonic stem cells. *Nat. Commun.* **8**, 1456 (2017).
36. Yau, R. G. et al. Assembly and function of heterotypic ubiquitin chains in cell-cycle and protein quality control. *Cell* **171**, 918–933 (2017).
37. Consortium, G.-H. Identification of genetic factors that modify clinical onset of Huntington's Disease. *Cell* **162**, 516–526 (2015).
38. Su, H. et al. Mammalian hyperplastic discs homolog EDD regulates miRNA-mediated gene silencing. *Mol. Cell* **43**, 97–109 (2011).
39. Sanchez, A. et al. BMI1-UBR5 axis regulates transcriptional repression at damaged chromatin. *Proc. Natl Acad. Sci. USA* **113**, 11243–11248 (2016).
40. Mishra, A. et al. E6-AP promotes misfolded polyglutamine proteins for proteasomal degradation and suppresses polyglutamine protein aggregation and toxicity. *J. Biol. Chem.* **283**, 7648–7656 (2008).
41. de Pril, R., Fischer, D. F., Roos, R. A. & van Leeuwen, F. W. Ubiquitin-conjugating enzyme E2-25K increases aggregate formation and cell death in polyglutamine diseases. *Mol. Cell. Neurosci.* **34**, 10–19 (2007).
42. Kalchman, M. A. et al. Huntingtin is ubiquitinated and interacts with a specific ubiquitin-conjugating enzyme. *J. Biol. Chem.* **271**, 19385–19394 (1996).
43. Raychaudhuri, S., Sinha, M., Mukhopadhyay, D. & Bhattacharyya, N. P. HYPK, a Huntingtin interacting protein, reduces aggregates and apoptosis induced by N-terminal Huntingtin with 40 glutamines in Neuro2a cells and exhibits chaperone-like activity. *Hum. Mol. Genet.* **17**, 240–255 (2008).
44. Kitamura, A. et al. Cytosolic chaperonin prevents polyglutamine toxicity with altering the aggregation state. *Nat. Cell Biol.* **8**, 1163–1170 (2006).
45. Tam, S., Geller, R., Spiess, C. & Frydman, J. The chaperonin TRiC controls polyglutamine aggregation and toxicity through subunit-specific interactions. *Nat. Cell Biol.* **8**, 1155–1162 (2006).
46. Kawaguchi, Y. et al. CAG expansions in a novel gene for Machado-Joseph disease at chromosome 14q32.1. *Nat. Genet.* **8**, 221–228 (1994).
47. Ranum, L. P. et al. Spinocerebellar ataxia type 1 and Machado-Joseph disease: incidence of CAG expansions among adult-onset ataxia patients from 311 families with dominant, recessive, or sporadic ataxia. *Am. J. Hum. Genet.* **57**, 603–608 (1995).
48. Koch, P. et al. Excitation-induced ataxin-3 aggregation in neurons from patients with Machado-Joseph disease. *Nature* **480**, 543–546 (2011).
49. Lenzi, J. et al. ALS mutant FUS proteins are recruited into stress granules in induced pluripotent stem cell-derived motoneurons. *Dis. Model Mech.* **8**, 755–766 (2015).
50. Chio, A. et al. A de novo missense mutation of the FUS gene in a “true” sporadic ALS case. *Neurobiol. Aging* **32**, e523–e556 (2011).
51. Zinsner, H. et al. binds RNA in vivo and engages in nucleo-cytoplasmic shuttling. *J. Cell. Sci.* **110**, 1741–1750 (1997).
52. Gal, J. et al. Nuclear localization sequence of FUS and induction of stress granules by ALS mutants. *Neurobiol. Aging* **32**, e2327–e2340 (2011).
53. Vance, C. et al. Mutations in FUS, an RNA processing protein, cause familial amyotrophic lateral sclerosis type 6. *Science* **323**, 1208–1211 (2009).
54. Bentmann, E., Haass, C. & Dormann, D. Stress granules in neurodegeneration—lessons learnt from TAR DNA binding protein of 43 kDa and fused in sarcoma. *FEBS J.* **280**, 4348–4370 (2013).
55. Vonsattel, J. P., Keller, C. & Del Pilar Amaya, M. Neuropathology of Huntington's disease. *Handb. Clin. Neurol.* **89**, 599–618 (2008).
56. Ma, L. et al. Human embryonic stem cell-derived GABA neurons correct locomotion deficits in quinolinic acid-lesioned mice. *Cell Stem Cell* **10**, 455–464 (2012).
57. Mehta, R. et al. Proteasomal regulation of the hypoxic response modulates aging in *C. elegans*. *Science* **324**, 1196–1198 (2009).
58. Brignull, H. R., Moore, F. E., Tang, S. J. & Morimoto, R. I. Polyglutamine proteins at the pathogenic threshold display neuron-specific aggregation in a pan-neuronal *Caenorhabditis elegans* model. *J. Neurosci.* **26**, 7597–7606 (2006).
59. Timmons, L., Court, D. L. & Fire, A. Ingestion of bacterially expressed dsRNAs can produce specific and potent genetic interference in *Caenorhabditis elegans*. *Gene* **263**, 103–112 (2001).
60. Sijen, T. et al. On the role of RNA amplification in dsRNA-triggered gene silencing. *Cell* **107**, 465–476 (2001).
61. Gudjonsson, T. et al. TRIP12 and UBR5 suppress spreading of chromatin ubiquitylation at damaged chromosomes. *Cell* **150**, 697–709 (2012).
62. Cuanalo-Contreras, K., Mukherjee, A. & Soto, C. Role of protein misfolding and proteostasis deficiency in protein misfolding diseases and aging. *Int. J. Cell Biol.* **2013**, 638083 (2013).
63. Kinsella, E. et al. Use of a conditional Ubr5 mutant allele to investigate the role of an N-end rule ubiquitin-protein ligase in hedgehog signalling and embryonic limb development. *PLoS ONE* **11**, e0157079 (2016).
64. Park, I. H. et al. Reprogramming of human somatic cells to pluripotency with defined factors. *Nature* **451**, 141–146 (2008).
65. Chambers, S. M. et al. Highly efficient neural conversion of human ES and iPS cells by dual inhibition of SMAD signaling. *Nat. Biotechnol.* **27**, 275–280 (2009).
66. Pardo, R. et al. pARIS-htt: an optimised expression platform to study huntingtin reveals functional domains required for vesicular trafficking. *Mol. Brain* **3**, 17 (2010).
67. Olzscha, H. et al. Amyloid-like aggregates sequester numerous metastable proteins with essential cellular functions. *Cell* **144**, 67–78 (2011).
68. Saez, I., Koyuncu, S., Gutierrez-Garcia, R., Dieterich, C. & Vilchez, D. Insights into the ubiquitin-proteasome system of human embryonic stem cells. *Sci. Rep.* **8**, 4092 (2018).
69. Kanehisa, M., Sato, Y., Kawashima, M., Furumichi, M. & Tanabe, M. KEGG as a reference resource for gene and protein annotation. *Nucleic Acids Res.* **44**, D457–D462 (2016).
70. Kim, E., Sun, L., Gabel, C. V. & Fang-Yen, C. Long-term imaging of *Caenorhabditis elegans* using nanoparticle-mediated immobilization. *PLoS ONE* **8**, e53419 (2013).

Acknowledgements

This work was supported by the European Research Council (ERC Starting Grant-677427 StemProteostasis), Else Kröner-Fresenius-Stiftung (2015_A118), Alexander von Humboldt Stiftung and Deutsche Forschungsgemeinschaft (DFG) (CECAD and VI742/

1-1). This work was also supported by the European Research Council (ERC Consolidator Grant-616499) to T.H. In addition, this article is based upon work from COST Action (PROTEOSTASIS BM1307). W.P. thanks the Polish National Science Center (grant UMO-2016/23/B/NZ3/00753). We are grateful to Mahmoud A. Pouladi for corrected isogenic lines of HD Q180-iPSCs. We would also like to thank Alessandro Rosa and Irene Bozzoni for ALS-iPSC lines. We thank the CECAD Proteomics and Imaging Facilities for their advice and contribution to proteomics and imaging experiments, respectively.

Author contributions

S.K. and I.S. performed most of the experiments, data analysis and interpretation through discussions with D.V., H.J.L. performed analysis of aggresomes/ β -amyloid aggregation and helped with other experiments. R.G.-G. carried out *C. elegans* motility and imaging experiments. W.P. contributed to HTT ubiquitination assays and provided critical advice for other experiments. A.F. performed analysis of pluripotent stem cell lines and helped with neuronal differentiation experiments. T.H. contributed with his knowledge in proteostasis and provided critical advice for the project. D.V. planned and supervised the project. The manuscript was written by D.V. All the authors discussed the results and commented on the manuscript.

Additional information

Supplementary Information accompanies this paper at <https://doi.org/10.1038/s41467-018-05320-3>.

Competing interests: The authors declare no competing interests.

Reprints and permission information is available online at <http://npg.nature.com/reprintsandpermissions/>

Publisher's note: Springer Nature remains neutral with regard to jurisdictional claims in published maps and institutional affiliations.



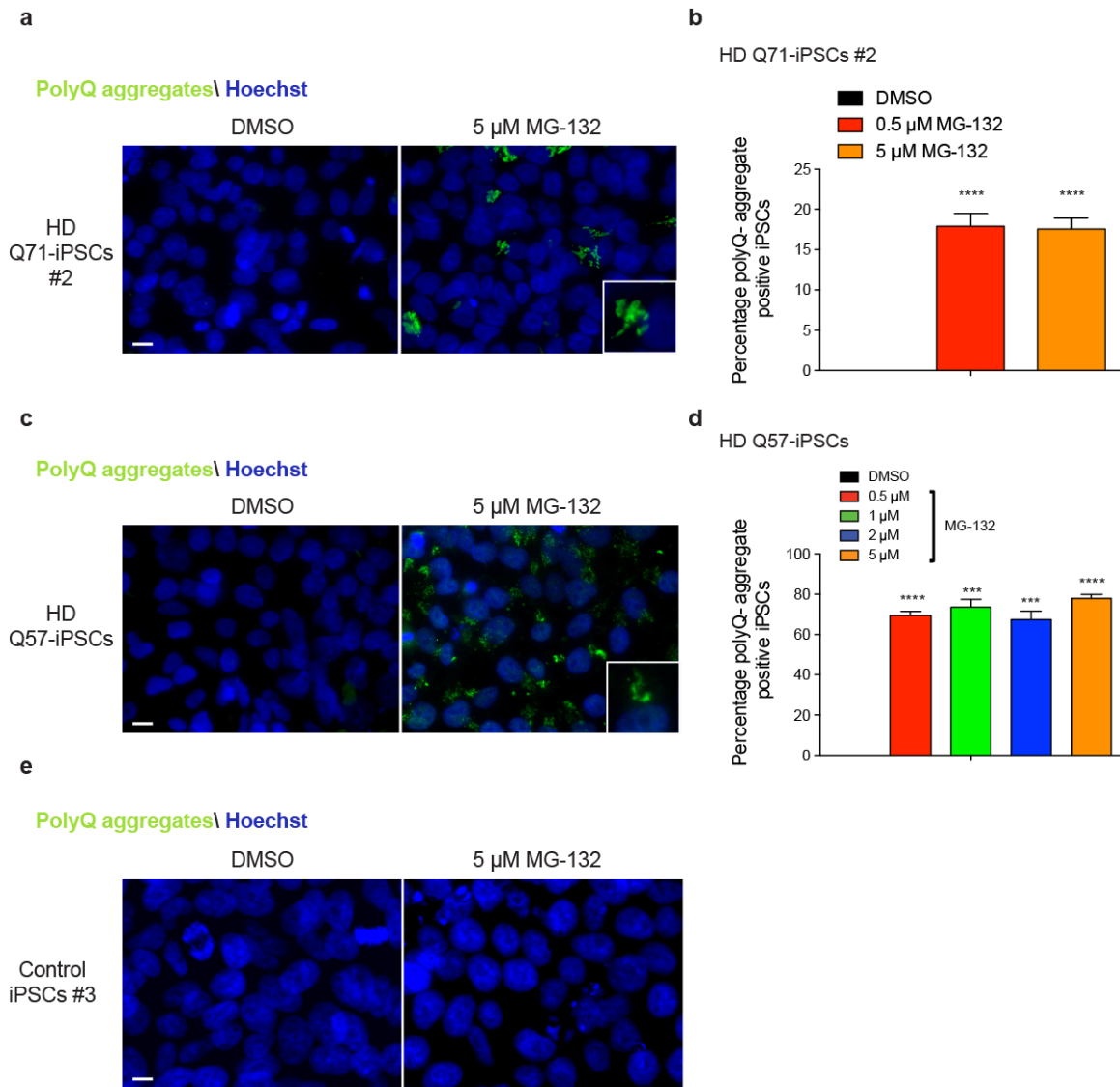
Open Access This article is licensed under a Creative Commons Attribution 4.0 International License, which permits use, sharing, adaptation, distribution and reproduction in any medium or format, as long as you give appropriate credit to the original author(s) and the source, provide a link to the Creative Commons license, and indicate if changes were made. The images or other third party material in this article are included in the article's Creative Commons license, unless indicated otherwise in a credit line to the material. If material is not included in the article's Creative Commons license and your intended use is not permitted by statutory regulation or exceeds the permitted use, you will need to obtain permission directly from the copyright holder. To view a copy of this license, visit <http://creativecommons.org/licenses/by/4.0/>.

© The Author(s) 2018

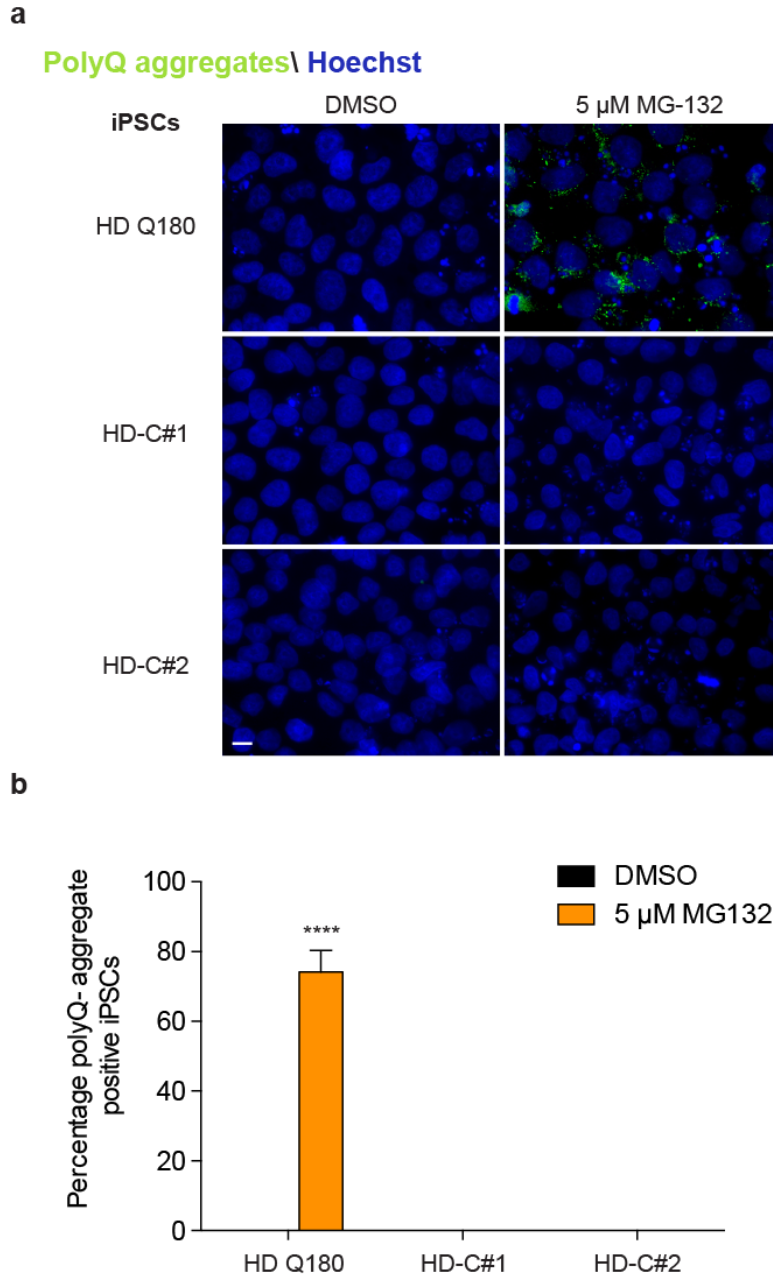
Supplementary Information

The ubiquitin ligase UBR5 suppresses proteostasis collapse in pluripotent stem cells from Huntington's disease patients

Koyuncu et al.



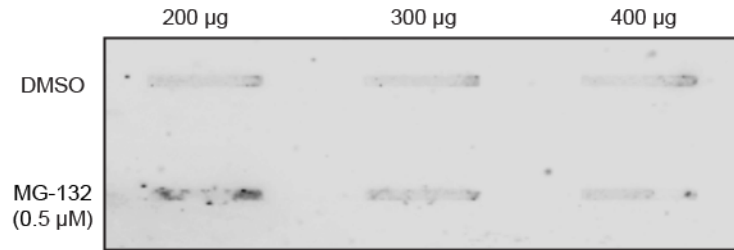
Supplementary Figure 1. Proteasome inhibition induces aggregation of polyQ-expanded HTT in distinct HD-iPSC lines. **a**, Immunocytochemistry with antibody against polyQ-expanded proteins of HD Q71-iPSC line #2 treated with 5 μ M MG-132 for 12 h. Cell nuclei were stained with Hoechst 33342. The images are representative of four independent experiments. **b**, Graph represents the percentage of polyQ aggregate-positive cells/total nuclei in HD Q71-iPSC line #2 (mean \pm s.e.m., 4 independent experiments, 300-350 total cells per treatment). **c**, Immunocytochemistry with antibody against polyQ-expanded proteins of HD Q57-iPSCs treated with 5 μ M MG-132 (12 h). The images are representative of four independent experiments. **d**, Graph represents the percentage of polyQ aggregate-positive cells/total nuclei in HD Q57-iPSCs (mean \pm s.e.m., 4 independent experiments, 250-300 total cells per treatment). **e**, Immunocytochemistry of control iPSC line #3 with antibody against polyQ-expanded proteins. The images are representative of two independent experiments. In **a**, **c** and **e**, scale bar represents 10 μ m. All the statistical comparisons were made by Student's t-test for unpaired samples. P-value: *** (P<0.001), **** (P<0.0001).



Supplementary Figure 2. Proteasome inhibition does not induce HTT aggregation in two corrected isogenic counterparts of Q180-iPSCs. **a**, Immunocytochemistry of Q180-iPSCs and two isogenic counterparts (*i.e.*, HD-C#1 and HD-C#2), in which the 180 CAG expansion was corrected to a nonpathological repeat length. Proteasome inhibition treatment: 5 μ M MG-132 for 12 h. We used an antibody against polyQ-expanded protein to detect mutant HTT aggregates. Cell nuclei were stained with Hoechst 33342. Scale bar represents 10 μ m. The images are representative of three independent experiments. **b**, Graph represents the percentage of polyQ aggregate-positive cells/total nuclei in Q180-iPSCs and their corrected isogenic counterparts (mean \pm s.e.m., 3 independent experiments, 250-300 total cells per treatment for each line).

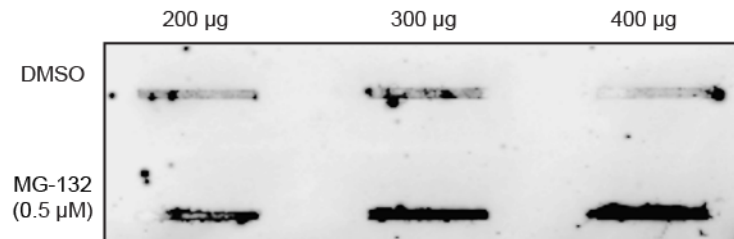
a

Control iPSC #2 (Q33)



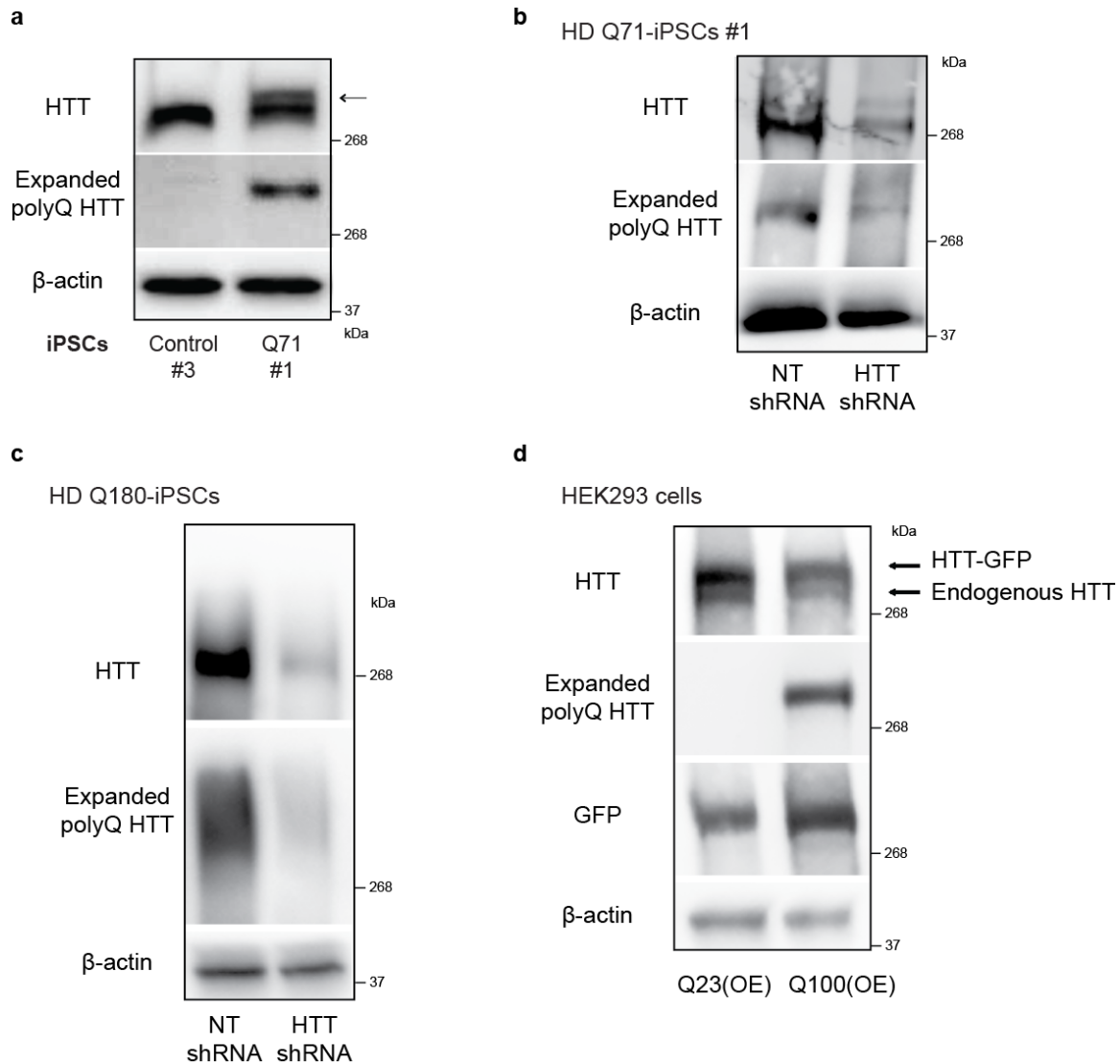
b

HD iPSC #2 (Q180)

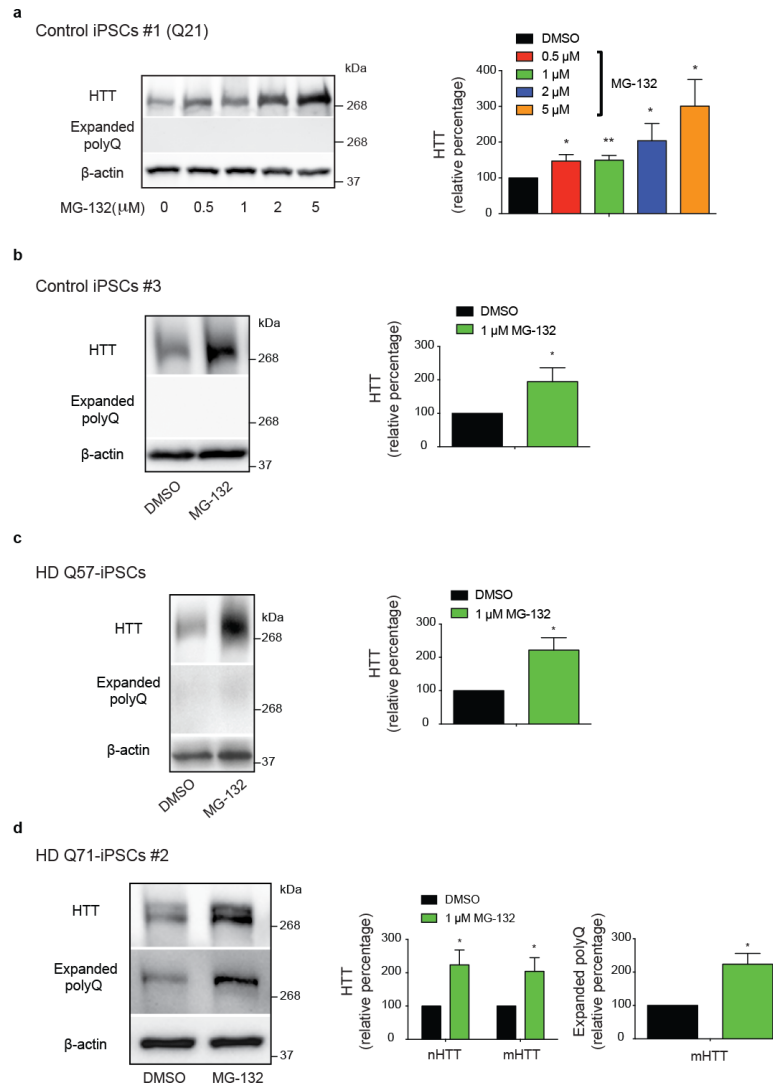


SDS-resistant
polyQ aggregates

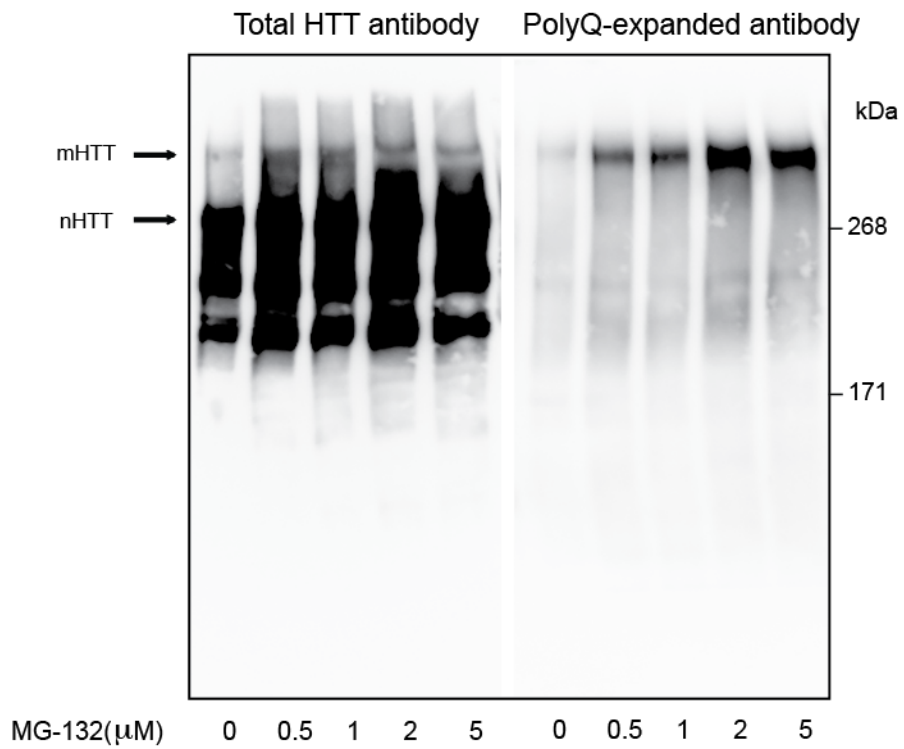
Supplementary Figure 3. Filter trap assay detects aggregation of endogenous polyQ-expanded HTT in HD iPSCs treated with proteasome inhibitor. a, Filter trap analysis of control iPSCs #2 (Q33) treated with MG-132 for 12 h using anti-polyQ-expansion diseases marker antibody. We did not observe differences when we loaded higher amounts of total protein from the cell lysate, indicating that the weak signal detected in this assay corresponds to background signal. **b,** Filter trap analysis of HD Q180-iPSCs treated with MG-132 for 12 h using anti-polyQ-expansion diseases marker. In MG-132-treated samples, the levels of detected polyQ-expanded aggregates correlate with the amount of total protein loaded. However, the background signal does not change in DMSO-treated cells regardless the total amount of protein loaded. The images are representative of two independent experiments.



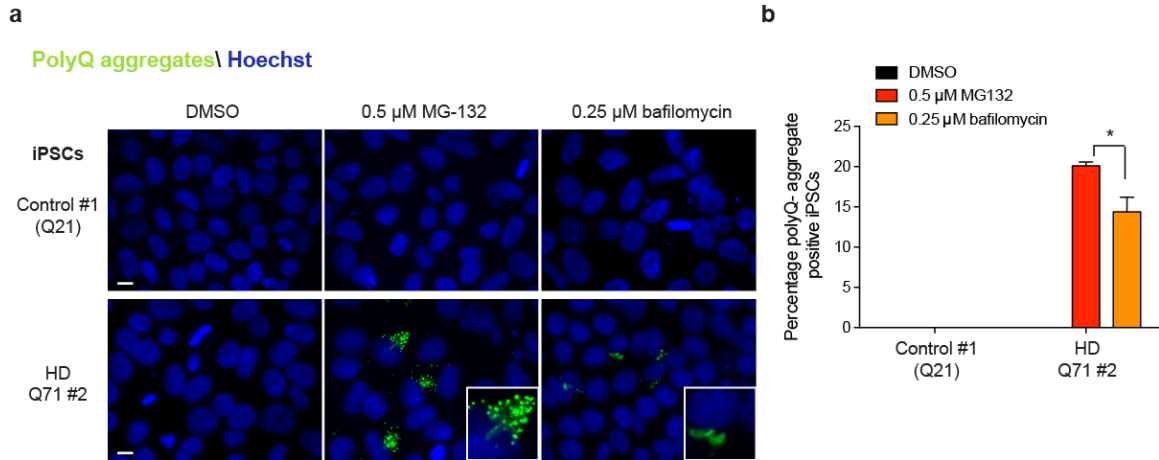
Supplementary Figure 4. Validation of antibodies to total HTT and anti-polyQ-expansion diseases marker. **a**, Western blot analysis of control iPSCs #3 and HD Q71-iPSCs #1 with antibodies to total HTT, polyQ-expanded proteins and β-actin. Arrow indicates mutant HTT detected with total HTT antibody in the HD Q71-iPSC line. The images are representative of three independent experiments. **b**, Western blot analysis of HD Q71-iPSCs #1 upon HTT knockdown. The images are representative of two independent experiments. **c**, Western blot analysis of HD Q180-iPSCs upon HTT knockdown. The images are representative of two independent experiments. **d**, Western blot analysis of Q23-HTT and Q100-HTT overexpressing (OE)-HEK293 cells with antibodies to total HTT, polyQ-expanded proteins, GFP and β-actin. The images are representative of two independent experiments.



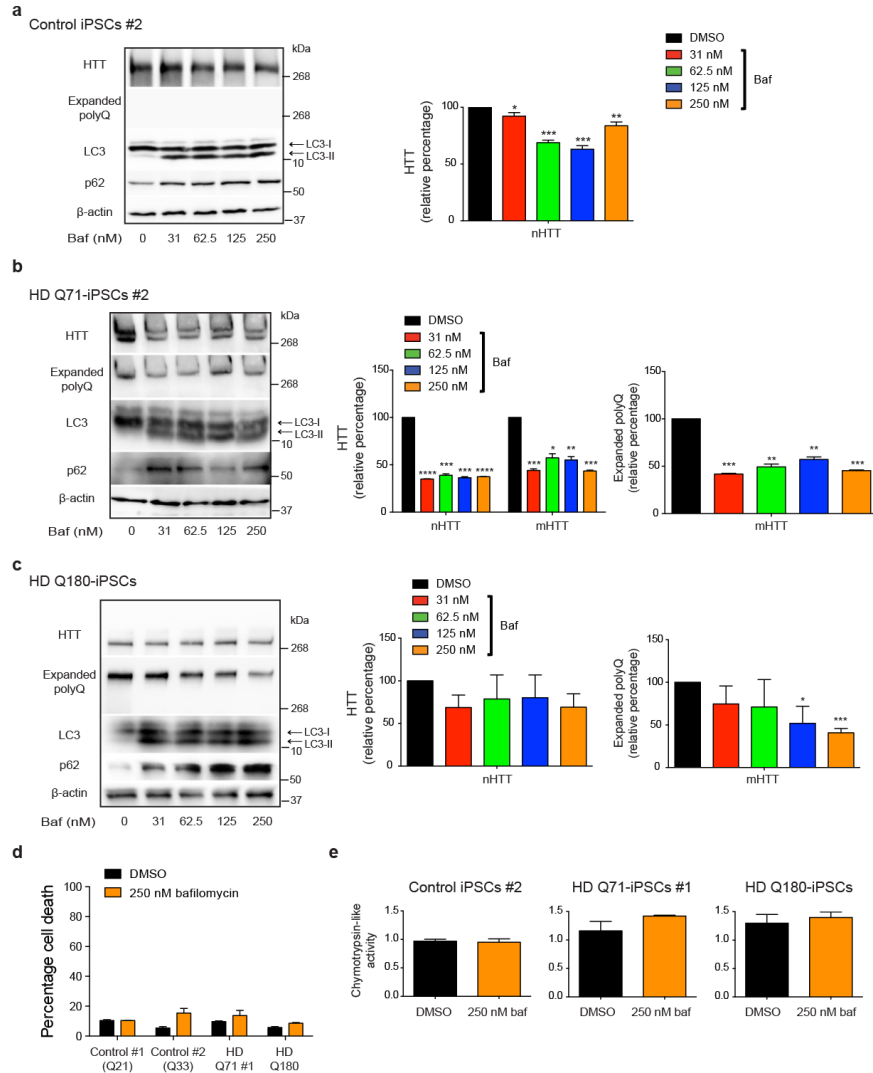
Supplementary Figure 5. Proteasome inhibition increases HTT protein levels in distinct iPSC lines. **a**, Western blot analysis with antibodies to total HTT and polyQ-expanded proteins of control iPSC line #1 treated with different concentrations of MG-132 (12 h). The graph represents the HTT relative percentage values to DMSO-treated iPSCs corrected for β -actin loading control (mean \pm s.e.m. of three independent experiments). **b**, Western blot analysis of control iPSC line #3 treated with 1 μ M MG-132 (12 h). The graph represents the HTT relative percentage values (corrected for β -actin) to DMSO-treated iPSCs (mean \pm s.e.m. of three independent experiments). **c**, Western blot analysis of HD Q57-iPSC line treated with 1 μ M MG-132 for 12 h. The graph represents the relative percentage value to DMSO-treated iPSCs (corrected for β -actin) of total HTT levels detected with anti-HTT antibody (mean \pm s.e.m. of three independent experiments). **d**, Western blot analysis of HD Q71-iPSC line #2 treated with 1 μ M MG-132 for 12 h. The graphs represent the relative percentage values to DMSO-treated iPSCs (corrected for β -actin) of normal (nHTT) and mutant HTT (mHTT) detected with antibodies to total HTT and polyQ-expanded proteins (mean \pm s.e.m. of three independent experiments). All the statistical comparisons were made by Student's t-test for unpaired samples. P-value: *($P < 0.05$), **($P < 0.05$).



Supplementary Figure 6. Higher exposure time of the membrane presented in **Fig. 2e** for a better comparison of mutant HTT (mHTT) levels detected with total HTT antibody in HD Q180-iPSCs.

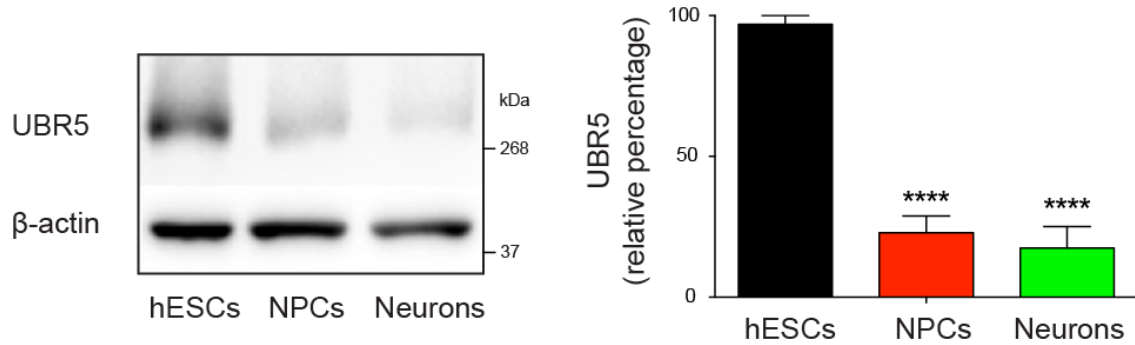


Supplementary Figure 7. Autophagy inhibition triggers accumulation of polyQ-expanded HTT aggregates to a lesser extent when compared to proteasome inhibition. a, Immunocytochemistry of control iPSC line #1 (Q21) and HD Q71-iPSC line #2 treated with 0.5 μ M MG-132 or 0.25 μ M bafilomycin for 12 h. We used an antibody against polyQ-expanded protein to detect mutant HTT aggregates. Cell nuclei were stained with Hoechst 33342. Scale bar represents 10 μ m. The images are representative of three independent experiments. **b,** Graph represents the percentage of polyQ aggregate-positive cells/total nuclei in the indicated iPSC lines with 0.5 μ M MG-132 or 0.25 μ M bafilomycin for 12 h (mean \pm s.e.m., 3 independent experiments, 200-250 total cells per treatment for each line).

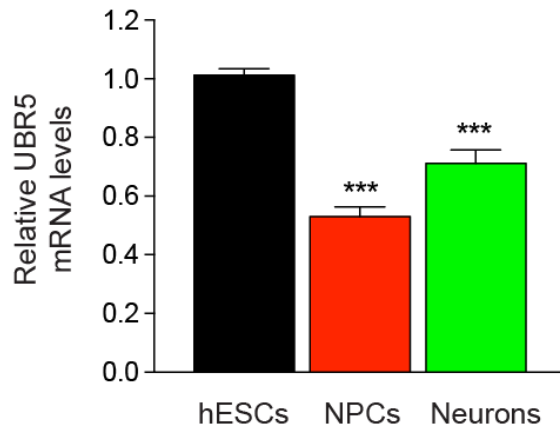


Supplementary Figure 8. Autophagy inhibition does not increase HTT protein levels in iPSCs. a, Western blot analysis of control iPSC line #2 treated with bafilomycin (12 h) using antibodies to total HTT, polyQ-expanded proteins, LC3 and P62. β -actin is the loading control. The graph represents the relative percentage values to DMSO-treated iPSCs of nHTT detected with total HTT antibody and corrected for β -actin loading control (mean \pm s.e.m. of three independent experiments). **b,** Western blot analysis of HD Q71-iPSC line #2 treated with bafilomycin (12 h) The graphs represent the relative percentage values to DMSO-treated iPSCs (corrected for β -actin) of normal (nHTT) and mutant (mHTT) huntingtin detected with antibodies to total HTT and polyQ-expanded proteins (mean \pm s.e.m. of three independent experiments). **c,** Western blot analysis of HD Q180-iPSCs treated with bafilomycin (12 h). The graphs represent the relative percentage values to DMSO-treated iPSCs (corrected for β -actin) of nHTT and mHTT detected with antibodies to total HTT and polyQ-expanded proteins, respectively (mean \pm s.e.m. of three independent experiments). **d,** Graph represents the percentage of propidium iodide-positive cells/total nuclei in the indicated iPSC lines treated with bafilomycin (12 h) (mean \pm s.e.m., 3 independent experiments, 200-300 total cells for each line). **e,** Chymotrypsin-like proteasome activity in the indicated iPSC lines treated with bafilomycin for 12 h (relative slope to the respective DMSO-iPSCs). Graph represents the mean \pm s.e.m. of three independent experiments. All the statistical comparisons were made by Student's t-test for unpaired samples. P-value: * ($P < 0.05$), ** ($P < 0.01$), *** ($P < 0.001$), **** ($P < 0.0001$).

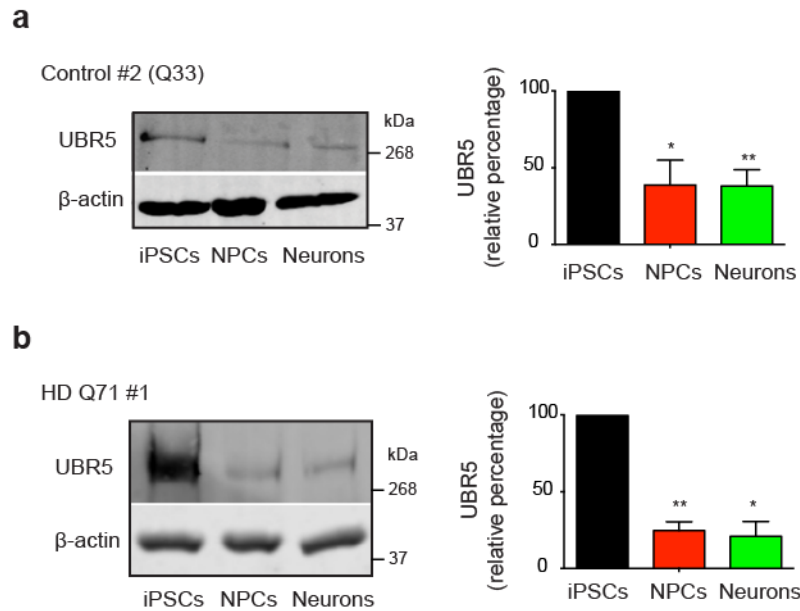
a



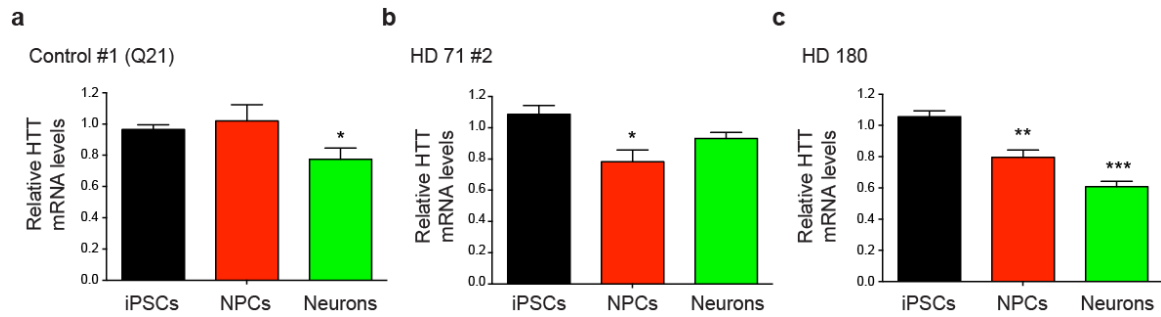
b



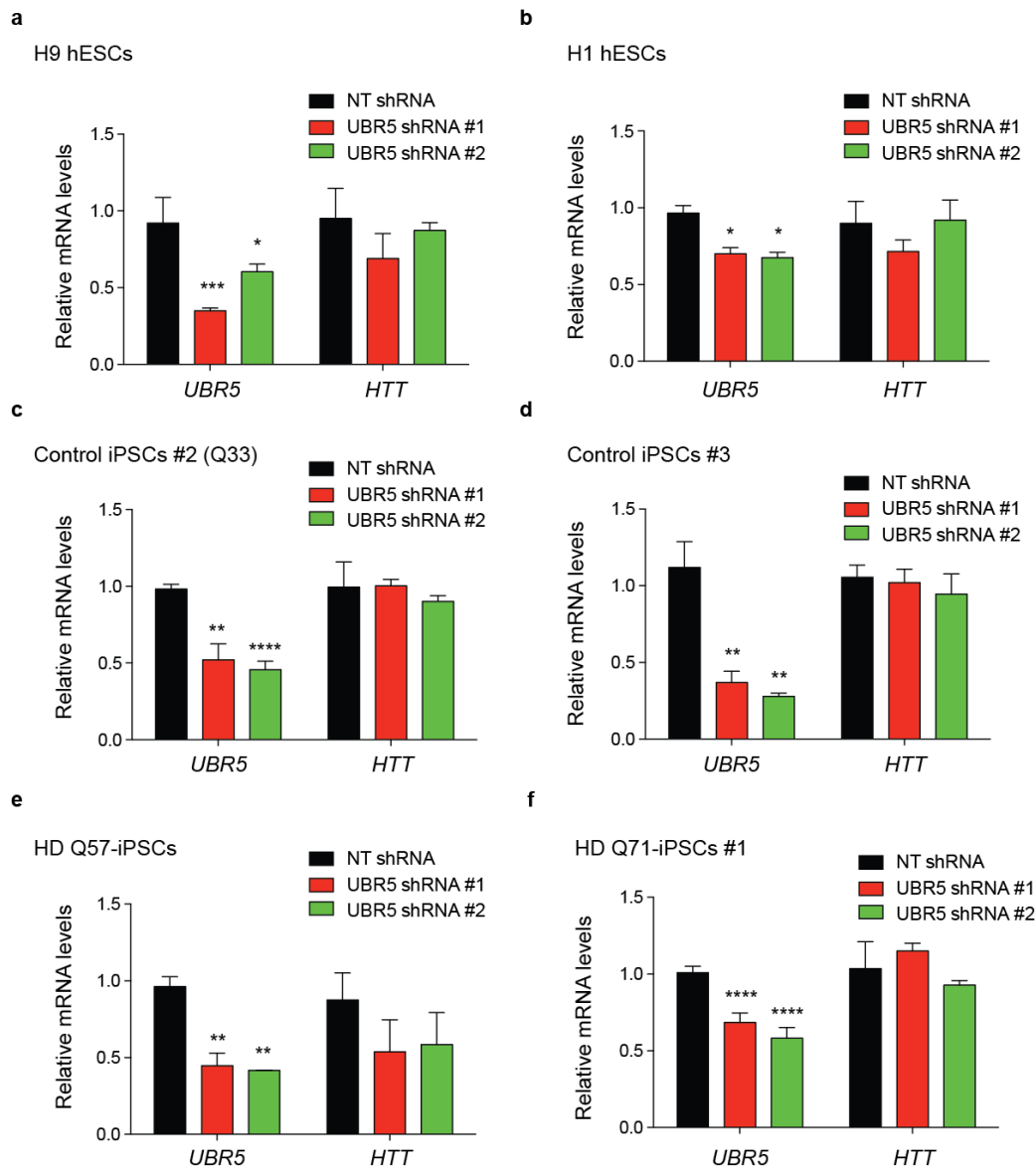
Supplementary Figure 9. UBR5 levels decrease during differentiation of H9 hESCs. a, Western blot analysis of UBR5 levels in H9 hESCs compared with their neural progenitor cell (NPC) and terminally differentiated neuronal counterparts. β -actin is the loading control. The graph represents the UBR5 relative percentage values (corrected for β -actin loading control) to H9 hESCs (mean \pm s.e.m. of five independent experiments). **b,** qPCR of UBR5 mRNA levels. Graph represents the mean \pm s.e.m. (relative expression to H9 hESCs) of three independent experiments. All the statistical comparisons were made by Student's t-test for unpaired samples. P-value: ***($P < 0.001$), ****($P < 0.0001$).



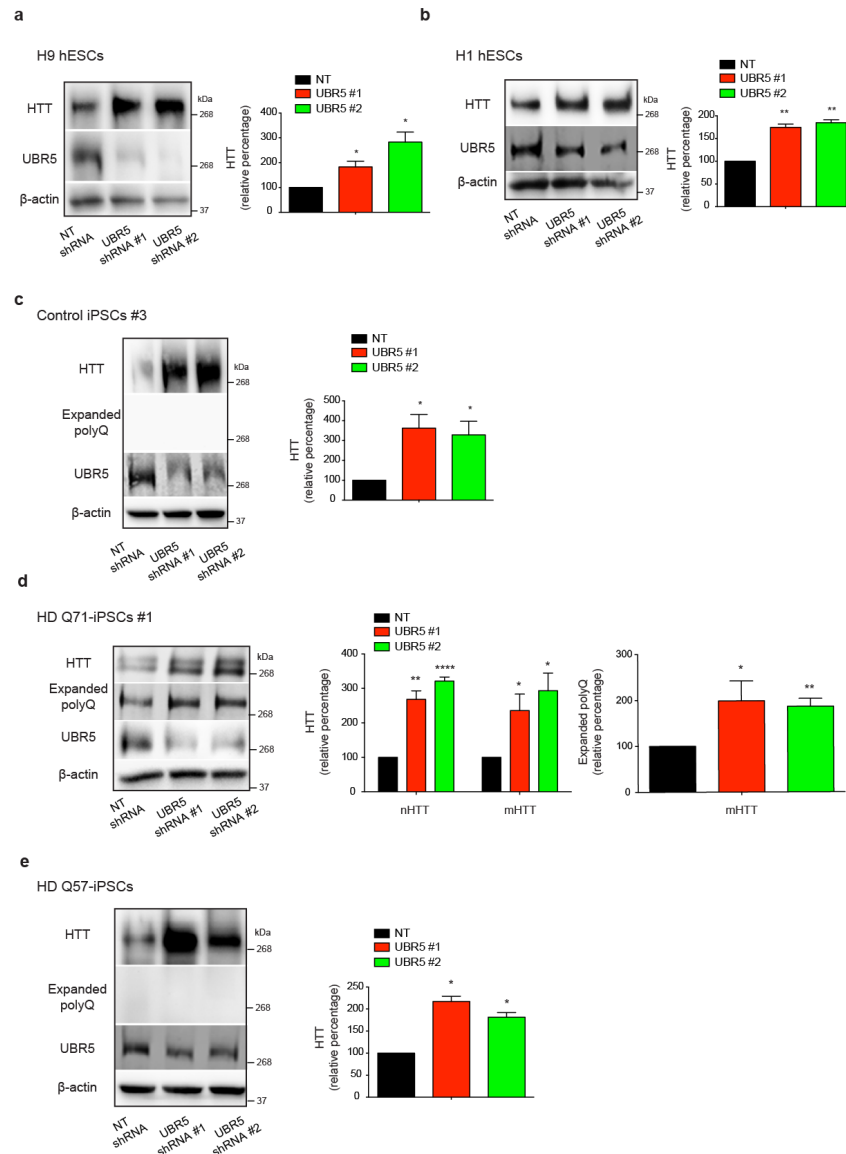
Supplementary Figure 10. UBR5 levels decrease during differentiation of control and HD-iPSC lines. **a**, Western blot of UBR5 levels in control #2 iPSCs (Q33) compared with their neural progenitor cell (NPC) and striatal neuron counterparts. The graph represents the UBR5 relative percentage values to iPSCs corrected for β -actin loading control (mean \pm s.e.m. of three independent experiments). **b**, Western blot of UBR5 levels in HD Q71 iPSCs #1 compared with their NPC and striatal neuronal counterparts. The graph represents the UBR5 relative percentage values to iPSCs corrected for β -actin loading control (mean \pm s.e.m. of three independent experiments). All the statistical comparisons were made by Student's t-test for unpaired samples. P-value: *($P < 0.05$), ** ($P < 0.01$).



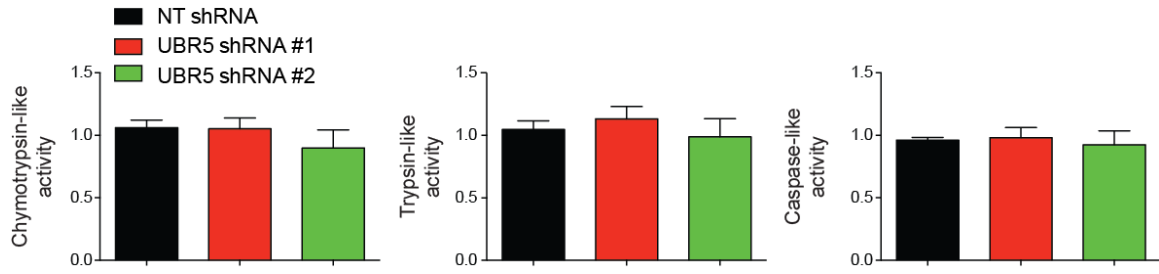
Supplementary Figure 11. Analysis of HTT mRNA levels in iPSCs and their differentiated counterparts. qPCR of HTT mRNA levels in (a) control #1 (Q21), (b) HD 71 #2 and (c) HD 180. Graphs represents the mean \pm s.e.m. (relative expression to iPSCs) of three independent experiments. All the statistical comparisons were made by Student's t-test for unpaired samples. P-value: *(P<0.05), **(P<0.01), *** (P<0.001).



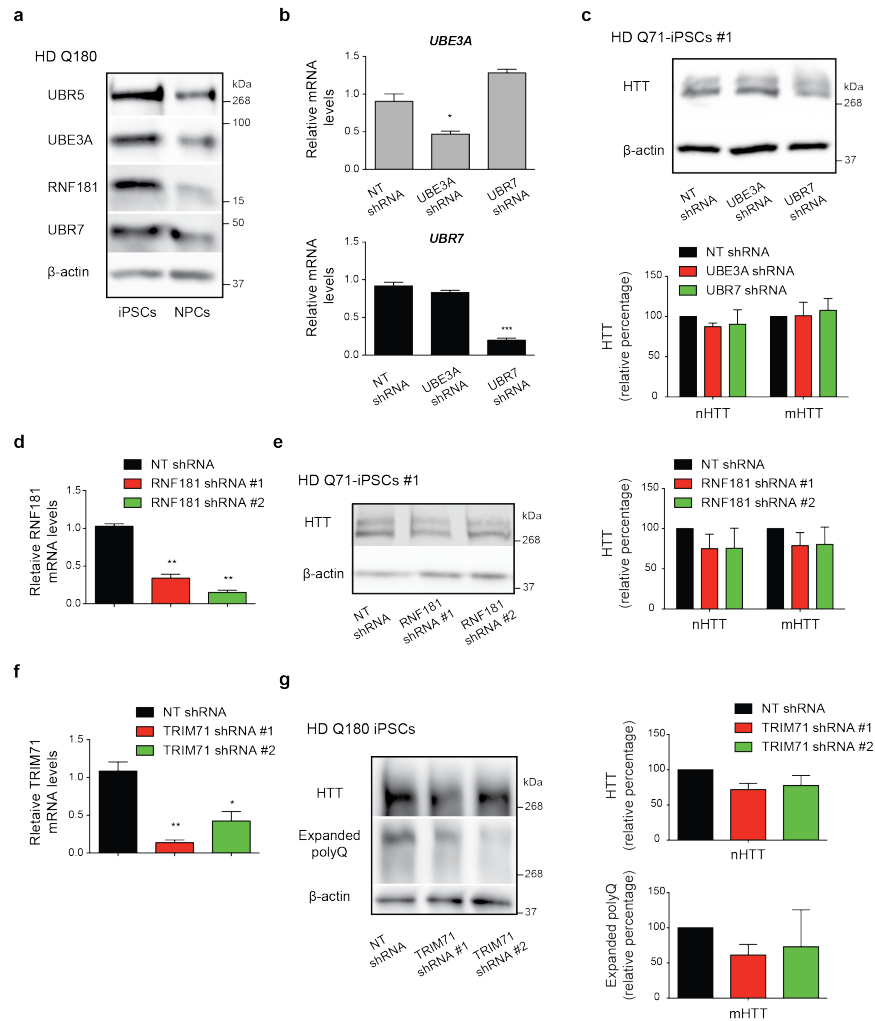
Supplementary Figure 12. Loss of intrinsic high levels of UBR5 does not change HTT mRNA levels in human pluripotent stem cells. **a**, qPCR analysis of UBR5 and HTT mRNA levels in H9 hESCs. Graph (relative expression to non-targeting (NT) shRNA) represents the mean \pm s.e.m. of four independent experiments. **b**, qPCR analysis in H1 hESCs (mean \pm s.e.m, n= 3 independent experiments). **c**, qPCR analysis in control iPSCs #2 (mean \pm s.e.m, n= 4 independent experiments). **d**, qPCR analysis in control iPSCs #3 (mean \pm s.e.m, n= 3 independent experiments). **e**, qPCR analysis in HD Q57-iPSCs (mean \pm s.e.m, n= 3 independent experiments). **f**, qPCR analysis in HD Q71-iPSCs #1 (mean \pm s.e.m, n= 5 independent experiments). All the statistical comparisons were made by Student's t-test for unpaired samples. P-value: *(P<0.05), ***(P<0.001), **** (P<0.0001).



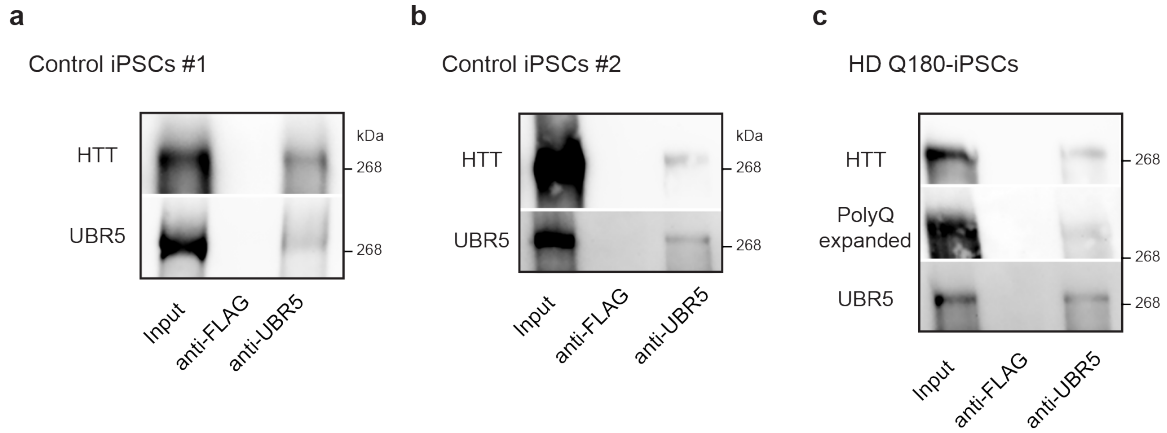
Supplementary Figure 13. Knockdown of UBR5 results in increased levels of HTT in hESCs, control iPSCs and HD iPSCs. **a**, Western blot analysis of HTT levels in H9 hESCs upon UBR5 knockdown. The graph represents the HTT relative percentage values to NT shRNA-H9 hESCs corrected for β-actin loading control (mean ± s.e.m. of three independent experiments). **b**, Western blot analysis of H1 hESCs. The graph represents the HTT relative percentage values to NT shRNA-H1 hESCs corrected for β-actin loading control (mean ± s.e.m. of two independent experiments). **c**, Western blot analysis of control iPSCs #3. The graph represents the HTT relative percentage values to NT shRNA-control iPSCs #3 corrected for β-actin loading control (mean ± s.e.m. of two independent experiments). **d**, Western blot analysis of HD Q71-iPSC line #1 upon UBR5 knockdown. The graphs represent the relative percentage values to NT shRNA-iPSCs (corrected for β-actin) of nHTT and mHTT detected with antibodies to total HTT and polyQ-expanded proteins (mean ± s.e.m. of three independent experiments). **e**, Western blot analysis of HD Q57-iPSCs. The graph represents the relative percentage value to NT shRNA-iPSCs (corrected for β-actin) of total HTT levels detected with anti-HTT antibody (mean ± s.e.m. of two independent experiments). All the statistical comparisons were made by Student's t-test for unpaired samples. P-value: * (P<0.05), ** (P<0.01), **** (P<0.0001).



Supplementary Figure 14. Knockdown of UBR5 does not change proteasome activities in iPSCs. Proteasome activities in control iPSC line #2 (Q33) upon UBR5 knockdown (relative slope to NT shRNA iPSCs). Graphs represent the mean \pm s.e.m. of three independent experiments. All the statistical comparisons were made by Student's t-test for unpaired samples.



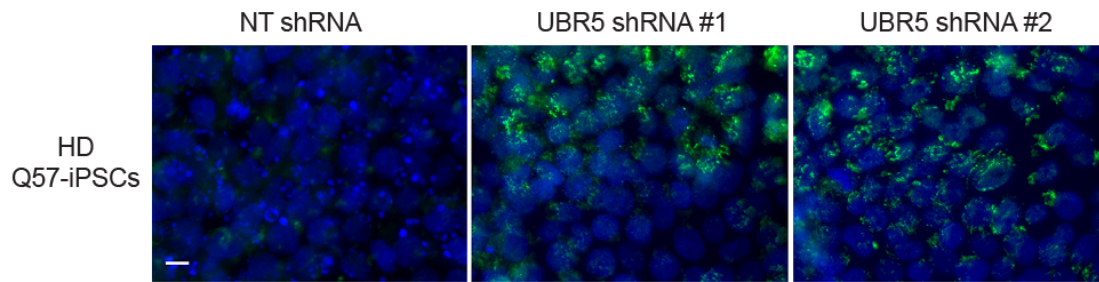
Supplementary Figure 15. Besides UBR5, knockdown of other up-regulated E3 enzymes in iPSCs does not increase HTT protein levels. **a**, Western blot analysis of HD Q180-iPSC lysates with antibodies to UBR5, UBE3A, RNF181 and UBR7 E3 enzymes. β -actin is the loading control. The images are representative of two independent experiments. **b**, qPCR analysis of UBE3A and UBR7 mRNA levels in HD Q71-iPSC line #3. Graph (relative expression to non-targeting (NT) shRNA) represents the mean \pm s.e.m. of three independent experiments. **c**, Western blot analysis of HD Q71-iPSC line #1 upon knockdown of either UBE3A or UBR7. The graph represents the relative percentage values to NT shRNA iPSCs (corrected for β -actin) of nHTT and mHTT detected with antibody to total HTT (mean \pm s.e.m. of two independent experiments). **d**, qPCR analysis of RNF181 mRNA levels in HD Q71-iPSC line #1. Graph (relative expression to NT shRNA) represents the mean \pm s.e.m. of two independent experiments. **e**, Western blot analysis of HTT levels in HD Q71-iPSC line #1 upon knockdown of RNF181. The graph represents the relative percentage values to NT shRNA iPSCs (corrected for β -actin) of nHTT and mHTT detected with antibody to total HTT (mean \pm s.e.m. of two independent experiments). **f**, qPCR analysis of TRIM71 mRNA levels in HD Q180-iPSCs. Graph (relative expression to NT shRNA) represents the mean \pm s.e.m. of two independent experiments. **g**, Western blot analysis of HD Q180-iPSCs upon knockdown of TRIM71 with antibodies to total HTT, polyQ-expanded proteins and β -actin. The graphs represent the relative percentage values to NT shRNA iPSCs (corrected for β -actin) of nHTT and mHTT detected with antibodies to total HTT and polyQ-expanded proteins, respectively (mean \pm s.e.m. of three independent experiments). All the statistical comparisons were made by Student's t-test for unpaired samples. P-value: *($P < 0.05$), **($P < 0.01$), ***($P < 0.001$).



Supplementary Figure 16. UBR5 binds HTT protein in iPSCs. **a**, Co-immunoprecipitation with UBR5 and FLAG antibodies in control iPSC line #1 (Q21) followed by western blot with HTT and UBR5 antibodies. The images are representative of two independent experiments. **b**, Co-immunoprecipitation with UBR5 and FLAG antibodies in control iPSC line #2 (Q33). The images are representative of two independent experiments. **c**, Co-immunoprecipitation with UBR5 and FLAG antibodies in HD Q180-iPSCs followed by western blot with HTT, polyQ-expanded and UBR5 antibodies. The images are representative of two independent experiments.

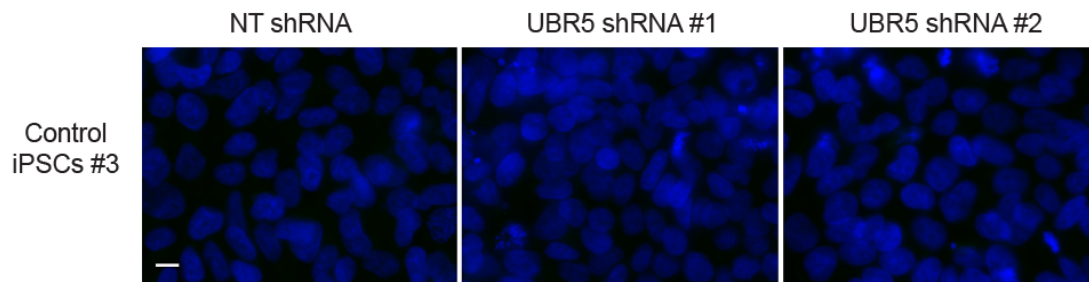
a

PolyQ aggregates\ Hoechst

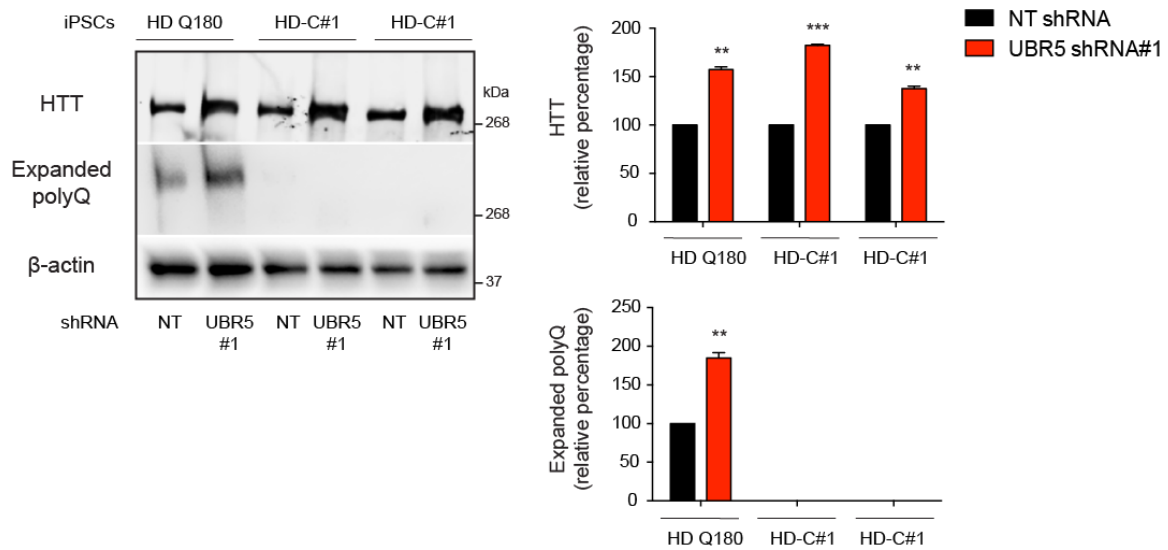


b

PolyQ aggregates\ Hoechst

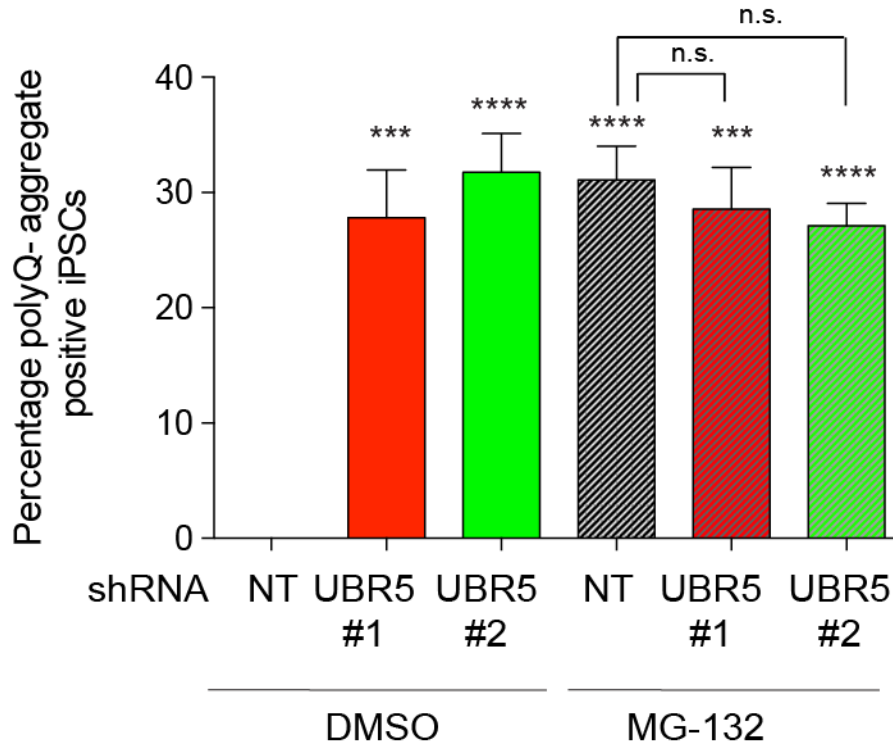


Supplementary Figure 17. UBR5 prevents accumulation of mutant HTT aggregates in HD-iPSCs. a, Immunocytochemistry of HD Q57-iPSCs upon UBR5 knockdown. PolyQ-expanded and Hoechst 33342 staining were used as markers of aggregates and nuclei, respectively. Scale bar represents 10 μ m. The images are representative of three independent experiments. **b,** Immunocytochemistry of control iPSC line #3 upon UBR5 knockdown. Scale bar represents 10 μ m. The images are representative of two independent experiments.



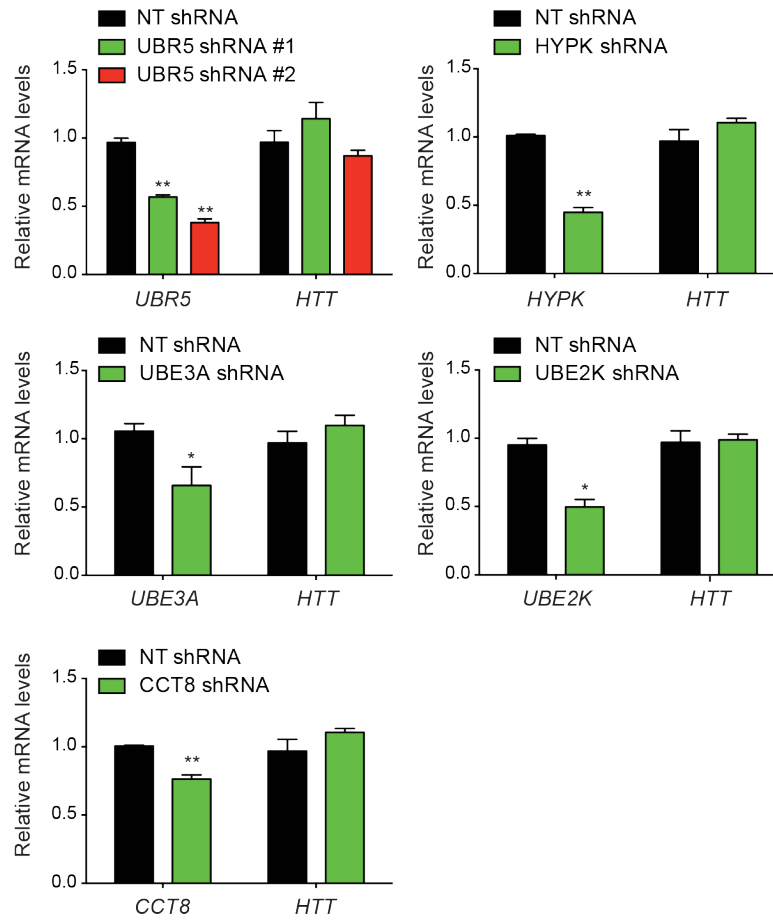
Supplementary Figure 18. Knockdown of UBR5 induces accumulation of normal HTT in corrected isogenic counterparts of Q180-iPSCs. Western blot of Q180-iPSCs and two isogenic counterparts (*i.e.*, HD-C#1 and HD-C#2), in which the 180 CAG expansion was corrected to a nonpathological repeat length. The graphs represent the relative percentage values to the respective NT shRNA-iPSCs (corrected for β -actin) of nHTT and mHTT detected with antibodies to total HTT and polyQ-expanded proteins, respectively (mean \pm s.e.m. of three independent experiments).

HD Q71-iPSCs #1

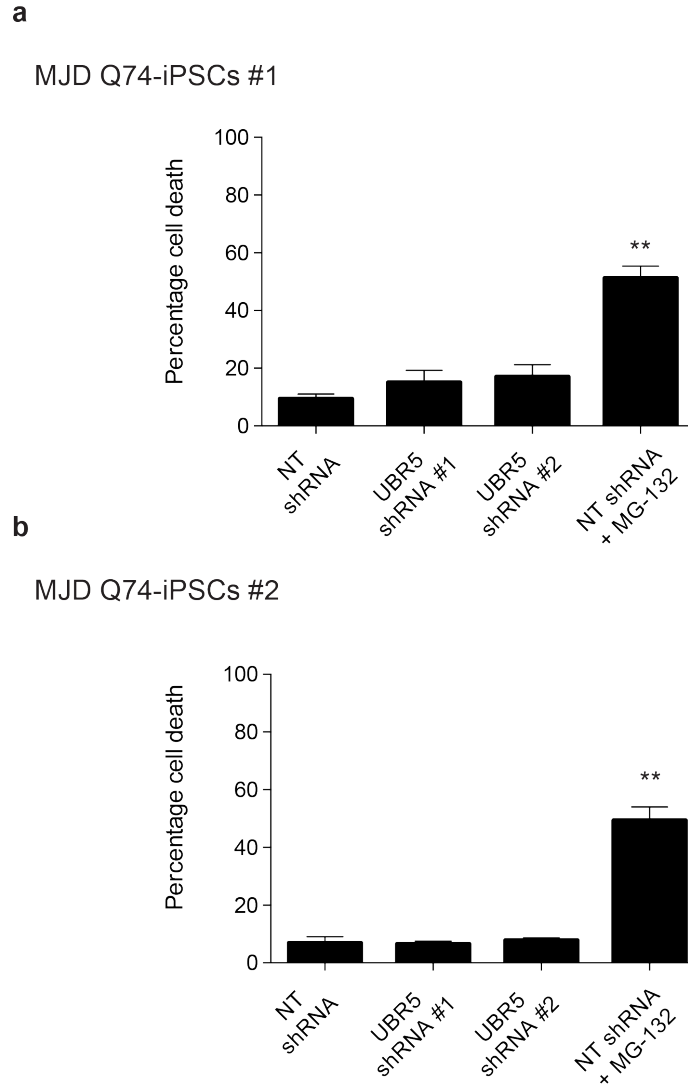


Supplementary Figure 19. Proteasome inhibition does not further increase the accumulation of polyQ-aggregates induced by loss of UBR5. Graph represents the percentage of polyQ aggregate-positive cells/total nuclei in HD Q71-iPSC line #1 (mean \pm s.e.m., 3 independent experiments, 300-400 total cells per condition). Proteasome inhibitor treatment: 5 μ M MG-132 for 12 h. PolyQ-expanded and Hoechst 33342 staining were used as markers of aggregates and nuclei, respectively. All the statistical comparisons were made by Student's t-test for unpaired samples. P-value: *** (P<0.001), **** (P<0.0001).

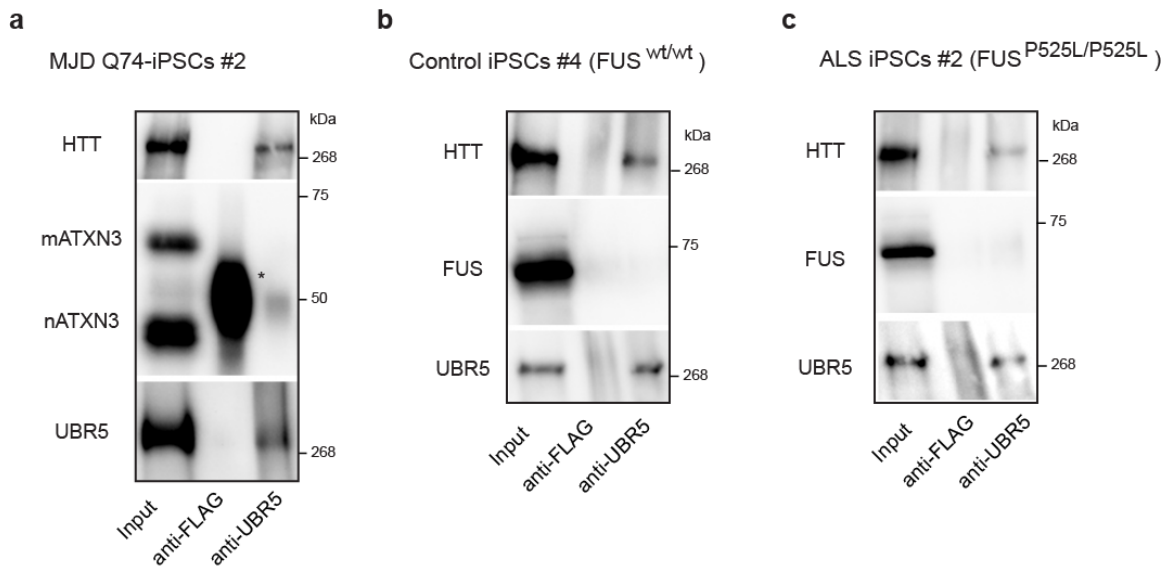
HD Q71-iPSCs #1



Supplementary Figure 20. Knockdown of distinct proteostasis components in HD-iPSCs does not impair HTT mRNA levels. qPCR analysis of HD Q71-iPSC line #1 upon knockdown of distinct proteostasis components. Graph (relative expression to non-targeting (NT) shRNA) represents the mean \pm s.e.m. of three independent experiments. All the statistical comparisons were made by Student's t-test for unpaired samples. P-value: * (P<0.05), ** (P<0.01).

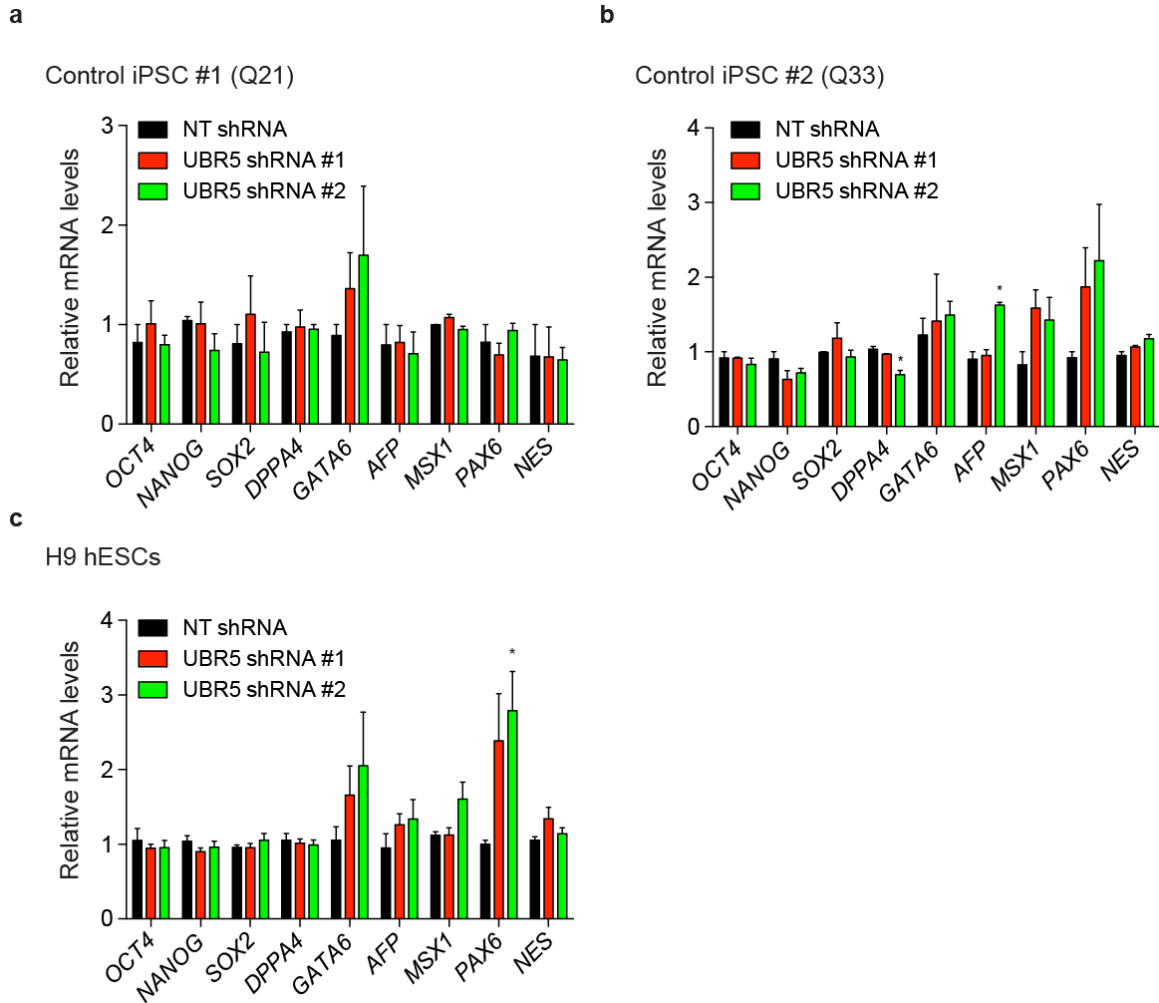


Supplementary Figure 21. Percentage of cell death in MJD-iPSC lines. **a**, Graph represents the percentage of propidium iodide-positive cells/total nuclei in MJD-iPSC line #1 (mean \pm s.e.m., 2 independent experiments, 400-500 total cells). **b**, Percentage of propidium iodide-positive cells/total nuclei in MJD-iPSC line #2 (mean \pm s.e.m., 2 independent experiments, 400-500 total cells). Proteasome inhibitor treatment: 5 μ M MG-132 for 6 h. All the statistical comparisons were made by Student's t-test for unpaired samples. P-value: ** (P<0.01).

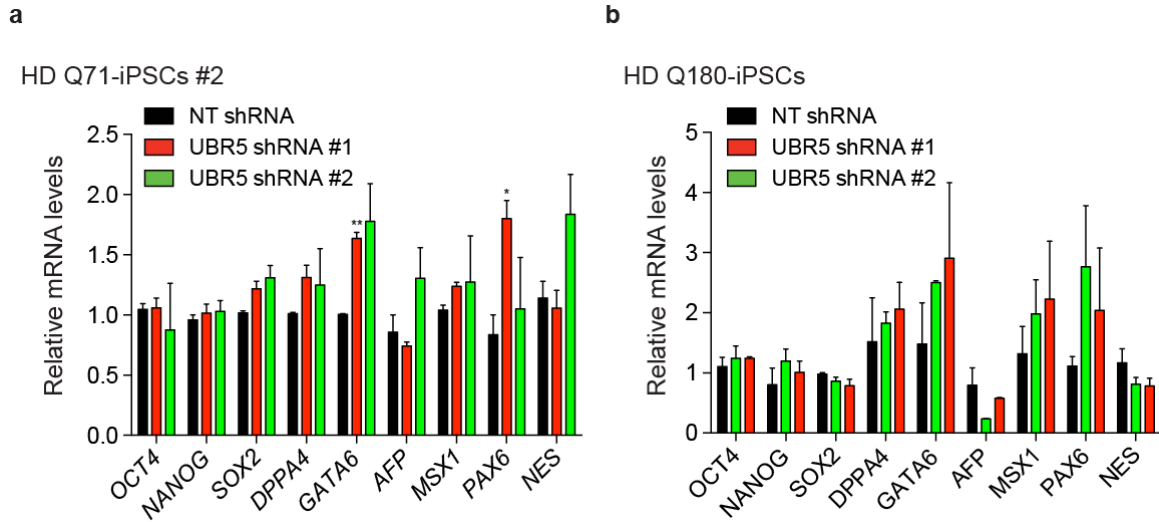


Supplementary Figure 22. UBR5 does not interact with ATXN3 and FUS proteins in iPSCs.

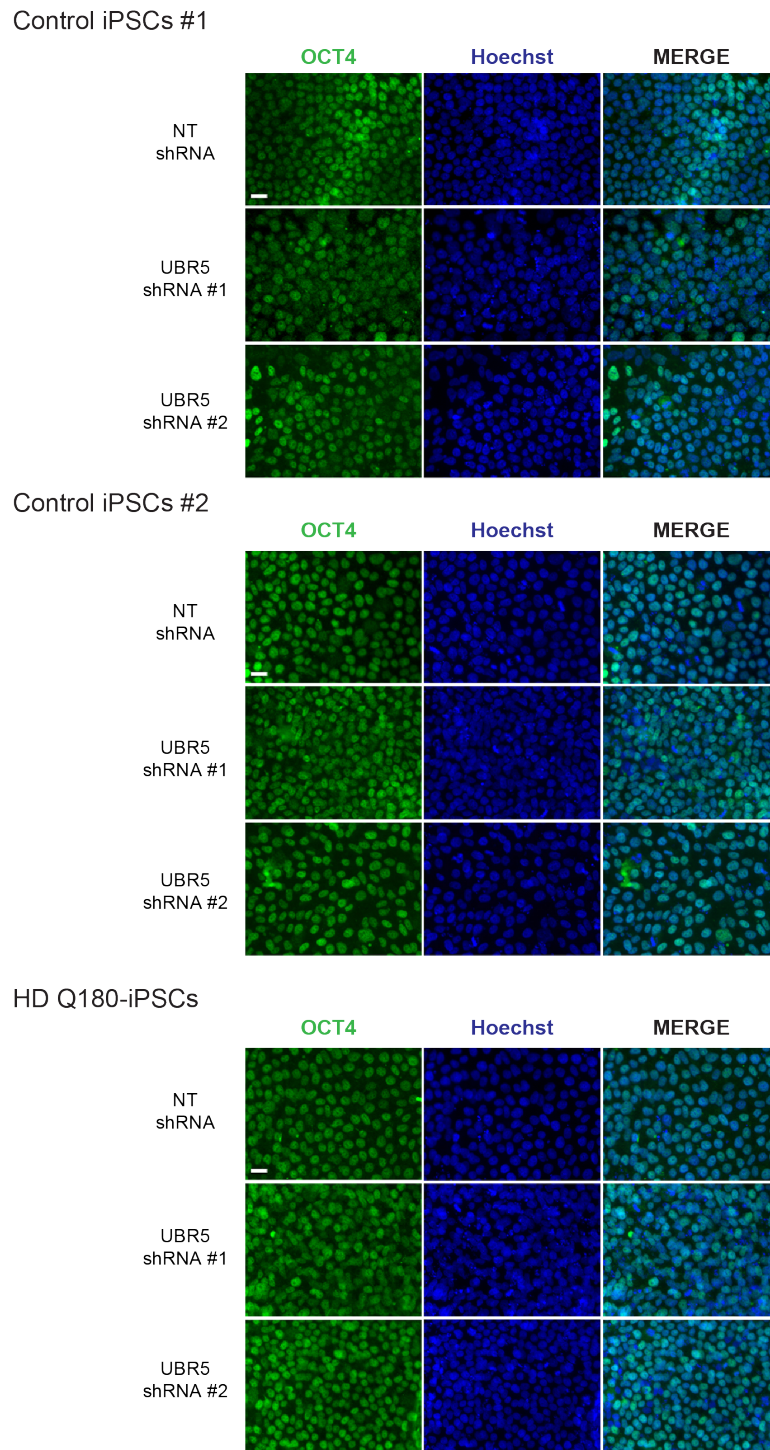
a, Co-immunoprecipitation with UBR5 and FLAG antibodies in MJD Q74-iPSC line #2 followed by western blot with HTT, ATXN3 and UBR5 antibodies. * indicates IgG. The images are representative of two independent experiments. **b**, Co-immunoprecipitation with UBR5 and FLAG antibodies in control iPSCs #4 (FUS^{wt/wt}), followed by western blot with HTT, FUS and UBR5 antibodies. The images are representative of two independent experiments. **c**, Co-immunoprecipitation with UBR5 and FLAG antibodies in ALS-iPSCs #2 (FUS^{P525L/P525L}), followed by western blot with HTT, FUS and UBR5 antibodies. The images are representative of two independent experiments.



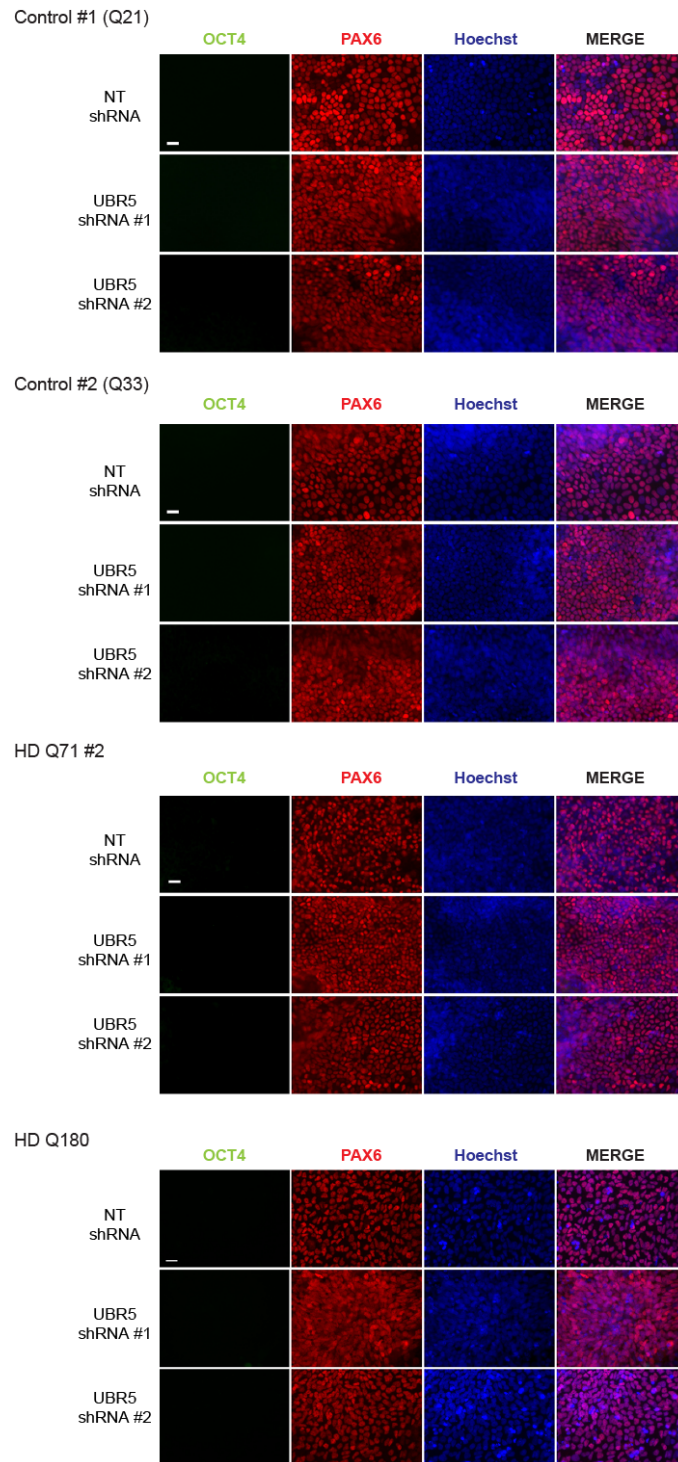
Supplementary Figure 23. Loss of UBR5 does not affect expression of pluripotency and germ layer markers in control pluripotent stem cells. **a**, qPCR analysis in control iPSC line #1 (Q21). The graph represents the relative expression to NT shRNA (mean \pm s.e.m., $n = 3$ independent experiments). **b**, Control iPSC line #2 (Q33) (mean \pm s.e.m., $n = 3$ independent experiments). **c**, H9 hESCs (mean \pm s.e.m., $n = 4$ independent experiments). All the statistical comparisons were made by Student's t-test for unpaired samples. P-value: * ($P < 0.05$).



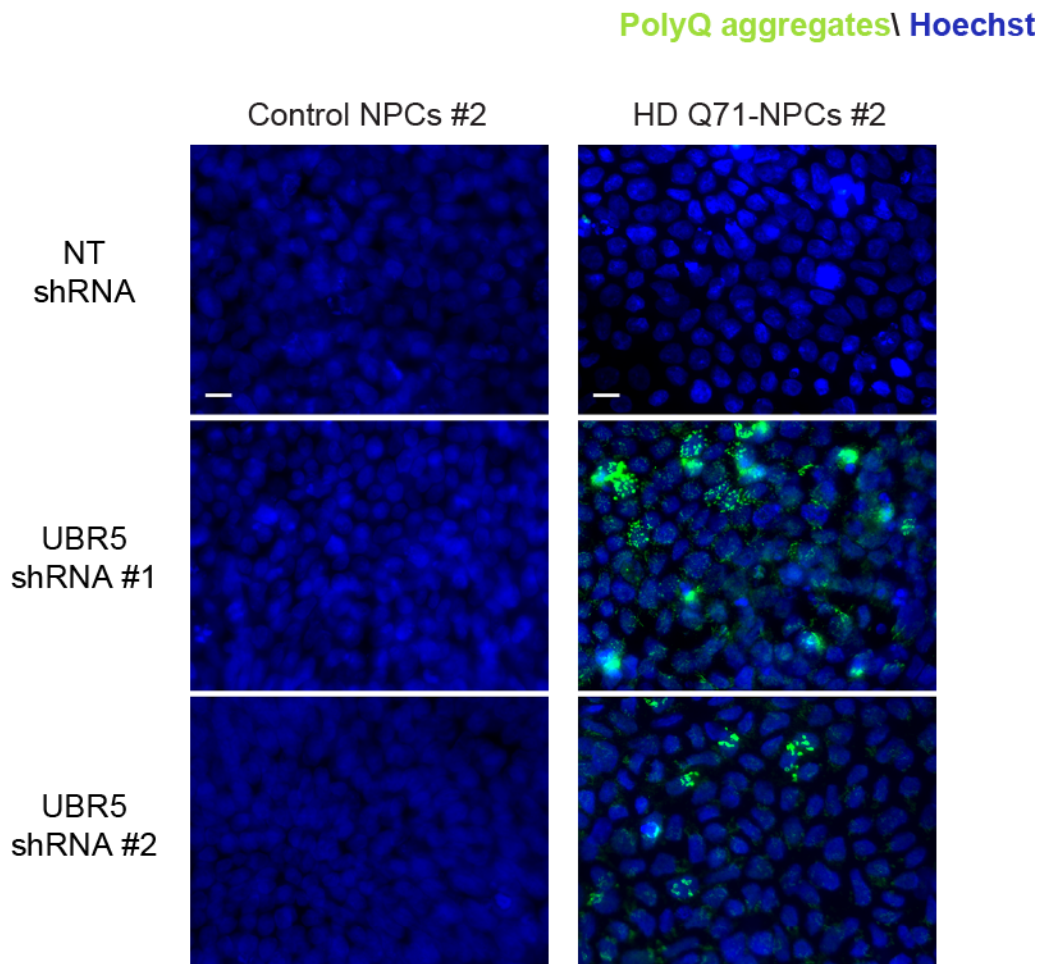
Supplementary Figure 24. Accumulation of polyQ-expanded HTT aggregates upon UBR5 knockdown does not affect pluripotency expression levels. qPCR analysis of pluripotency markers in (a) HD Q71-iPSC line #2 and (b) HD Q180-iPSC line. The graphs represent the relative expression to NT shRNA HD-iPSCs (mean \pm s.e.m. (n= 3 independent experiments for each line)). All the statistical comparisons were made by Student's t-test for unpaired samples. P-value: * (P<0.05), ** (P<0.01).



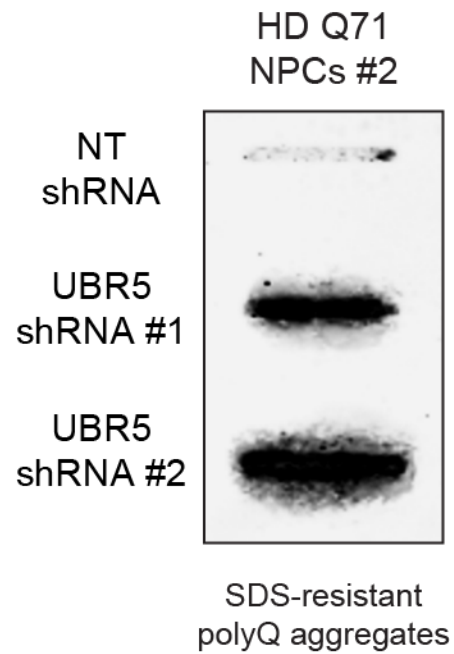
Supplementary Figure 25. UBR5 knockdown does not induce loss of OCT4 expression. Immunocytochemistry of control iPSCs #1, control iPSCs #2 and HD Q180-iPSCs. OCT4 and Hoechst 33342 staining were used as markers of pluripotency and nuclei, respectively. Scale bar represents 20 μ m. The images are representative of three independent experiments.



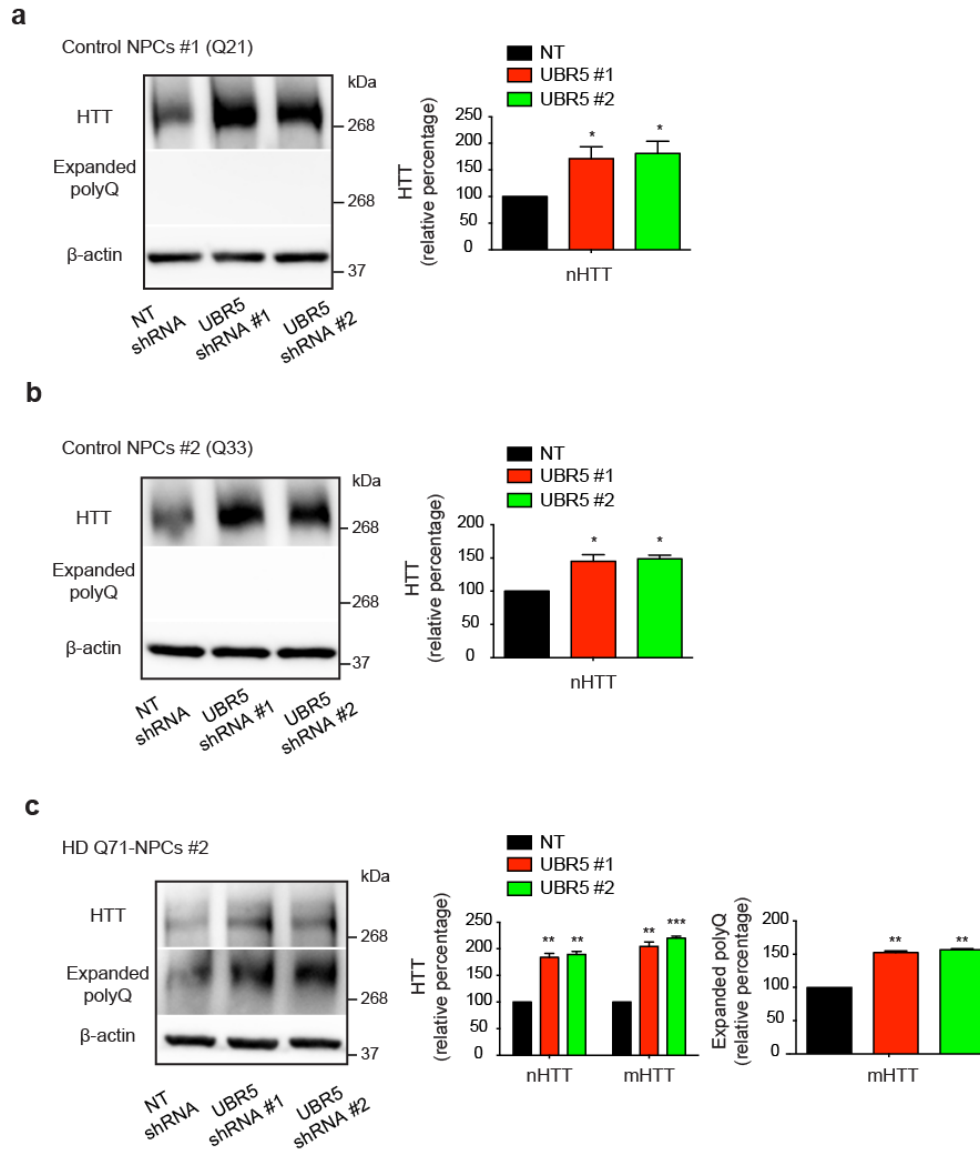
Supplementary Figure 26. Loss of UBR5 does not impair neural differentiation of control and HD-iPSCs. After neural induction of the indicated iPSCs lines with down-regulated levels of UBR5, we did not observe differences in their ability to differentiate into PAX6-positive cells compared with their respective NT shRNA controls. Scale bar represents 20 μ m. The images are representative of three independent experiments.



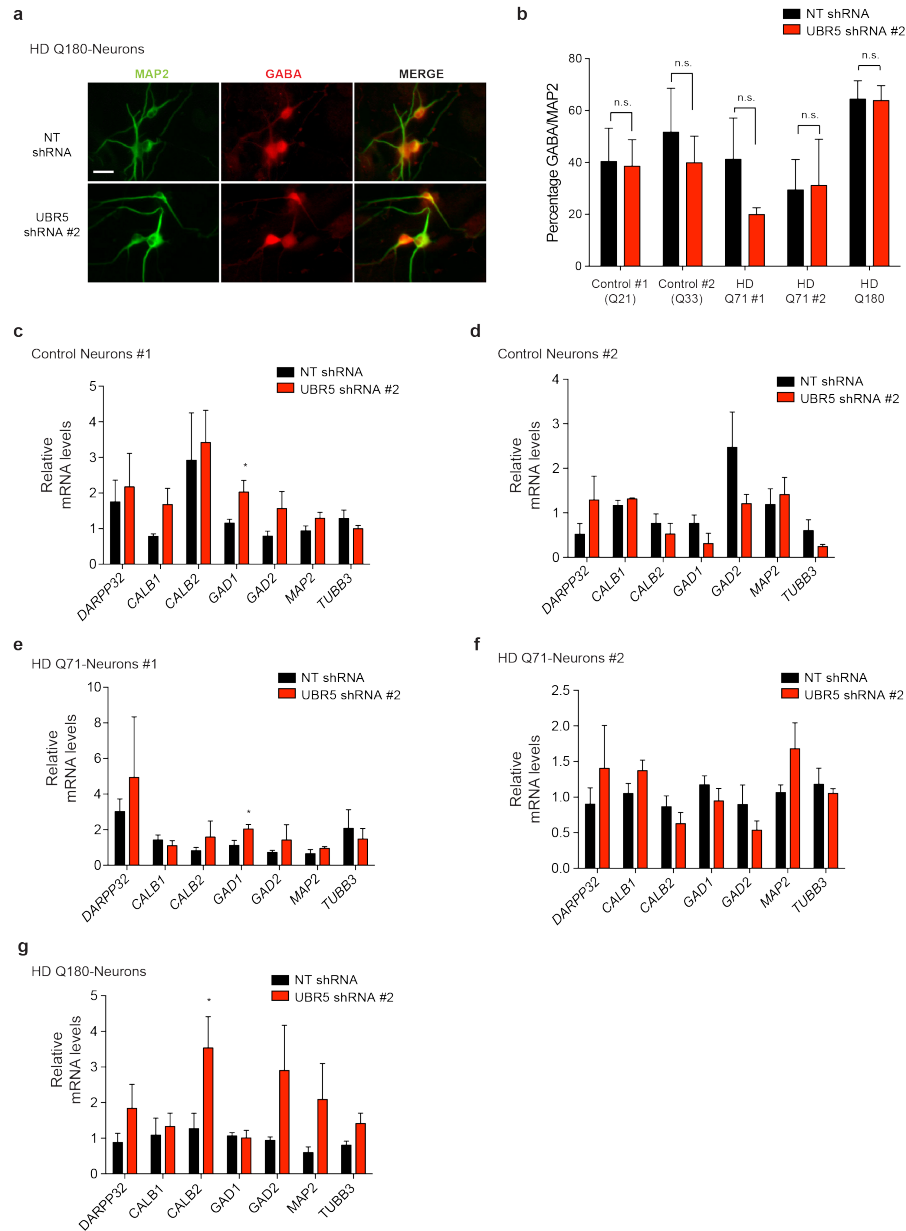
Supplementary Figure 27. HD-iPSCs with downregulated levels of UBR5 differentiate into NPCs with aggregates. Upon neural induction of HD Q71-iPSC line #2 with down-regulated levels of UBR5, NPCs accumulate polyQ-expanded HTT aggregates. PolyQ-expanded and Hoechst 33342 staining were used as markers of aggregates and nuclei, respectively. Scale bar represents 10 μ m. The images are representative of three independent experiments.



Supplementary Figure 28. Filter trap of HD Q71-NPCs #2 derived from iPSCs with downregulated levels of UBR5. Upon neural induction of HD Q71-iPSC line #2 with downregulated levels of UBR5, NPCs accumulate mutant HTT aggregates as assessed by filter trap experiments with anti-polyQ-expansion diseases marker antibody. The images are representative of three independent experiments.

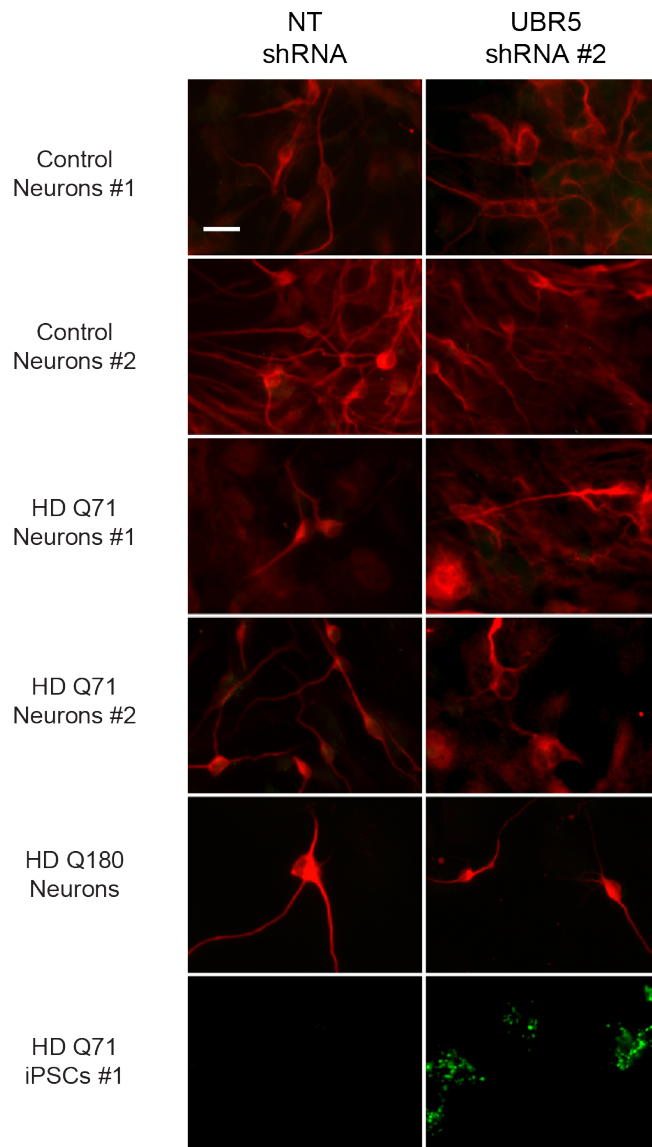


Supplementary Figure 29. iPSCs with downregulated levels of UBR5 differentiate into NPCs with high expression of HTT upon neural induction. **a**, Control iPSCs #1 with downregulated levels of UBR5 were differentiated into NPCs and analyzed by western blot. The graph represents the HTT relative percentage values to NT shRNA NPCs (corrected for β -actin) detected with antibody to total HTT (mean \pm s.e.m. of three independent experiments). **b**, Western blot analysis of NPCs derived from control iPSCs #2 with downregulated levels of UBR5. The graph represents the HTT relative percentage values to NT shRNA NPCs (corrected for β -actin) detected with antibody to total HTT (mean \pm s.e.m. of three independent experiments). **c**, Western blot analysis of NPCs derived from HD Q71-iPSCs #2 with downregulated levels of UBR5. The graph represents the HTT relative percentage values to NT shRNA NPCs (corrected for β -actin) detected with antibody to total HTT (mean \pm s.e.m. of two independent experiments). All the statistical comparisons were made by Student's t-test for unpaired samples. P-value: *($P < 0.05$), **($P < 0.01$), ***($P < 0.001$).

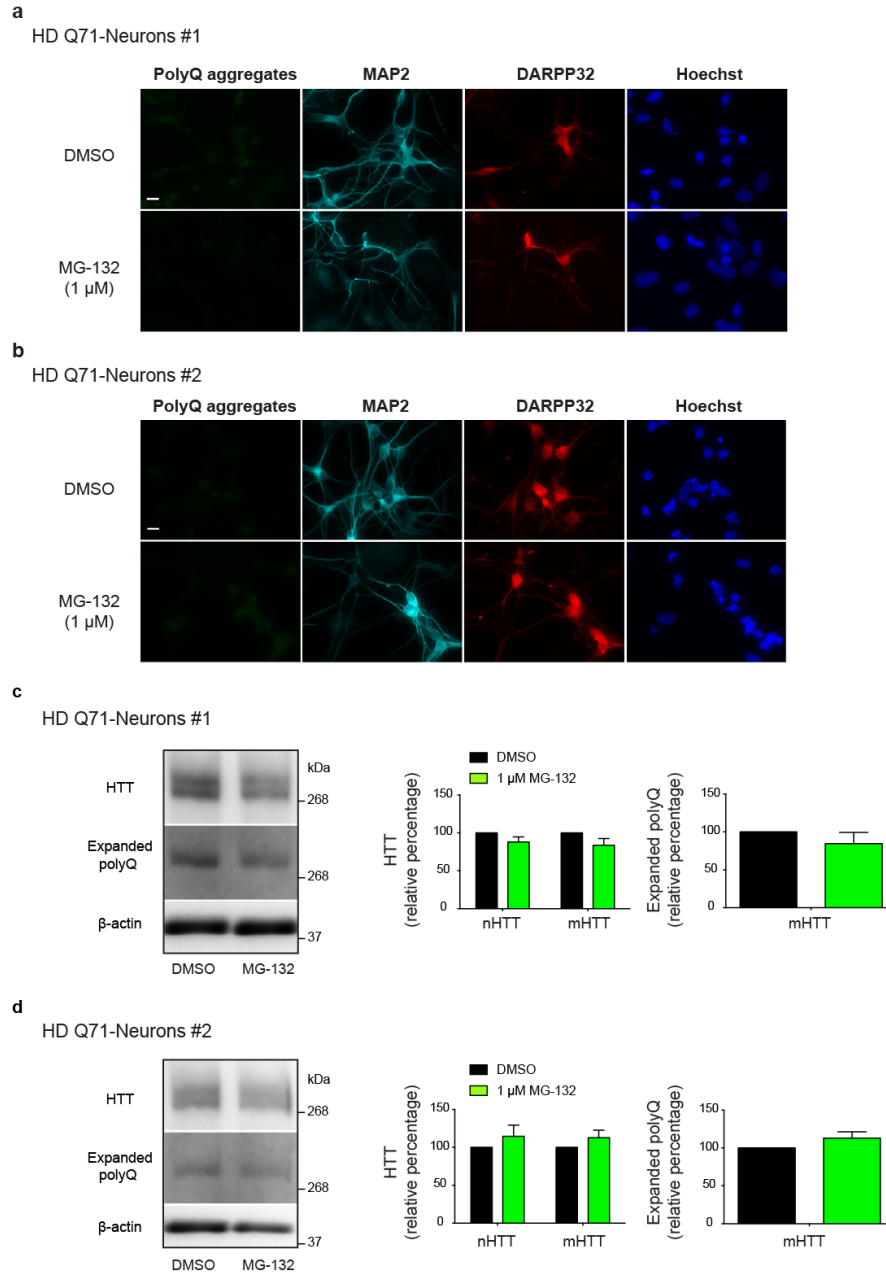


Supplementary Figure 30. iPSCs with downregulated levels of UBR5 can differentiate into striatal neurons. **a**, Striatal neuronal differentiation of HD Q180-iPSCs with downregulated levels of UBR5. GABA staining was used as a marker of striatal neurons. MAP2 and Hoechst 33342 staining were used as markers of neurons and nuclei, respectively. Scale bar represents 20 μ m. The images are representative of three independent experiments. **b**, Quantification of GABA cell populations among MAP2-positive neurons upon striatal neuronal differentiation (mean \pm s.e.m., three independent experiments, 1500-2000 cells per condition for each line). Knockdown of UBR5 was performed at the iPSC stage. **c**, qPCR analysis of striatal neuronal markers (*DARPP32*, *CALB1*, *CALB2*, *GAD1*, *GAD2*) and pan-neuronal markers (*MAP2*, *TUBB3*) in neurons derived from control iPSCs #1 with downregulated levels of UBR5. The graph represents the relative expression to NT shRNA neurons (mean \pm s.e.m. (n= 4 independent experiments)). **d**, Control neurons #2 (n= 3 independent experiments). **e**, HD Q71-Neurons #1 (n= 3 independent experiments). **f**, HD Q71-Neurons #2 (n= 2 independent experiments). **g**, HD Q180-Neurons (n= 3 independent experiments). All the statistical comparisons were made by Student's t-test for unpaired samples. P-value: *(P<0.05).

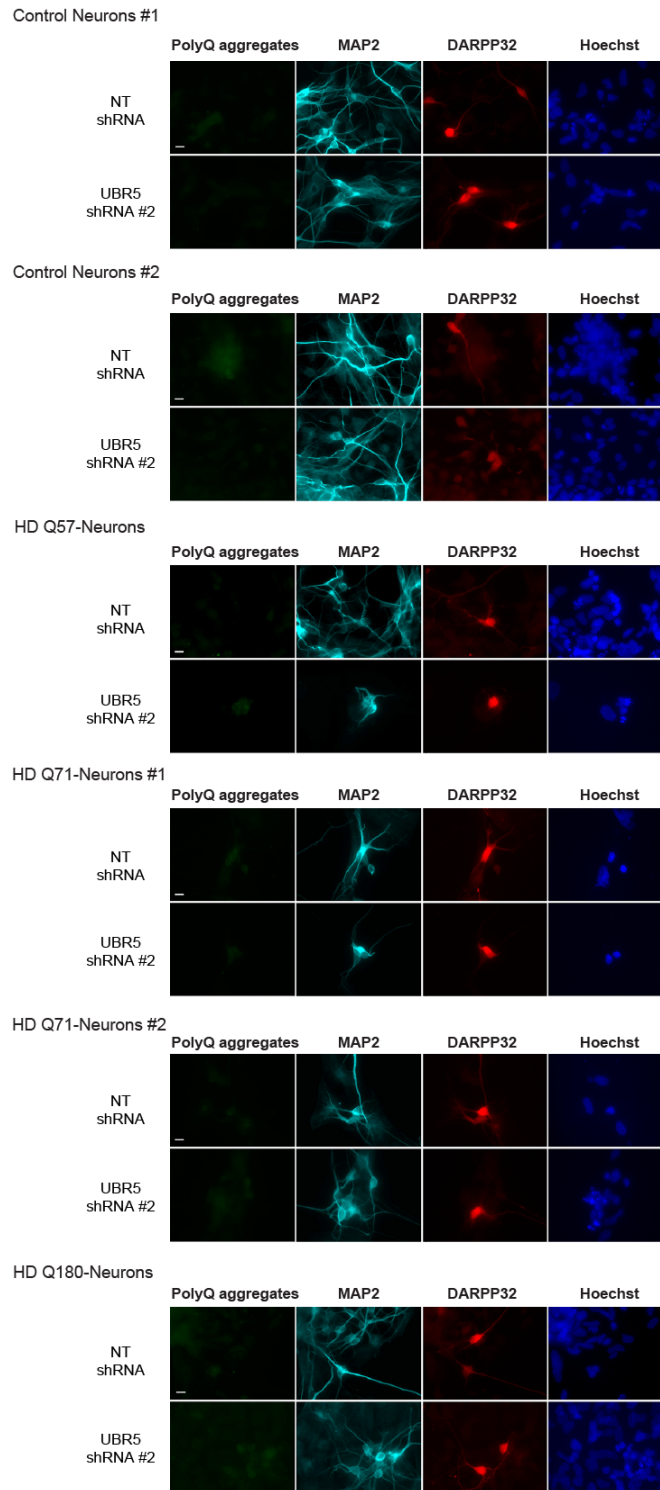
PolyQ aggregates \ MAP2



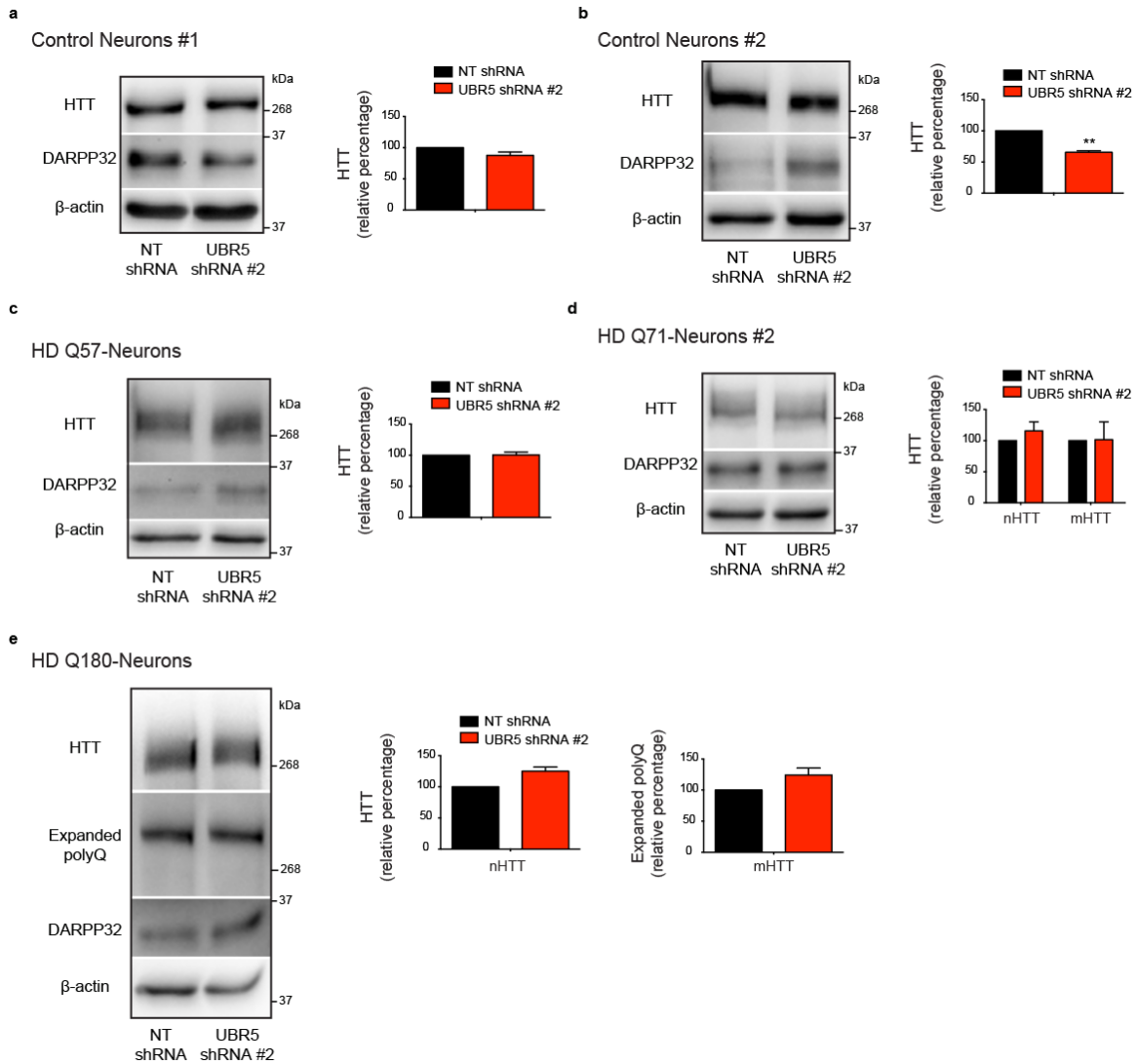
Supplementary Figure 31. Lack of polyQ-expanded HTT aggregates in terminally differentiated neurons derived from HD-iPSCs with downregulated levels of UBR5. Striatal neuronal differentiation of distinct control and HD-iPSCs with downregulated levels of UBR5. PolyQ-expanded and MAP2 staining were used as markers of polyQ-expanded aggregates and neurons, respectively. Scale bar represents 20 μ m. The images are representative of three independent experiments.



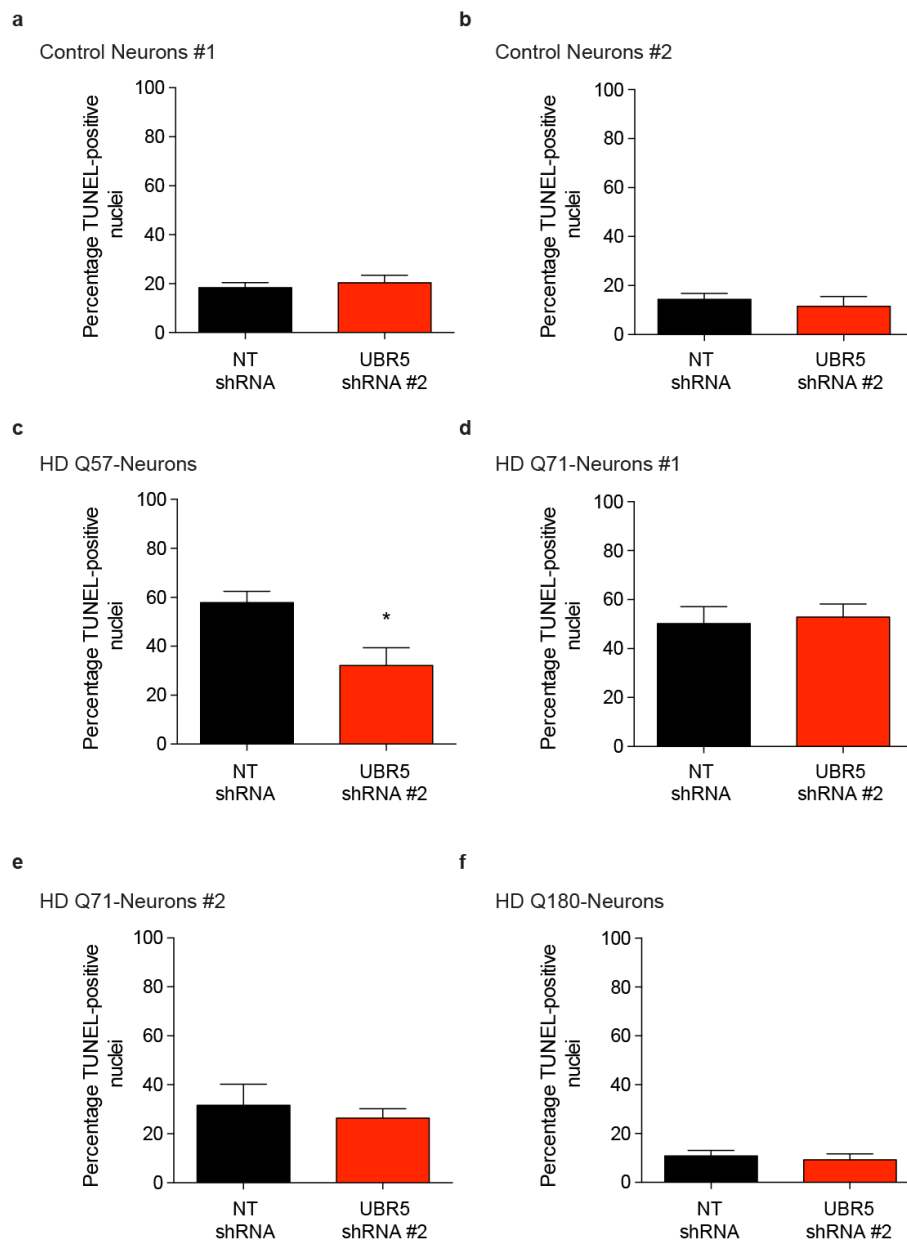
Supplementary Figure 32. Proteasome inhibition does not trigger aggregation of polyQ-expanded HTT in MSNs derived from HD-iPSCs. **a, b**, Immunocytochemistry with antibody against polyQ-expanded proteins of HD Q71-neurons lines #1 (**a**) and #2 (**b**) treated with 1 μ M MG-132 for 16 h. MAP2 was used as a pan-neuronal marker whereas DARPP32 was used as a marker of striatal neurons. Cell nuclei were stained with Hoechst 33342. Scale bar represents 10 μ m. The images are representative of two independent experiments. **c, d**, Western blot analysis of HD Q71-neurons lines #1 (**c**) and #2 (**d**) treated with 1 μ M MG-132 for 16 h. The graphs represent the relative percentage values to the respective DMSO-treated neurons (corrected for β -actin) of normal (nHTT) and mutant HTT (mHTT) detected with antibodies to total HTT and polyQ-expanded proteins (mean \pm s.e.m. of two independent experiments). No significant differences were found. All the statistical comparisons were made by Student's t-test for unpaired samples.



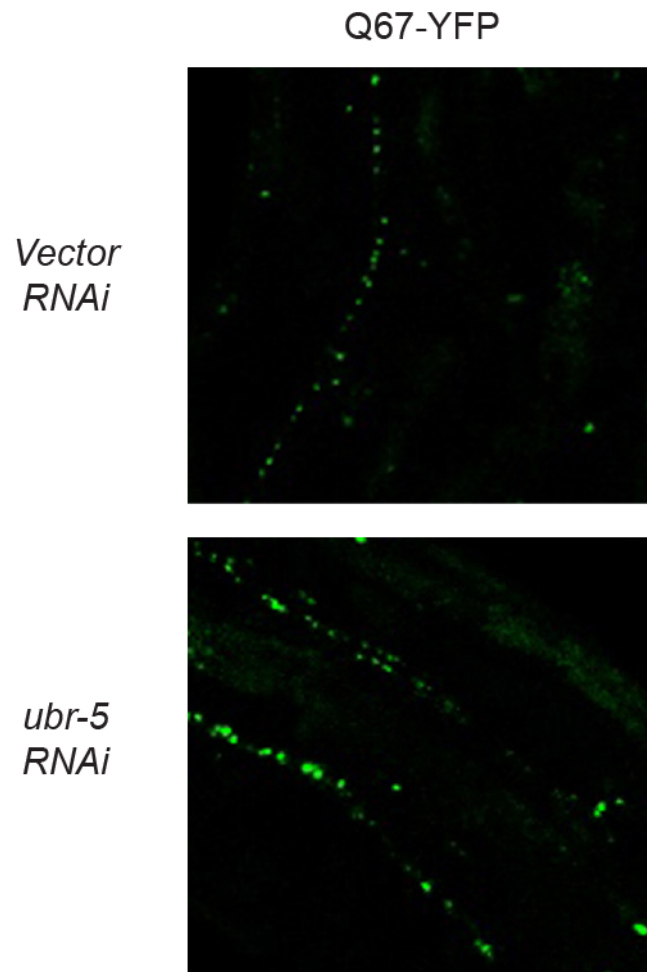
Supplementary Figure 33. Loss of UBR5 does not induce aggregation of mutant HTT in MSNs derived from HD-iPSCs. Immunocytochemistry with antibody against polyQ-expanded proteins in the indicated neurons. MAP2 was used as a pan-neuronal marker whereas DARPP32 was used as a marker of striatal neurons. Cell nuclei were stained with Hoechst 33342. Scale bar represents 10 μ m. The images are representative of three independent experiments.



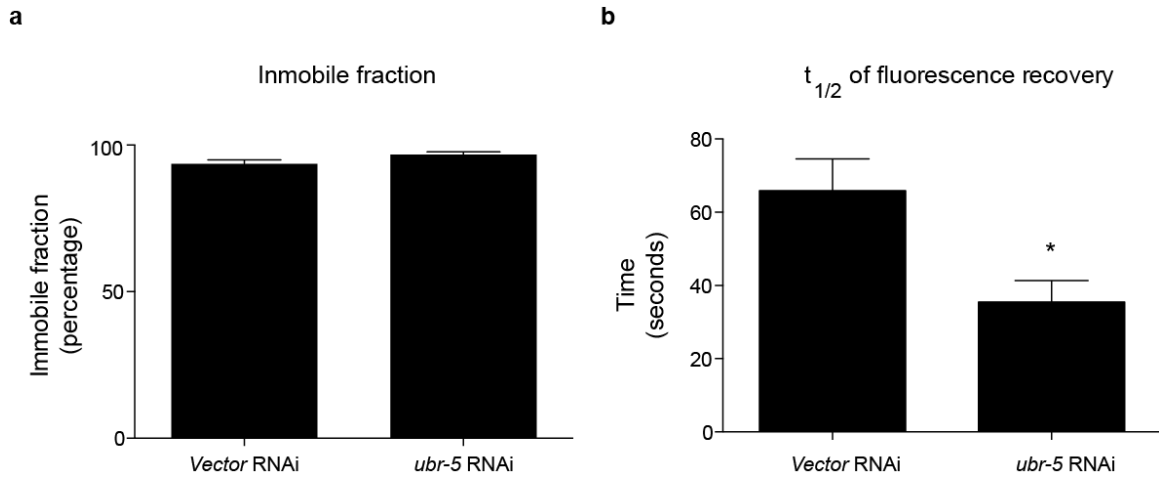
Supplementary Figure 34. Knockdown of UBR5 in MSN cultures derived from iPSCs does not increase HTT levels. **a, b,** Western blot analysis of the indicated control neuronal cultures with antibodies to HTT and DARPP32. The graphs represent the HTT relative percentage values to the respective NT shRNA neurons corrected for β -actin loading control (mean \pm s.e.m. of three independent experiments). **c,** Western blot analysis of HD Q57-neurons. The graph represents the relative percentage value to NT shRNA neurons (corrected for β -actin) of total HTT levels detected with anti-HTT antibody (mean \pm s.e.m. of three independent experiments). **d,** Western blot analysis of HD Q71-neurons #2. The graph represents the relative percentage values to NT shRNA neurons (corrected for β -actin) of nHTT and mHTT detected with anti-HTT antibody (mean \pm s.e.m. of four independent experiments). **e,** Western blot analysis of HD Q180-neurons. The graphs represent the relative percentage values to NT shRNA neurons (corrected for β -actin) of nHTT and mHTT detected with antibodies to HTT and polyQ-expanded proteins, respectively (mean \pm s.e.m. of three independent experiments).



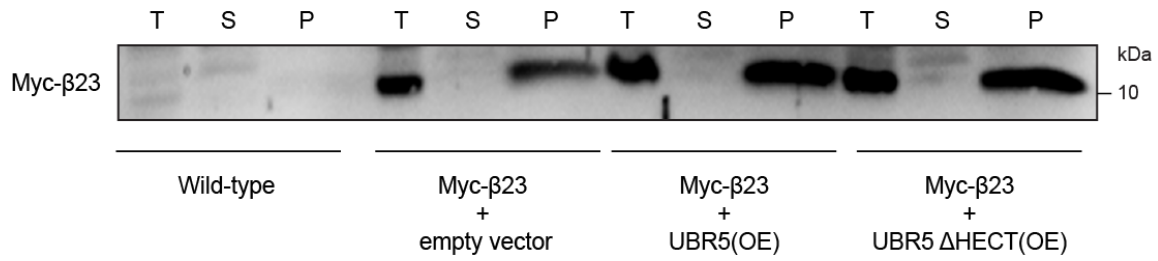
Supplementary Figure 35. Loss of UBR5 does not induce apoptosis in MSN cultures derived from iPSCs. Percentage of TUNEL-positive nuclei in the indicated MSN cultures: **a**, Control Neurons #1, **b**, Control Neurons #2, **c**, HD Q57-Neurons, **d**, HD Q71-Neurons #1, **e**, HD Q71-Neurons #2, **f**, HD Q180-Neurons. In **a-f**, total number of cells was evidenced after staining of nuclei with Hoechst 33342. Each graph represents the mean \pm s.e.m. of the percentage observed in 3 independent neuronal differentiation experiments (we assessed approximately 200-300 total nuclei in each independent experiment for each line). All the statistical comparisons were made by Student's t-test for unpaired samples. P-value: *($P < 0.05$).



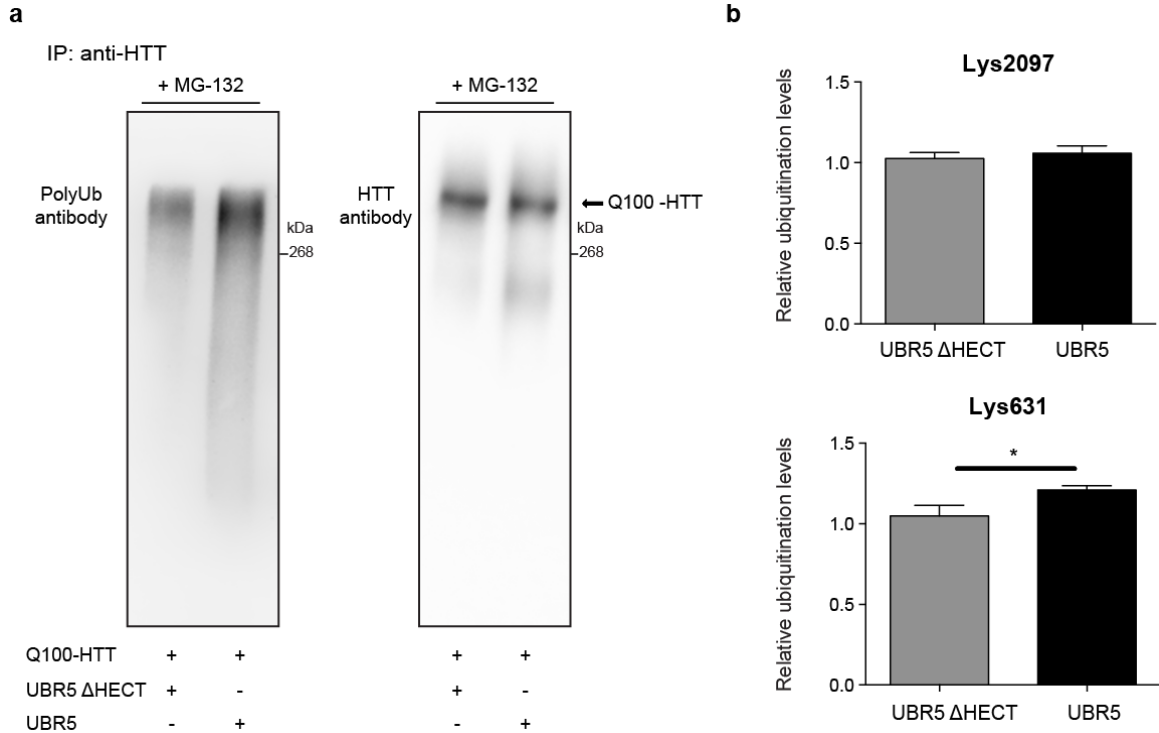
Supplementary Figure 36. Higher magnification of *C. elegans* mid-body of the images presented in **Figure 9c**.



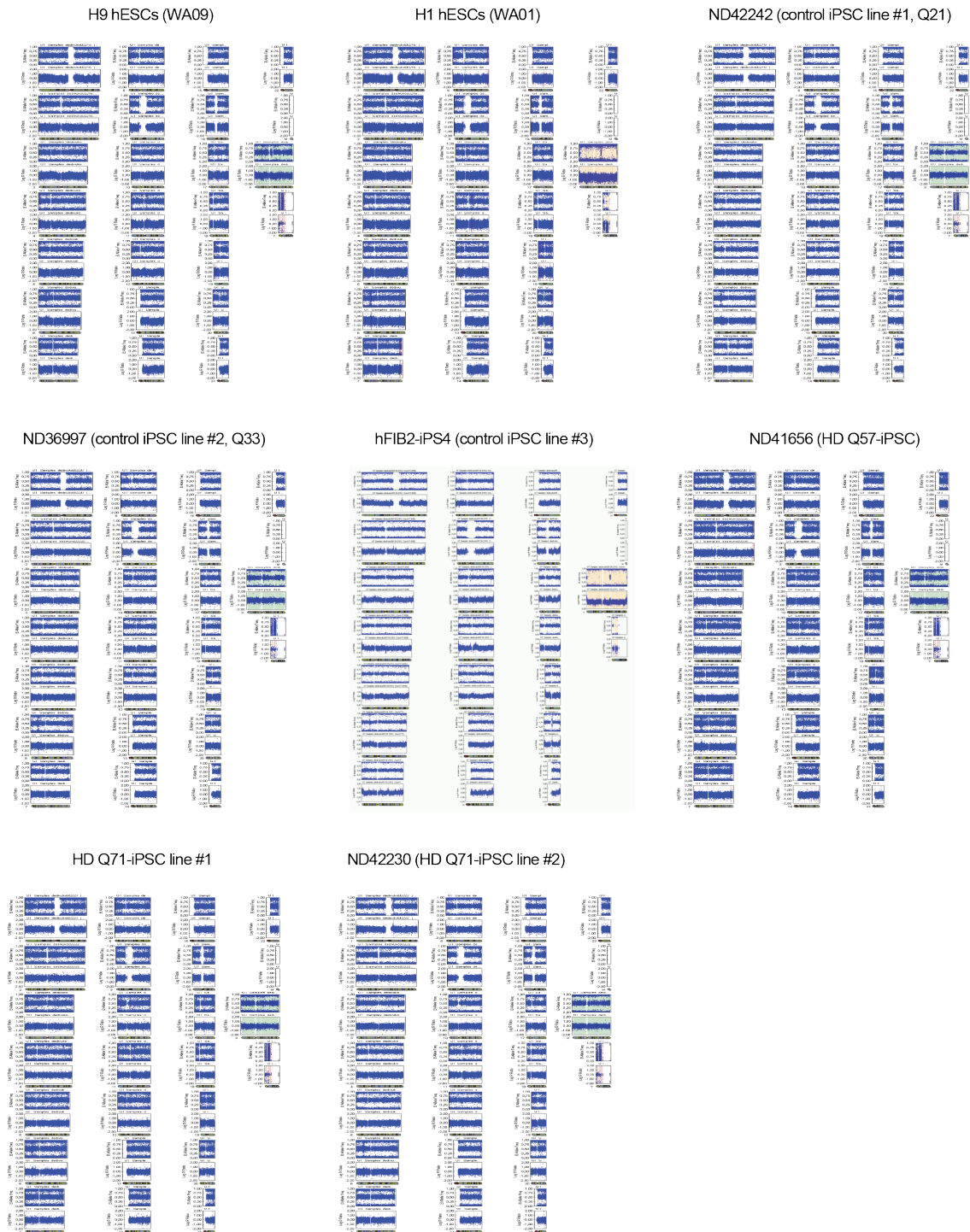
Supplementary Figure 37. FRAP analysis of Q67-YFP-expressing worms. Worms fed with empty vector or *ubr-5* RNAi were immobilized and regions containing polyQ-YFP foci in the head neurons were bleached. Subsequently, pictures were taken once every 2 seconds for 90 times. **a**, Graph represents percentage of immobile fraction. **b**, Graph represents the half-life of fluorescence recovery. In (**a**, **b**) data represents the mean \pm s.e.m. of 9 worms from two independent experiments. All the statistical comparisons were made by Student's t-test for unpaired samples. P-value: *($P < 0.05$).



Supplementary Figure 38. Ectopic expression of UBR5 does not reduce aggregation of β -amyloid fibrils. Upon cell fractionation of HEK293 cells, β 23 polypeptide with N-terminal c-Myc-epitope is largely recovered in the insoluble fraction. Overexpression of UBR5 does not increase the solubility of β 23 fibrils, as we did not detect the protein in the soluble fraction under this condition. Anti-Myc antibody was used to detect β 23 protein in the distinct cell fractions. T, total lysate; S, soluble fraction; P, pellet fraction. The images are representative of four independent experiments.



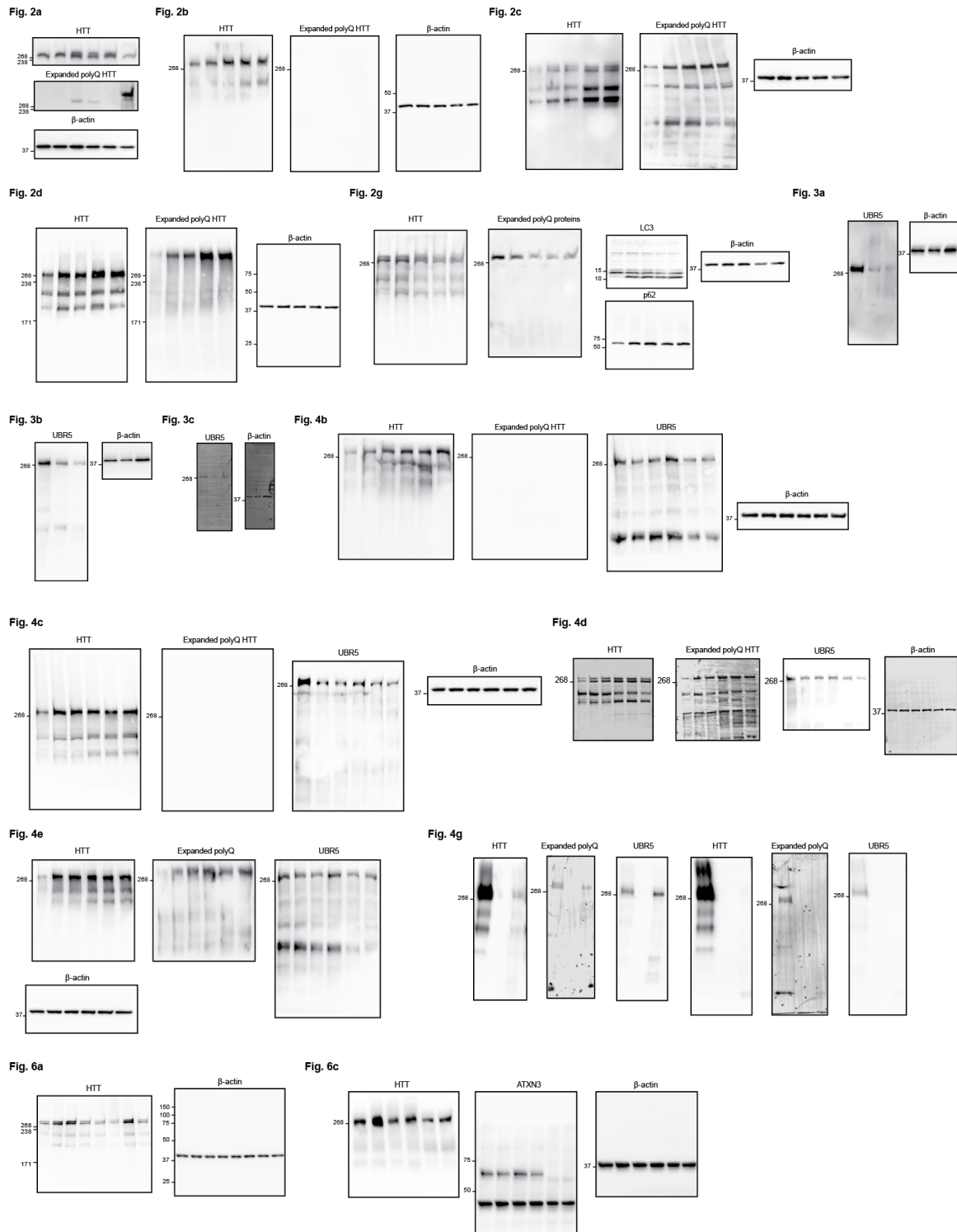
Supplementary Figure 39. Identification of HTT ubiquitination sites. a, Immunoprecipitation with anti-HTT antibody in Q100-HTT(OE) HEK293 cells treated with 0.5 μ M MG-132 for 16 h. Immunoprecipitation was followed by western blot with antibodies to HTT and polyubiquitinated proteins (polyUb) to detect immunoprecipitated total HTT protein and polyUb-HTT, respectively. These data validate increased polyubiquitination of HTT upon wild-type UBR5 overexpression when compared to catalytic inactive UBR5 mutant of the samples analyzed by proteomics for identification of ubiquitination sites. **b,** Relative ubiquitination levels of Lys2097 and Lys631 of HTT in Q100-HTT(OE) HEK293 cells upon overexpression of catalytic inactive mutant or wild-type UBR5. HTT was immunoprecipitated with anti-HTT antibody and analyzed by mass spectrometry. Lys631 and 2097 of HTT were found to be ubiquitinated. The ubiquitination intensity of each lysine was normalized by the total HTT level in every condition. The graphs show ubiquitination levels normalized to the levels of ubiquitination in samples overexpressing UBR5 catalytically catalytic inactive UBR5 mutant (mean \pm s.e.m. of three independent experiments). All the statistical comparisons were made by Student's t-test for unpaired samples. P-value: *(P<0.05).



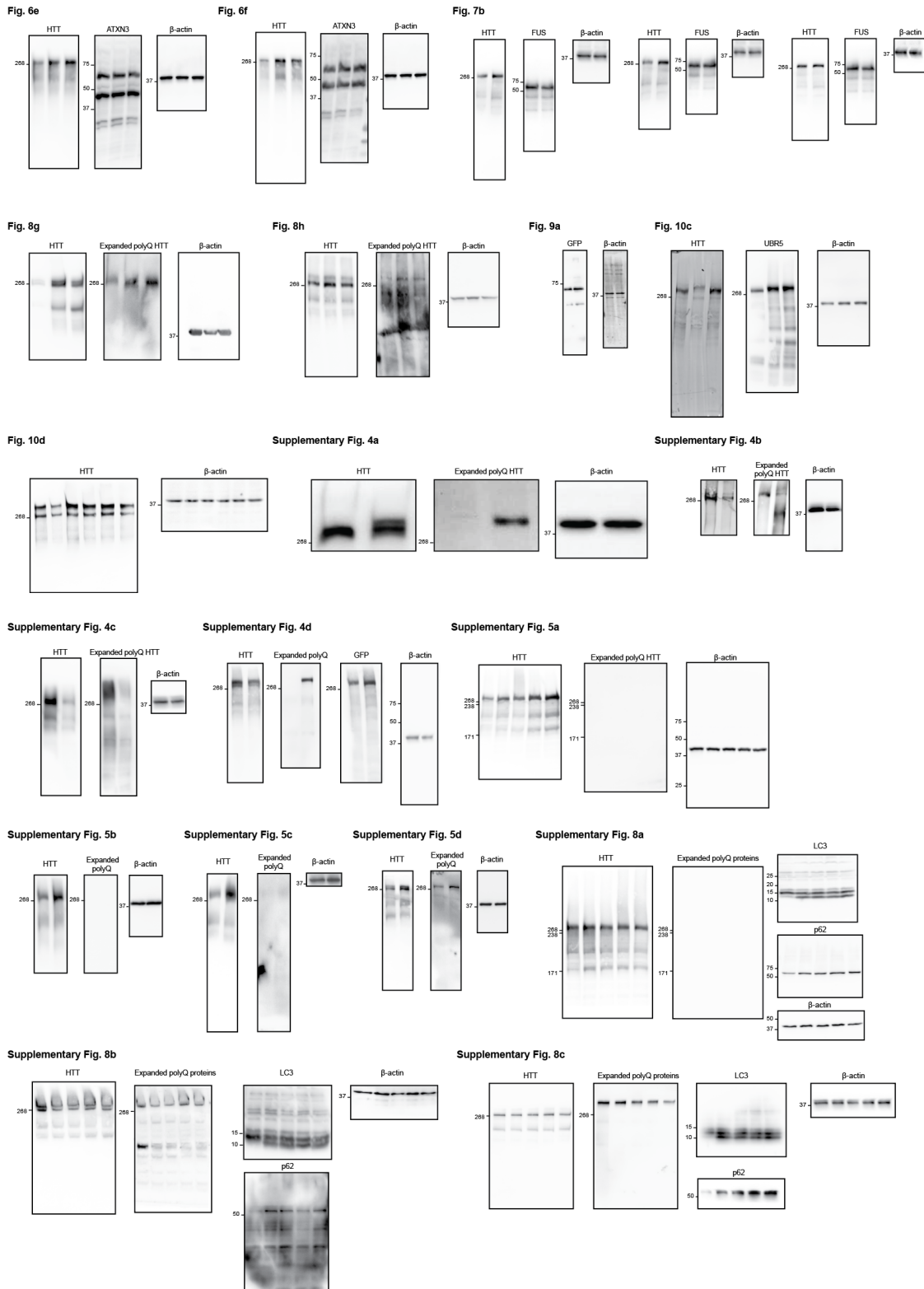
Supplementary Figure 40. SNP genotyping of hESCs and iPSCs used in this study.



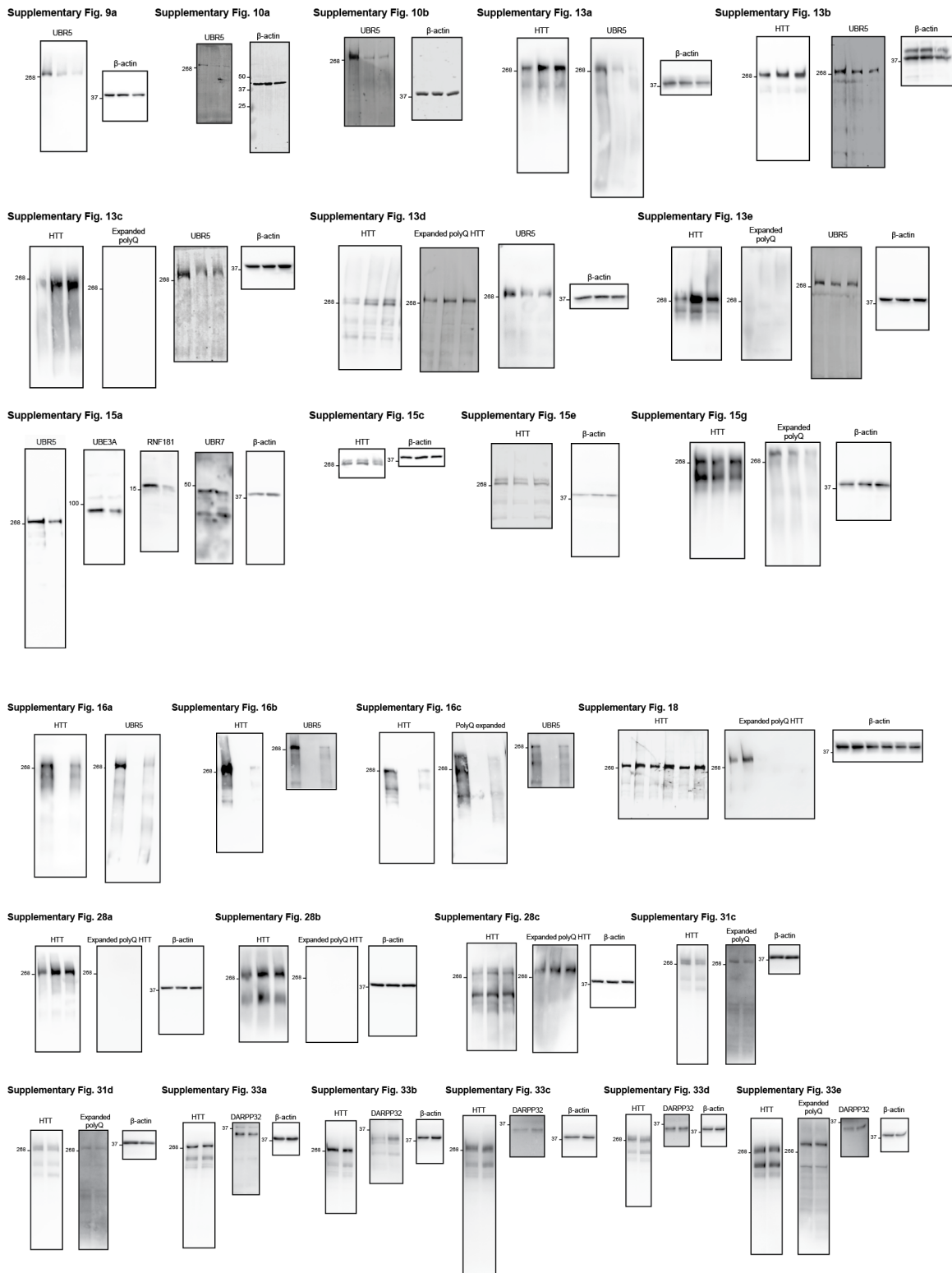
Supplementary Figure 40 (continuation). SNP genotyping of hESCs and iPSCs used in this study.



Supplementary Figure 41. Uncropped images are presented with molecular weight ladders.



Supplementary Figure 41 (continuation). Uncropped images are presented with molecular weight ladders.



Supplementary Figure 41 (continuation). Uncropped images are presented with molecular weight ladders.

iPSC line	Age at sampling	Age of onset	Sex	Relevant gene for disease	Clinical information
HD Q71 lines #1/#2	20	14	Female	Q71HTT/ Q19HTT	Rigid form of HD, hypokinetic variant of HD with dystonia and marked tremor, ataxic wide-based gait, symptomatic
HD Q180	6	<6	Male	Q180HTT/ Q18HTT	Juvenile HD, symptomatic
HD Q57	29		Female	Q57HTT/ Q17HTT	Post-juvenile HD, pre-symptomatic
MJD Q74 line #1	40	30	Male	Q74ATXN3/ Q21ATXN3	Scale for the Assessment and Rating of Ataxia (SARA): 23,0. Additional symptoms: parkinsonism, restless legs, spasticity, neuropathy
MJD Q74 line #2	38	31	Male	Q74ATXN3/ Q22ATXN3	SARA: 22,5. Additional symptoms: parkinsonism, restless legs, spasticity, neuropathy
ALS line #1	39	Mid-late age	Male	FUS ^{R521C/WT}	Affected by ALS in mid-late age
ALS line #2	Generated from control iPSCs #4 by TALEN-directed mutagenesis		Male	FUS ^{P525L/P525L}	Patient carrying this mutation displayed severe and juvenile onset of ALS

Supplementary Table 1. Patient information for disease-iPSC lines.

E3 ubiquitin ligases increased in hESCs	hESC vs neuron ratio	q-value
TRIM71	17.26	0.029
TRIM28	2.61	0.015
UBR5	2.49	0.007
RGPD1	2.46	0.010
RGPD2	2.41	0.010
RGPD8	2.36	0.013
UBR7	2.35	0.007
RGPD4	2.26	0.011
SART1	2.26	0.011
RGPD5	2.26	0.011
TRIM33	2.24	0.009
RGPD3	2.19	0.012
UBE4B	1.95	0.011
RNF20	1.94	0.017
ARIH2	1.80	0.037
RNF181	1.69	0.004
UBR4	1.61	0.021
PRPF19	1.48	0.019
HECTD1	1.46	0.010
KCMF1	1.43	0.012
UBE3A	1.30	0.007
TRIP12	1.30	0.014
RNF40	1.27	0.034
TRAF2	1.21	0.008
HERC1	1.17	0.011
HUWE1	1.09	0.028

Supplementary Table 2. List of E3 enzymes significantly increased in hESCs compared with their neuronal counterparts. Tandem mass tag (TMT) quantitative proteomics comparing H9 hESCs with neurons. Statistical comparisons were made by Student's t-test (n= 3). False Discovery Rate (FDR) adjusted p-value (q-value) <0.05 was considered significant.

a)

Locus ID	Alleles	
	H9 hESCs	H1 hESCs
vWA	17, 17	15, 17
TH01	9.3, 9.3	9.3, 9.3
TP0X	10, 11	8, 11
CSF1P0	11, 11	12, 13
D5S818	11, 12	9, 11
D13S317	9, 9	8, 11
D7S820	9, 11	8, 12
D16S539	12, 13	9, 13

b)

Locus ID	Alleles	
	MJD-iPSC line #1	MJD iPSC line #2
TH01	6, 10	9, 9.3
CSF1P0	10, 11	9, 10
D5S818	12, 13	10, 12
D13S317	8, 10	11, 11
D7S820	10, 12	9, 11
D16S539	11, 14	9, 12

Supplementary Table 3. STR profiles of hESC and MJD-iPSC lines. **a,** The H9 and H1 hESCs used in our study matches exactly the published STR profile of these cells across the 8 STR loci analysed. **b,** The MJD-iPSCs used in our study matches exactly the STR profile of their parental fibroblasts provided by the depositor of the lines. The STR profile is not presented in full to protect the donor's identity as requested by the provider of the cells (EBiSC consortium).

	Allele size in base pairs					
	TPOX	CSFIPO	THO1	vWA	D17S1303	D16S539
	Allele1, Allele2	Allele1, Allele2	Allele1, Allele2		Allele1, Allele2	Allele1, Allele2
ND30014	242, 242	306, 318	169, 172	146, 151	223, 227	154, 159
Control iPSCs #1	242, 242	306, 318	169, 172	146, 151	223, 227	154, 159
GMO2183	231, 231	315, 315	169, 172	146, 159	231, 235	150, 154
Control iPSCs #2	231, 231	315, 315	169, 172	146, 159	231, 235	150, 154
GMO4281	231, 242	306, 310	165, 169	146, 154	223, 223	154, 159
HD Q71-iPSCs #1	231, 242	306, 310	165, 169	146, 154	223, 223	154, 159
HD Q71-iPSCs #2	231, 242	306, 310	165, 169	146, 154	223, 223	154, 159
GMO9197	231, 234	306, 310	155, 172	135, 145	231, 235	142, 159
HD Q180-iPSCs	231, 234	306, 310	155, 172	135, 145	231, 235	142, 159
HD-C#1 (isogenic corrected line)	231, 234	306, 310	155, 172	135, 145	231, 235	142, 159
HD-C#2 (isogenic corrected line)	231, 234	306, 310	155, 172	135, 145	231, 235	142, 159
ND33392	237, 241	309, 314	164, 171	140, 145	223, 235	154, 159
HD Q57-iPSCs	237, 241	309, 314	164, 171	140, 145	223, 235	154, 159
Control iPSCs #4	231, 231	306, 311	169, 172	140, 155	223, 235	159, 168
ALS-iPSCs #2	231, 231	306, 311	169, 172	140, 155	223, 235	159, 168

Supplementary Table 4. Confirmation of genetic identity of HD-iPSCs lines with the corresponding parental fibroblasts by STR analysis. Since ALS-iPSCs #2 were raised from control iPSCs #4 by TALEN-directed mutagenesis, we confirmed that the STR profile of the ALS-iPSCs #2 used in our experiments matches with the profile of control iPSCs #4.

Gene	Forward (5' → 3')	Reverse (5' → 3')
ACTB	CTGGCACCCAGCACAATG	CCGATCCACACGGAGTACTTG
GAPDH	GCACCGTCAAGGCTGAGAAC	GGATCTCGCTCCTGGAAGATG
UBR5	TGGAGTGAATCTGAGCCTTACAGA	AATGTTGCTCGTGGATGATGTAAT
HTT	GATTGGATGGGCACCATTAGA	GATTGGATGGGCACCATTAGA
0CT4	GGAGGAAGCTGACAACAATGAAA	GGCCTGCACGAGGGTTT
NANOG	AAATCTAAGAGGTGGCAGAAAAACA	GCCTTCTGCGTCACACCATT
SOX2	TGCGAGCGCTGCACAT	TCATGAGCGCTTGGTTTTCC
DPPA4	CTGGTGCCAACAATTGAAGCT	AGGCACACAGGCGCTTATATG
GATA6	AGCGCGTGCCCTTCATCA	GTGGTAGTTGTGGTGTGACAGTTG
AFP	GAGGGAGCGGCTGACATTATT	ACCAGGGTTTACTGGAGTCATTTTC
MSX1	CTCCGCAAACACAAGACGAAC	CACATGGGCCCGTGTAGAGTC
NES	TGAAGGGCAATCACAACAGG	TGACCCCAACATGACCTCTG
PAX6	CATACCAAGCGTGTCAATAAAC	TGCGCCCATCTGTTGCT
UBE3A	GACTCAAAGTTAGACGTGACCATATCA	CTTCAAGTCTGCAGGATTTTCCA
UBR7	TGCCGGCTCTAGTTCTGAATC	TTCTGCGTTGAGGCTTTTATT
RNF181	CCTTGCCATCACCTTTTCCA	GGACAGGAATTTGTCTTGCTTAG
TRIM71	CGGCGAGGCATAAGAAAGC	GCTTTCACCTGGCGGATCT
DARPP32	CCTGAAGGTCATCAGGCAGT	GGTCTTCCACTTGGTCTCTCA
CALB1	TCAGGACGGCAATGGATACA	AAGAGCAAGATCCGTTTCGGT
CALB2	TGGCGGAAGTACGACACAGA	GGAATCCCTTGAGCTCATTGG
GAD1	CCAAGGTGCTGGACTTTTCAT	AAATCGAGGATGACCTGTGC
GAD2	CGAGCCTGGTGCCAAGTG	CAGGGCGCACAGTTTGT
MAP2	AAAGAAGCTCAACATAAAGACCAGACT	GTGGAGAAGGAGGCAGATTAGC
TUBB3	GGCCAAGTTCTGGGAAGTCA	CGAGTCGCCCACGTAGTTG

Supplementary Table 5. List of primers used for qPCR experiments.

ARTICLE

Received 29 Mar 2016 | Accepted 19 Oct 2016 | Published 28 Nov 2016

DOI: 10.1038/ncomms13649

OPEN

Somatic increase of CCT8 mimics proteostasis of human pluripotent stem cells and extends *C. elegans* lifespan

Alireza Noormohammadi^{1,*}, Amirabbas Khodakarami^{1,*}, Ricardo Gutierrez-Garcia¹, Hyun Ju Lee¹, Seda Koyuncu¹, Tim König¹, Christina Schindler¹, Isabel Saez¹, Azra Fatima¹, Christoph Dieterich² & David Vilchez¹

Human embryonic stem cells can replicate indefinitely while maintaining their undifferentiated state and, therefore, are immortal in culture. This capacity may demand avoidance of any imbalance in protein homeostasis (proteostasis) that would otherwise compromise stem cell identity. Here we show that human pluripotent stem cells exhibit enhanced assembly of the TRiC/CCT complex, a chaperonin that facilitates the folding of 10% of the proteome. We find that ectopic expression of a single subunit (CCT8) is sufficient to increase TRiC/CCT assembly. Moreover, increased TRiC/CCT complex is required to avoid aggregation of mutant Huntingtin protein. We further show that increased expression of CCT8 in somatic tissues extends *Caenorhabditis elegans* lifespan in a TRiC/CCT-dependent manner. Ectopic expression of CCT8 also ameliorates the age-associated demise of proteostasis and corrects proteostatic deficiencies in worm models of Huntington's disease. Our results suggest proteostasis is a common principle that links organismal longevity with hESC immortality.

¹Cologne Excellence Cluster for Cellular Stress Responses in Aging-Associated Diseases (CECAD), University of Cologne, Joseph Stelzmann Strasse 26, Cologne 50931, Germany. ²Section of Bioinformatics and Systems Cardiology, Department of Internal Medicine III and Klaus Tschira Institute for Computational Cardiology, Neuenheimer Feld 669, University Hospital, Heidelberg 69120, Germany. * These authors contributed equally to this work. Correspondence and requests for materials should be addressed to D.V. (email: dvilchez@uni-koeln.de).

The survival of an organism is linked to its ability to maintain the integrity of the cellular proteome. Oxidative or thermal stress, misfolding-prone mutations and aging challenge the structure of proteins. Damaged proteins form toxic aggregates and disrupt cellular membranes, overwhelming the cellular machinery required for their degradation and causing cell malfunction and death¹. The quality of the proteome is controlled by proteostasis, a complex network of competing and integrated cellular pathways that regulate the synthesis, folding, aggregation, trafficking, interaction and degradation of proteins². With age, post-mitotic cells lose extensive control of proteostasis: widespread, aberrant changes in translation, a generalized downregulation of chaperones and a loss of function in protein degradation machineries often appear in differentiated cells across time^{3,4}. This demise in proteostasis is considered one of the hallmarks of aging and contributes to the functional loss characteristic of old organisms^{2,3}. Proteostasis dysfunction is associated with multiple age-related disorders such as Huntington's disease (HD), Alzheimer's or Parkinson's disease^{2,3}. In contrast, preservation or enhancement of proteostasis surveillance systems until late in life improves resistance to proteotoxic stress and slows down the aging process^{4,5}.

Embryonic stem cells (ESCs) demonstrate a striking capacity to proliferate indefinitely while maintaining their pluripotency⁶—a capacity that necessarily demands avoidance of any imbalance in proteostasis that would otherwise compromise their function and immortality. Furthermore, ESCs require high global translational rates to maintain their pluripotency⁷. These observations raise an intriguing question: how do ESCs maintain the quality of their proteome under enhanced protein synthesis and proliferation rates? Thus, we hypothesize that ESCs can provide a novel paradigm to study proteostasis and its demise with age. Human ESCs (hESCs) and induced pluripotent stem cells (iPSCs) exhibit high proteasome activity compared with their differentiated counterparts⁸. However, pluripotent stem cells are remarkably more sensitive ($100\times$) to proteasome inhibitors than progenitor or terminally differentiated cells^{8,9}. Increased proteasome activity of human pluripotent stem cells is induced by enhanced levels of the proteasome subunit PSMD11/RPN-6 (ref. 8). Interestingly, RPN-6 overexpression (OE) in somatic tissues is sufficient to induce proteotoxic resistance and extend lifespan in the organismal model *Caenorhabditis elegans*¹⁰. Besides increased proteasome activity, we hypothesize that other proteostasis components are also enhanced in hESCs/iPSCs to maintain their pluripotency and immortality.

In this study, we focused on the chaperome network, a key node of proteostasis. The human chaperome is formed by 332 chaperones and co-chaperones that regulate the folding and function of proteins¹¹. The binding of chaperones to nascent proteins assists their folding into the correct structure. Furthermore, chaperones assure the proper folding and cellular localization of proteins throughout their life cycle¹². Gene expression analysis of human brain aging shows a striking repression of 32% of the chaperome, including ATP-dependent chaperone machines such as cytosolic HSP90, HSP70 family members (for example, HSPA8 and HSPA14) and subunits of the T-complex protein-1 ring complex/chaperonin containing TCP1 (TRiC/CCT) complex. In contrast, 19.5% of the chaperome is induced during human brain aging¹¹. In addition, these repression and induction are enhanced in the brains of those with HD, Alzheimer's or Parkinson's disease compared with their age-matched controls¹¹. Notably, knockdown of specific chaperome components that are repressed during aging such as CCT subunits, HSPA14 or HSPA8 induces proteotoxicity in HD *C. elegans* and mammalian cell models¹¹. Therefore, defining

differences in the levels and regulation of chaperone machines between immortal hESCs and their differentiated counterparts could be of central importance not only for understanding hESC identity but also the aging process.

Here we show that human pluripotent stem cells exhibit increased assembly of the chaperonin TRiC/CCT complex, a mechanism induced by high levels of specific CCT subunits. By studying proteostasis of pluripotent stem cells, we find that CCT8 is sufficient to increase TRiC/CCT assembly. Furthermore, enhanced TRiC/CCT assembly is required for the striking ability of pluripotent stem cells to maintain proteostasis of aggregation-prone huntingtin (HTT), the mutant protein underlying HD. Our results indicate that the differentiation process correlates with a decline in the expression of CCT subunits and TRiC/CCT assembly. Since the levels of CCT subunits are further decreased in somatic tissues during organismal aging¹¹, we examined whether modulation of CCT8 can delay the aging process and proteostasis dysfunction by using *C. elegans* as a model organism. Notably, upregulation of CCT8 levels in somatic tissues triggers TRiC/CCT assembly and extends organismal lifespan particularly under proteotoxic conditions. Thus, we define CCT8 as a key modulator of TRiC/CCT assembly and establish a link between TRiC/CCT chaperonin, hESC identity and youthfulness.

Results

CCT subunits decrease during hESC differentiation. To examine changes in the chaperome network during differentiation, we performed quantitative analysis of both the transcriptome and proteome comparing hESCs with their neural progenitor cell (NPC) and neuronal counterparts (Supplementary Figs 1 and 2 and Supplementary Data 1 and 2). In our transcriptome analysis, we identified 279 chaperome components. Among them, 119 genes were downregulated and 44 genes were upregulated during differentiation into NPCs (Supplementary Fig. 1 and Supplementary Data 1). At the protein level, we found that 36 out of 122 identified chaperome components decrease during differentiation into NPCs (Supplementary Fig. 2 and Supplementary Data 2). In contrast, 27 chaperome components were increased during neural differentiation. Among the 44 chaperome components decreased in terminally differentiated neurons compared with hESCs, 28 proteins were already downregulated during differentiation into NPCs (Supplementary Data 2).

Notably, several subunits of the chaperonin TRiC/CCT complex decreased at both transcript and protein levels during neural differentiation of hESCs (Supplementary Fig. 3 and Supplementary Table 1). TRiC/CCT is required for cell viability as a key component of the proteostasis network that facilitates the folding of $\sim 10\%$ of the eukaryotic proteome^{13,14}. TRiC/CCT not only assists the folding of newly synthesized proteins¹⁵ but also binds to misfolded proteins regulating their aggregation¹⁶. In eukaryotes, the hetero-oligomeric TRiC/CCT complex consists of two stacked rings of eight paralogous subunits each¹⁷. In our quantitative proteomics assay, we found that CCT3, CCT4 and CCT8 subunits are significantly increased in hESC compared with NPCs (Supplementary Table 1). We confirmed these results by western blot analysis and found that other subunits also decrease during neural and neuronal differentiation (that is, CCT2, CCT6A and CCT7; Fig. 1a). The decrease in the protein amount of CCT subunits correlated with a reduction of the mRNA levels during differentiation (Fig. 1b). This downregulation of CCT subunits was not a specific phenomenon associated with the neural lineage as differentiation into either endoderm or mesoderm induced a similar decrease (Fig. 1c–f). Because hESC lines can vary in their characteristics, we differentiated a distinct hESC line as well as two iPSC lines,

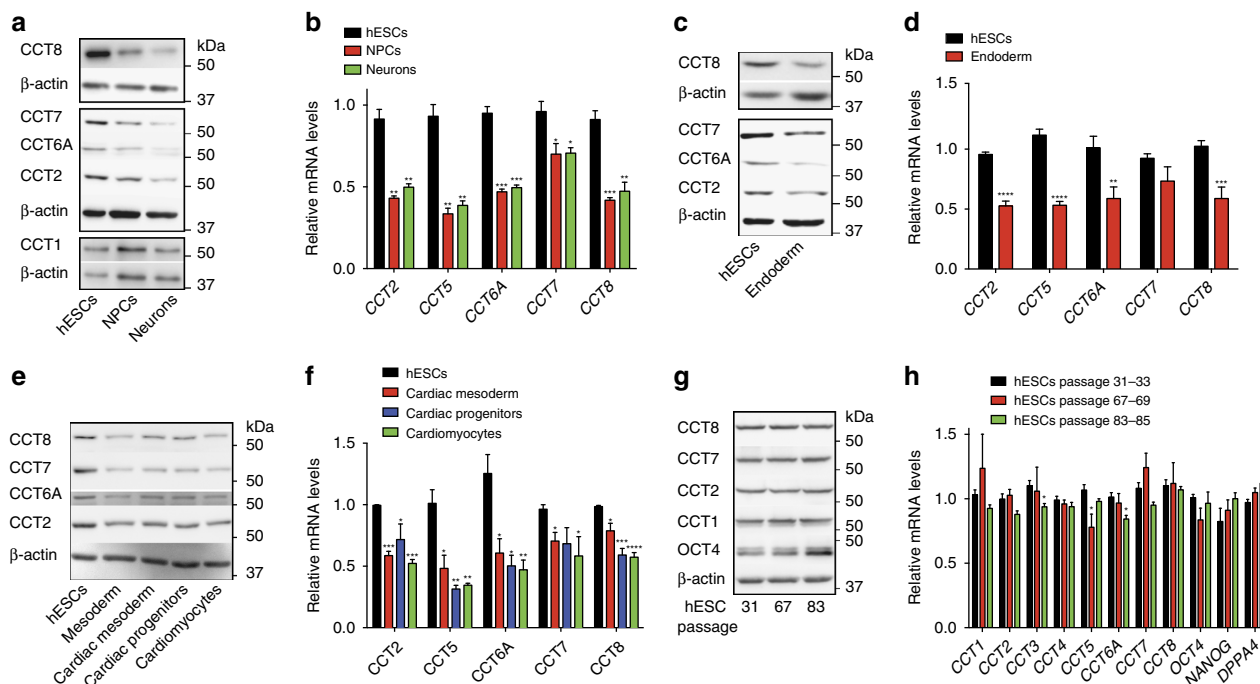


Figure 1 | The expression of CCT subunits decreases during differentiation. (a,c,e) Western blot analysis with antibodies to CCT8, CCT7, CCT6A, CCT2 and CCT1. β-actin is the loading control. The images are representative of two independent experiments. In a,c the differentiation was performed with the H9 hESC line whereas in e we used H1 hESCs. (b) CCT subunits relative expression to H9 hESCs represents the mean ± s.e.m. of three independent experiments. (d) CCT subunits relative expression to H9 hESCs represents the mean ± s.e.m. ($n = 7$ independent experiments). (f) CCT subunits relative expression to H1 hESCs represents the mean ± s.e.m. of three independent experiments. (g) The protein levels of CCT subunits do not differ with passage in H9 hESCs. β-actin is the loading control. The images are representative of two independent experiments. (h) Data represent the mean ± s.e.m. of the relative expression levels to H9 hESCs passage 31–33 ($n = 3$ independent experiments). All the statistical comparisons were made by Student's *t* test for unpaired samples. *P* value: * $P < 0.05$, ** $P < 0.01$, *** $P < 0.001$, **** $P < 0.0001$.

and obtained similar results (Supplementary Figs 4 and 5). Consistent with the ability of pluripotent stem cells to self-renew indefinitely while maintaining their undifferentiated state⁶, the expression of CCT subunits and pluripotency markers did not decline with passage (Fig. 1g,h). Taken together, our results indicate that human pluripotent stem cells are able to maintain enhanced expression of CCT subunits under unlimited proliferation in their undifferentiated state. However, the levels of subunits such as CCT8 or CCT2 decrease when hESCs/iPSCs differentiate into distinct cell lineages. Thus, increased levels of CCT subunits could be an intrinsic characteristic of human pluripotent stem cells linked to their immortality and identity.

Increased expression of CCT8 induces TRiC/CCT assembly.

Prompted by these findings, we asked whether increased levels of CCT subunits resulted into more assembled TRiC/CCT complexes in human pluripotent stem cells. Although both hESCs and NPCs have similar levels of total CCT1 subunits (Figs 1a and 2a, Supplementary Fig. 4 and Supplementary Table 1), hESCs lines exhibited a dramatic increase in the assembly of TRiC/CCT in the form of two stacked rings (Fig. 2a and Supplementary Fig. 4). Similarly, iPSCs also had increased TRiC/CCT assembly compared with differentiated cells (Supplementary Fig. 5). Since all the subunits are required for TRiC/CCT function¹⁸, down-regulated CCT subunits could become structural limiting factors during differentiation and modulate the decrease of TRiC/CCT assembly. An intriguing possibility is that specific subunits can also function as assembly activators. A comparison between the levels (relative to CCT1) of the different subunits in hESCs and NPCs showed that CCT8 is the most abundant subunit in both

cell types despite decreasing during differentiation (Fig. 2b). These findings indicate that CCT8 is not stoichiometric limiting for TRiC/CCT assembly. Thus, we asked whether an increase in the total protein levels of CCT8 could trigger TRiC/CCT assembly. Strikingly, ectopic expression of CCT8 induced an increase in TRiC/CCT assembly whereas the total protein levels of CCT1 remained similar (Fig. 2c). In contrast, we found a decrease in the levels of CCT1 in its monomeric form on CCT8 OE (Fig. 2c). Collectively, our results suggest that human pluripotent stem cells have an intrinsic proteostasis network characterized by high levels of TRiC/CCT complex. However, the levels of several CCT subunits decrease during differentiation resulting in diminished assembly of TRiC/CCT chaperonin. In addition, we identified CCT8 as a potential activator of TRiC/CCT assembly by using hESCs/iPSCs as a model to study proteostasis.

Loss of CCT subunits affects hESC identity. With the strong connection between hESC/iPSC identity, CCT8 expression and enhanced assembly of TRiC/CCT complex, we asked whether increased levels of CCT8 contribute to maintain pluripotency. Given that TRiC/CCT is essential for cell viability¹³, loss of CCT subunits induced cell death and detachment of hESCs (Supplementary Fig. 6a). To avoid these effects, we induced a mild knockdown of ~30–50% (Fig. 3a). Notably, downregulation of CCT8 resulted in decreased levels of pluripotency markers (Fig. 3a). We hypothesized that high CCT8 expression impinges on hESC function via enhanced assembly of TRiC/CCT complex. Since mutation or loss of a single subunit is sufficient to impair the activity of the complex¹⁸, we knocked down other subunits

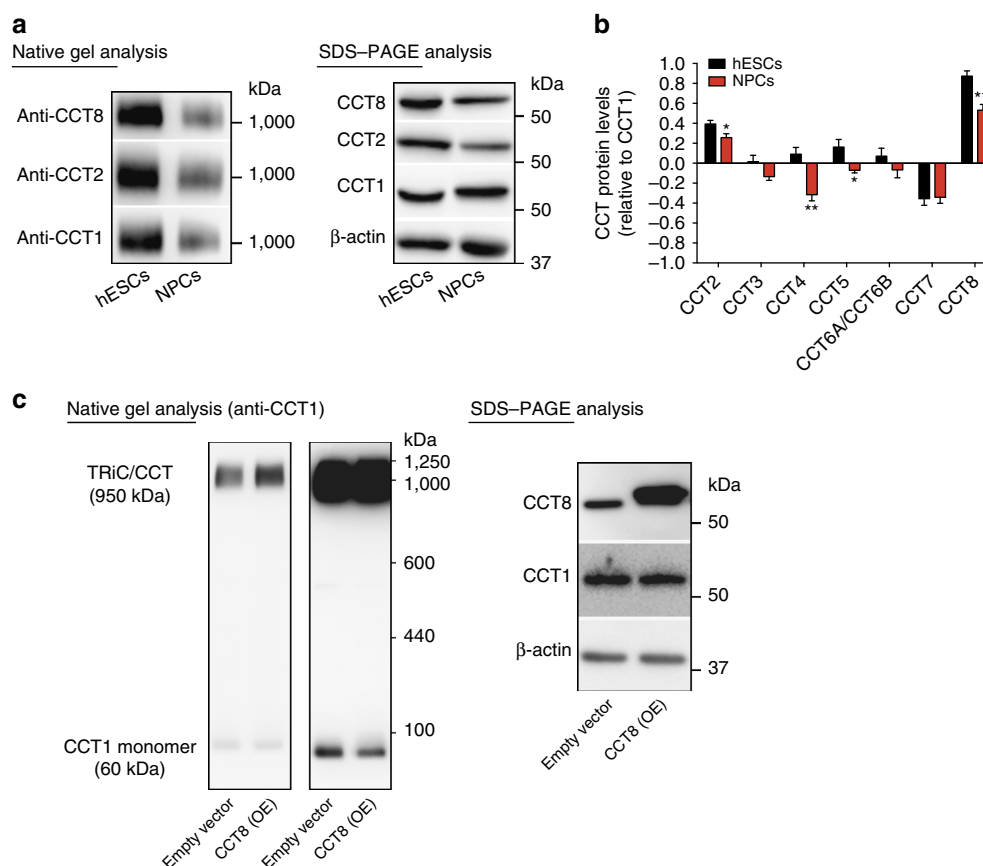


Figure 2 | Ectopic expression of CCT8 is sufficient to increase TRiC/CCT assembly. (a) Native gel electrophoresis of H9 hESCs and NPCs extracts followed by immunoblotting with CCT antibodies. Extracts were resolved by SDS-PAGE and immunoblotting for analysis of total CCT subunit levels and β -actin loading control. The images are representative of three independent experiments. (b) Label-free quantification (LFQ) of CCT protein levels relative to CCT1. All detected CCT subunits were quantified by their log₂ fold change in LFQ intensities relative to CCT1. Graphs represent the mean \pm s.e.m. (hESCs ($n = 9$), NPCs ($n = 6$)). All the statistical comparisons were made by Student's t-test for unpaired samples. P-value: * $P < 0.05$, ** $P < 0.01$, *** $P < 0.001$. (c) Native gel electrophoresis of HEK293T cell extracts followed by immunoblotting with CCT1 antibody (two different exposure times of the same membrane are shown). Extracts were resolved by SDS-PAGE and immunoblotting for analysis of total CCT8 and CCT1 subunit levels. β -actin is the loading control. The images are representative of three independent experiments.

(that is, CCT2, CCT6A and CCT7) to determine whether increased TRiC/CCT is required for hESC function. As with CCT8 knockdown, decreased levels of other subunits affected the expression of pluripotency markers (Fig. 3a,b). We performed these experiments in an independent hESC line as well as two iPSC lines and obtained similar results (Supplementary Fig. 6b–d). In addition, loss of CCT levels induced the expression of markers of the distinct germ layers (Fig. 3c and Supplementary Fig. 7). Since we observed an upregulation in specific markers of the three germ layers (Fig. 3c and Supplementary Fig. 7), our data suggest that hESCs/iPSCs undergo a decline of pluripotency on knockdown of CCT subunits but they do not differentiate into a particular cell lineage. Although we cannot discard a role of free monomeric CCT subunits, our results indicate that increased levels of the TRiC/CCT complex are required for human pluripotent stem cell identity.

TRiC determines proteostasis of pluripotent stem cells. Because the TRiC/CCT complex modulates aggregation of damaged and misfolded proteins¹⁶, we asked whether this chaperonin is required for increased proteostasis of pluripotent stem cells. To examine this hypothesis, we used iPSCs derived from HD. HD is an autosomal dominant neurodegenerative disorder caused by the expansion of a CAG triplet repeat region in the *huntingtin* gene

(*HTT*), which translates into a polyglutamine stretch (polyQ) in the protein resulting in proteotoxicity and aggregation¹⁹. In its wild-type form, HTT contains 6–35 glutamine residues. However, in individuals affected by HD, it contains > 35 glutamine residues and longer repeats predict younger disease onset¹⁹. Here we used three different control iPSC lines and HD-iPSCs from four donors with different allelic series (that is, polyQ57, polyQ60, polyQ71 and polyQ180). These HD-iPSC lines possess one mutant copy of *huntingtin* gene but also one normal allele (Fig. 4a,b). Although the levels of mutant HTT were lower compared with the normal protein, HD-iPSCs exhibited significant amounts of mutant polyQ-expanded HTT protein (Fig. 4a,b). In iPSCs that express longer CAG repeat expansions (polyQ180), the differences between the levels of mutant and normal HTT were more dramatic (Fig. 4b). Nevertheless, we confirmed the expression of mutant HTT in these iPSCs by using an antibody that detects remarkably better polyQ-expanded HTT than wild-type HTT (refs 20,21; Fig. 4b,e). To examine the aggregation of mutant HTT in HD-iPSCs, we performed filter trap analysis that allows for quantification of polyQ aggregates¹⁰. Although HD-iPSCs expressed significant levels of polyQ-expanded HTT, these cells did not exhibit accumulation of detectable polyQ aggregates compared with control iPSCs as assessed by both filter trap and immunohistochemistry analyses (Fig. 4c,e and Supplementary Fig. 8). In HD organismal models

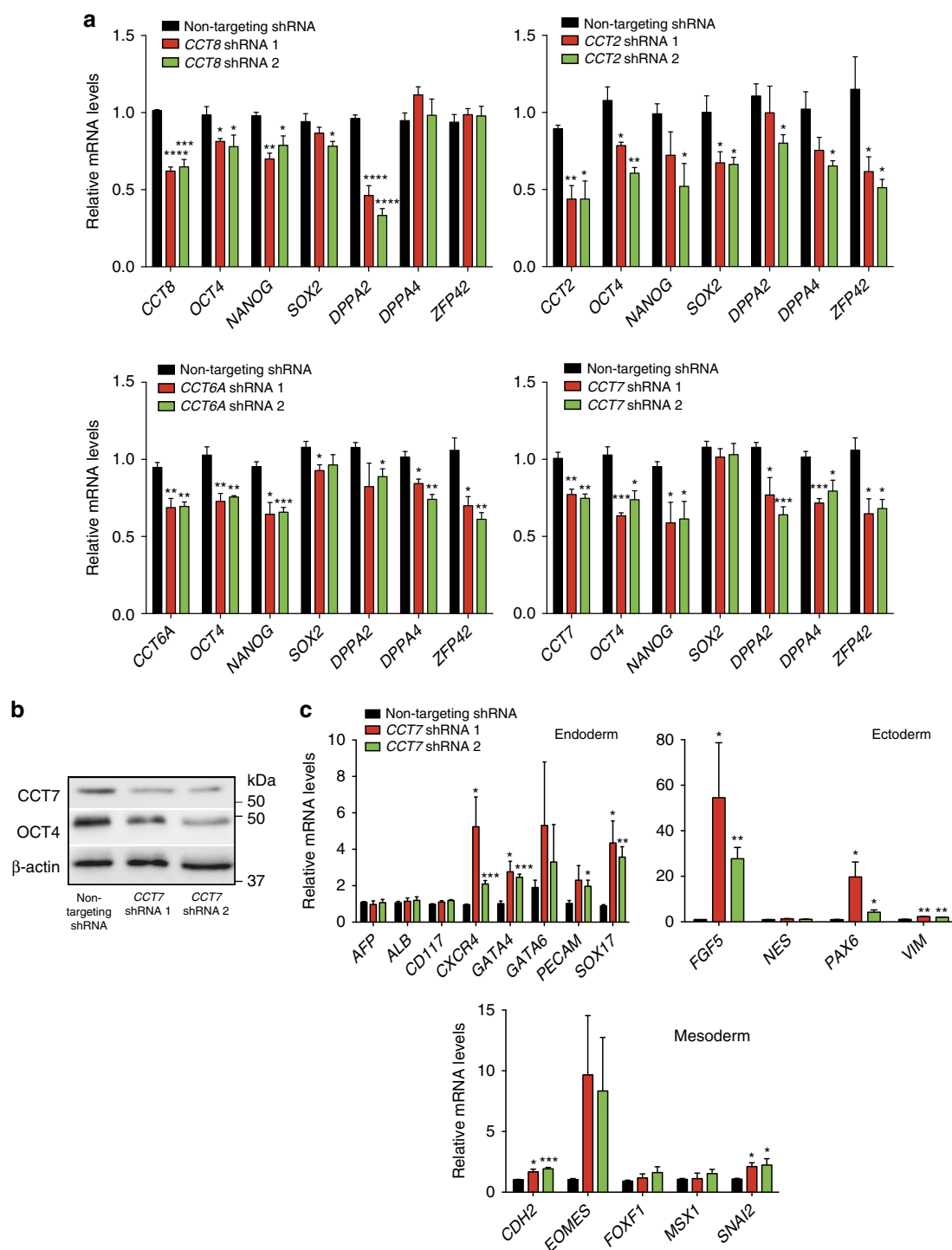


Figure 3 | Knockdown of CCT subunits affects pluripotency of hESCs. (a) Real-time PCR analysis of pluripotency markers in H9 hESCs. Graphs (relative expression to NT shRNA) represent the mean \pm s.e.m. of at least three independent experiments. Knockdown of *CCT8* ($n=3$), *CCT2* ($n=3$), *CCT6A* ($n=4$) and *CCT7* ($n=4$) decrease the expression of pluripotency markers. (b) Knockdown of *CCT7* induces a decrease in OCT4 protein levels. β -actin is the loading control. The images are representative of three independent experiments. (c) Real-time PCR analysis of germ-layer markers in H9 hESCs (relative expression to NT shRNA). Graph represents the mean \pm s.e.m. of four independent experiments. All the statistical comparisons were made by Student's *t* test for unpaired samples. *P* value: * $P<0.05$, ** $P<0.01$, *** $P<0.001$, **** $P<0.0001$.

and mammalian cells, the inhibition of HSP90 induces heat-shock response (HSR) and reduces polyQ-expanded protein aggregation²². We found that the treatment with an inhibitor of HSP90 did not further decrease the signal observed in HD-iPSCs by filter trap, reinforcing that these cells do not accumulate detectable aggregates of mutant HTT (Supplementary Fig. 8a).

However, a collapse in proteostasis induced by proteasome inhibition triggered the accumulation of polyQ aggregates in HD-iPSCs (ref. 23; Supplementary Fig. 8b–c).

Loss of CCT subunits enhances aggregation of mutant HTT and worsens HD-related changes in yeast, *C. elegans* and mammalian neuronal models^{24–26}. Thus, increased TRiC/CCT

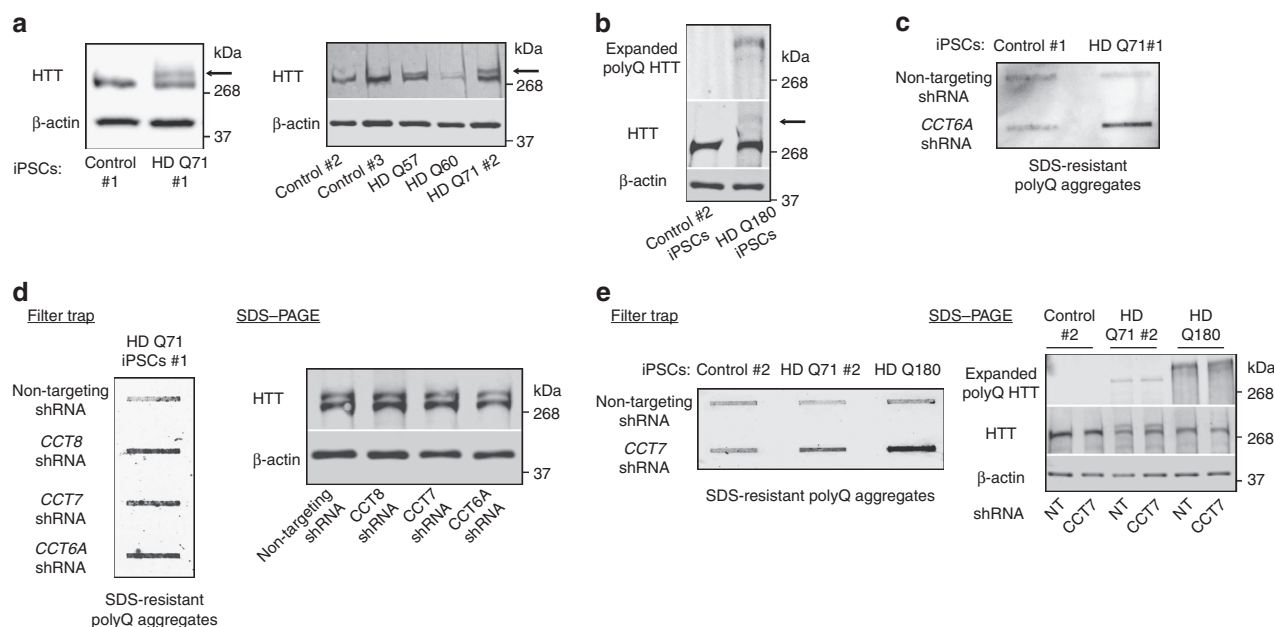


Figure 4 | Knockdown of CCT subunits impairs proteostasis of pluripotent stem cells. (a) Western blot analysis of control and HD-iPSC lysates with antibodies to HTT and β -actin. Arrow indicates mutant polyQ-expanded HTT. The images are representative of three independent experiments. (b) In HD polyQ180-expressing iPSCs, the levels of mutant HTT are dramatically decreased compared with normal HTT copy. The expression of polyQ180 HTT was confirmed by using an antibody that detects polyQ-expanded mutant HTT. The images are representative of three independent experiments. (c) Filter trap analysis shows that HD-iPSCs do not have increased levels of polyQ aggregates compared with control iPSCs (detected by anti-polyQ-expansion diseases marker antibody). However, knockdown of a single CCT subunit triggers the accumulation of polyQ aggregates. The images are representative of three independent experiments. (d) Knockdown of different CCT subunits in HD polyQ71 iPSC line #1 results in a similar increase of polyQ aggregates. Right panel: SDS-PAGE analysis with antibodies to HTT and β -actin loading control. The images are representative of three independent experiments. (e) Knockdown of a single CCT subunit triggers the accumulation of polyQ aggregates in both polyQ71 iPSC line #2 and polyQ180 iPSCs. Right panel: polyQ-expansion diseases marker antibody was used to confirm that the total protein levels of mutant HTT do not change on knockdown of CCT subunits. The images are representative of two independent experiments.

assembly induced by high levels of CCT subunits could contribute to maintain the proteostasis of mutant HTT in iPSCs. We found that knockdown of CCT8 and other CCT subunits trigger the accumulation of polyQ aggregates without affecting the mutant HTT total protein levels in HD-iPSCs (Fig. 4d,e and Supplementary Fig. 9). These results were observed in all the HD-iPSC lines tested whereas knockdown of CCT subunits did not induce accumulation of polyQ aggregates in control iPSCs (Fig. 4c–e and Supplementary Fig. 10). Remarkably, loss of different CCT subunits (that is, CCT2, CCT6A, CCT7 and CCT8) had similar effects (Fig. 4d and Supplementary Fig. 9), indicating that the TRiC/CCT complex modulates polyQ aggregation in HD-iPSCs.

HD-iPSCs represent a valuable resource to gain mechanistic insights into HD (ref. 20). Neuronal dysfunction and death occurs in many brain regions in HD, but striatal neurons expressing cyclic AMP-regulated phosphoprotein (DARPP32) undergo the greatest neurodegeneration²⁷. HD-iPSCs can be terminally differentiated into neurons (including DARPP32-positive cells) that exhibit HD-associated phenotypes such as cumulative risk of death over time and increased vulnerability to excitotoxic stressors²⁰. Furthermore, proteotoxicity induced via autophagy inhibition or oxidative stress results in higher neurodegeneration of HD cells compared with controls²⁰. Despite these phenotypes, mutant HTT-expressing neurons present important limitations for disease modelling such as lack of robust neurodegeneration, polyQ aggregates and gene expression changes resembling HD (refs 20,23). Despite the efforts to detect polyQ aggregates under different conditions (for example, adding cellular stressors), the presence of inclusions has not been observed in neurons derived

from HD-iPSCs (refs 20,23). The lack of inclusions in these cells could reflect the long period of time before aggregates accumulate in HD (ref. 20). Consistently, HD human neurons do not accumulate detectable polyQ aggregates at 12 weeks after transplantation into HD rat models whereas these inclusions are observed after 33 weeks of transplantation²³. To assess whether loss of CCT subunits triggers neurodegeneration and polyQ aggregation in these cells, we differentiated three HD-iPSC lines (Q57, Q71 and Q180) into striatal neurons²⁸. Among those cells expressing the neuronal marker MAP2, ~50% also expressed DARPP32 (Supplementary Fig. 11a). As with proteasome inhibitor treatment, we could not detect polyQ aggregates in mutant HTT-expressing neurons on knockdown of different CCT subunits (that is, CCT2, CCT6, CCT7 and CCT8) by either immunohistochemistry (Supplementary Fig. 11b) or filter trap (Supplementary Fig. 11c). However, knockdown of CCTs resulted in increased cell death of HD neuronal cultures as assessed by activation of caspase-3 whereas it did not induce neurodegeneration of control cells (Supplementary Fig. 11d). In contrast, proteasome inhibition triggered cell death at the same extent in both control and HD neurons (Supplementary Fig. 11d). These results indicate that mutant HTT-expressing neurons are more susceptible to TRiC/CCT dysfunction than controls, providing a link between downregulation of CCTs with onset of neurodegeneration in HD during aging.

Somatic overexpression of CCT8 extends organismal lifespan. Our results indicate that increased TRiC/CCT complex is a key determinant of proteostasis of immortal hESCs/iPSCs. However,

the levels of CCT subunits decreased on differentiation. During human brain aging, the expression of CCTs is further repressed¹¹. With the strong correlation between *cct* levels, differentiation and aging, we asked whether inducing TRiC/CCT assembly in somatic post-mitotic cells could have a positive role in longevity. To examine the impact of TRiC/CCT on organismal aging and proteotoxic resistance, we used the nematode *C. elegans*. In this organism, CCT transcripts are detected in most tissues and developmental stages²⁹. The role of TRiC/CCT complex in proliferating cells during *C. elegans* development has been extensively studied³⁰. Disruption of TRiC/CCT assembly by knockdown of different CCT subunits causes a variety of defects in cell division and results in embryonic lethality^{30–32}. These effects are partially mediated by a collapse in microtubule function as a consequence of diminished folding of tubulin by TRiC/CCT (ref. 30). In addition, loss of different *cct* subunits during post-embryonic developmental stages results in larval arrest, body morphology alterations as well as defects in developing gonads and sterility, indicating a key role of the TRiC/CCT complex in *C. elegans* development³⁰. In adult worms, the only proliferating cells are found in the germline whereas somatic tissues are formed exclusively by post-mitotic cells³³. To examine the expression of CCTs in germ cells, we dissected the germline and intestine from adult *C. elegans* and compared the levels of CCT subunits by immunohistochemistry. We found that CCT1 subunit is enhanced in germ cells compared with the intestine (Supplementary Fig. 12a), suggesting that CCTs are highly expressed in the germline. Notably, knockdown of *cct* subunits during adulthood dramatically decreased the number of germ cells destabilizing the germline (Supplementary Fig. 12b). Accordingly, we observed a dramatic decrease in the number of laid eggs after 1 day of *cct* RNA interference (RNAi) treatment during adulthood (Supplementary Fig. 12c). Overall, these data suggest that high levels of TRiC/CCT complex are essential for proliferating cells and germline stability. However, knockdown of *cct* subunits during adulthood did not decrease lifespan in wild-type worms (Supplementary Fig. 13 and Supplementary Data 3).

To assess the expression of CCT subunits in somatic tissues of adult *C. elegans*, we generated a green fluorescent protein (GFP) transcriptional reporter construct for *cct-8* gene. Although we did not observe GFP expression in germ cells as a result of germline silencing of transgenes^{34,35}, these experiments confirmed wide expression of *cct-8* in somatic cells including neurons or body wall muscle cells (Supplementary Fig. 14). Somatic expression pattern of *cct-8* resembled other *cct* subunits (for example, *cct-1*, *cct-2* and *cct-7*) showing a high expression in pharynx and tail^{30,35} (Supplementary Fig. 14). In aging organisms, post-mitotic somatic tissues undergo a gradual deterioration and become particularly susceptible to age-associated protein aggregation diseases. Thus, we asked whether increasing the levels of the TRiC/CCT complex in somatic tissues could delay the aging of post-reproductive organisms. To examine this hypothesis we overexpressed CCT8, a subunit that promotes TRiC/CCT assembly in mammalian cells (Fig. 2c). For this purpose, we induced ectopic expression of *cct-8* under *sur-5* promoter (Fig. 5a), which is expressed ubiquitously in somatic tissues but not in the germline^{10,36}. Notably, somatic OE of *cct-8* was sufficient to extend the lifespan of *C. elegans* under normal conditions (20 °C; Fig. 5b and Supplementary Data 3). These worms exhibited up to 20% increased median lifespan compared with the control strain and other *cct*-overexpressing worms (Fig. 5b). We observed similar results in two independent OE lines of the different *cct* subunits tested (Supplementary Data 3). Since OE of a single *cct* subunit did not change the levels of other subunits, the longevity phenotype can be attributed specifically to

cct-8 (Fig. 5a). Interestingly, the lifespan extension induced by ectopic expression of *cct-8* was more dramatic at 25 °C, a condition that results in mild heat stress (Fig. 5c). Under this temperature, *cct-8(OE)* *C. elegans* lived up to 40% longer than the control strain. Overexpression of *cct-2* also increased lifespan significantly at 25 °C, although to a lesser extent than *cct-8* (Fig. 5c). Since heat stress challenges the structure of proteins and triggers the accumulation of misfolded proteins, our results indicate that both *cct-8* and *cct-2* extend longevity by sustaining the integrity of the proteome during adulthood.

To examine whether these pro-longevity effects are induced through modulation of the TRiC/CCT complex, we knocked down the expression of a different subunit. Given that *cct* subunits are required during larval development, we initiated RNAi treatment during adulthood. Interestingly, knockdown of *cct-6* partially reduces the longevity phenotype of both *cct-8(OE)* and *cct-2(OE)* worms whereas it did not affect the lifespan of the control strain (Fig. 5d and Supplementary Fig. 15). By native gel electrophoresis analysis, we confirmed that OE of *cct-8* in somatic tissues increases TRiC/CCT assembly in the form of two stacked rings (Fig. 5e). Collectively, these results suggest that somatic OE of *cct-8* induces longevity via modulation of TRiC/CCT assembly, particularly under proteotoxic conditions.

CCT8 determines proteotoxic stress resistance. During aging, organisms lose their ability to maintain proteostasis and respond to proteotoxic stress^{3,5}. With age, the expression of several *cct* subunits significantly decreased in *C. elegans* whereas the levels of *cct-1* remained similar (Fig. 6a and Supplementary Fig. 16). At day 5 of adulthood, several *cct* subunits (for example, *cct-2*, *cct-5* and *cct-8*) were already downregulated (Fig. 6a and Supplementary Fig. 16). To examine whether somatic *cct-8(OE)* ameliorates the age-associated demise in proteotoxic stress responses, we induced acute heat stress (34 °C) at different ages (that is, days 1 and 5). Severe heat stress dramatically affects survival and activates the HSR, an essential mechanism to ensure proper cytosolic protein folding and alleviate proteotoxic stress³⁷. Under heat stress (34 °C), *cct-8(OE)* worms did not survive significantly longer compared with control strain at day 1 of adulthood (Fig. 6b and Supplementary Data 3). However, *cct-8(OE)* worms were markedly more resistant to proteotoxicity than control strains when subjected to heat stress at day 5 of adulthood (Fig. 6c). Although to a lesser extent, *cct-2(OE)* also conferred resistance to heat stress (Fig. 6c). As a more formal test, we asked whether animals with reduced HSR had increased survival when *cct-8* was overexpressed (Fig. 6d). Heat-shock transcription factor activates the HSR and is required for proteotoxicity resistance and adult lifespan³⁸. Thus, we induced downregulation of HSR via silencing *hsf-1* expression. Notably, *hsf-1*-RNAi-treated *cct-8(OE)* worms lived markedly longer compared with control worms under the same treatment (Fig. 6d). These results indicate that *cct-8(OE)* *C. elegans* can significantly overcome the loss of a key transcription factor such as *hsf-1*, which is not only required for HSR but also lifespan.

Growing evidence suggest that the TRiC/CCT complex could be a therapeutic target in HD (refs 24,26). For instance, simultaneous OE of all eight CCT subunits ameliorates polyQ-expanded HTT aggregation and neuronal death²⁴. Intrigued by the protection that *cct-8* could confer, we tested whether increased levels of this subunit are sufficient to protect from polyQ-expanded aggregation. For this purpose, we used a *C. elegans* model that expresses polyQ peptides throughout the nervous system. In these worms, neurotoxicity correlates with increased length of the polyQ repeat and age^{8,39}. The neurotoxic effects can be monitored by worm motility, which is markedly

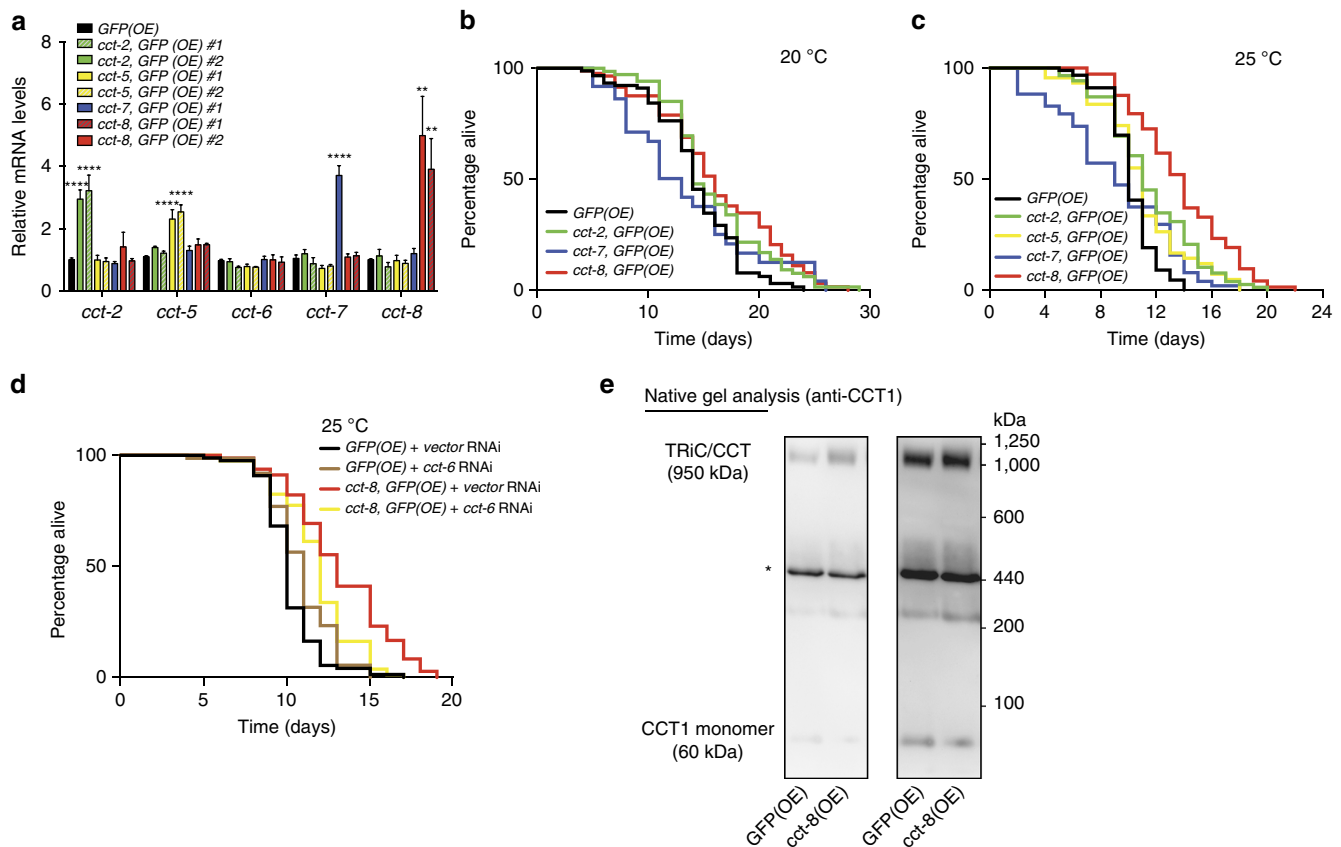


Figure 5 | Somatic increased expression of *cct-8* induces TRiC/CCT assembly and extends longevity. (a) Data represent the mean \pm s.e.m. of the relative expression levels to *GFP(OE)* worms ($n = 4$ independent experiments). Statistical comparisons were made by Student's t test for unpaired samples. P value: ** $P < 0.01$, **** $P < 0.0001$. (b,c,d) Each lifespan graph shows a Kaplan-Meier survival plot of a single representative experiment. In each graph, experimental and control animals were grown in parallel. n = total number of uncensored animals/total number (uncensored + censored) of animals observed in each experiment. P values refer to experimental and control animals in a single lifespan experiment. See Supplementary Data 3 for statistical analysis, replicate data and independent OE lines results of lifespan experiments. (b) *cct-8(OE)* extends lifespan at 20 °C (log rank, $P < 0.0001$). *GFP(OE)*: median = 14, $n = 73/96$; *cct-2, GFP(OE)*: median = 14, $n = 65/96$; *cct-7, GFP(OE)*: median = 13, $n = 46/74$; *cct-8, GFP(OE)*: median = 16, $n = 70/96$. (c) Both *cct-8(OE)* and *cct-2(OE)* worms live longer compared with control *GFP(OE)* strain at 25 °C (log rank, $P < 0.0001$). *cct-8(OE)* worms live longer compared with *cct-2(OE)* and other *cct(OE)* strains (log rank, $P < 0.0001$). *GFP(OE)*: median = 10, $n = 89/96$; *cct-2, GFP(OE)*: median = 11, $n = 79/96$; *cct-5, GFP(OE)*: median = 11, $n = 42/50$; *cct-7, GFP(OE)*: median = 9, $n = 56/77$; *cct-8, GFP(OE)*: median = 14, $n = 82/96$. (d) Knockdown of *cct-6* reduces the long lifespan induced by *cct-8(OE)* (log rank, $P = 0.0001$). In contrast, loss of *cct-6* does not decrease the lifespan of *GFP(OE)* worms. RNAi was initiated at day 1 of adulthood. *GFP(OE)* fed empty vector RNAi bacteria: median = 10, $n = 74/96$; *GFP(OE)* fed *cct-6* RNAi bacteria: median = 11, $n = 73/96$; *cct-8, GFP(OE)* fed empty vector bacteria: median = 13, $n = 77/96$; *cct-8, GFP(OE)* fed *cct-6* RNAi bacteria: median = 12, $n = 79/96$. (e) Native gel electrophoresis of *GFP(OE)* and *cct-8, GFP(OE)* worm extracts followed by immunoblotting with CCT-1 antibody (two different exposure times of the same membrane are shown). Overexpression of *cct-8* induces an increase in the assembly of TRiC/CCT in the form of two stacked rings. * indicates a complex of ~ 475 kDa which is strongly detected in worm lysates. The molecular weight suggests that this signal corresponds to single ring TRiC/CCT assembled forms. The images are representative of two independent experiments.

reduced by the aggregation of polyQ peptides with a pathogenic threshold at a length of 35–40 glutamines³⁹. We found that ectopic expression of *cct-8* reduced toxicity and improve motility of worms expressing polyQ67 either at 20 °C or 25 °C (Fig. 6e and Supplementary Fig. 17). Similarly, *cct-2(OE)* also ameliorated the neurotoxic effects of polyQ67 aggregation although the impact of *cct-8* is more dramatic (Fig. 6e and Supplementary Fig. 17). Moreover, filter trap analysis showed that *cct-8(OE)* reduced polyQ67 aggregates without decreasing the total protein levels of polyQ67 (Fig. 6f). In fact, we observed higher expression of total polyQ67 protein in *cct-8(OE)* worms probably because they are in a healthier state than controls. Taken together, these results indicate CCT8 as a novel candidate to sustain proteostasis during aging.

Longevity promoting pathways such as reduced insulin–insulin-like growth factor signalling (IIS) and dietary restriction

(DR) delay the onset of age-related diseases associated with proteostasis dysfunction⁴. These pathways confer increased proteome integrity and resistance to proteotoxic stress during aging^{4,5}, mechanisms that contribute to lifespan extension. Thus, we hypothesized that the TRiC/CCT complex could be required for the longevity phenotype induced by DR and reduced IIS. Notably, loss of function of TRiC/CCT complex significantly decreased longevity of long-lived IIS and DR genetic models whereas it did not affect the lifespan of wild-type worms (Fig. 7a). In *C. elegans*, the aging of somatic tissues is regulated by signals from the germline⁴⁰. Concomitantly, ablation of germ cells extends lifespan and induces heightened resistance to proteotoxic stress in post-mitotic tissues^{10,40}. We found that TRiC/CCT dysfunction reduces the lifespan of germline-lacking genetic worm models (Fig. 7b). We have previously reported that removal of germ cells induces increased expression of key

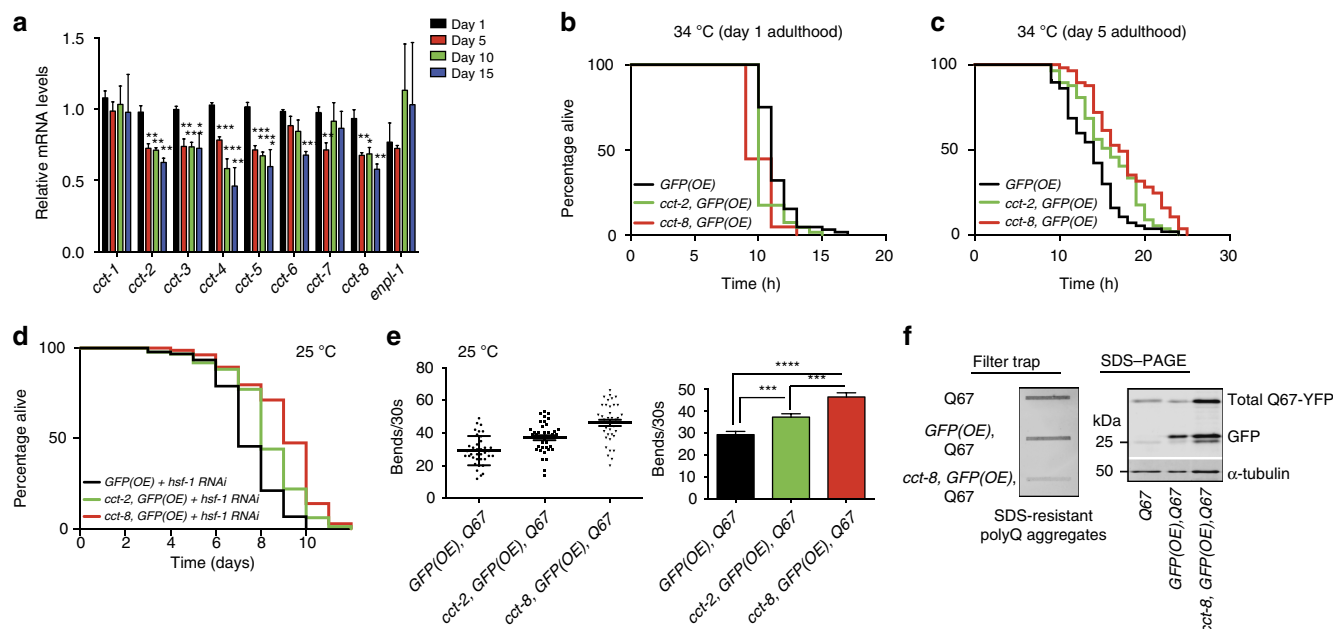


Figure 6 | *cct-8* determines proteotoxic stress resistance during aging and protects from polyQ aggregation. (a) The expression of several *cct* subunits decreases with age. In contrast, we did not find significant differences in *cct-1* and *enpl-1*, the *C. elegans* orthologue to the human chaperone *HSP90B1*. Data represent the mean \pm s.e.m. of the relative expression levels to day 1 adult worms grown at 20 °C ($n = 4$ independent experiments). These experiments were performed with the sterile control strain *fer-15(b26)II;fem-1(hc17)*. (b) When subjected to heat stress (34 °C) at day 1 of adulthood, both *cct-8(OE)* and *cct-2(OE)* worms show similar survival rates compared with the control strain (*GFP(OE)*: median = 11, $n = 70/72$; *cct-2, GFP(OE)*: median = 10, $n = 71/72$; *cct-8, GFP(OE)*: median = 9, $n = 70/72$). (c) In contrast, *cct-8(OE)* (log rank, $P < 0.0001$) and *cct-2(OE)* (log rank, $P = 0.0036$) worms survive longer than control strain when subjected to heat stress at day 5 of adulthood (*GFP(OE)*: median = 14, $n = 57/58$; *cct-2, GFP(OE)*: median = 16, $n = 57/57$; *cct-8, GFP(OE)*: median = 17, $n = 57/57$). (d) *hsf-1*-RNAi-treated *cct(OE)* worms were long-lived compared with control strain under the same treatment (log rank, $P < 0.0001$). RNAi was initiated at day 1 of adulthood. *GFP(OE)* fed *hsf-1* RNAi bacteria: median = 7, $n = 90/96$; *cct-2, GFP(OE)* fed *hsf-1* RNAi bacteria: median = 8, $n = 82/96$; *cct-8, GFP(OE)* fed *hsf-1* RNAi bacteria: median = 9, $n = 72/96$. (e) Ectopic expression of *cct-8* and *cct-2* improve motility in polyQ67 worms grown at 25 °C. In the left panel, each point represents the average thrashing rate of a single 3 day-adult animal over a period of 30 s. In the right panel, bar graphs represent average \pm s.e.m. of these data (*GFP(OE);Q67* ($n = 37$), *cct-2;GFP(OE);Q67* ($n = 38$), *cct-8;GFP(OE);Q67* ($n = 38$)). All the statistical comparisons were made by Student's *t* test for unpaired samples. P value: *** $P < 0.001$, **** $P < 0.0001$. (f) Filter trap indicates that *cct-8* OE results in decreased polyQ aggregates (detected by anti-GFP antibody). Right panel: SDS-PAGE analysis with antibodies to GFP and α -tubulin loading control. The images are representative of two independent experiments. See Supplementary Data 3 for statistical analysis and replicate data of lifespan and stress assays experiments.

proteasome subunits in somatic tissues¹⁰. An intriguing possibility is that the germline also modulates the levels of CCT subunits in somatic tissues. Indeed, germline-lacking *C. elegans* showed upregulation of CCT expression in somatic tissues (Fig. 7c,d). Altogether, our data suggest that the TRiC/CCT complex could be a key determinant of proteotoxic resistance and longevity.

Discussion

Our findings establish enhanced assembly of the TRiC/CCT complex as an intrinsic characteristic of pluripotent stem cells. This increased assembly correlates with an upregulation of several CCT subunits. Notably, human pluripotent stem cells are able to maintain high expression of CCT subunits during unlimited proliferation. However, pluripotent stem cells lose their high levels of CCT subunits on differentiation and this decline is already significant in multipotent cells (for example, NPCs) before terminal differentiation. Therefore, enhanced TRiC/CCT assembly could be linked to the immortal and pluripotent characteristics of hESCs/iPSCs. Indeed, we found that slight dysfunctions of the TRiC/CCT complex induce a decrease in pluripotency markers and, concomitantly, an increase in differentiation markers. Defining the mechanisms by which increased TRiC/CCT regulates hESC/iPSC identity could open a

new door to a better understanding of pluripotency and differentiation. Although the exact mechanisms are still unknown, the TRiC/CCT complex could impinge on hESC/iPSC function in several (and non-exclusive) manners. TRiC/CCT assists the folding of a significant percentage of nascent proteins such as actin and tubulin^{14,41}. Thus, one possibility is that enhanced TRiC/CCT assembly is required for the proper folding of specific regulatory or structural proteins involved either in maintenance of hESC/iPSC identity or generation of healthy differentiated cells. Interestingly, a study performed in calreticulin^{-/-} mouse ESCs showed a downregulation in the expression of *Cct2*, *Cct3* and *Cct7* (ref. 42) in these cells. Calreticulin, a chaperone that binds to misfolded proteins preventing their export from the endoplasmic reticulum, is essential for cardiac development in mice⁴³ and required for proper myofibril formation during cardiomyocyte differentiation of mouse ESCs *in vitro*⁴⁴. Since the TRiC/CCT complex regulates folding and actin dynamics, the downregulation of *Cct* subunits in calreticulin^{-/-} mouse ESCs could forecast the myofibrillar disarray observed in their cardiomyocytes counterparts⁴². As TRiC/CCT also regulates the aggregation of misfolded and damaged proteins, increased TRiC/CCT levels could be linked to the biological purpose of pluripotent stem cells and their intrinsic properties such as high global protein synthesis rates and immortality. Given the ability of hESCs to replicate indefinitely

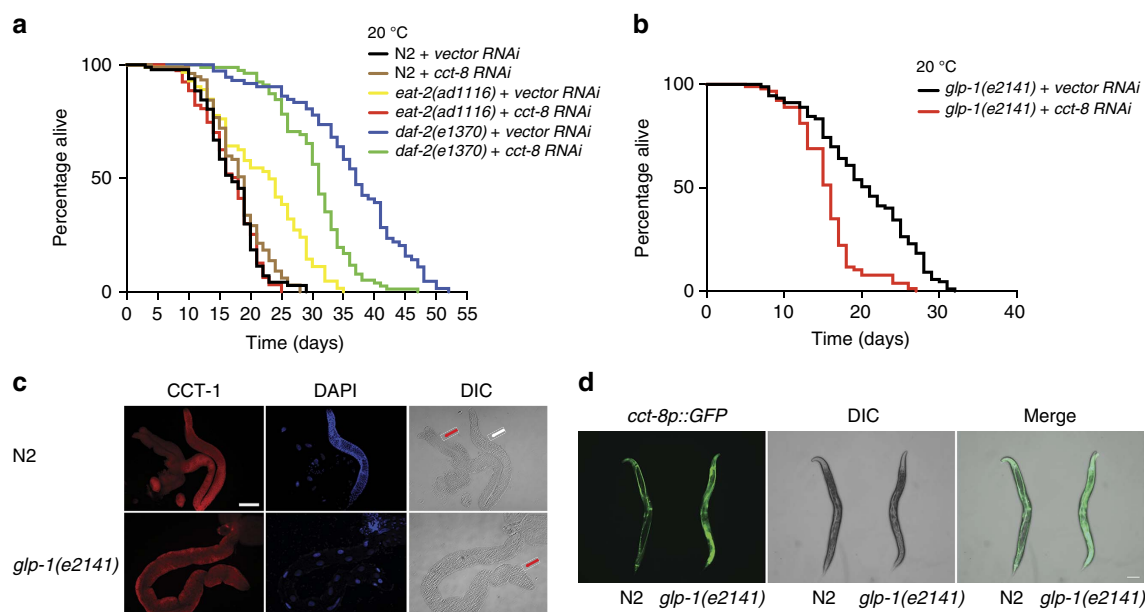


Figure 7 | TRiC/CCT is required for the longevity phenotype of long-lived *C. elegans* mutants. (a) Knockdown of *cct-8* decreases lifespan of IIS (*daf-2*) and DR (*eat-2*) long-lived mutant worms at 20 °C (log rank, $P < 0.0001$). N2 (wild-type worms) + vector RNAi: median = 17, $n = 72/9$; N2 + *cct-8* RNAi: median = 19, $n = 66/96$; *eat-2(ad1116)* + vector RNAi: median = 23, $n = 66/96$; *eat-2(ad1116)* + *cct-8* RNAi: median = 18, $n = 67/96$; *daf-2(e1370)* + vector RNAi: median = 37, $n = 68/96$; *daf-2(e1370)* + *cct-8* RNAi: median = 31, $n = 77/96$. (b) Knockdown of *cct-8* decreases lifespan of germline-lacking mutant worms (log rank, $P < 0.0001$). *glp-1(e2141)* + vector RNAi: median = 21, $n = 88/96$; *glp-1(e2141)* + *cct-8* RNAi: median = 16, $n = 86/96$. (c) Gonad and intestine immunostaining with CCT-1 antibody of wild-type and germline-lacking (*glp-1(e2141)*) worms. Long-lived germline-lacking nematodes have increased levels of CCT-1 in the intestine compared with wild-type worms. Cell nuclei were stained with DAPI. White arrow indicates gonad and red arrow indicates intestine. DIC, differential interference contrast. Scale bar represents 50 μm . (d) Representative images of GFP expressed under control of the *cct-8* promoter in adult wild-type and germline-lacking (*glp-1(e2141)*) worms. Scale bar represents 100 μm . In c,d the images are representative of three independent experiments. See Supplementary Data 3 for statistical analysis and replicate data of lifespan experiments.

and generate every other cell type in the body, the TRiC/CCT complex could be a key quality control mechanism to maintain a global intact proteome for either self-renewal or the generation of progenitor cells. In this context, the accumulation of damaged and misfolded proteins caused by proteostasis defects may affect hESC/iPSC function and immortality. With the asymmetric divisions invoked by these cells, the passage of damaged proteins to progenitor cells could also compromise development and organismal aging. In support of this hypothesis, we found that the TRiC/CCT complex determines the ability of pluripotent stem cells to maintain proteostasis of mutant huntingtin.

Another important question is how pluripotent stem cells achieve their high TRiC/CCT levels. Interestingly, specific subunits such as CCT4 are relatively more abundant compared to CCT1 in hESCs whereas this proportion is reversed in NPCs (Fig. 2b). Therefore, these subunits could become limiting assembly factors during differentiation. Despite decreasing during neural differentiation, other CCT subunits (that is, CCT8 and CCT2) were more abundant relatively to the rest of subunits in both hESCs and NPCs suggesting that they could be activators of TRiC/CCT assembly rather than limiting factors. Indeed, increasing the expression of CCT8, the most abundant subunit, triggers TRiC/CCT assembly regardless the levels of other subunits such as CCT1 in both mammalian cells and *C. elegans*. Further studies will be required to understand how CCT8 promotes TRiC/CCT assembly. A fascinating hypothesis is that CCT8 could act as a scaffold protein that triggers the interaction between the different subunits.

Our findings in human pluripotent stem cells led us to identify CCT8 as a powerful candidate to sustain proteostasis during organismal aging. The somatic induction of TRiC/CCT assembly

via CCT8 OE extends lifespan and protects from proteotoxic stress in *C. elegans*. Notably, somatic CCT8 OE can partially protect this nematode from knockdown of *hsf-1*, a transcription factor that coordinates cellular protein-misfolding responses. The precise mechanism by which the TRiC/CCT complex ameliorates the detrimental effects triggered by loss HSF1 is not yet understood. In response to proteotoxic stress, HSF1 binds heat-shock elements in the promoters of target genes and triggers their expression⁴⁵. In mammalian cells, all the CCT subunits contain heat-shock elements and are transcriptionally activated by HSF1 (ref. 46). Thus, ectopic expression of CCT8 could ameliorate the effects induced by a decrease of CCT subunits on HSF1 knockdown. In addition, a direct regulatory interaction between TRiC/CCT activity and induction of proteotoxic stress response by HSF1 has been recently reported^{47,48}. HSF1A, a chemical activator of HSF1, binds to the TRiC/CCT complex and inhibits its folding activity^{47,48}. Both the inactivation of TRiC/CCT complex by HSF1A or its depletion by loss of CCT subunits induce HSF1 activity⁴⁷. Since TRiC/CCT chaperonin interacts with HSF1 (ref. 47), TRiC/CCT could have a direct repressor role in regulating HSF1 (ref. 47). However, a decrease in TRiC/CCT activity mediated by either HSF1A or knockdown of CCT subunits can also lead to the accumulation of misfolded proteins that trigger the HSF1-induced proteotoxic response⁴⁷. In support of this hypothesis, our results suggest that increased TRiC/CCT assembly induced by CCT8 reduces the accumulation of misfolded proteins and, therefore, ameliorates the deleterious impact of reduced HSF1-mediated signalling.

During organismal aging, loss of proteostasis in somatic tissues could contribute to the late onset of age-related diseases such as HD (refs 3,11). Hence, the decrease in the levels of several CCT

subunits during human brain aging¹¹ may induce TRiC/CCT dysfunction, proteotoxic stress and neurodegeneration. In support of this hypothesis, knockdown of CCT subunits hastens aggregation of mutant HTT and worsens HD-related changes in HD models^{11,24–26}. Previous studies have shown that simultaneous OE of all eight CCT subunits ameliorates polyQ-expanded HTT aggregation and neuronal death²⁴. Furthermore, OE of CCT1 remodels the morphology of HTT aggregates and reduces neurotoxicity²⁶. Although CCT1 OE does not increase TRiC/CCT assembly, this subunit modulates the interaction between HTT and TRiC/CCT complex²⁶. Since CCT8 is sufficient to increase TRiC/CCT assembly, this subunit could be a candidate to correct deficiencies in age-related diseases associated with proteostasis dysfunction. Indeed, we found that OE of CCT8 can protect from the accumulation of polyQ-expanded proteins. Recently, a link between CCT8 and mutant HTT expression was observed in an integrated genomics and proteomics study of knock-in HD mouse models expressing the human *HTT* exon1 carrying different CAG lengths (polyQ20, Q80, Q92, Q111, Q140 or Q175)⁴⁹. Notably, highly expanded-polyQ *HTT* exon1 (Q175) induces a significant increase of CCT8 at both transcript and protein levels in the striatum of young mice (6 months) whereas other subunits were not altered⁴⁹. In contrast, CCT8 induction was not observed in knock-in mice expressing mutant HTT with lower than 175 polyQ repeats. These findings suggest that upregulation of CCT8 could be a compensatory mechanism to protect from polyQ aggregation.

While expression of CCT subunits decrease during both differentiation and biological aging, our results indicate that mimicking proteostasis of pluripotent stem cells by modifying either the chaperome or proteasome network⁸ delays the aging of somatic cells and extends organismal lifespan. Given the link between sustained proteostasis in somatic cells and healthy aging, our findings raise an intriguing question: why the levels of CCT8 decrease during differentiation if this subunit could have beneficial effects on organismal longevity and proteotoxic stress resistance? In this regard, it is important not to diminish potential detrimental effects of mimicking proteostasis of pluripotent stem cells in somatic tissues. For instance, cancer cells and pluripotent stem cells not only share their immortality features but also increased proteostasis nodes such as proteasome activity and specific chaperones^{50–52}. Proteasome and chaperone levels in cancer cells are consistent with the special requirements of these cells, such as elimination of aberrant proteins. Interestingly, the expression of CCT8 is increased in gliomas and hepatocellular carcinoma whereas its knockdown induces a decrease in the proliferation and invasion capacity of these cells^{53,54}. Similarly, other CCT subunits have been linked to cancer⁵⁵. Whereas proteasome inhibitors and interventions of the chaperome network have been suggested as potential strategies for anti-cancer therapy^{52,56}, an abnormal activation of these mechanisms in somatic dividing cells could have the opposite effect inducing their abnormal proliferation. However, although the TRiC/CCT complex is important for the proliferation of cancer cells, this chaperonin is also required for the proper folding of p53 and, therefore, promotes tumour suppressor responses⁵⁷. Thus, the TRiC/CCT complex could be an important factor to avoid misfolding of tumour suppressors and the increase incidence of cancer during the aging process. Besides its link with cancer, other factors could explain the decline of CCT subunits during differentiation. In support of the disposable soma theory of aging⁵⁸, a fascinating hypothesis is that downregulation of the TRiC/CCT complex during differentiation is part of an organismal genetic programme that ensures a healthy progeny whereas somatic tissues undergo a progressive demise in their homeostasis and function. Due to the limitation of nutrients in

nature, organisms divide the available metabolic resources between reproduction and maintenance of the non-reproductive soma. Evolutionary pressure has been theorized to force a re-allocation of the resources to prevent or eliminate damage to the germline and progeny, while little resources are placed on the maintenance of somatic cells⁵⁸. In support of this hypothesis, signals from the germline modulate the aging of somatic tissues and removal of the germline extends lifespan⁴⁰. Interestingly, our results indicate that germline-lacking worms exhibit increased levels of TRiC/CCT in post-mitotic cells.

Collectively, we underscore the importance of defining proteostasis of pluripotent stem cells to uncover novel mechanisms of organismal healthspan extension. Besides CCT subunits, other chaperome components also decrease during differentiation and, therefore, could be interesting targets to be studied in the context of aging. In addition, it will be fascinating to explore whether other proteostasis components are also divergent in pluripotent stem cells and if mimicking these mechanisms in somatic cells extends organismal healthspan.

Methods

hESCs/iPSCs culture. The human H9 (WA09) and H1 (WA01) hESC lines were obtained from WiCell Research Institute. The human control iPSC line #1 (hFIB2-iPS4 (ref. 59)) and HD Q71-iPSC line #1 (ref. 60) were a gift from G.Q. Daley. These iPSC lines were derived and fully characterized for pluripotency in refs 59,60. ND42242 (control iPSC line #2, Q21), ND36997 (control iPSC line #3, Q33), ND41656 (HD Q57-iPSC), ND36998 (HD Q60-iPSC), ND42229 (HD Q71-iPSC line #2) and ND36999 (HD Q180-iPSC) were obtained from NINDS Human Cell and Data Repository (NHCDR) through Coriell Institute. Parental fibroblasts GM02183 (control Q33), GM03621 (HD Q60), GM04281 (HD Q71) and GM09197 (HD Q180) were obtained from Coriell Institute whereas ND30014 (control Q21) and ND33392 (HD Q57) fibroblasts were obtained from NHCDR through RUCDR Infinite Biologicals at Rutgers University. hESCs and iPSCs were maintained on Geltrex (ThermoFisher Scientific) using mTeSR1 (Stem Cell Technologies). hESCs and iPSCs colonies were passaged using a solution of dispase (2 mg ml⁻¹), and scraping the colonies with a glass pipette. The hESC and iPSC lines used in our experiments had a normal diploid karyotype as indicated by single nucleotide polymorphism (SNP) genotyping (Supplementary Fig. 18). Genetic identity of hESCs was assessed by short tandem repeat (STR) analysis. The H9 and H1 hESC lines used in our study matches exactly the known STR profile of these cells across the 8 STR loci analysed (Supplementary Table 2). No STR polymorphisms other than those corresponding to H9 and H1 were found in the respective cell lines, indicating correct hESC identity and no contamination with any other human cell line. By STR analysis, we also confirmed correct genetic identity of the iPSCs used in our study with the corresponding parental fibroblast lines when fibroblasts were available (that is, ND42242, ND36997, ND41656, ND36998, ND42229, ND36999 and HD Q71-iPSC line #1; Supplementary Table 3). All the cell lines used in this study were tested for mycoplasma contamination at least once every 3 weeks. No mycoplasma contamination was detected. Research involving hESC lines was performed with approval of the German Federal competent authority (Robert Koch Institute).

Pan-neuronal differentiation. Neural differentiation of H9 hESCs, H1 hESCs and iPSCs was performed using the monolayer culture protocol following the STEMdiff Neural Induction Medium (Stem Cell Technologies) method based on ref. 61. Undifferentiated pluripotent stem cells were rinsed once with PBS and then we added 1 ml of Gentle Dissociation Reagent (Stem Cell Technologies) for 10 min. After the incubation period, we gently dislodged pluripotent cells and add 2 ml of Dulbecco's Modified Eagle Medium (DMEM)-F12 + 10 µM ROCK inhibitor (Abcam). Then, we centrifuged cells at 300g for 10 min. Cells were resuspended on STEMdiff Neural Induction Medium + 10 µM ROCK inhibitor and plated on polyornithine (15 µg ml⁻¹)/laminin (10 µg ml⁻¹)-coated plates (200,000 cells cm⁻²). For neuronal differentiation, NPCs were dissociated with Accutase (Stem Cell Technologies) and plated into neuronal differentiation medium (DMEM/F12, N2, B27 (ThermoFisher Scientific), 1 µg ml⁻¹ laminin (ThermoFisher Scientific), 20 ng ml⁻¹ brain-derived neurotrophic factor (BDNF) (Peprotech), 20 ng ml⁻¹ glial cell-derived neurotrophic factor (GDNF) (Peprotech), 1 mM dibutyryl-cyclic AMP (Sigma) and 200 nM ascorbic acid (Sigma)) onto polyornithine/laminin-coated plates as described in ref. 8. Cells were differentiated for 1–2 months, with weekly feeding of neuronal differentiation medium.

Striatal neuron differentiation. iPSCs were differentiated into striatal neuron by induction with sonic hedgehog in a defined medium as reported in ref. 28. Briefly, iPSCs were detached by incubating with dispase (1 mg ml⁻¹) for 20 min. The detached colonies were cultured in suspension as free-floating embryoid bodies

(EBs) in the differentiation medium consisting of DMEM/F12, 20% knockout serum replacement, $1 \times$ MEM non-essential amino acids, 2 mM L-glutamine, and 100 μ M β -Mercaptoethanol. On day 4, the medium was replaced with a neural induction medium consisting of DMEM/F12, N2 supplement, $1 \times$ MEM non-essential amino acids, 2 mM glutamine and 2 μ g ml⁻¹ heparin. On day 7, the EBs were attached to laminin-coated substrate in a 35-mm culture petri dish and cultured in the neural induction medium. In the next week, the EBs flattened and columnar neuroepithelia organized into rosette appeared in the centre of individual colonies. On day 12, sonic hedgehog (200 ng ml⁻¹) was added for 14 days (until day 25). From day 26, neuroepithelial spheres were dissociated with Accutase (1 unit ml⁻¹, Invitrogen) at 37 °C for 5 min and placed onto polyornithine/laminin-coated coverslips in the neurobasal medium in the presence of valproic acid (VPA, 10 μ M, Sigma) for 1 week, followed by a set of trophic factors, including brain derived neurotrophic factor (BDNF, 20 ng ml⁻¹), glial-derived neurotrophic factor (10 ng ml⁻¹), insulin-like growth factor 1 (10 ng ml⁻¹) and cyclic AMP (1 μ M) (all from R&D Systems). DARPP32-expressing neurons appeared by day 35.

Endoderm differentiation. Endoderm differentiation of H9 hESCs was performed using STEMdiff Definitive Endoderm Kit (Stem Cell Technologies).

Cardiomyocyte differentiation. Cardiomyocyte differentiation was performed as described in ref. 62. Confluent H1 hESCs were dissociated into single cells with Accutase at 37 °C for 10 min followed by inactivation using two volumes of F12/DMEM. Cells were counted and 230,000 cells cm⁻² were plated in ITS medium (Corning), containing 1.25 μ M CHIR 99021 (AxonMedchem) and 1.25 ng ml⁻¹ BMP4 (R&D), and seeded on Matrigel-coated 24-well plates. After 24 h, medium was changed to TS (transferrin/selenium) medium. After 48 h, medium was changed to TS medium supplemented with 10 μ M canonical Wnt-Inhibitor IWP-2 (Santa Cruz) for 48 h. Then, medium was changed to fresh TS until beating cells were observed at days 8–10. Finally, medium was changed to Knockout DMEM (ThermoFisher Scientific) supplemented with 2% FCS, L-Glutamine and Penicillin/Streptomycin until cells were used for downstream analysis.

SNP genotyping. The molecular karyotype was analysed by SNP genotyping using Illumina's HumanOmniExpressExome-8-v1.2 BeadArray (Illumina, Inc., San Diego, CA, USA) at the Institute for Human Genetics (Department of Genomics, Life & Brain Center, University of Bonn, Germany). Processing was performed on genomic DNA following the manufacturer's procedures. Copy number regions were detected using the cnvPartition version 3.1.6.

STR typing. STR analysis of H9 and H1 hESC lines was conducted using the Promega PowerPlex 21 system (Promega Corporation) by Eurofins Genomics (Germany). We analysed loci D5S818, D13S317, D7S820, D16S539, vWA, TH01, TPOX and CSF1P0 to compare with the known STR profile of these hESC lines⁶³. Genotype analysis of iPSCs lines and their parental fibroblasts was performed using the following microsatellite markers: D17S1303, D16S539, D10S526, vWA, TH01, D5S818, CSF1P0 and TPOX. Fluorescently labelled PCR products were electrophoresed and detected on an automated 3730 DNA Analyzer and data were analysed using Genemapper software version 3.0 to compare allele sizes between iPSCs and their parental fibroblasts (Applied Biosystems).

Lentiviral infection of human stem cells. Lentivirus (LV)-non targeting shRNA control, LV-shCCT2#1 (clone number TRCN0000029499), LV-shCCT2#2 (TRCN0000029500), LV-shCCT6A#1 (TRCN0000062514), LV-shCCT6A#2 (TRCN0000062515), LV-shCCT7#1 (TRCN0000147373), LV-shCCT7#2 (TRCN0000149108), LV-shCCT8#1 (TRCN0000442235) and LV-shCCT8#2 (TRCN0000438803) in pLKO.1-puro vector were obtained from Mission shRNA (Sigma). Transient infection experiments were performed as follows. hESC/iPSC colonies growing on Geltrex were incubated with mTesR1 medium containing 10 μ M ROCK inhibitor (Abcam) for 2 h and individualized using Accutase. Hundred thousand cells were plated on Geltrex plates and incubated with mTesR1 medium containing 10 μ M ROCK inhibitor for 1 day. Cells were infected with 5 μ l of concentrated lentivirus. Plates were centrifuged at 800g for 1 h at 30 °C. Cells were fed with fresh media the day after to remove virus. After 1 day, cells were selected for lentiviral integration using 1 μ g ml⁻¹ puromycin (ThermoFisher Scientific). Cells were collected for experimental assays after 4–6 days of infection. Alternatively, we generated stable transfected hESCs. In this case, hESC colonies growing on Geltrex were incubated with mTesR1 medium containing 10 μ M ROCK inhibitor for 1 h and individualized using Accutase. Fifty thousand cells were infected with 20 μ l of concentrated lentivirus in the presence of 10 μ M ROCK inhibitor for 1 h. Cell suspension was centrifuged to remove virus, passed through a mesh of 40 μ m to obtain individual cells, and plated back on a feeder layer of fresh mitotically inactive mouse embryonic fibroblasts in hESC media (DMEM/F12, 20% knockout serum replacement (ThermoFisher Scientific), 1 mM L-glutamine, 0.1 mM non-essential amino acids, β -mercaptoethanol and 10 ng ml⁻¹ bFGF (Joint Protein Central)) supplemented with 10 μ M ROCK inhibitor. After a few

days in culture, small hESC colonies arose. Then, we performed 1 μ g ml⁻¹ puromycin selection during 2 days and colonies were manually passed onto fresh mouse embryonic fibroblasts to establish new hESC lines.

Transfection of HEK293T cells. HEK293T cells (ATCC) were plated on 0.1% gelatin-coated plates and grown in DMEM supplemented with 10% FCS and 1% non-essential amino acids (ThermoFisher Scientific) at 37 °C, 5% CO₂ conditions. Cells were transfected once they reached 80–90% confluency. 1 μ g CCT8 OE plasmid (Sino Biological HG11492-UT) or pCDNA3.1 empty vector plasmid (Life Technologies V870-20) were used for transfection, using Eugene HD (Promega) following manufacturer's instructions. 24 h after transfection, the cells were treated with 500 μ g ml⁻¹ Hygromycin B gold (InvivoGen) during 16 h to select for transfected cells. After 24 h incubation in normal medium, the cells were harvested for TRIC/CCT assembly experiments.

Immunohistochemistry. Cells were fixed with paraformaldehyde (4% in PBS) for 20 min, followed by permeabilization (0.2% Triton X-100 in PBS for 10 min) and blocking (3% BSA in 0.2% Triton X-100 in PBS for 10 min). Cells were incubated in primary antibody overnight at 4 °C (Mouse anti-Polyglutamine-Expansion Diseases Marker Antibody (Merck Millipore, MAB1574, 1:50), Rabbit anti-Cleaved Caspase-3 (Cell Signaling, 9661, 1:400), Rabbit anti-DARPP32 (Abcam, ab40801, 1:100), Chicken anti-MAP2 (Abcam, ab5392, 1:1,000). After washing with PBS, cells were incubated in secondary antibody (Alexa Fluor 488 goat anti-mouse (ThermoFisher Scientific, A-11029, 1:1,000), Alexa Fluor 647 donkey anti-chicken (Jackson ImmunoResearch, 703-605-155, 1:1,000), Alexa Fluor 568 goat anti-Rabbit (ThermoFisher Scientific A-21067, 1:1,000)) and co-stained with 2 μ g ml⁻¹ Hoechst 33342 (Life technologies). Finally, coverslips were covered with Mowiol (Sigma).

mRNA sequencing. For hESCs, NPCs and neurons (1, 2 and 4 weeks of differentiation) total RNA was extracted using RNeasy (Tel-Test Inc.). Total RNA was rRNA-depleted and libraries were prepared using TruSeq Stranded Total RNA Library Prep Kit (Illumina). RNA-seq libraries were then sequenced 100 bp single end with HiSeq 2500 System. 100 bp short reads were trimmed and quality clipped with Flexbar⁶⁴. All remaining reads (> 18 bp in length) were mapped against the human 45S rRNA precursor sequence (NR_046235) to remove rRNA contaminant reads. We used the human genome sequence and annotation (Ensembl 79) together with the splice-aware STAR read aligner⁶⁵ (release 2.5.1b) to map and assemble our reference transcriptome. Subsequent transcriptome analyses on differential gene and transcript abundance were carried out with the cufflinks package⁶⁶. Supplementary Data 4 provides the statistical analysis of the transcriptome data.

Sample preparation for label-free quantitative proteomics and analysis. Cells were scratched in urea buffer (containing 8 M urea, 50 mM ammonium bicarbonate and $1 \times$ complete protease inhibitor mix with EDTA (Roche)), homogenized with a syringe and cleared using centrifugation (16,000g, 20 min). Supernatants were reduced (1 mM DTT, 30 min), alkylated (5 mM IAA, 45 min) and digested with trypsin at a 1:100 w/w ratio after diluting urea concentration to 2 M. The day after, samples were cleared (16,000g, 20 min) and supernatant was acidified. Peptides were cleaned up using stage tip extraction⁶⁷. In short, peptides were eluted from C18 tips with 30 μ l of 0.1% formic acid in 80% acetonitrile, concentrated in a speed vac to complete dryness and resuspended in 10 μ l buffer A (0.1% formic acid). The liquid chromatography tandem mass spectrometry (LC-MS/MS) equipment consisted out of an EASY nLC 1000 coupled to the quadrupole based QExactive instrument (Thermo Scientific) via a nano-spray electroionization source. Peptides were separated on an in-house packed 50 cm column (1.9 μ m C18 beads, Dr Maisch) using a binary buffer system: A) 0.1% formic acid and B) 0.1% formic acid in acetonitrile. The content of buffer B was raised from 7 to 23% within 120 min and followed by an increase to 45% within 10 min. Then, within 5 min buffer B fraction was raised to 80% and held for further 5 min after which it was decreased to 5% within 2 min and held there for further 3 min before the next sample was loaded on the column. Eluting peptides were ionized by an applied voltage of 2.2 kV. The capillary temperature was 275 °C and the S-lens RF level was set to 60. MS1 spectra were acquired using a resolution of 70,000 (at 200 m/z), an Automatic Gain Control target of 3e6 and a maximum injection time of 20 ms in a scan range of 300–1,750 Th. In a data dependent mode, the 10 most intense peaks were selected for isolation and fragmentation in the higher-energy collisional dissociation (HCD) cell using a normalized collision energy of 25 at an isolation window of 2.1 Th. Dynamic exclusion was enabled and set to 20 s. The MS/MS scan properties were: 17,500 resolution at 200 m/z, an Automatic Gain Control target of 5e5 and a maximum injection time of 60 ms. All proteomics data sets (at least 5 biological replicates per condition) were analysed with the MaxQuant software⁶⁸ (release 1.5.3.30). Spectra were searched against the 'all peptides' database from Ensembl release 79 (Homo_sapiens.GRCh38.pep.all.fasta). We employed the label-free quantitation mode⁶⁹ and used MaxQuant default settings for protein identification and LFQ quantification. All downstream analyses were carried out on LFQ values, which have been subjected to the variance stabilization transformation method (limma)⁷⁰. We identified differentially abundant protein

groups by linear modelling including cell type and experimental batch as variable using limma's moderated *t*-statistics framework. We retain all protein groups with an adjusted *P* value (*q*-value) of <0.05. For the characterization of protein level differences in the chaperome network, we extracted the annotated human chaperome from Brehme *et al.*¹¹ and intersected this dataset with our computed protein abundance fold changes and test for differential abundance. All tables and figures were generated with custom R scripts⁷¹. Supplementary Data 5 provides the statistical analysis of the quantitative proteomics data comparing neurons versus hESCs and NPCs versus hESCs.

C. elegans. strains and generation of transgenic lines. Wild-type (N2), CF512 (*fer-15(b26)II;fem-1(hc17)IV*), CB4037 (*glp-1(e2141)III*), DA1116 (*eat-2(ad1116)III*) *C. elegans* strains were obtained from the *Caenorhabditis* Genetic Center, which is funded by NIH Office of Research Infrastructure Programs (P40OD010440). CF1041 (*daf-2(e1370)III*) was a gift from C. Kenyon. *C. elegans* were handled using standard methods⁷².

For the generation of worm strains DVG48–DVG49 (N2, *ocbEx48[psur5::cct-8, pmyo3::GFP]* and N2, *ocbEx49[psur5::cct-8, pmyo3::GFP]*), a DNA plasmid mixture containing 70 ng μl^{-1} of the plasmid *psur5::cct-8* and 20 ng μl^{-1} pPD93_97 (*pmyo3::GFP*) was injected into the gonads of adult N2 hermaphrodite animals, using standard methods⁷³. GFP-positive *F*₁ progeny were selected. Individual *F*₂ worms were isolated to establish independent lines. Following this method we generated the worm strains DVG47 (N2, *ocbEx47[psur5::cct-2, pmyo3::GFP]*), DVG50 (N2, *ocbEx50[psur5::cct-2, pmyo3::GFP]*), DVG41 (N2, *ocbEx41[psur5::cct-5, pmyo3::GFP]*), DVG58 (N2, *ocbEx55[psur5::cct-5, pmyo3::GFP]*) and DVG44 (N2, *ocbEx44[psur5::cct-7, pmyo3::GFP]*). Control worms DVG9 (N2, *ocbEx9[myo3p::GFP]*) were generated by microinjecting N2 worms with 20 ng μl^{-1} pPD93_97.

AM716 (*rmls284[pF25B3.3::Q67::YFP]*) was a gift from R. I. Morimoto. For the generation of worm strains DVG59 ([*rmls284[pF25B3.3::Q67::YFP;ocbEx9[myo3p::GFP]*], DVG55 ([*rmls284[pF25B3.3::Q67::YFP;ocbEx49[psur5::cct-8, pmyo3::GFP]*]) and DVG57 ([*rmls284[pF25B3.3::Q67::YFP;ocbEx50[psur5::cct-2, pmyo3::GFP]*]), AM716 was crossed to DVG9, DVG49 and DVG50, respectively.

Lifespan studies. Synchronized animals were raised and fed OP50 *E. coli* at 20 °C until day 1 of adulthood. Then, worms were transferred onto plates with RNAi clones. 96 animals were used per condition and scored every day or every other day⁷⁴. From the initial worm population, the worms that are lost or burrow into the medium as well as those that exhibit 'protruding vulva' or undergo bagging were censored. *n* = total number of uncensored animals/total number (uncensored + censored) of animals observed in each experiment. Lifespans were conducted at either 20 °C or 25 °C as stated in the figure legends. For non-integrated lines DVG9, DVG41, DVG44, DVG47–50 and DVG58, GFP-positive worms were selected for lifespan studies. PRISM 6 software was used for statistical analysis to determine median and percentiles. In all cases, *P* values were calculated using the log-rank (Mantel–Cox) method. The *P* values refer to experimental and control animals in a single experiment. In the main text, each graph shows a representative experiment. See Supplementary Data 3 for statistical analysis and replicate data.

Construction of *cct* *C. elegans* expression plasmids. To construct the *cct* *C. elegans* expression plasmids, pPD95.77 from the Fire Lab kit was digested with SphI and XmaI to insert 3.6KB of the *sur5* promoter. The resultant vector was then digested with KpnI and EcoRI to excise GFP and insert a multi-cloning site containing KpnI, NheI, NotI, XbaI and EcoRI. T21B10.7.1 (*cct-2*), C07G2.3a.1 (*cct-5*), F01F1.8a.1 (*cct-6*) and T10B5.5a (*cct-7*) were PCR amplified from cDNA to include 5' NheI and 3' NotI restriction sites then cloned into the aforementioned vector. Y55F3AR.3a (*cct-8*) was amplified with 5' NheI and 3' EcoRI. All constructs were sequence verified.

Construction of *cct-8* expression construct. To construct pDV077, pPD95.77 from the Fire Lab kit was digested with XbaI and XmaI. The promoter region and part of the first intron of Y55F3AR.3a (*cct-8*) was PCR amplified from N2 gDNA to include –600 to 100 and then cloned into the aforementioned vector using the same enzymes.

RNAi constructs. RNAi-treated strains were fed *E. coli* (HT115) containing an empty control vector (L4440) or expressing double-stranded RNAi. *cct-2*, *cct-6*, *cct-7* and *cct-8* RNAi constructs were obtained from the Vidal RNAi library. *cct-5* and *hsf-1* RNAi constructs were obtained from the Ahinger RNAi library. All constructs were sequence verified.

C. elegans germline and gut immunostaining. N2 and CB4037 strains were grown at 25 °C from hatching on OP50. Worms were dissected in dissection buffer (0.2% Tween 20, 1 × Egg buffer, 20 mM Sodium Azide) on a coverslip. Fixation was performed by adding formaldehyde buffer (1 × Egg buffer, 0.2% Tween 20 and 3.7% formaldehyde) and animals were frozen on dry ice between the coverslip and a poly-lysine coated slide (Thermo Scientific). The coverslips were removed and the

slides were placed for 1 min at –20 °C in methanol, then washed twice with PBS 0.1% Tween 20. After blocking for 30 min in PBST 10% donkey serum, anti-TCP1 alpha (Abcam, ab90357) antibody was added (1:1,000) followed by overnight incubation in a humid chamber. Anti Rat secondary antibody (Alexa Fluor 546) was added (1:400) for 2 h at room temperature. Finally, slides were mounted with Precision coverslip (Roth) using DAPI Fluoromount-G (Southern Biotech). Anti-TCP1 alpha is profiled for use in *C. elegans* by Abcam. We validated by western blot analysis that anti-TCP1 alpha recognizes this subunit in worms at the correct molecular weight. Native gel experiments confirmed that anti-TCP1 alpha recognizes CCT1 in its monomeric form as well as part of the TRIC/CCT complex.

Nuclear staining in RNAi-treated *C. elegans*. N2 wild-type worms were grown on *E. coli* (HT115) containing an empty control vector (L4440) from hatching until adulthood. The animals were then either kept on empty vector bacteria or fed with RNAi bacteria to *cct-2* or *cct-8* until day 4 of adulthood. Animals were then harvested and washed three times in M9 buffer. After 1 h incubation in methanol, worms were washed again three times with M9 buffer and mounted on a slide using DAPI Fluoromount-G (Southern Biotech).

Heat stress assays. For day 1 adulthood heat-shock assays, eggs were transferred to plates seeded with *E. coli* (OP50) bacteria and grown to day 1 of adulthood at 20 °C. Worms were then transferred to fresh plates with *E. coli* (HT115) containing L4440 and heat shocked at 34 °C. Worms were checked every hour for viability. For day 5 adulthood heat-shock assays, adult worms were transferred to fresh plates with *E. coli* (HT115) containing L4440 every day and then heat shocked at 34 °C at day 5. PRISM 6 software was used for statistical analysis and *P* values were calculated using the log-rank (Mantel–Cox) method.

Motility assay. Thrashing rates were determined as described in ref. 39. Animals were grown at 20 °C until L4 stage and then grown at 20 °C or 25 °C for the rest of the experiment. Worms were fed with *E. coli* (OP50) bacteria. Worms were transferred at day 3 of adulthood to a drop of M9 buffer and after 30 s of adaptation the number of body bends was counted for 30 s. A body bend was defined as change in direction of the bend at the midbody.

Western blot. Cells were collected from tissue culture plates by cell scraping and lysed in protein cell lysis buffer (10 mM Tris–HCl, pH 7.4, 10 mM EDTA, 50 mM NaCl, 50 mM NaF, 1% Triton X-100, 0.1% SDS supplemented with 2 mM sodium orthovanadate, 1 mM phenylmethylsulphonyl fluoride and complete mini protease) for 1 h at 1,000 r.p.m. and 4 °C in a Thermomixer. Samples were centrifuged at 10,000g for 15 min at 4 °C and the supernatant was collected. Protein concentrations were determined with a standard BCA protein assay (Thermo Scientific). Approximately 20–30 μg of total protein was separated by SDS–polyacrylamide gel electrophoresis (SDS–PAGE), transferred to nitrocellulose membranes (Whatman) and subjected to immunoblotting. Western blot analysis was performed with anti-TCP1 alpha (Abcam, ab90357, 1:1,000), anti-CCT2 (Abcam, ab92746, 1:10,000), anti-CCT6A (Abcam, ab140142, 1:1,000), anti-CCT7 (Abcam, ab170861, 1:10,000), anti-CCT8 (Proteintech, 12263-1-AP, 1:1,000), anti-OCT4 (Stem Cell Technologies, #60093, 1:5,000), anti-HTT (Cell Signaling, ab5656, 1:1,000), anti-polyQ-expansion diseases marker antibody (Millipore, MAB1574, 1:1,000), anti-GFP (ImmunoKontakt, 210-PS-1GFP, 1:5,000), anti- α -tubulin (Sigma, T6199, 1:5,000), anti-GAPDH (Abcam, ab9484, 1:5,000) and anti- β -actin (Abcam, ab8226, 1:5,000). In *C. elegans*, we tested all the CCT subunit antibodies indicated above but only anti-TCP1 alpha (Abcam, ab90357) was positive (as already profiled for use in this organism by Abcam). Uncropped versions of all important western blots are presented in Supplementary Fig. 19.

RNA isolation and quantitative RT-PCR. For human cell samples, total RNA was extracted using RNeasy (Tel-Test Inc.). cDNA was generated using qScript Flex cDNA synthesis kit (Quantabio). SybrGreen real-time qPCR experiments were performed with a 1:20 dilution of cDNA using a CFC384 Real-Time System (Bio-Rad) following the manufacturer's instructions. Data were analysed with the comparative $2\Delta\Delta C_t$ method using the geometric mean of *ACTB* and *GAPDH* as housekeeping genes. For *C. elegans* samples, total RNA was isolated from synchronized populations of ~2,000 adults using QIAzol lysis reagent (Qiagen). Data were analysed with the comparative $2\Delta\Delta C_t$ method using the geometric mean of *cdc-42* and *pmp-3* as endogenous control⁷⁵. See Supplementary Tables 4 and 5 for details about the primers used for this assay.

Filter trap. Worms were grown at 20 °C until L4 stage and then grown at 25 °C for the rest of the experiment. Day 3 adult worms were collected with M9 buffer and worm pellets were frozen with liquid N₂. Frozen worm pellets were thawed on ice and worm extracts were generated by glass bead disruption on ice in non-denaturing lysis buffer (50 mM Hepes pH 7.4, 150 mM NaCl, 1 mM EDTA, 1% Triton X-100) supplemented with EDTA-free protease inhibitor cocktail (Roche). Worm and cellular debris was removed with 8,000g spin for 5 min. Approximately 100 μg of protein extract was supplemented with SDS at a final concentration of 0.5%

and loaded onto a cellulose acetate membrane assembled in a slot blot apparatus (Bio-Rad). The membrane was washed with 0.1% SDS and retained Q67-GFP was assessed by immunoblotting for GFP (ImmunoKontakt, 210-PS-1GFP, 1:5,000). Extracts were also analysed by SDS-PAGE to determine protein expression levels.

iPSCs were collected in non-denaturing lysis buffer supplemented with EDTA-free protease inhibitor cocktail and lysed by passing 10 times through a 27 gauge needle attached to a 1 ml syringe. Then, we followed the filter trap protocol described above. The membrane was washed with 0.1% SDS and retained polyQ proteins were assessed by immunoblotting for anti-polyQ-expansion diseases marker antibody (Millipore, MAB1574, 1:5,000). This antibody recognizes polyQ-containing proteins like HTT and detects remarkably better polyQ-expanded HTT than wild-type HTT (refs 20,21). Extracts were also analysed by SDS-PAGE to determine HTT protein expression levels.

Blue native gel immunoblotting of TRiC/CCT complex. For experiments with hESCs (H9 and H1) and their NPC counterparts, cells were collected in lysis buffer (50 mM Tris-HCl (pH 7.5), 1 mM dithiothreitol and 10% glycerol supplemented with protease inhibitor cocktail (Roche)) and lysed by passing 10 times through a 27 gauge needle attached to a 1 ml syringe. Lysate was centrifuged at 16,000g for 10 min at 4°C. 50 µg of total protein was run on a 3–13% gel in deep blue cathode buffer (50 mM Tricine, 7.5 mM Imidazole and 0.02% Coomassie G250) at 4°C for 3 h at 100 V and then exchange deep blue cathode buffer to slightly blue cathode buffer (50 mM Tricine, 7.5 mM Imidazole, and 0.002% Coomassie G250) and run at 100 V overnight. Proteins were then transferred to a polyvinylidene difluoride membrane at 400 mV for 3 h by semi-dry blotting. Western blot analysis was performed with anti-TCPI alpha (Abcam, ab90357, 1:1,000), anti-CCT2 (Abcam, ab92746, 1:10,000) and anti-CCT8 (Proteintech, 12263-1-AP, 1:1,000). Extracts were also analysed by SDS-PAGE to determine CCT subunit expression levels and loading control. Uncropped versions of all important native and SDS-PAGE gels are presented in Supplementary Fig. 19.

Data availability. The mass spectrometry proteomics data have been deposited to the ProteomeXchange Consortium via the PRIDE partner repository under accession code PXD005123. Transcriptome data have been deposited in the Sequence Read Archive (SRA) under the accession code SRP091319. All the other data are also available from the corresponding author upon request.

References

- Bennett, E. J., Bence, N. F., Jayakumar, R. & Kopito, R. R. Global impairment of the ubiquitin-proteasome system by nuclear or cytoplasmic protein aggregates precedes inclusion body formation. *Mol. Cell* **17**, 351–365 (2005).
- Powers, E. T., Morimoto, R. I., Dillin, A., Kelly, J. W. & Balch, W. E. Biological and chemical approaches to diseases of proteostasis deficiency. *Annu. Rev. Biochem.* **78**, 959–991 (2009).
- Lopez-Otin, C., Blasco, M. A., Partridge, L., Serrano, M. & Kroemer, G. The hallmarks of aging. *Cell* **153**, 1194–1217 (2013).
- Vilchez, D., Saez, I. & Dillin, A. The role of protein clearance mechanisms in organismal ageing and age-related diseases. *Nat. Commun.* **5**, 5659 (2014).
- Taylor, R. C. & Dillin, A. Aging as an event of proteostasis collapse. *Cold Spring Harb. Perspect. Biol.* **3**, pii: a004440 (2011).
- Miura, T., Mattson, M. P. & Rao, M. S. Cellular lifespan and senescence signaling in embryonic stem cells. *Aging Cell* **3**, 333–343 (2004).
- You, K. T., Park, J. & Kim, V. N. Role of the small subunit processome in the maintenance of pluripotent stem cells. *Genes Dev.* **29**, 2004–2009 (2015).
- Vilchez, D. et al. Increased proteasome activity in human embryonic stem cells is regulated by PSMD11. *Nature* **489**, 304–308 (2012).
- Assou, S. et al. A gene expression signature shared by human mature oocytes and embryonic stem cells. *BMC Genomics* **10**, 10 (2009).
- Vilchez, D. et al. RPN-6 determines *C. elegans* longevity under proteotoxic stress conditions. *Nature* **489**, 263–268 (2012).
- Brehme, M. et al. A chaperone subnetwork safeguards proteostasis in aging and neurodegenerative disease. *Cell Rep.* **9**, 1135–1150 (2014).
- Hartl, F. U., Bracher, A. & Hayer-Hartl, M. Molecular chaperones in protein folding and proteostasis. *Nature* **475**, 324–332 (2011).
- Lopez, T., Dalton, K. & Frydman, J. The mechanism and function of group II chaperonins. *J. Mol. Biol.* **427**, 2919–2930 (2015).
- Yam, A. Y. et al. Defining the TRiC/CCT interactome links chaperonin function to stabilization of newly made proteins with complex topologies. *Nat. Struct. Mol. Biol.* **15**, 1255–1262 (2008).
- Etchells, S. A. et al. The cotranslational contacts between ribosome-bound nascent polypeptides and the subunits of the hetero-oligomeric chaperonin TRiC probed by photocross-linking. *J. Biol. Chem.* **280**, 28118–28126 (2005).
- Priya, S., Sharma, S. K. & Goloubinoff, P. Molecular chaperones as enzymes that catalytically unfold misfolded polypeptides. *FEBS Lett.* **583**, 1981–1987 (2013).
- Leitner, A. et al. The molecular architecture of the eukaryotic chaperonin TRiC/CCT. *Structure* **20**, 814–825 (2012).
- Spiess, C., Meyer, A. S., Reissmann, S. & Frydman, J. Mechanism of the eukaryotic chaperonin: protein folding in the chamber of secrets. *Trends Cell Biol.* **14**, 598–604 (2004).
- Finkbeiner, S. Huntington's Disease. *Cold Spring Harb. Perspect. Biol.* **3**, pii: a007476 (2011).
- Consortium, H. D. i. Induced pluripotent stem cells from patients with Huntington's disease show CAG-repeat-expansion-associated phenotypes. *Cell Stem Cell* **11**, 264–278 (2012).
- Trottier, Y. et al. Polyglutamine expansion as a pathological epitope in Huntington's disease and four dominant cerebellar ataxias. *Nature* **378**, 403–406 (1995).
- Herbst, M. & Wanker, E. E. Small molecule inducers of heat-shock response reduce polyQ-mediated huntingtin aggregation. A possible therapeutic strategy. *Neurodegener. Dis.* **4**, 254–260 (2007).
- Jeon, I. et al. Neuronal properties, *in vivo* effects, and pathology of a Huntington's disease patient-derived induced pluripotent stem cells. *Stem Cells* **30**, 2054–2062 (2012).
- Kitamura, A. et al. Cytosolic chaperonin prevents polyglutamine toxicity with altering the aggregation state. *Nat. Cell Biol.* **8**, 1163–1170 (2006).
- Nollen, E. A. et al. Genome-wide RNA interference screen identifies previously undescribed regulators of polyglutamine aggregation. *Proc. Natl Acad. Sci. USA* **101**, 6403–6408 (2004).
- Tam, S., Geller, R., Spiess, C. & Frydman, J. The chaperonin TRiC controls polyglutamine aggregation and toxicity through subunit-specific interactions. *Nat. Cell Biol.* **8**, 1155–1162 (2006).
- Vonsattel, J. P., Keller, C. & Del Pilar Amaya, M. Neuropathology of Huntington's disease. *Handb. Clin. Neurol.* **89**, 599–618 (2008).
- Ma, L. et al. Human embryonic stem cell-derived GABA neurons correct locomotion deficits in quinolinic acid-lesioned mice. *Cell Stem Cell* **10**, 455–464 (2012).
- Hill, A. A., Hunter, C. P., Tsung, B. T., Tucker-Kellogg, G. & Brown, E. L. Genomic analysis of gene expression in *C. elegans*. *Science* **290**, 809–812 (2000).
- Lundin, V. F., Srayko, M., Hyman, A. A. & Leroux, M. R. Efficient chaperone-mediated tubulin biogenesis is essential for cell division and cell migration in *C. elegans*. *Dev. Biol.* **313**, 320–334 (2008).
- Gonczy, P. et al. Functional genomic analysis of cell division in *C. elegans* using RNAi of genes on chromosome III. *Nature* **408**, 331–336 (2000).
- Green, R. A. et al. A high-resolution *C. elegans* essential gene network based on phenotypic profiling of a complex tissue. *Cell* **145**, 470–482 (2011).
- Hubbard, E. J. *Caenorhabditis elegans* germ line: a model for stem cell biology. *Dev. Dyn.* **236**, 3343–3357 (2007).
- Kelly, W. G., Xu, S., Montgomery, M. K. & Fire, A. Distinct requirements for somatic and germline expression of a generally expressed *Caenorhabditis elegans* gene. *Genetics* **146**, 227–238 (1997).
- McKay, S. J. et al. Gene expression profiling of cells, tissues, and developmental stages of the nematode *C. elegans*. *Cold Spring Harb. Symp. Quant. Biol.* **68**, 159–169 (2003).
- Gu, T., Orita, S. & Han, M. *Caenorhabditis elegans* SUR-5, a novel but conserved protein, negatively regulates LET-60 Ras activity during vulval induction. *Mol. Cell Biol.* **18**, 4556–4564 (1998).
- Vabulas, R. M., Raychaudhuri, S., Hayer-Hartl, M. & Hartl, F. U. Protein folding in the cytoplasm and the heat shock response. *Cold Spring Harb. Perspect. Biol.* **2**, a004390 (2010).
- Morimoto, R. I. The heat shock response: systems biology of proteotoxic stress in aging and disease. *Cold Spring Harb. Symp. Quant. Biol.* **76**, 91–99 (2011).
- Brignull, H. R., Moore, F. E., Tang, S. J. & Morimoto, R. I. Polyglutamine proteins at the pathogenic threshold display neuron-specific aggregation in a pan-neuronal *Caenorhabditis elegans* model. *J. Neurosci.* **26**, 7597–7606 (2006).
- Khodakarami, A., Mels, J., Saez, I. & Vilchez, D. Mediation of organismal aging and somatic proteostasis by the germline. *Front. Mol. Biosci.* **2**, 3 (2015).
- Gao, Y., Thomas, J. O., Chow, R. L., Lee, G. H. & Cowan, N. J. A cytoplasmic chaperonin that catalyzes beta-actin folding. *Cell* **69**, 1043–1050 (1992).
- Faustino, R. S. et al. Decoded calreticulin-deficient embryonic stem cell transcriptome resolves latent cardiophenotype. *Stem Cells* **28**, 1281–1291 (2010).
- Mesaali, N. et al. Calreticulin is essential for cardiac development. *J. Cell Biol.* **144**, 857–868 (1999).
- Li, J. et al. Calreticulin reveals a critical Ca(2+) checkpoint in cardiac myofibrillogenesis. *J. Cell Biol.* **158**, 103–113 (2002).
- Akerfelt, M., Morimoto, R. I. & Sistonen, L. Heat shock factors: integrators of cell stress, development and lifespan. *Nat. Rev. Mol. Cell Biol.* **11**, 545–555 (2010).
- Kubota, H., Matsumoto, S., Yokota, S., Yanagi, H. & Yura, T. Transcriptional activation of mouse cytosolic chaperonin CCT subunit genes by heat shock factors HSF1 and HSF2. *FEBS Lett.* **461**, 125–129 (1999).
- Neef, D. W. et al. A direct regulatory interaction between chaperonin TRiC and stress-responsive transcription factor HSF1. *Cell Rep.* **9**, 955–966 (2014).
- Neef, D. W., Turski, M. L. & Thiele, D. J. Modulation of heat shock transcription factor 1 as a therapeutic target for small molecule intervention in neurodegenerative disease. *PLoS Biol.* **8**, e1000291 (2010).

49. Langfelder, P. *et al.* Integrated genomics and proteomics define huntingtin CAG length-dependent networks in mice. *Nat. Neurosci.* **19**, 623–633 (2016).
50. Saez, I. & Vilchez, D. The mechanistic links between proteasome activity, aging and age-related diseases. *Curr. Genomics* **15**, 38–51 (2014).
51. Vilchez, D., Simic, M. S. & Dillin, A. Proteostasis and aging of stem cells. *Trends Cell Biol.* **24**, 161–170 (2014).
52. Whitesell, L. & Lindquist, S. L. HSP90 and the chaperoning of cancer. *Nat. Rev. Cancer* **5**, 761–772 (2005).
53. Huang, X. *et al.* Chaperonin containing TCP1, subunit 8 (CCT8) is upregulated in hepatocellular carcinoma and promotes HCC proliferation. *APMIS* **122**, 1070–1079 (2014).
54. Qiu, X. *et al.* Overexpression of CCT8 and its significance for tumor cell proliferation, migration and invasion in glioma. *Pathol. Res. Pract.* **211**, 717–725 (2015).
55. Boudiaf-Benmammar, C., Cresteil, T. & Melki, R. The cytosolic chaperonin CCT/TRiC and cancer cell proliferation. *PLoS ONE* **8**, e60895 (2013).
56. Rappa, F. *et al.* HSP-molecular chaperones in cancer biogenesis and tumor therapy: an overview. *Anticancer Res.* **32**, 5139–5150 (2012).
57. Trinidad, A. G. *et al.* Interaction of p53 with the CCT complex promotes protein folding and wild-type p53 activity. *Mol. Cell* **50**, 805–817 (2013).
58. Kirkwood, T. B. Evolution of ageing. *Nature* **270**, 301–304 (1977).
59. Park, I. H. *et al.* Reprogramming of human somatic cells to pluripotency with defined factors. *Nature* **451**, 141–146 (2008).
60. Park, I. H. *et al.* Disease-specific induced pluripotent stem cells. *Cell* **134**, 877–886 (2008).
61. Chambers, S. M. *et al.* Highly efficient neural conversion of human ES and iPSC cells by dual inhibition of SMAD signaling. *Nat. Biotechnol.* **27**, 275–280 (2009).
62. Rao, J. *et al.* Stepwise clearance of repressive roadblocks drives cardiac induction in human ESCs. *Cell Stem Cell* **18**, 341–353 (2016).
63. Josephson, R. *et al.* A molecular scheme for improved characterization of human embryonic stem cell lines. *BMC Biol.* **4**, 28 (2006).
64. Dodt, M., Roehr, J. T., Ahmed, R. & Dieterich, C. FLEXBAR-flexible barcode and adapter processing for next-generation sequencing platforms. *Biology (Basel)* **1**, 895–905 (2012).
65. Dobin, A. *et al.* STAR: ultrafast universal RNA-seq aligner. *Bioinformatics* **29**, 15–21 (2013).
66. Trapnell, C. *et al.* Differential gene and transcript expression analysis of RNA-seq experiments with TopHat and Cufflinks. *Nat. Protoc.* **7**, 562–578 (2012).
67. Rappsilber, J., Ishihama, Y. & Mann, M. Stop and go extraction tips for matrix-assisted laser desorption/ionization, nanoelectrospray, and LC/MS sample pretreatment in proteomics. *Anal. Chem.* **75**, 663–670 (2003).
68. Cox, J. & Mann, M. MaxQuant enables high peptide identification rates, individualized p.p.b.-range mass accuracies and proteome-wide protein quantification. *Nat. Biotechnol.* **26**, 1367–1372 (2008).
69. Cox, J. *et al.* Accurate proteome-wide label-free quantification by delayed normalization and maximal peptide ratio extraction, termed MaxLFQ. *Mol. Cell. Proteomics* **13**, 2513–2526 (2014).
70. Ritchie, M. E. *et al.* limma powers differential expression analyses for RNA-sequencing and microarray studies. *Nucleic Acids Res.* **43**, e47 (2015).
71. R Development Core Team. R: A Language and Environment for Statistical Computing. (The R Foundation for Statistical Computing, Vienna, Austria, 2011). <http://www.R-project.org/>.
72. Brenner, S. The genetics of *Caenorhabditis elegans*. *Genetics* **77**, 71–94 (1974).
73. Mello, C. C., Kramer, J. M., Stinchcomb, D. & Ambros, V. Efficient gene transfer in *C.elegans*: extrachromosomal maintenance and integration of transforming sequences. *EMBO J.* **10**, 3959–3970 (1991).
74. Amrit, F. R., Ratnappan, R., Keith, S. A. & Ghazi, A. The *C. elegans* lifespan assay toolkit. *Methods* **68**, 465–475 (2014).
75. Hoogewijs, D., Houthoofd, K., Matthijssens, F., Vandesompele, J. & Vanfleteren, J. R. Selection and validation of a set of reliable reference genes for quantitative sod gene expression analysis in *C. elegans*. *BMC Mol. Biol.* **9**, 9 (2008).

Acknowledgements

We thank D. Bartsch and L. Kurian for their suggestions and performing mesoderm differentiation. We thank T. Langer for his advice on the study of TRiC/CCT assembly. The following funding sources supported this research: Deutsche Forschungsgemeinschaft (DFG) (VI742/1-1 and CECAD), University of Cologne Advanced Postdoc Grant, Else Kröner-Fresenius-Stiftung (2015_A118) and European Research Council (ERC Starting Grant-677427 StemProteostasis). Proteomics experiments were performed at the CECAD Proteomics Facility. Some of the nematode strains used in this work were provided by the *Caenorhabditis* Genetics Center (University of Minnesota), which is supported by the NIH Office of Research Infrastructure Programs (P40 OD010440).

Author contributions

A.N. and A.K. performed most of the experiments, data analysis and interpretation through discussions with D.V., R.G.-G. and S.K. performed filter trap experiments and helped with other experiments. H.J.L. and T.K. performed TRiC/CCT assembly experiments. C.S. helped with and performed some of the experiments. I.S. carried out the proteomics and RNA sequencing experiments. A.F. performed neuronal differentiation and analysis of HD-iPSC lines. C.D. performed bioinformatic analysis of proteomics and transcriptomics data. D.V. planned and supervised the project. The manuscript was written by D.V. All the authors discussed the results and commented on the manuscript.

Additional information

Supplementary Information accompanies this paper at <http://www.nature.com/naturecommunications>

Competing financial interests: The authors declare no competing financial interests.

Reprints and permission information is available online at <http://npg.nature.com/reprintsandpermissions/>

How to cite this article: Noormohammadi, A. *et al.* Somatic increase of CCT8 mimics proteostasis of human pluripotent stem cells and extends *C. elegans* lifespan. *Nat. Commun.* **7**, 13649 doi: 10.1038/ncomms13649 (2016).

Publisher's note: Springer Nature remains neutral with regard to jurisdictional claims in published maps and institutional affiliations.



This work is licensed under a Creative Commons Attribution 4.0 International License. The images or other third party material in this article are included in the article's Creative Commons license, unless indicated otherwise in the credit line; if the material is not included under the Creative Commons license, users will need to obtain permission from the license holder to reproduce the material. To view a copy of this license, visit <http://creativecommons.org/licenses/by/4.0/>

© The Author(s) 2016

4) DISCUSSION

1) Analysis of the role of E3 ligases in pluripotency

Proteostasis is essential for organismal development and cell function (van Oosten-Hawle and Morimoto 2014). ESCs have unlimited self-renewal capacity in cell culture and do not undergo senescence (Miura, Mattson et al. 2004). This unlimited self-renewal capacity needs a specialized high level of quality control mechanisms to maintain the integrity of the genome and cell function (Nagaria, Robert et al. 2013). Recent studies have shown that pluripotent stem cells have enhanced proteasome activity which is critical to maintain their proteostasis (Vilchez, Boyer et al. 2012, Vilchez, Morante et al. 2012, Noormohammadi, Khodakarami et al. 2016). This increased proteasome activity is mediated by PSMD11/RPN6 which is a subunit required for the proteasome assembly (Vilchez, Boyer et al. 2012). However, the mechanisms by which proteasome activity regulates hESC function remain unknown. Therefore, we proposed that elucidating the regulation of the proteostasis network in hESCs may shed light on hESC identity and the aging process. In this study, we elucidated the mechanisms by which increased proteasome activity regulates hESC identity by focusing on the E3 ubiquitin ligases which promote ubiquitin transfer to a specific substrate. For this aim, we analyzed proteomics data in which hESCs were compared with their neuronal differential counterparts. We identified 44 E3 ligases differentially regulated, from which 35 were upregulated in hESC. Three E3 (HUWE1, TRIM33 and RNF40) which were upregulated in our proteomics data have been shown to have a role in stem cell identity, thus supporting our approach (Zhao, Heng et al. 2008, Dupont, Mamidi et al. 2009, Fuchs, Shema et al. 2012). First, we validated our proteomics results through Western blot and also analyzed the change of these E3 ligases at the mRNA level. Since we did not observe a decrease in their mRNA levels during neuronal differentiation, these E3s probably are regulated on the post-transcriptional or post-translational level. To delineate whether the downregulation of these E3 ligases also occurred during differentiation into other germ layers, we also compared hESC with endoderm precursors. This comparison revealed that this downregulation is not specific to neuronal differentiation. Furthermore, to assess the possible substrate of these E3 ligases which could participate in stem cell identity, we investigated the interactome of these up-regulated E3 ligases. We combined these data with a shot label free proteomic experiment in E3 knockdown hESCs as well as proteasome-inhibitor experiments. Unexpectedly, we found relatively low numbers of potential targets of the E3 ligases which is also upregulated when inhibiting the proteasome. Although we only identified a low number of potential substrates of the E3 ligases, our data contributes to discover potential

proteasomal targets in hESCs. Among the identified possible targets, we validated the interaction of HECTD1 with EXOC5 (Exocyst complex component 5) and RNF181 with PSMD3 (26S proteasome non-ATPase regulatory subunit 3). It has been previously reported that the identification of E3 ligase substrates is difficult due to several technical challenges (Iconomou and Saunders 2016). First, ubiquitylation is a dynamic process and it is under control of both E3 ligases and DUBs which can remove ubiquitin chains (Komander, Reyes-Turcu et al. 2009). Secondly, the weak interaction and the fast dissociation rate between E3 ligases and their substrate results in difficulties for the identification using immunoprecipitation techniques (Pierce, Kleiger et al. 2009). Furthermore, the low abundance of substrate also challenges the identification of interactors. Finally, some substrates can be ubiquitylated by multiple E3s ligases at different sites or a E3 ligases ubiquitylate multiple substrate in response to different conditions (Jain and Barton 2009). Therefore, we cannot rule out that the interactor partners of the E3 ligase identified could still be targets of the proteasome, their activity/function could be modified by ubiquitylation or they could be part of a E3-containing protein complex. In addition to the challenge for the identification of the substrates of the E3 ligases, we need to consider the effect of inhibiting the proteasome. Proteasome inhibition promotes the accumulation of polyubiquitylated proteins and severe shortage of monoubiquitin at the cellular level. This can promote the activation of other degradation pathways such as autophagy (Bustamante, Gonzalez et al. 2018). Therefore, the exposure time and the amount of inhibitor can alter the experimental results and activating other degradative pathways can also impair substrate identification. To evaluate whether these E3 ligases have role in hESCs identity, we performed loss-of-function experiments and then analyzed the pluripotency level and differentiation capacities of the hESCs. However, we did not observe a significant change in stem cell markers or their differentiation capacity upon silencing these E3 ligases. Potential functional redundancies between E3 ligases could explain these results (Rubenstein and Hochstrasser 2010). For instance, the tumor suppressor p53 can be degraded through multiple E3 ligases such as E4F1, WWP1 and COP1 (Lee and Gu 2010). Another example is the yeast α cell-specific transcriptional repressor $\alpha 2$, which can be targeted to the proteasome through ubiquitination by the E3 enzymes Doa10 and Slx5/Slx8 (Xie, Rubenstein et al. 2010). These redundant mechanisms could be important to ensure tightly regulated, proper degradation of a particular substrate when one of the E3s is not functioning or saturated by the number of targets for ubiquitination. Besides, some E3s can show subtle differences in terms of ubiquitination of the same substrate based on their different subcellular localizations and lead to ubiquitination of the same substrate in an intracellular dependent manner. As an example, Doa10 and

Slx5/Slx8, which are involved in ubiquitylation of $\alpha 2$, have different subcellular localization (Rubenstein and Hochstrasser 2010). Therefore, both the redundant and compensatory mechanisms of the E3s could be essential for the maintenance of the proteome of pluripotent stem cells and this could hinder the study of the impact of one single E3 ligase. Moreover, to compensate the effect of the knockdown of these E3 ligases, E3-depleted hESCs could activate other proteostatic pathways such as autophagy (Bustamante, Gonzalez et al. 2018).

As mentioned previously, we also inhibited the proteasome using MG132 and performed quantitative proteomics. Analyses of quantitative proteomics of MG132- treated hESCs revealed that the proteasome is coupled to other important biological processes of hESCs identity in addition to its role in proteostasis of hESCs. For example, impairment in proteasome activity increases the levels of activators of ribosome biogenesis and translation. This could be an adaptation mechanism to compensate the decrease in proteolytic activity. On the other hand, it could affect stem cell pluripotency and differentiation capacity due to the need of enhanced expression of ribosomal subunits and global translational rates in hESCs (Ingolia, Lareau et al. 2011, You, Park et al. 2015). Furthermore, we observed a down-regulation of proteins involved in mRNA transport such as the nuclear pore complex protein NUP153, which has been shown to be important for ESC pluripotency (Jacinto, Benner et al. 2015). Interestingly, proteasome dysfunction also caused the down-regulation of proteins involved in telomere maintenance, such as NOP10, and which are essential to sustain hESCs function (Zeng, Liu et al. 2014). In addition, proteasome dysfunction promoted a decrease in the levels of multiple proteins, which are key metabolic regulators. Specifically, hexokinase II (HK2), which sustains high levels of glycolysis in hESCs, was downregulated. These alterations in the metabolic enzymes are important since hESC have distinct metabolic characteristics that are required for their energetic needs (Varum, Rodrigues et al. 2011).

In summary, although we did not observe a strong phenotype of our target E3s on pluripotency and differentiation in the loss-of-function experiments, our results are important for the identification of the potential candidates of these E3 ligases in hESCs. In addition, we cannot discard the possibility that these E3 ligases could be involved in stem cell identity under different stress conditions and their high levels would be necessary in these situations. Under different stress conditions, these E3 ligases could be involved in the rapid modification of the cell cycle, removal of damaged protein and regulation of transcription to sustain their stemness. Moreover, our proteomics data from the proteasome inhibited experiments indicated that in hESCs, the proteasome is involved in other biological processes such as telomere maintenance, RNA biogenesis and metabolism as well as sustaining proteostasis. Taken together, this study

is important for the characterization of the UPS in hESCs and provide valuable data for a further understanding of hESCs.

2) The investigation of the role of UBR5 in the proteostasis of HTT

Pluripotent stem cells have enhanced cellular quality control mechanisms to maintain their pluripotency and stemness. Several studies suggested that, in addition to a tight regulation of gene expression, epigenetic and signaling networks, pluripotent stem cells have enhanced proteasome activity to maintain their proteostasis, which is essential for the proper cellular function and organismal development (Buckley, Aranda-Orgilles et al. 2012, Vilchez, Boyer et al. 2012, Noormohammadi, Khodakarami et al. 2016, Garcia-Prat, Sousa-Victor et al. 2017). Impairment in proteostasis results in the accumulation of misfolded, damaged and aggregated proteins that might affect the stemness and pluripotency of ESCs. Moreover, defects in proteostasis are also associated with the early onset of age-related diseases such as AD, PD and HD. Notably, human pluripotent stem cells, especially iPSC, are an invaluable source to investigate the mechanisms and pathologies of neurodegenerative diseases by recapitulating diseases and allow to screen drug candidates for potential therapeutic treatments. Therefore, the analysis of the mechanisms of enhanced proteostasis capacities in pluripotent stem cells derived from patients could provide valuable information to understand the disease pathology and regulation. This mechanism, which is required for this super-vigilant proteostasis, could also be mimicked in somatic tissues as a therapeutic approach.

Remarkably, although HD-iPSCs express mHTT, they do not accumulate polyQ-expanded aggregates (Consortium 2012, Jeon, Lee et al. 2012, Noormohammadi, Khodakarami et al. 2016). Moreover, the length of expansion of polyQ does not influence pluripotency, self-renewal and survival of HD-iPSCs. However, they show HD- associated phenotypes such as increased vulnerability to stress and variations in gene expression when they are differentiated into neural progenitor cells and neurons (Park, Arora et al. 2008, Consortium 2012). In this part of the study, we investigated the underlying mechanisms to suppress the aggregation of polyQ-expanded HTT in HD-iPSCs mediated by enhanced proteasome activity by focusing on the E3 ubiquitin ligase network. First, we analyzed how proteasome dysfunction affected polyQ-expanded HTT aggregate formation in HD-iPSCs. We observed that enhanced proteasome activity in HD-iPSCs regulates the levels of both normal and mutant HTT and ameliorates polyQ-expanded HTT aggregation. To study whether the effect of the proteasome on mHTT aggregation was associated with a reduction in the cell viability, we also examined how proteasome inhibition affected cell viability. We observed the accumulation of polyQ-expanded

HTT even with short proteasome inhibition which in turn did not promote any cell death. Moreover, higher concentrations of the proteasome inhibitor triggered only a mild increase (~8%) in cell death. This data excluded the possibility that the impact of declined proteasome activity on polyQ-expanded HTT aggregation was related with a decrease in cell viability. Although our data suggest a direct link between proteasome activity and HTT regulation, we cannot rule out that proteasome inhibition could trigger global proteostasis collapse. To elucidate this, we inhibited the autophagy-lysosome system, which is also involved in proteostasis of HTT (Koyuncu, Fatima et al. 2017). Although autophagy impairment triggered the formation of aggregates, these aggregates were less compact and the amount of aggregate-containing cells was also lower than the ones with proteasome inhibition. Moreover, autophagy inhibition caused a decline in the amount of HTT protein. We showed that this decrease in HTT protein was not associated with cell viability or induced a compensatory upregulation of the proteasome. These results highlighted the direct link between the proteasome activity with HTT protein levels and polyQ-expanded HTT aggregation. Remarkably, we found that intrinsic high expression of UBR5 E3 ligases was a key component of the UPS to control of HTT level in iPSCs. UBR5 is a highly conserved HECT ligase in metazoans and is involved in several distinct biological processes such as DNA damage response, development, metabolism and transcription (Shearer, Iconomou et al. 2015). We observed that UBR5 interacts with both normal and mutant HTT and mediates its proteasomal degradation. The depletion of UBR5 lead to dysregulation in HTT levels and the accumulation of polyQ-expanded HTT in HD-iPSCs. Therefore, our data showed that UBR5 is a key regulator of HTT and polyQ-expanded HTT aggregation in HD-iPSCs. Moreover, we also found that the HECT domain-containing the E3 ligase activity of UBR5 is needed for the degradation of HTT, revealing a further link between enhanced proteasome activity and modulation of mHTT levels. To investigate whether the other E3 ligases upregulated in pluripotent stem cells were involved in the regulation of HTT level, we downregulated several of them (TRIM71, UBR7, UBE3A, RNF181) and we did not observe any direct role in the modulation of HTT levels or accumulation of polyQ-expanded HTT aggregation. On the other hand, the study of the impact of the other upregulated E3s could provide a further understanding in the regulation of HTT and polyQ-expanded HTT aggregation in pluripotent stem cells. Since our findings demonstrated a role of UBR5 in the regulation of HTT, we also examined whether this regulation caused an alteration in pluripotency. Previously, a study had reported that Ubr5 knockdown lead to significant loss of pluripotency markers in murine ESCs whereas another study suggested that Ubr5 RNAi treatment did not cause change in stem cell identity (Buckley, Aranda-Orgilles et al. 2012, Kinsella, Dora et al.

2016). In iPSCs, we did not observe any change in pluripotency and germ layer markers upon loss of function of UBR5. This suggested that the accumulation of aggregates upon UBR5 knockdown is not associated with an impairment in the pluripotency markers. In addition, these data showed that the formation of aggregates upon UBR5 knockdown did not impair pluripotency markers. Furthermore, we also analyzed whether UBR5 is required for the generation of GABAergic medium spiny neurons (MSNs) from iPSCs via a method based on the induction of hedgehog signaling. We also did not observe any variation in the differentiation efficiency between the control and UBR5 knock down cells. This finding was also surprising because knockdown of Ubr5 in murine pluripotent stem cells decreases the induction of Sonic hedgehog upon retinoic-acid treatment (Kinsella, Dora et al. 2016). Although the loss of Ubr5 led to on average shorter limbs than control limbs, the effects were not statistically significant. Moreover, in these lines, a conditional Ubr5 mutant mouse showed a perturbation in hedgehog signaling in the developing limb while the mutants did not have obvious morphological defects (Kinsella, Dora et al. 2016). These differences in pluripotency and differentiation could be related with genetic differences between mice and humans. Hence, it has been reported that human and mouse ESCs differ enormously in the transcriptional networks and signaling pathways that regulate pluripotency and lineage development (Schnerch, Cerdan et al. 2010). Furthermore, mouse ESCs require leukemia inhibitory factor (LIF)/STAT3 for their maintenance in an undifferentiated state and show a naive state that is similar to the pluripotent state in the inner cell mass of the pre-implantation embryo. However, hESCs and iPSCs do not require LIF signaling and also show a more primed state that is similar to post-implantation embryonic configurations (Weinberger, Ayyash et al. 2016). Since HD-iPSCs did not show any change in stem cell identity and were able to differentiate after knocking down UBR5, we speculate that enhanced proteasome activity may be necessary to eliminate the generation of precursor cells that accumulate protein aggregates at early developmental stages of organism. To support this hypothesis, in vivo experiments might be necessary. Interestingly, in contrast to what happens at the iPSCs state, we couldn't find any aggregates in HD-iPSCs differentiated into MSNs upon UBR5 knockdown. There could be several reasons for this. Firstly, although the knockdown levels of UBR5 were very strong, it could have been lost during differentiation into MSNs. Secondly, during terminal neuronal differentiation, additional proteostatic mechanisms could have been activated in order to avoid the accumulation of aggregates. Moreover, the differentiation protocol could be also crucial to define the role of UBR5 in the regulation of HTT protein and polyQ-expanded HTT aggregation in the neuronal level. It is important to note that recent studies have suggested that modeling

HD by using neurons differentiated from HD-iPSCs is challenging because neurons differentiated from HD-iPSC do not exhibit aggregates or a strong cell death phenotype (Consortium 2012, Jeon, Lee et al. 2012, Victor, Richner et al. 2018). Therefore, a different neuronal differentiation protocol could be required to study the impact of UBR5 knock down in the regulation of polyQ-expanded HTT aggregation in neuronal level. For instance, recent studies have shown the direct reprogramming of fibroblast into neural stem cells (Son, Ichida et al. 2011, Victor, Richner et al. 2018, Xiao, Liu et al. 2018). It has been revealed that MSNs derived from HD patient fibroblasts by using microRNA-based neuronal conversion maintain age signatures of original fibroblasts. These MSNs showed polyQ-expanded HTT aggregates as well as mitochondrial dysfunction and mHTT-dependent DNA damage during culturing (Victor, Richner et al. 2018). This method could be helpful to study of the role of UBR5 in the HTT regulation in neurons. Moreover, identifying the mechanisms which are responsible for the lack of aggregates in neurons differentiated from HD-iPSCs would be key for their implications for organismal aging and development.

Remarkably, genome-wide association (GWA) study has shown that genetic variations in a region of chromosome 8 - the one which contains UBR5- are associated with the age of neurological onset of HD (Genetic Modifiers of Huntington's Disease 2015). Our results highlight that impairment in UBR5 function could be one of the regulators in the onset of HD. To further investigate the impact of UBR5 in the regulation of aggregates, we analyzed whether ectopic expression of UBR5 is sufficient to hasten the accumulation of polyQ-expanded HTT aggregation and polyQ-expanded HTT protein levels. We found that ectopic expression of UBR5 diminished accumulation of aggregates and increases the degradation of HTT by mediating proteasomal degradation. Moreover, the ectopic expression of a catalytic inactive UBR5 mutant protein (Gudjonsson, Altmeyer et al. 2012) did not ameliorate the aggregates nor polyQ-expanded HTT protein levels. These findings also supported that UBR5 controlled HTT levels via proteasome and for this the E3 ligase activity was required. Our immunoprecipitation experiment confirmed an interaction between HTT and UBR5. The overexpression of UBR5 caused an increase in polyubiquitination of mHTT. Since we observed a dramatic increase in polyubiquitination of mHTT upon ectopic expression of UBR5, we performed proteomics analyses to determine potential lysine sites modified by UBR5. Our findings are supported by a recent study that suggested that UBR5 knockdown caused a modification of HTT protein with K11/K48 in HeLa cells. They also showed that this modification happened at Lys337 of HTT (Yau, Doerner et al. 2017). In our proteomic analyses, we found two other ubiquitinated lysine sites: Lys631 and Lys2097. Nevertheless, only levels of Lys2097 showed significant

differences between overexpression of wild-type and catalytically dead UBR5. On the other hand, it will be fascinating to investigate more putative ubiquitinated lysine sites by applying different methods. For instance, ubiquitome proteomic approaches could be applied to investigate novel potential ubiquitinated lysine sites. In this method, identification of possible ubiquitin sites is based on pull-down of diglycine peptides which result from the cleavage of the isopeptide-linked ubiquitin by trypsin (Jadhav and Wooten 2009). Moreover, characterization of these ubiquitination sites could be interesting to further understand the regulation of HTT protein by UBR5 which in turn could be used as a target for a potential therapeutic approach.

Due to the challenges, we faced while using MSNs derived from HD- iPSC, we used the *C. elegans* model to further investigate the impact of UBR5 on polyQ-expanded aggregation with age. We also observed that UBR5 hastens polyQ- expanded aggregation and ameliorates neurotoxicity in a *C. elegans* model of HD. It is important to remark that in this *C. elegans* model of HD, only the polyQ-expanded peptide and not the whole HTT protein is overexpressed. Therefore, our findings do not rule out that UBR5 could also be involved in the regulation of other polyQ-expanded aggregates. To examine this hypothesis, we analyzed the impact of UBR5 on different polyQ-containing protein such as ATAXIN-3 (ATXN3). An abnormal CAG expansion (>52) in *ATXN3* causes Machado-Joseph disease (MJD), a neurodegenerative disease characterized by progressive cerebellar dysfunction (Kawaguchi, Okamoto et al. 1994). We performed UBR5 loss of function experiments in MJD-iPSCs and found that UBR5 does not regulate ATXN3 proteostasis. These data revealed that UBR5 does not modulate all polyQ-containing proteins, but the effect on HTT would be more specific. In addition, to confirm this hypothesis, we also use two other models in which proteins aggregate. First, we used iPSCs derived from amyotrophic lateral sclerosis (ALS) patients and which carry a diseases-mimicking mutation in the RNA-binding protein FUS (Lenzi, De Santis et al. 2015). ALS is a fatal neurodegenerative disorder characterized by loss of motor neurons in the spinal cord and brain and progressive decline in muscles. FUS is one of the RNA-binding proteins involved in ALS and it is part of stress granules (SG) and control SG assembly (Bentmann, Haass et al. 2013). Normally, FUS is mostly localized in the nucleus but it can shuttle between the nucleus and cytoplasm. In ALS, the mutations in FUS disrupt the nuclear import of the protein, causing aggregation of FUS in the cytoplasm (Lenzi, De Santis et al. 2015). UBR5 knock down experiments performed in ALS-iPSC revealed that UBR5 does not regulate FUS protein or stress granules formation. In addition, we also analyzed the effect of UBR5 on solubility of aggregation-prone β -amyloid protein. In several neurodegenerative diseases such

as AD and PD, specific proteins have tendency to structural rearrangements leading to misfolded proteins. This causes the formation of amyloid-like fibrils with cross- β structure and these amyloid-like fibrils formation is responsible for the prototoxicity (Stroo, Koopman et al. 2017). We found that the overexpression of UBR5 does not decrease the insolubility of aggregation-prone β -amyloid protein (Olzscha, Schermann et al. 2011). Taken together, these results point to a specific role of UBR5 in HTT regulation. However, we cannot exclude the possibility that UBR5 could be involved in the control of other aggregation-prone proteins associated with different disease. Finally, we also asked whether UBR5 controlled the global proteostasis capacity of human pluripotent stem cells. Notably, we found that depletion of UBR5 induced the accumulation of aggresomes in pluripotent stem cells. Overwhelming the proteolytic system can lead to the accumulation of misfolded and damaged proteins into aggresomes. This remarkable result suggested that UBR5 is also essential for the degradation of misfolded proteins ensued from normal metabolism. Further investigations in the role of UBR5 in the global capacity of human pluripotent stem cells will offer valuable insights into understanding the balance between normal protein homeostasis and an alteration in several disease conditions.

In summary, our results in pluripotent stem cells uncovered UBR5 as a novel modulator of the super-vigilant proteostasis and suggest that UBR5 could be used as a potential therapeutic target in HD.

5) CONCLUSIONS

Although growing evidence indicates that the UPS regulates stem cell identity, there are still numerous questions which remain unanswered regarding the underlying mechanisms. Therefore, our studies shed light on the characterization of UPS in hESCs and provide valuable implications for understanding how proteostasis regulates stemness and pluripotency. In addition, in the second part of our studies, by working with HD-iPSCs, we highlight the role of UBR5, a member of the UPS network, as a mediator of HD progression and pathology. Our findings provide a better understanding of the role of the proteasome in HD. Furthermore, our results evidence the importance of enhanced proteasome activity after reprogramming for properly maintaining proteostasis in iPSCs. Taken together, our studies provide a strong link between UBR5 and the progression of HD and highlight its role in the modulation of the super-vigilant proteostasis in pluripotent stem cells, which makes UBR5 a putative candidate for therapeutic approach. The characterization and understanding of proteostasis in pluripotent

stem cells has also shown to have potential implications for organismal aging and aging-related disorders.

6) DECLARATION OF CONTRIBUTION AS CO-AUTHOR

I am joint first-author in all studies included in this thesis which leads to two papers published in Scientific Reports and Nature Communications, respectively. The first paper is “Insights into the ubiquitin- proteasome system of human embryonic stem cells” and the second paper is entitled “The ubiquitin ligase UBR5 suppresses proteostasis collapse in pluripotent stem cells from Huntington’s disease patients “. In addition to these two projects, I also contributed in another publication of our laboratory which appeared in Nature Communications in 2016 and has the title “Somatic increase of CCT8 mimics proteostasis of human pluripotent stem cells and extends *C. elegans* lifespan”. I was involved in performing the experiments on inducible pluripotent stem cells from Huntington’s Disease and was therefore placed as the 5th author of the manuscript. I contributed majorly or equally in the following experiments and processes in these studies listed in below:

- Study design
- Cell culture experiments (maintaining and culturing of iPSCs, hESCs, HEK293, differentiated cells such as NPC, transfection and infection of cells, differentiation from pluripotent to differentiated counterparts)
- Western blots experiment
- Immunoprecipitation experiments
- Immunocytochemistry experiments
- Filter trap assay
- Molecular cloning
- Quantitative real time polymerase chain reaction(qRT-PCR)
- *C. elegans* experiments (analysis of the aggregates using biochemical as well as imaging techniques)
- Flurosence recovery after photobleaching (FRAP) experiments
- Proteomics and analysis of data by using computational tools
- Data interpretation
- Statistical analysis

7) REFERENCES

- Adams, J. (2003). "The proteasome: structure, function, and role in the cell." *Cancer Treat Rev* **29 Suppl 1**: 3-9.
- Assou, S., D. Cerecedo, S. Tondeur, V. Pantesco, O. Hovatta, B. Klein, S. Hamamah and J. De Vos (2009). "A gene expression signature shared by human mature oocytes and embryonic stem cells." *BMC Genomics* **10**: 10.
- Atkinson, S. P., J. Collin, N. Irina, G. Anyfantis, B. K. Kyung, M. Lako and L. Armstrong (2012). "A putative role for the immunoproteasome in the maintenance of pluripotency in human embryonic stem cells." *Stem Cells* **30**(7): 1373-1384.
- Babaie, Y., R. Herwig, B. Greber, T. C. Brink, W. Wruck, D. Groth, H. Lehrach, T. Burdon and J. Adjaye (2007). "Analysis of Oct4-dependent transcriptional networks regulating self-renewal and pluripotency in human embryonic stem cells." *Stem Cells* **25**(2): 500-510.
- Baharvand, H., M. Hajheidari, S. K. Ashtiani and G. H. Salekdeh (2006). "Proteomic signature of human embryonic stem cells." *Proteomics* **6**(12): 3544-3549.
- Baig, U. I., B. J. Bhadbhade and M. G. Watve (2014). "Evolution of aging and death: what insights bacteria can provide." *Q Rev Biol* **89**(3): 209-223.
- Balch, W. E., R. I. Morimoto, A. Dillin and J. W. Kelly (2008). "Adapting proteostasis for disease intervention." *Science* **319**(5865): 916-919.
- Balchin, D., M. Hayer-Hartl and F. U. Hartl (2016). "In vivo aspects of protein folding and quality control." *Science* **353**(6294): aac4354.
- Bates, G. (2003). "Huntingtin aggregation and toxicity in Huntington's disease." *Lancet* **361**(9369): 1642-1644.
- Ben-David, U., O. Kopper and N. Benvenisty (2012). "Expanding the boundaries of embryonic stem cells." *Cell Stem Cell* **10**(6): 666-677.
- Bence, N. F., R. M. Sampat and R. R. Kopito (2001). "Impairment of the ubiquitin-proteasome system by protein aggregation." *Science* **292**(5521): 1552-1555.
- Bennett, E. J., N. F. Bence, R. Jayakumar and R. R. Kopito (2005). "Global impairment of the ubiquitin-proteasome system by nuclear or cytoplasmic protein aggregates precedes inclusion body formation." *Mol Cell* **17**(3): 351-365.
- Bentmann, E., C. Haass and D. Dormann (2013). "Stress granules in neurodegeneration--lessons learnt from TAR DNA binding protein of 43 kDa and fused in sarcoma." *FEBS J* **280**(18): 4348-4370.
- Bjorkoy, G., T. Lamark, A. Brech, H. Outzen, M. Perander, A. Overvatn, H. Stenmark and T. Johansen (2005). "p62/SQSTM1 forms protein aggregates degraded by autophagy and has a protective effect on huntingtin-induced cell death." *J Cell Biol* **171**(4): 603-614.
- Borissenko, L. and M. Groll (2007). "Diversity of proteasomal missions: fine tuning of the immune response." *Biol Chem* **388**(9): 947-955.
- Borovecki, F., L. Lovrecic, J. Zhou, H. Jeong, F. Then, H. D. Rosas, S. M. Hersch, P. Hogarth, B. Bouzou, R. V. Jensen and D. Krainc (2005). "Genome-wide expression profiling of human blood reveals biomarkers for Huntington's disease." *Proc Natl Acad Sci U S A* **102**(31): 11023-11028.
- Bradley, C. K., H. A. Scott, O. Chami, T. T. Peura, B. Dumevska, U. Schmidt and T. Stojanov (2011). "Derivation of Huntington's disease-affected human embryonic stem cell lines." *Stem Cells Dev* **20**(3): 495-502.
- Brehme, M., C. Voisine, T. Rolland, S. Wachi, J. H. Soper, Y. Zhu, K. Orton, A. Vilella, D. Garza, M. Vidal, H. Ge and R. I. Morimoto (2014). "A chaperome subnetwork safeguards proteostasis in aging and neurodegenerative disease." *Cell Rep* **9**(3): 1135-1150.
- Buckley, S. M., B. Aranda-Orgilles, A. Strikoudis, E. Apostolou, E. Loizou, K. Moran-Crusio, C. L. Farnsworth, A. A. Koller, R. Dasgupta, J. C. Silva, M. Stadtfeld, K. Hochedlinger, E. I.

Chen and I. Aifantis (2012). "Regulation of pluripotency and cellular reprogramming by the ubiquitin-proteasome system." Cell Stem Cell **11**(6): 783-798.

Buetow, L. and D. T. Huang (2016). "Structural insights into the catalysis and regulation of E3 ubiquitin ligases." Nat Rev Mol Cell Biol **17**(10): 626-642.

Bulteau, A. L., L. I. Szweda and B. Friguet (2002). "Age-dependent declines in proteasome activity in the heart." Arch Biochem Biophys **397**(2): 298-304.

Bustamante, H. A., A. E. Gonzalez, C. Cerda-Troncoso, R. Shaughnessy, C. Otth, A. Soza and P. V. Burgos (2018). "Interplay Between the Autophagy-Lysosomal Pathway and the Ubiquitin-Proteasome System: A Target for Therapeutic Development in Alzheimer's Disease." Front Cell Neurosci **12**: 126.

Carmona, J. J. and S. Michan (2016). "Biology of Healthy Aging and Longevity." Rev Invest Clin **68**(1): 7-16.

Carter, R. L. and A. W. Chan (2012). "Pluripotent stem cells models for Huntington's disease: prospects and challenges." J Genet Genomics **39**(6): 253-259.

Cha, J. H. (2007). "Transcriptional signatures in Huntington's disease." Prog Neurobiol **83**(4): 228-248.

Chen, B., M. Retzlaff, T. Roos and J. Frydman (2011). "Cellular strategies of protein quality control." Cold Spring Harb Perspect Biol **3**(8): a004374.

Chen, Y. and D. J. Klionsky (2011). "The regulation of autophagy - unanswered questions." J Cell Sci **124**(Pt 2): 161-170.

Chondrogianni, N. and E. S. Gonos (2005). "Proteasome dysfunction in mammalian aging: steps and factors involved." Exp Gerontol **40**(12): 931-938.

Chondrogianni, N., I. Petropoulos, S. Grimm, K. Georgila, B. Catalgol, B. Friguet, T. Grune and E. S. Gonos (2014). "Protein damage, repair and proteolysis." Mol Aspects Med **35**: 1-71.

Chondrogianni, N., F. L. Stratford, I. P. Trougakos, B. Friguet, A. J. Rivett and E. S. Gonos (2003). "Central role of the proteasome in senescence and survival of human fibroblasts: induction of a senescence-like phenotype upon its inhibition and resistance to stress upon its activation." J Biol Chem **278**(30): 28026-28037.

Chondrogianni, N., K. Voutetakis, M. Kapetanou, V. Delitsikou, N. Papaevgeniou, M. Sakellari, M. Lefaki, K. Filippopoulou and E. S. Gonos (2015). "Proteasome activation: An innovative promising approach for delaying aging and retarding age-related diseases." Ageing Res Rev **23**(Pt A): 37-55.

Ciechanover, A. and P. Brundin (2003). "The ubiquitin proteasome system in neurodegenerative diseases: sometimes the chicken, sometimes the egg." Neuron **40**(2): 427-446.

Consortium, H. D. i. (2012). "Induced pluripotent stem cells from patients with Huntington's disease show CAG-repeat-expansion-associated phenotypes." Cell Stem Cell **11**(2): 264-278.

Cortez, L. and V. Sim (2014). "The therapeutic potential of chemical chaperones in protein folding diseases." Prion **8**(2).

Cummings, C. J., M. A. Mancini, B. Antalffy, D. B. DeFranco, H. T. Orr and H. Y. Zoghbi (1998). "Chaperone suppression of aggregation and altered subcellular proteasome localization imply protein misfolding in SCA1." Nat Genet **19**(2): 148-154.

da Fonseca, P. C., J. He and E. P. Morris (2012). "Molecular model of the human 26S proteasome." Mol Cell **46**(1): 54-66.

Dasuri, K., L. Zhang, P. Ebenezer, S. O. Fernandez-Kim, A. J. Bruce-Keller, L. I. Szweda and J. N. Keller (2011). "Proteasome alterations during adipose differentiation and aging: links to impaired adipocyte differentiation and development of oxidative stress." Free Radic Biol Med **51**(9): 1727-1735.

Davies, S. W., M. Turmaine, B. A. Cozens, M. DiFiglia, A. H. Sharp, C. A. Ross, E. Scherzinger, E. E. Wanker, L. Mangiarini and G. P. Bates (1997). "Formation of neuronal

intranuclear inclusions underlies the neurological dysfunction in mice transgenic for the HD mutation." *Cell* **90**(3): 537-548.

Deshaies, R. J. and C. A. Joazeiro (2009). "RING domain E3 ubiquitin ligases." *Annu Rev Biochem* **78**: 399-434.

Diaz-Hernandez, M., A. G. Valera, M. A. Moran, P. Gomez-Ramos, B. Alvarez-Castelao, J. G. Castano, F. Hernandez and J. J. Lucas (2006). "Inhibition of 26S proteasome activity by huntingtin filaments but not inclusion bodies isolated from mouse and human brain." *J Neurochem* **98**(5): 1585-1596.

DiFiglia, M., E. Sapp, K. O. Chase, S. W. Davies, G. P. Bates, J. P. Vonsattel and N. Aronin (1997). "Aggregation of huntingtin in neuronal intranuclear inclusions and dystrophic neurites in brain." *Science* **277**(5334): 1990-1993.

Dolmetsch, R. and D. H. Geschwind (2011). "The human brain in a dish: the promise of iPSC-derived neurons." *Cell* **145**(6): 831-834.

Dupont, S., A. Mamidi, M. Cordenonsi, M. Montagner, L. Zacchigna, M. Adorno, G. Martello, M. J. Stinchfield, S. Soligo, L. Morsut, M. Inui, S. Moro, N. Modena, F. Argenton, S. J. Newfeld and S. Piccolo (2009). "FAM/USP9x, a deubiquitinating enzyme essential for TGFbeta signaling, controls Smad4 monoubiquitination." *Cell* **136**(1): 123-135.

Eldridge, A. G. and T. O'Brien (2010). "Therapeutic strategies within the ubiquitin proteasome system." *Cell Death Differ* **17**(1): 4-13.

Ferrington, D. A. and D. S. Gregerson (2012). "Immunoproteasomes: structure, function, and antigen presentation." *Prog Mol Biol Transl Sci* **109**: 75-112.

Ferrington, D. A., A. D. Husom and L. V. Thompson (2005). "Altered proteasome structure, function, and oxidation in aged muscle." *FASEB J* **19**(6): 644-646.

Finkbeiner, S. (2011). "Huntington's Disease." *Cold Spring Harb Perspect Biol* **3**(6).

Finkbeiner, S. and S. Mitra (2008). "The ubiquitin-proteasome pathway in Huntington's disease." *ScientificWorldJournal* **8**: 421-433.

Fuchs, G., E. Shema, R. Vesterman, E. Kotler, Z. Wolchinsky, S. Wilder, L. Golomb, A. Pribluda, F. Zhang, M. Haj-Yahya, E. Feldmesser, A. Brik, X. Yu, J. Hanna, D. Aberdam, E. Domany and M. Oren (2012). "RNF20 and USP44 regulate stem cell differentiation by modulating H2B monoubiquitylation." *Mol Cell* **46**(5): 662-673.

Garcia-Prat, L., P. Sousa-Victor and P. Munoz-Canoves (2017). "Proteostatic and Metabolic Control of Stemness." *Cell Stem Cell* **20**(5): 593-608.

Genetic Modifiers of Huntington's Disease, C. (2015). "Identification of Genetic Factors that Modify Clinical Onset of Huntington's Disease." *Cell* **162**(3): 516-526.

Glick, D., S. Barth and K. F. Macleod (2010). "Autophagy: cellular and molecular mechanisms." *J Pathol* **221**(1): 3-12.

Glickman, M. H. and A. Ciechanover (2002). "The ubiquitin-proteasome proteolytic pathway: destruction for the sake of construction." *Physiol Rev* **82**(2): 373-428.

Groll, M., L. Ditzel, J. Lowe, D. Stock, M. Bochtler, H. D. Bartunik and R. Huber (1997). "Structure of 20S proteasome from yeast at 2.4 Å resolution." *Nature* **386**(6624): 463-471.

Grune, T., T. Jung, K. Merker and K. J. Davies (2004). "Decreased proteolysis caused by protein aggregates, inclusion bodies, plaques, lipofuscin, ceroid, and 'aggresomes' during oxidative stress, aging, and disease." *Int J Biochem Cell Biol* **36**(12): 2519-2530.

Gudjonsson, T., M. Altmeyer, V. Savic, L. Toledo, C. Dinant, M. Grofte, J. Bartkova, M. Poulsen, Y. Oka, S. Bekker-Jensen, N. Mailand, B. Neumann, J. K. Heriche, R. Shearer, D. Saunders, J. Bartek, J. Lukas and C. Lukas (2012). "TRIP12 and UBR5 suppress spreading of chromatin ubiquitylation at damaged chromosomes." *Cell* **150**(4): 697-709.

Gumeni, S. and I. P. Trougakos (2016). "Cross Talk of Proteostasis and Mitostasis in Cellular Homeodynamics, Ageing, and Disease." *Oxid Med Cell Longev* **2016**: 4587691.

Hageman, J., M. A. Rujano, M. A. van Waarde, V. Kakkar, R. P. Dirks, N. Govorukhina, H. M. Oosterveld-Hut, N. H. Lubsen and H. H. Kampinga (2010). "A DNAJB chaperone

subfamily with HDAC-dependent activities suppresses toxic protein aggregation." *Mol Cell* **37**(3): 355-369.

Hargus, G., M. Ehrlich, A. L. Hallmann and T. Kuhlmann (2014). "Human stem cell models of neurodegeneration: a novel approach to study mechanisms of disease development." *Acta Neuropathol* **127**(2): 151-173.

Hartl, F. U., A. Bracher and M. Hayer-Hartl (2011). "Molecular chaperones in protein folding and proteostasis." *Nature* **475**(7356): 324-332.

Hartl, F. U. and M. Hayer-Hartl (2002). "Molecular chaperones in the cytosol: from nascent chain to folded protein." *Science* **295**(5561): 1852-1858.

Haslbeck, M. and E. Vierling (2015). "A first line of stress defense: small heat shock proteins and their function in protein homeostasis." *J Mol Biol* **427**(7): 1537-1548.

Hay, D. G., K. Sathasivam, S. Tobaben, B. Stahl, M. Marber, R. Mestrlil, A. Mahal, D. L. Smith, B. Woodman and G. P. Bates (2004). "Progressive decrease in chaperone protein levels in a mouse model of Huntington's disease and induction of stress proteins as a therapeutic approach." *Hum Mol Genet* **13**(13): 1389-1405.

Hipp, M. S., C. N. Patel, K. Bersuker, B. E. Riley, S. E. Kaiser, T. A. Shaler, M. Brandeis and R. R. Kopito (2012). "Indirect inhibition of 26S proteasome activity in a cellular model of Huntington's disease." *J Cell Biol* **196**(5): 573-587.

Hochstrasser, M. (1996). "Ubiquitin-dependent protein degradation." *Annu Rev Genet* **30**: 405-439.

Hughes, K. A., J. A. Alipaz, J. M. Drnevich and R. M. Reynolds (2002). "A test of evolutionary theories of aging." *Proc Natl Acad Sci U S A* **99**(22): 14286-14291.

Iconomou, M. and D. N. Saunders (2016). "Systematic approaches to identify E3 ligase substrates." *Biochem J* **473**(22): 4083-4101.

Inagaki, R., K. Tagawa, M. L. Qi, Y. Enokido, H. Ito, T. Tamura, S. Shimizu, K. Oyanagi, N. Arai, I. Kanazawa, E. E. Wanker and H. Okazawa (2008). "Omi / HtrA2 is relevant to the selective vulnerability of striatal neurons in Huntington's disease." *Eur J Neurosci* **28**(1): 30-40.

Ingolia, N. T., L. F. Lareau and J. S. Weissman (2011). "Ribosome profiling of mouse embryonic stem cells reveals the complexity and dynamics of mammalian proteomes." *Cell* **147**(4): 789-802.

Iwai, K. and F. Tokunaga (2009). "Linear polyubiquitination: a new regulator of NF-kappaB activation." *EMBO Rep* **10**(7): 706-713.

Jacinto, F. V., C. Benner and M. W. Hetzer (2015). "The nucleoporin Nup153 regulates embryonic stem cell pluripotency through gene silencing." *Genes Dev* **29**(12): 1224-1238.

Jadhav, T. and M. W. Wooten (2009). "Defining an Embedded Code for Protein Ubiquitination." *J Proteomics Bioinform* **2**: 316.

Jain, A. K. and M. C. Barton (2009). "Regulation of p53: TRIM24 enters the RING." *Cell Cycle* **8**(22): 3668-3674.

Jana, N. R., P. Dikshit, A. Goswami, S. Kotliarova, S. Murata, K. Tanaka and N. Nukina (2005). "Co-chaperone CHIP associates with expanded polyglutamine protein and promotes their degradation by proteasomes." *J Biol Chem* **280**(12): 11635-11640.

Jana, N. R. and N. Nukina (2005). "BAG-1 associates with the polyglutamine-expanded huntingtin aggregates." *Neurosci Lett* **378**(3): 171-175.

Jana, N. R., E. A. Zemskov, G. Wang and N. Nukina (2001). "Altered proteasomal function due to the expression of polyglutamine-expanded truncated N-terminal huntingtin induces apoptosis by caspase activation through mitochondrial cytochrome c release." *Hum Mol Genet* **10**(10): 1049-1059.

Jeon, I., N. Lee, J. Y. Li, I. H. Park, K. S. Park, J. Moon, S. H. Shim, C. Choi, D. J. Chang, J. Kwon, S. H. Oh, D. A. Shin, H. S. Kim, J. T. Do, D. R. Lee, M. Kim, K. S. Kang, G. Q. Daley, P. Brundin and J. Song (2012). "Neuronal properties, in vivo effects, and pathology of a

Huntington's disease patient-derived induced pluripotent stem cells." *Stem Cells* **30**(9): 2054-2062.

Jin, K. (2010). "Modern Biological Theories of Aging." *Aging Dis* **1**(2): 72-74.

Johnson, S. C., P. S. Rabinovitch and M. Kaeblerlein (2013). "mTOR is a key modulator of ageing and age-related disease." *Nature* **493**(7432): 338-345.

Kakkar, V., M. Meister-Broekema, M. Minoia, S. Carra and H. H. Kampinga (2014). "Barcoding heat shock proteins to human diseases: looking beyond the heat shock response." *Dis Model Mech* **7**(4): 421-434.

Kapphahn, R. J., B. M. Giwa, K. M. Berg, H. Roehrich, X. Feng, T. W. Olsen and D. A. Ferrington (2006). "Retinal proteins modified by 4-hydroxynonenal: identification of molecular targets." *Exp Eye Res* **83**(1): 165-175.

Katsiki, M., N. Chondrogianni, I. Chinou, A. J. Rivett and E. S. Gonos (2007). "The olive constituent oleuropein exhibits proteasome stimulatory properties in vitro and confers life span extension of human embryonic fibroblasts." *Rejuvenation Res* **10**(2): 157-172.

Katsuno, M., C. Sang, H. Adachi, M. Minamiyama, M. Waza, F. Tanaka, M. Doyu and G. Sobue (2005). "Pharmacological induction of heat-shock proteins alleviates polyglutamine-mediated motor neuron disease." *Proc Natl Acad Sci U S A* **102**(46): 16801-16806.

Kawaguchi, Y., T. Okamoto, M. Taniwaki, M. Aizawa, M. Inoue, S. Katayama, H. Kawakami, S. Nakamura, M. Nishimura, I. Akiguchi and et al. (1994). "CAG expansions in a novel gene for Machado-Joseph disease at chromosome 14q32.1." *Nat Genet* **8**(3): 221-228.

Kaye, J. A. and S. Finkbeiner (2013). "Modeling Huntington's disease with induced pluripotent stem cells." *Mol Cell Neurosci* **56**: 50-64.

Kazemi-Esfarjani, P. and S. Benzer (2000). "Genetic suppression of polyglutamine toxicity in Drosophila." *Science* **287**(5459): 1837-1840.

Keck, S., R. Nitsch, T. Grune and O. Ullrich (2003). "Proteasome inhibition by paired helical filament-tau in brains of patients with Alzheimer's disease." *J Neurochem* **85**(1): 115-122.

Kinsella, E., N. Dora, D. Mellis, L. Lettice, P. Deveney, R. Hill and M. Ditzel (2016). "Use of a Conditional Ubr5 Mutant Allele to Investigate the Role of an N-End Rule Ubiquitin-Protein Ligase in Hedgehog Signalling and Embryonic Limb Development." *PLoS One* **11**(6): e0157079.

Kitamura, A., H. Kubota, C. G. Pack, G. Matsumoto, S. Hirayama, Y. Takahashi, H. Kimura, M. Kinjo, R. I. Morimoto and K. Nagata (2006). "Cytosolic chaperonin prevents polyglutamine toxicity with altering the aggregation state." *Nat Cell Biol* **8**(10): 1163-1170.

Komander, D., F. Reyes-Turcu, J. D. Licchesi, P. Odenwaelder, K. D. Wilkinson and D. Barford (2009). "Molecular discrimination of structurally equivalent Lys 63-linked and linear polyubiquitin chains." *EMBO Rep* **10**(5): 466-473.

koyuncu, s. (2015). "Defining the General Principles of Stem Cell Aging: Lessons from Organismal Models." *Current Stem Cell Reports* **1**(3): 162-169.

Koyuncu, S., A. Fatima, R. Gutierrez-Garcia and D. Vilchez (2017). "Proteostasis of Huntingtin in Health and Disease." *Int J Mol Sci* **18**(7).

Kozziel, R., R. Greussing, A. B. Maier, L. Declercq and P. Jansen-Durr (2011). "Functional interplay between mitochondrial and proteasome activity in skin aging." *J Invest Dermatol* **131**(3): 594-603.

Krahn, J. H., F. Kaschani and M. Kaiser (2017). "Turning-ON Proteasomes." *Cell Chem Biol* **24**(6): 653-655.

Kratter, I. H. and S. Finkbeiner (2010). "PolyQ disease: too many Qs, too much function?" *Neuron* **67**(6): 897-899.

Labbadia, J. and R. I. Morimoto (2015). "The biology of proteostasis in aging and disease." *Annu Rev Biochem* **84**: 435-464.

Lee, J. T. and W. Gu (2010). "The multiple levels of regulation by p53 ubiquitination." *Cell Death Differ* **17**(1): 86-92.

Leitman, J., F. Ulrich Hartl and G. Z. Lederkremer (2013). "Soluble forms of polyQ-expanded huntingtin rather than large aggregates cause endoplasmic reticulum stress." Nat Commun **4**: 2753.

Lenzi, J., R. De Santis, V. de Turris, M. Morlando, P. Laneve, A. Calvo, V. Caliendo, A. Chio, A. Rosa and I. Bozzoni (2015). "ALS mutant FUS proteins are recruited into stress granules in induced pluripotent stem cell-derived motoneurons." Dis Model Mech **8**(7): 755-766.

Li, W., B. Gao, S. M. Lee, K. Bennett and D. Fang (2007). "RLE-1, an E3 ubiquitin ligase, regulates *C. elegans* aging by catalyzing DAF-16 polyubiquitination." Dev Cell **12**(2): 235-246.

Li, W. W., J. Li and J. K. Bao (2012). "Microautophagy: lesser-known self-eating." Cell Mol Life Sci **69**(7): 1125-1136.

Li, X. J., H. Li and S. Li (2010). "Clearance of mutant huntingtin." Autophagy **6**(5): 663-664.

Li, Z. and P. Srivastava (2004). "Heat-shock proteins." Curr Protoc Immunol **Appendix 1**: Appendix 1T.

Lin, Y. J., L. Seroude and S. Benzer (1998). "Extended life-span and stress resistance in the *Drosophila* mutant methuselah." Science **282**(5390): 943-946.

Liu, X., B. R. Miller, G. V. Rebec and D. E. Clemmer (2007). "Protein expression in the striatum and cortex regions of the brain for a mouse model of Huntington's disease." J Proteome Res **6**(8): 3134-3142.

Liu, Y., C. L. Hettinger, D. Zhang, K. Rezvani, X. Wang and H. Wang (2014). "Sulforaphane enhances proteasomal and autophagic activities in mice and is a potential therapeutic reagent for Huntington's disease." J Neurochem **129**(3): 539-547.

Longo, V. D. and B. K. Kennedy (2006). "Sirtuins in aging and age-related disease." Cell **126**(2): 257-268.

Lopez-Otin, C., M. A. Blasco, L. Partridge, M. Serrano and G. Kroemer (2013). "The hallmarks of aging." Cell **153**(6): 1194-1217.

Lovrecic, L., A. Kastrin, J. Kobal, Z. Pirtosek, D. Krainc and B. Peterlin (2009). "Gene expression changes in blood as a putative biomarker for Huntington's disease." Mov Disord **24**(15): 2277-2281.

Mangiarini, L., K. Sathasivam, M. Seller, B. Cozens, A. Harper, C. Hetherington, M. Lawton, Y. Trotter, H. Lehrach, S. W. Davies and G. P. Bates (1996). "Exon 1 of the HD gene with an expanded CAG repeat is sufficient to cause a progressive neurological phenotype in transgenic mice." Cell **87**(3): 493-506.

Martinez-Vicente, M. and A. M. Cuervo (2007). "Autophagy and neurodegeneration: when the cleaning crew goes on strike." Lancet Neurol **6**(4): 352-361.

Martinez-Vicente, M., Z. Tallozy, E. Wong, G. Tang, H. Koga, S. Kaushik, R. de Vries, E. Arias, S. Harris, D. Sulzer and A. M. Cuervo (2010). "Cargo recognition failure is responsible for inefficient autophagy in Huntington's disease." Nat Neurosci **13**(5): 567-576.

Maucksch, C., E. M. Vazey, R. J. Gordon and B. Connor (2013). "Stem cell-based therapy for Huntington's disease." J Cell Biochem **114**(4): 754-763.

McNaught, K. S., D. P. Perl, A. L. Brownell and C. W. Olanow (2004). "Systemic exposure to proteasome inhibitors causes a progressive model of Parkinson's disease." Ann Neurol **56**(1): 149-162.

Mendez, M. F. (1994). "Huntington's disease: update and review of neuropsychiatric aspects." Int J Psychiatry Med **24**(3): 189-208.

Metzger, M. B., V. A. Hristova and A. M. Weissman (2012). "HECT and RING finger families of E3 ubiquitin ligases at a glance." J Cell Sci **125**(Pt 3): 531-537.

Miura, T., M. P. Mattson and M. S. Rao (2004). "Cellular lifespan and senescence signaling in embryonic stem cells." Aging Cell **3**(6): 333-343.

Moreno-Gonzalez, I. and C. Soto (2011). "Misfolded protein aggregates: mechanisms, structures and potential for disease transmission." Semin Cell Dev Biol **22**(5): 482-487.

Muchowski, P. J. and J. L. Wacker (2005). "Modulation of neurodegeneration by molecular chaperones." Nat Rev Neurosci **6**(1): 11-22.

Nagaria, P., C. Robert and F. V. Rassool (2013). "DNA double-strand break response in stem cells: mechanisms to maintain genomic integrity." Biochim Biophys Acta **1830**(2): 2345-2353.

Niclis, J., A. O. Trounson, M. Dottori, A. Ellisdon, S. P. Bottomley, Y. Verlinsky and D. Cram (2009). "Human embryonic stem cell models of Huntington disease." Reprod Biomed Online **19**(1): 106-113.

Noormohammadi, A., G. Calculli, R. Gutierrez-Garcia, A. Khodakarami, S. Koyuncu and D. Vilchez (2018). "Mechanisms of protein homeostasis (proteostasis) maintain stem cell identity in mammalian pluripotent stem cells." Cell Mol Life Sci **75**(2): 275-290.

Noormohammadi, A., A. Khodakarami, R. Gutierrez-Garcia, H. J. Lee, S. Koyuncu, T. Konig, C. Schindler, I. Saez, A. Fatima, C. Dieterich and D. Vilchez (2016). "Somatic increase of CCT8 mimics proteostasis of human pluripotent stem cells and extends *C. elegans* lifespan." Nat Commun **7**: 13649.

Okita, Y. and K. I. Nakayama (2012). "UPS delivers pluripotency." Cell Stem Cell **11**(6): 728-730.

Olzscha, H., S. M. Schermann, A. C. Woerner, S. Pinkert, M. H. Hecht, G. G. Tartaglia, M. Vendruscolo, M. Hayer-Hartl, F. U. Hartl and R. M. Vabulas (2011). "Amyloid-like aggregates sequester numerous metastable proteins with essential cellular functions." Cell **144**(1): 67-78.

Park, I. H., N. Arora, H. Huo, N. Maherali, T. Ahfeldt, A. Shimamura, M. W. Lensch, C. Cowan, K. Hochedlinger and G. Q. Daley (2008). "Disease-specific induced pluripotent stem cells." Cell **134**(5): 877-886.

Perez, M. K., H. L. Paulson, S. J. Pendse, S. J. Saionz, N. M. Bonini and R. N. Pittman (1998). "Recruitment and the role of nuclear localization in polyglutamine-mediated aggregation." J Cell Biol **143**(6): 1457-1470.

Pföh, R., I. K. Ladao and V. Saridakis (2015). "Deubiquitinases and the new therapeutic opportunities offered to cancer." Endocr Relat Cancer **22**(1): T35-54.

Pickart, C. M. (2001). "Mechanisms underlying ubiquitination." Annu Rev Biochem **70**: 503-533.

Pickart, C. M. and M. J. Eddins (2004). "Ubiquitin: structures, functions, mechanisms." Biochim Biophys Acta **1695**(1-3): 55-72.

Pierce, N. W., G. Kleiger, S. O. Shan and R. J. Deshaies (2009). "Detection of sequential polyubiquitylation on a millisecond timescale." Nature **462**(7273): 615-619.

Pouladi, M. A., A. J. Morton and M. R. Hayden (2013). "Choosing an animal model for the study of Huntington's disease." Nat Rev Neurosci **14**(10): 708-721.

Powers, E. T., R. I. Morimoto, A. Dillin, J. W. Kelly and W. E. Balch (2009). "Biological and chemical approaches to diseases of proteostasis deficiency." Annu Rev Biochem **78**: 959-991.

Ravikumar, B., C. Vacher, Z. Berger, J. E. Davies, S. Luo, L. G. Oroz, F. Scaravilli, D. F. Easton, R. Duden, C. J. O'Kane and D. C. Rubinsztajn (2004). "Inhibition of mTOR induces autophagy and reduces toxicity of polyglutamine expansions in fly and mouse models of Huntington disease." Nat Genet **36**(6): 585-595.

Rose, M. R., T. Flatt, J. L. Graves, L. F. Greer, D. E. Martinez, M. Matos, L. D. Mueller, R. J. Shmookler Reis and P. Shahrestani (2012). "What is Aging?" Front Genet **3**: 134.

Ross, C. A. and S. J. Tabrizi (2011). "Huntington's disease: from molecular pathogenesis to clinical treatment." Lancet Neurol **10**(1): 83-98.

Rotin, D. and S. Kumar (2009). "Physiological functions of the HECT family of ubiquitin ligases." Nat Rev Mol Cell Biol **10**(6): 398-409.

Rubenstein, E. M. and M. Hochstrasser (2010). "Redundancy and variation in the ubiquitin-mediated proteolytic targeting of a transcription factor." Cell Cycle **9**(21): 4282-4285.

Rubinsztajn, D. C. (2006). "The roles of intracellular protein-degradation pathways in neurodegeneration." Nature **443**(7113): 780-786.

Rubinsztein, D. C., J. E. Gestwicki, L. O. Murphy and D. J. Klionsky (2007). "Potential therapeutic applications of autophagy." *Nat Rev Drug Discov* **6**(4): 304-312.

Rui, Y. N., Z. Xu, B. Patel, Z. Chen, D. Chen, A. Tito, G. David, Y. Sun, E. F. Stimming, H. J. Bellen, A. M. Cuervo and S. Zhang (2015). "Huntingtin functions as a scaffold for selective macroautophagy." *Nat Cell Biol* **17**(3): 262-275.

Saez, I. and D. Vilchez (2014). "The Mechanistic Links Between Proteasome Activity, Aging and Age-related Diseases." *Curr Genomics* **15**(1): 38-51.

Safren, N., A. El Ayadi, L. Chang, C. E. Terrillion, T. D. Gould, D. F. Boehning and M. J. Monteiro (2014). "Ubiquilin-1 overexpression increases the lifespan and delays accumulation of Huntingtin aggregates in the R6/2 mouse model of Huntington's disease." *PLoS One* **9**(1): e87513.

Saftig, P., W. Beertsen and E. L. Eskelinen (2008). "LAMP-2: a control step for phagosome and autophagosome maturation." *Autophagy* **4**(4): 510-512.

Saibil, H. (2013). "Chaperone machines for protein folding, unfolding and disaggregation." *Nat Rev Mol Cell Biol* **14**(10): 630-642.

Sakai, Y., A. Koller, L. K. Rangell, G. A. Keller and S. Subramani (1998). "Peroxisome degradation by microautophagy in *Pichia pastoris*: identification of specific steps and morphological intermediates." *J Cell Biol* **141**(3): 625-636.

Saraswat, K. and S. I. Rizvi (2017). "Novel strategies for anti-aging drug discovery." *Expert Opin Drug Discov* **12**(9): 955-966.

Sarkar, S., E. O. Perlstein, S. Imarisio, S. Pineau, A. Cordenier, R. L. Maglathlin, J. A. Webster, T. A. Lewis, C. J. O'Kane, S. L. Schreiber and D. C. Rubinsztein (2007). "Small molecules enhance autophagy and reduce toxicity in Huntington's disease models." *Nat Chem Biol* **3**(6): 331-338.

Saudou, F. and S. Humbert (2016). "The Biology of Huntingtin." *Neuron* **89**(5): 910-926.

Scherzinger, E., R. Lurz, M. Turmaine, L. Mangiarini, B. Hollenbach, R. Hasenbank, G. P. Bates, S. W. Davies, H. Lehrach and E. E. Wanker (1997). "Huntingtin-encoded polyglutamine expansions form amyloid-like protein aggregates in vitro and in vivo." *Cell* **90**(3): 549-558.

Schnerch, A., C. Cerdan and M. Bhatia (2010). "Distinguishing between mouse and human pluripotent stem cell regulation: the best laid plans of mice and men." *Stem Cells* **28**(3): 419-430.

Schwarz, S. C. and J. Schwarz (2010). "Translation of stem cell therapy for neurological diseases." *Transl Res* **156**(3): 155-160.

Seo, H., K. C. Sonntag, W. Kim, E. Cattaneo and O. Isacson (2007). "Proteasome activator enhances survival of Huntington's disease neuronal model cells." *PLoS One* **2**(2): e238.

Shearer, R. F., M. Ionomou, C. K. Watts and D. N. Saunders (2015). "Functional Roles of the E3 Ubiquitin Ligase UBR5 in Cancer." *Mol Cancer Res* **13**(12): 1523-1532.

Shirasaki, D. I., E. R. Greiner, I. Al-Ramahi, M. Gray, P. Boontheung, D. H. Geschwind, J. Botas, G. Coppola, S. Horvath, J. A. Loo and X. W. Yang (2012). "Network organization of the huntingtin proteomic interactome in mammalian brain." *Neuron* **75**(1): 41-57.

Smith, E. D., T. L. Kaeberlein, B. T. Lydum, J. Sager, K. L. Welton, B. K. Kennedy and M. Kaeberlein (2008). "Age- and calorie-independent life span extension from dietary restriction by bacterial deprivation in *Caenorhabditis elegans*." *BMC Dev Biol* **8**: 49.

Son, E. Y., J. K. Ichida, B. J. Wainger, J. S. Toma, V. F. Rafuse, C. J. Woolf and K. Eggan (2011). "Conversion of mouse and human fibroblasts into functional spinal motor neurons." *Cell Stem Cell* **9**(3): 205-218.

Spratt, D. E., H. Walden and G. S. Shaw (2014). "RBR E3 ubiquitin ligases: new structures, new insights, new questions." *Biochem J* **458**(3): 421-437.

Strikoudis, A., M. Guillaumot and I. Aifantis (2014). "Regulation of stem cell function by protein ubiquitylation." *EMBO Rep* **15**(4): 365-382.

Stroo, E., M. Koopman, E. A. Nollen and A. Mata-Cabana (2017). "Cellular Regulation of Amyloid Formation in Aging and Disease." Front Neurosci **11**: 64.

Suhr, S. T., M. C. Senut, J. P. Whitelegge, K. F. Faull, D. B. Cuizon and F. H. Gage (2001). "Identities of sequestered proteins in aggregates from cells with induced polyglutamine expression." J Cell Biol **153**(2): 283-294.

Sun, L. and Z. J. Chen (2004). "The novel functions of ubiquitination in signaling." Curr Opin Cell Biol **16**(2): 119-126.

Szutorisz, H., A. Georgiou, L. Tora and N. Dillon (2006). "The proteasome restricts permissive transcription at tissue-specific gene loci in embryonic stem cells." Cell **127**(7): 1375-1388.

Tagawa, K., S. Marubuchi, M. L. Qi, Y. Enokido, T. Tamura, R. Inagaki, M. Murata, I. Kanazawa, E. E. Wanker and H. Okazawa (2007). "The induction levels of heat shock protein 70 differentiate the vulnerabilities to mutant huntingtin among neuronal subtypes." J Neurosci **27**(4): 868-880.

Takahashi, K., K. Tanabe, M. Ohnuki, M. Narita, T. Ichisaka, K. Tomoda and S. Yamanaka (2007). "Induction of pluripotent stem cells from adult human fibroblasts by defined factors." Cell **131**(5): 861-872.

Tam, S., R. Geller, C. Spiess and J. Frydman (2006). "The chaperonin TRiC controls polyglutamine aggregation and toxicity through subunit-specific interactions." Nat Cell Biol **8**(10): 1155-1162.

Tatar, M., A. Bartke and A. Antebi (2003). "The endocrine regulation of aging by insulin-like signals." Science **299**(5611): 1346-1351.

Taylor, R. C. and A. Dillin (2011). "Aging as an event of proteostasis collapse." Cold Spring Harb Perspect Biol **3**(5).

Thomson, J. A., J. Itskovitz-Eldor, S. S. Shapiro, M. A. Waknitz, J. J. Swiergiel, V. S. Marshall and J. M. Jones (1998). "Embryonic stem cell lines derived from human blastocysts." Science **282**(5391): 1145-1147.

Tonoki, A., E. Kuranaga, T. Tomioka, J. Hamazaki, S. Murata, K. Tanaka and M. Miura (2009). "Genetic evidence linking age-dependent attenuation of the 26S proteasome with the aging process." Mol Cell Biol **29**(4): 1095-1106.

Torres, C., L. Lewis and V. J. Cristofalo (2006). "Proteasome inhibitors shorten replicative life span and induce a senescent-like phenotype of human fibroblasts." J Cell Physiol **207**(3): 845-853.

Tsai, Y. C., P. S. Fishman, N. V. Thakor and G. A. Oyler (2003). "Parkin facilitates the elimination of expanded polyglutamine proteins and leads to preservation of proteasome function." J Biol Chem **278**(24): 22044-22055.

van Leeuwen, F. W., D. P. de Kleijn, H. H. van den Hurk, A. Neubauer, M. A. Sonnemans, J. A. Sluijs, S. Koycu, R. D. Ramdjielal, A. Salehi, G. J. Martens, F. G. Grosveld, J. Peter, H. Burbach and E. M. Hol (1998). "Frameshift mutants of beta amyloid precursor protein and ubiquitin-B in Alzheimer's and Down patients." Science **279**(5348): 242-247.

van Oosten-Hawle, P. and R. I. Morimoto (2014). "Organismal proteostasis: role of cell-nonautonomous regulation and transcellular chaperone signaling." Genes Dev **28**(14): 1533-1543.

Varum, S., A. S. Rodrigues, M. B. Moura, O. Momcilovic, C. A. t. Easley, J. Ramalho-Santos, B. Van Houten and G. Schatten (2011). "Energy metabolism in human pluripotent stem cells and their differentiated counterparts." PLoS One **6**(6): e20914.

Verlinsky, Y., N. Strelchenko, V. Kukharensko, S. Rechitsky, O. Verlinsky, V. Galat and A. Kuliev (2005). "Human embryonic stem cell lines with genetic disorders." Reprod Biomed Online **10**(1): 105-110.

Victor, M. B., M. Richner, H. E. Olsen, S. W. Lee, A. M. Monteys, C. Ma, C. J. Huh, B. Zhang, B. L. Davidson, X. W. Yang and A. S. Yoo (2018). "Striatal neurons directly converted from

Huntington's disease patient fibroblasts recapitulate age-associated disease phenotypes." *Nat Neurosci* **21**(3): 341-352.

Vilchez, D., L. Boyer, M. Lutz, C. Merkwirth, I. Morantte, C. Tse, B. Spencer, L. Page, E. Masliah, W. T. Berggren, F. H. Gage and A. Dillin (2013). "FOXO4 is necessary for neural differentiation of human embryonic stem cells." *Aging Cell* **12**(3): 518-522.

Vilchez, D., L. Boyer, I. Morantte, M. Lutz, C. Merkwirth, D. Joyce, B. Spencer, L. Page, E. Masliah, W. T. Berggren, F. H. Gage and A. Dillin (2012). "Increased proteasome activity in human embryonic stem cells is regulated by PSMD11." *Nature* **489**(7415): 304-308.

Vilchez, D., I. Morantte, Z. Liu, P. M. Douglas, C. Merkwirth, A. P. Rodrigues, G. Manning and A. Dillin (2012). "RPN-6 determines *C. elegans* longevity under proteotoxic stress conditions." *Nature* **489**(7415): 263-268.

Vilchez, D., I. Saez and A. Dillin (2014). "The role of protein clearance mechanisms in organismal ageing and age-related diseases." *Nat Commun* **5**: 5659.

Vonsattel, J. P. (2008). "Huntington disease models and human neuropathology: similarities and differences." *Acta Neuropathol* **115**(1): 55-69.

Vonsattel, J. P. and M. DiFiglia (1998). "Huntington disease." *J Neuropathol Exp Neurol* **57**(5): 369-384.

Vonsattel, J. P., R. H. Myers, T. J. Stevens, R. J. Ferrante, E. D. Bird and E. P. Richardson, Jr. (1985). "Neuropathological classification of Huntington's disease." *J Neuropathol Exp Neurol* **44**(6): 559-577.

Waelter, S., A. Boeddrich, R. Lurz, E. Scherzinger, G. Lueder, H. Lehrach and E. E. Wanker (2001). "Accumulation of mutant huntingtin fragments in aggresome-like inclusion bodies as a result of insufficient protein degradation." *Mol Biol Cell* **12**(5): 1393-1407.

Warrick, J. M., H. Y. Chan, G. L. Gray-Board, Y. Chai, H. L. Paulson and N. M. Bonini (1999). "Suppression of polyglutamine-mediated neurodegeneration in *Drosophila* by the molecular chaperone HSP70." *Nat Genet* **23**(4): 425-428.

Weinberger, L., M. Ayyash, N. Novershtern and J. H. Hanna (2016). "Dynamic stem cell states: naive to primed pluripotency in rodents and humans." *Nat Rev Mol Cell Biol* **17**(3): 155-169.

Wilkinson, K. D. (2000). "Ubiquitination and deubiquitination: targeting of proteins for degradation by the proteasome." *Semin Cell Dev Biol* **11**(3): 141-148.

Wytenbach, A., J. Carmichael, J. Swartz, R. A. Furlong, Y. Narain, J. Rankin and D. C. Rubinsztein (2000). "Effects of heat shock, heat shock protein 40 (HDJ-2), and proteasome inhibition on protein aggregation in cellular models of Huntington's disease." *Proc Natl Acad Sci U S A* **97**(6): 2898-2903.

Xiao, D., X. Liu, M. Zhang, M. Zou, Q. Deng, D. Sun, X. Bian, Y. Cai, Y. Guo, S. Liu, S. Li, E. Shiang, H. Zhong, L. Cheng, H. Xu, K. Jin and M. Xiang (2018). "Direct reprogramming of fibroblasts into neural stem cells by single non-neural progenitor transcription factor Ptf1a." *Nat Commun* **9**(1): 2865.

Xie, Y., E. M. Rubenstein, T. Matt and M. Hochstrasser (2010). "SUMO-independent in vivo activity of a SUMO-targeted ubiquitin ligase toward a short-lived transcription factor." *Genes Dev* **24**(9): 893-903.

Yamamoto, A., J. J. Lucas and R. Hen (2000). "Reversal of neuropathology and motor dysfunction in a conditional model of Huntington's disease." *Cell* **101**(1): 57-66.

Yamanaka, T., H. Miyazaki, F. Oyama, M. Kurosawa, C. Washizu, H. Doi and N. Nukina (2008). "Mutant Huntingtin reduces HSP70 expression through the sequestration of NF-Y transcription factor." *EMBO J* **27**(6): 827-839.

Yang, H., X. Zhong, P. Ballar, S. Luo, Y. Shen, D. C. Rubinsztein, M. J. Monteiro and S. Fang (2007). "Ubiquitin ligase Hrd1 enhances the degradation and suppresses the toxicity of polyglutamine-expanded huntingtin." *Exp Cell Res* **313**(3): 538-550.

Yau, R. G., K. Doerner, E. R. Castellanos, D. L. Haakonsen, A. Werner, N. Wang, X. W. Yang, N. Martinez-Martin, M. L. Matsumoto, V. M. Dixit and M. Rape (2017). "Assembly and

Function of Heterotypic Ubiquitin Chains in Cell-Cycle and Protein Quality Control." Cell **171**(4): 918-933 e920.

You, K. T., J. Park and V. N. Kim (2015). "Role of the small subunit processome in the maintenance of pluripotent stem cells." Genes Dev **29**(19): 2004-2009.

Zeng, S., L. Liu, Y. Sun, P. Xie, L. Hu, D. Yuan, D. Chen, Q. Ouyang, G. Lin and G. Lu (2014). "Telomerase-mediated telomere elongation from human blastocysts to embryonic stem cells." J Cell Sci **127**(Pt 4): 752-762.

Zhao, X., J. I. Heng, D. Guardavaccaro, R. Jiang, M. Pagano, F. Guillemot, A. Iavarone and A. Lasorella (2008). "The HECT-domain ubiquitin ligase Huwe1 controls neural differentiation and proliferation by destabilizing the N-Myc oncoprotein." Nat Cell Biol **10**(6): 643-653.

Zuccato, C., M. Valenza and E. Cattaneo (2010). "Molecular mechanisms and potential therapeutic targets in Huntington's disease." Physiol Rev **90**(3): 905-981.

ACKNOWLEDGEMENT

I would like to extend my sincere thanks to my advisor Dr. David Vilchez not only for his guidance and constructive advices during my PhD but also for his support and encouragement for my academic life. I am really lucky as I had chance to work with his and I had opportunity to learn from him to develop my scientific perspective.

I would like to thank Prof. Dr. Thorsten Hoppe and Prof. Dr. Matthias Hammerschmidt for being members of my thesis committee and for their contributions to my thesis. I also would like to express my thanks Prof. Dr. Björn Schumacher and Dr. Markus Rinschen for their great feedback about my work during my PhD.

I am very thankful to our group, Dr. Isabel Sáez Martínez, Ricardo Gutiérrez García, Giuseppe Calculli Dr. Azra Fatima, Hafiza Alirzayeva, Dr. Hyun Ju Lee, Alireza Noormohammadi, Dr. Ernesto Llamas, Melissa Chmara, Orsolya Bilkei-Gorzo for their friendship, support and helps and creating such a warm working environment during my PhD. I want specially to thank Dr. Isabel Sáez Martínez. I started my PhD under supervision of her and working with her was a very pleasant experience with sharing so many nice memories. As both friend and supervisor, she helped me in every situation and kept me motivated during this long journey.

Moreover, I am very grateful to Giuseppe Calculli, Ricardo Gutiérrez García, Hafiza Alirzayeva. They were my second family in here. We shared a lot of great memories, fun and beautiful moments. They always supported me and with them, it was also easier to cope with any frustrating or bad situations. I cannot image my PhD without these precious people. I would like to acknowledge also our former lab members, Christina Schindler, Dr. Amirabbas Khodakarami, Dilber Irmak and Yasin Bahadir Erol for their friendship and helps.

I would also acknowledge Cologne Graduate School of Aging Research for financial support with a scholarship during my thesis study and all of their help and support. I would like to specifically thanks to Doris, Jenny, Daniela and Ruth for their great support.

Additionally, I am very thankful to Chiara Calabrese, Pablo Rivera Mejias and Christoph Wittich for their friendship and moral support. Moreover, I want to also thank to Yasin Tümtas and Kübra Narci. Although even we didn't live in even same country, they always supported me with their great friendship.

I would like to extend my thanks to CECAD lab groups because they provided supportive and peaceful environment for my research.

Finally, I would like to express my special, sincere thanks to my lovely family due to their infinite love, motivation, support and helps. They always believe and encourage me and their

support gives me power to my academic life. I would not be where I am today without them. I dedicated my studies to my lovely family.

8)Erklärung

Ich versichere, dass ich die von mir vorgelegte Dissertation selbständig angefertigt, die benutzten Quellen und Hilfsmittel vollständig angegeben und die Stellen der Arbeit einschließlich Tabellen, Karten und Abbildungen, die anderen Werken im Wortlaut oder dem Sinn nach entnommen sind, in jedem Einzelfall als Entlehnung kenntlich gemacht habe: dass diese Dissertation noch keener anderen Fakultät oder Universität zur Prüfung vorgelegen hat; dass sie – abgesehen von Teilpublikationen – noch nicht veröffentlicht worden ist sowie, dass ich eine solche Veröffentlichung vor Abschluss des Prüfungsverfahrens nicht vornehmen werde.

Die Bestimmungen dieser Promotionsordnung sind mir bekannt. Die von mir vorgelegte Dissertation ist von Dr. David Vilchez betreut worden.

Teilpublikationen sind unter “Publications” aufgeführt.

Ich versichere, dass ich alle Angaben wahrheitsgemäß nach bestem Wissen und Gewissen gemacht habe und verpflichte mich, jedmögliche, die obigen Angabe betreffenden Veränderungen, dem Dekanat unverzüglich mitzuteilen.

Datum Unterschrift

Köln, 2019

SEDA KOYUNCU

Adress(es): Am Sportpark Müngersdorf 1, Room number :21-11 Köln-Germany

Telephone(s): +4915775895773

E-mail(s): sedakyncu@gmail.com, skoyunc2@uni-koeln.de

HIGHER EDUCATION

2014-2019 –PhD candidate

University of Cologne-CECAD (Cologne Excellent in Aging Research)

Cologne, Germany

Thesis Title: “Mechanism suppressing proteostasis collapse in pluripotent stem cells and its demise in Huntington's disease”

Supervisor: Dr. David Vilchez

2012-2014 – Master of Science

Bilkent University- Molecular Biology and Genetics

Ankara-Turkey

Thesis title:” Prevention of Free Fatty Acid Induced Inflammasome Activation by Bioactive Lipokine”

Degree of Graduation:3.89/4.00

2007-2012 – Bachelor of Science

Middle East Technical University-Molecular Biology and Genetics

Ankara-Turkey

Degree of Graduation:3.17/4.00



RESEARCH EXPERIENCE

PhD student-CECAD, University of Cologne

OCTOBER 2014 – PRESENT

Supervisor: Dr.David Vilchez

- Thesis Title: Mechanism suppressing proteostasis collapse in pluripotent stem cells and its demise in Huntington's disease

-Insights into the ubiquitin-proteasome system of human embryonic stem cells

Master of Science –Molecular Biology and Genetics at Bilkent University Ankara, Turkey

SEPTEMBER 2012-AUGUST 2014

Supervisor: Assist. Prof Dr. Ebru Erbay

-Thesis Title: Prevention of Free Fatty Acid Induced Inflammasome Activation by Bioactive Lipokine

Member of International Genetically Engineered Machine(IGEM) team at Middle East Technical University (METU)–METU, Ankara, Turkey

NOVEMBER 2011-SEPTEMBER 2012

- Design of biological carbon monoxide filter by using advantage of synthetic biology

Intern –Molecular Biology and Genetics at METU, Ankara, Turkey

FEBRUARY 2012-JUNE 2012

Supervisor: Assist. Prof Dr. Tülin Yanik

-Preparation of DNA bank from schizophrenic patient blood

Intern –Ageing and Cell Death-Laboratory of Frank Madeo at University of Graz, Graz, Austria

JUNE 2011-SEPTEMBER 2011

Supervisor: Prof Dr. Frank Madeo

-Investigation of Alzheimer Disease on aging yeast as a model for neurodegenerative disorders



PUBLICATIONS

- 1) **Koyuncu, S***, Saez, I*, Lee, H.J., Gutierrez Garcia, Pokrzywa, W., Fatima, A., Hoppe, T. and Vilchez, D. (2018) The ubiquitin ligase UBR5 suppresses proteostasis collapse in pluripotent stem cells from Huntington's disease patients. *Nat. Commun.*, 9, 2886.
- 2) I. Saez*, **S. Koyuncu***, R. Gutierrez-Garcia, C. Dieterich and D. Vilchez (2018). Insights into the ubiquitin-proteasome system of human embryonic stem cells. *Scientific Reports* 8: 4092.
- 3) A. Noormohammadi, G. Calculli, R. Gutierrez-Garcia, A. Khodokarami, **S. Koyuncu** and D. Vilchez (2017). Mechanisms of protein homeostasis(proteostasis) maintain stem cell identity in mammalian pluripotent stem cells. *Cellular and Molecular Life Sciences* doi: 10.1007/s00018-017-2602-1
- 4) **S. Koyuncu**, A. Fatima, R. Gutierrez-Garcia and D. Vilchez (2017). Proteostasis of Huntingtin in Health and Disease. *International Journal of Molecular Sciences* 18(7): 1568 doi:10.3390/ijms18071568.
- 5) A. Noormohammadi, A. Khodokarami, R. Gutierrez-Garcia, H.J. Lee, **S. Koyuncu**, T. König, C. Schindler, I. Saez, A. Fatima, C. Dieterich and D. Vilchez (2016). Somatic increase of CCT8 mimics proteostasis of human pluripotent stem cells and extends *C. elegans* lifespan. *Nature Communications* **7**: 13649.
- 6) I. Cimen, B. Kocaturk, **S. Koyuncu**, et al. (2016). Prevention of atherosclerosis by bioactive palmitoleate through suppression of organelle stress and inflammasome activation. *Sci Transl Med* 8(358): 358ra126.
- 7) **S. Koyuncu**, D. Irmak, I. Saez & D. Vilchez, (2015). Defining the General Principles of Stem Cell Aging: Lessons from Organismal Models. *Current Stem Cell Reports*, 1-8



AWARDS&HONORS

- Full PhD scholarship awarded by Cologne Graduate School of Ageing Research-**2014-2017**
- Full scholarship awarded by TUBITAK (The Scientific and Technical Research Council of Turkey)-**2012-2014**
- Bilkent University Master Degree Education Scholarship-**2012-2014**
- Bronze Award gained by International Genetically Engineered Machine Competition-**2012**
- Finalist in 3. National Medical Ethics Project Competition (Obesity and Ethics)-**2012**
- Erasmus Internship Scholarship-**2011**
- Full scholarship awarded by TUBITAK (The Scientific and Technical Research Council of Turkey)-**2007-2012**
- Entered the Department of Molecular Biology and Genetics in METU as a 5th student according to the ranking of the Student Selection Exam(OSS) organized by the Student Selection and Placement Center -**2007**



RESEARCH RELATED EMPLOYMENTS

- Spring 2014- Teaching Assistant, Molecular Genetics, Bilkent University, TURKEY
- Spring 2013-Teaching Assistant, Biochemistry, Bilkent University, TURKEY
- Fall 2012 and Fall 2013-Teaching Asistant, Intoduction to modern Biology, Bilkent University, TURKEY



MEMBERSHIPS OF COMMUNITY, ORGANIZATION, ASSOCIATION

- Organization committee member in Ihsan Dogramaci Memorial Conference' The Endoplasmic Reticulum Homeostasis and Disease' Lecturers: Gökhan Hothamisligil and Peter Walter
- iGEM (International Genetically Engineered Machine) METU 2012 –team member
- Science and Technics Committee's administration member (2011-2012)



ATTENDANT SEMINARS, MEETING AND CONFERENCES

- Protein quality control: Success and failure in health and disease-2017-Girona/Spain
- Molecular Mechanisms of Ageing and Regeneration: From pluripotency to senescence-2016-Spetses/Greece
- Developmental Circuits in Aging -2015- Heraklion/Greece
- Bioinformatics for Anti-cancer Drug Discovery-2011-Ankara/Turkey
- Genetics of Neurological Disorders-2010-Istanbul/Turkey